

AN EXPLORATION OF THE ORIGINS, EVOLUTION, AND FATE OF INORGANIC  
CHEMICAL CONSTITUENTS IN METEORIC WATERS ON THE ISLAND OF O'AHU,  
HAWAI'I, USA

A DISSERTATION SUBMITTED TO THE GRADUATE DIVISION OF THE  
UNIVERSITY OF HAWAI'I AT MĀNOA IN PARTIAL FULFILLMENT  
OF THE REQUIREMENTS FOR THE DEGREE OF

DOCTOR OF PHILOSOPHY  
IN  
EARTH AND PLANETARY SCIENCE  
NOVEMBER 2023

By

Theodore M. Brennis

Dissertation Committee:  
Nicole Lautze (Chairperson)  
Robert Whittier  
Giuseppe Torri  
Donald Thomas  
Scott Rowland

Keywords: precipitation, stable isotopes of water,  $\delta^{18}\text{O}$ ,  $\delta^2\text{H}$ , dissolved ions, O'ahu, soil moisture, infiltration, groundwater, groundwater flow, recharge

## ACKNOWLEDGEMENTS

First, foremost, and in all things, I give thanks my Savior, the Good Shepard, the Great Physician, and the Creator of all things. I echo the psalmist's proclamation,

By the word of the LORD the heavens were made,

and by the breath of his mouth all their host.

He gathers the waters of the sea as a heap;

he puts the deeps in storehouses.

Let all the earth fear the LORD;

let all the inhabitants of the world stand in awe of him!

For he spoke, and it came to be;

he commanded, and it stood firm. (Psalm 33: 6-9, ESV)

Nowhere is the handiwork of God more apparent to me than in Hawai‘i. From the green, jagged peaks, down through the streams and waterfalls, out to the turquoise waters teaming with life, Hawai‘i cries out with the psalmist in exultation to God:

Praise the LORD from the earth you great sea creatures and all deeps,

fire and hail, snow and mist, stormy wind fulfilling his word! (Psalm 148: 7-8, ESV)

The last five years studying His creation in this wonderful place have been a joy and a privilege.

I will give thanks to the LORD with my whole heart;

I will recount all of your wonderful deeds.

I will be glad and exult in you;

I will sing praise to your name, O Most High. (Psalm 9: 1-2, ESV)

Secondly, I would like to thank my lovely wife, and best friend, Paige. This undertaking would have been impossible without her patience, encouragement, and constant support. Paige was my sounding board, my first line editor, my field companion, my anchor, and my motivation. I do not deserve to have such a wonderful woman as my wife, and I thank my God with my whole heart for His kindness in bringing us together.

I would like to express my love and gratitude to my parents, Gary and Suzanne, for their constant encouragement, support, kindness, and generosity.

I would like to thank my committee members. I am grateful to Nicole for bringing me on as an undergraduate and allowing me to continue working on this fascinating project through graduate school. I could not have asked for a better mentor and advisor. I am grateful to Bob Whittier for the many hours of one-on-one Teams meetings going through the minutia of soil mechanics and inorganic chemistry, for the fun fishing stories, and for all the career advice. I am grateful to Don, Giuseppe, and Scott, for selflessly carving out time to invest in my development, for pushing me to dig deeper, and for encouraging me to let the data speak for itself. I am grateful to Henrietta, Garrett, and Yin-Phan, along with the other members of my comprehensive examination committee for all the amazing resources, thought provoking questions, and flexibility working with my atypical circumstances.

I am grateful for the fine instruction, training, and support I have received within the University of Hawai‘i at Mānoa Department of Earth Sciences. I would like to thank Professors Tom Shea, Henrietta Dulai, Scott Rowland, and Rob Dunn for the fascinating and challenging courses. I would also like to thank Lily Shao, and all the other amazing staff within SOEST, who truly run a world class organization.

I am grateful to Michael and April Wolfe, the State of Hawai‘i Department of Health, the State of Hawai‘i Department of Land and Natural Resources, the Schofield Barracks Directorate of Public Works, Mililani High School, and the Ko‘olau Mountains Watershed Partnership for land access and sampling assistance.

Finally, I would like to express my gratitude to both the EPSCoR ‘Ike Wai and the DoD SMART programs for providing the financial support necessary to complete this project.

## DISSERTATION ABSTRACT

This study examines the inorganic composition of rainfall on O‘ahu, Hawai‘i, as part of a broader effort to apply natural conservative geochemical tracers to water resource management problems in the State. Pacific Islands grapple with unique water resource challenges due to environmental vulnerability, climate dynamics, and heavy groundwater reliance. Urbanization, population growth, and decreasing rainfall trends also stress O‘ahu's freshwater resources. To address these water resource challenges, understanding the links between meteoric, ground-, and surface waters is crucial. This research consists of three components that use the inorganic chemistry of precipitation to better understand such links. First, we analyzed major ion sources in O‘ahu's rainfall, which revealed that ocean sea spray is the primary dissolved ion source, with perturbations from Asian continental dust, local sediment, and agriculture as dictated by broader weather patterns. Second, we analyzed rainfall stable isotopes ( $^{18}\text{O}$  and  $^2\text{H}$ ), which indicated that there are distinct geographical, seasonal, and precipitation source-related influences. High-elevation spring sampling also indicated that there are significant fog contributions to groundwater recharge. Finally, we investigated how rainfall chemistry evolves as it infiltrates the soil and present a method to assess changes in the stable isotope composition of precipitation during infiltration. These studies illuminate several key meteorological and physiographic dynamics that affect precipitation chemistry on O‘ahu and provide a baseline from which to assess future fluctuations. They underscore the impact of microclimates and moisture source on the stable isotope composition of precipitation, and highlight the need for topographically diverse, event-based precipitation sampling. Results from the third study highlight the importance of understanding chemical changes to precipitation during the process of infiltration. Cumulatively, these findings lay groundwork for utilizing natural geochemical tracers to understand groundwater flow paths and recharge processes on O‘ahu.

## TABLE OF CONTENTS

Acknowledgements .....	ii
Dissertation Abstract .....	iv
List of Tables .....	ix
List of Figures .....	x
Chapter 1: Introduction .....	1
Chapter 2: Understanding the Origins of and Influences on Precipitation Major	
Ion Chemistry on the Island of O‘ahu, Hawai‘i.....	6
Chapter 2 Abstract .....	7
1. Introduction.....	8
2. Methods .....	10
2.1. Study Area.....	10
2.2. Precipitation Collection .....	14
2.3. Chemical Analysis .....	14
2.4. Weather Trend Analysis .....	15
2.5. Data Analysis.....	15
2.5.1. Sea Salt Aerosol Correction .....	16
2.5.2. Crustal & Marine Enrichment Factors .....	17
2.5.3. Regression Analysis .....	17
2.5.4. Principal Component Analysis.....	18
3. Results & Discussion .....	19
3.1. Sodium & Chloride .....	19
3.2. Calcium .....	28
3.3. Potassium .....	33
3.4. Sulfate & Magnesium .....	36
4. Conclusions.....	39
5. Chapter 2 References .....	40

Chapter 3: Understanding the Source and Evolution of Precipitation Stable Isotope Composition Across O‘ahu, Hawai‘i, USA .....	46
Chapter 3 Abstract .....	47
1. Introduction .....	48
2. Methods .....	51
2.1. Water Stable Isotope Fundamentals .....	51
2.2. Study Region Isoscape .....	51
2.3. Water Chemistry Data Collection .....	53
2.4. Chemical Analysis .....	53
2.5. Local Meteoric Water Line .....	54
2.6. Statistical Analysis: Amount and Altitude Effect.....	54
2.7. Weather Trend Analysis.....	55
3. Results .....	59
3.1. Rainfall H and O isotopic composition.....	59
3.2. Local Meteoric Water Line .....	59
3.3. Amount Effect .....	60
3.4. Altitude Effect .....	60
3.5. Deuterium Excess .....	61
4. Discussion .....	71
4.1. Altitude Effect .....	71
4.2. Fog .....	77
4.3. Influence of Microclimates .....	82
5. Conclusions.....	82
6. References .....	84
Chapter 4: A Method for Exploring the Impacts of Soil Moisture Dynamics on the Chemistry of Groundwater Infiltration .....	88
Chapter 4 Abstract .....	89
1. Introduction .....	90
2. Methods .....	91

2.1. Study Area Overview.....	91
2.2. Soil Moisture Dynamics Overview.....	97
2.3. Soil Moisture Monitoring Methods Overview .....	98
2.4. Stable Isotope Composition of Soil Water .....	98
2.5. Data Collection .....	99
2.5.1. Soil Tension .....	99
2.5.2. Soil Moisture Content .....	100
2.5.3. Meteorological Data .....	101
2.5.4. Soil Water Chemistry .....	102
2.6. Data Analysis .....	103
2.6.1. Soil Water Retention Curve .....	103
2.6.2. Soil Water Column Height .....	103
2.6.3. Evapotranspiration.....	104
2.6.4. Water Budget Calculations.....	105
2.6.5. Limitations .....	106
3. Findings .....	109
3.1. Soil Water Retention Curve .....	109
3.2. Infiltration Periods .....	109
3.3. Water Budget Amounts.....	109
3.4. Soil and Precipitation H and O isotopic composition .....	110
4. Discussion .....	118
4.1. Soil Water Retention Curve Performance.....	118
4.2. Water Budget Model Performance .....	119
4.3. Soil Moisture Dynamics Impacting Groundwater Chemistry .....	120
5. Conclusions.....	126
6. References .....	127
Chapter 5: Conclusions .....	131
Appendix A: Chapter 2 Supplementary Materials .....	136
Tab A.1 Processes Impacting Precipitation Inorganic Chemistry .....	136

Tab A.2 Major Ion Bulk Deposition .....	142
Tab A.3 Crustal Enrichment Factors.....	149
Tab A.4 Marine Enrichment Factors.....	156
Tab A.5 Non-Sea Salt Major Ion Concentrations.....	163
Tab A.6 Major Ion Raw Data .....	170
Appendix B: Chapter 3 Supplementary Materials.....	177
Appendix C: Chapter 4 Supplementary Materials.....	185
Tab C.1 Lower Manana Soil and Water Budget Data .....	185
Tab C.2 Upper Manana Soil and Water Budget Data.....	189
Tab C.3 Uluakupu Soil Chemistry Data.....	195
Tab C.4 Uluakupu Soil Tension and Moisture Data.....	196

## LIST OF TABLES

### Chapter 2

Table 1. Summary of precipitation collector locations .....	12
Table 2. Precipitation VWA major ion concentrations .....	20
Table 3. Seawater major ion regression analysis .....	22
Table 4. Principal component analysis loading matrix .....	23
Table 5. Regression analysis of rainfall rates vs. bulk deposition .....	30

### Chapter 3

Table 1. Precipitation VWA stable isotope composition .....	58
Table 2. Local meteoric water line regression analysis.....	65
Table 3. Amount effect regression analysis.....	67
Table 4. Stable isotope composition of Ka‘ala fog samples.....	81

### Chapter 4

Table 1. Study site equipment and characteristic table .....	96
Table 2. Summary of water budget model results .....	116

## LIST OF FIGURES

### Chapter 2

Figure 1. Study area map with 1000 mm rainfall isohyets .....	13
Figure 2. Interpolated precipitation VWA major ion maps.....	21
Figure 3. Time series of bulk precipitation $\text{Na}^+$ concentrations .....	26
Figure 4. Major ions relative to seawater ratios in bulk precipitation.....	27
Figure 5. Calcium marine enrichment factor map .....	31
Figure 6. Time series of bulk precipitation $\text{Ca}^{2+}$ concentrations .....	32
Figure 7. Potassium enrichment factor and bulk deposition maps .....	35
Figure 8. Time series of bulk precipitation $\text{Mg}^{2+}$ and $\text{SO}_4^{2-}$ concentrations ....	38

### Chapter 3

Figure 1. Study area map with 1000 mm rainfall isohyets .....	50
Figure 2. Perennial high elevation spring along Mount Ka‘ala Road.....	56
Figure 3. Bulk precipitation collector design .....	57
Figure 4. Precipitation VWA $\delta^{18}\text{O}$ (‰) map.....	62
Figure 5. Time series of precipitation $\delta^{18}\text{O}$ composition .....	63
Figure 6. Regional Local meteoric water lines .....	64
Figure 7. Seasonal local meteoric water lines for O‘ahu.....	66
Figure 8. Precipitation VWA $\delta^{18}\text{O}$ -elevation lapse rates.....	68
Figure 9. Precipitation VWA $\delta^2\text{H}$ -excess (‰) map.....	69
Figure 10. Precipitation VWA $\delta^2\text{H}$ -excess plotted against elevation .....	70
Figure 11. Storm correction of leeward Ko‘olau $\delta^{18}\text{O}$ -elevation lapse rates....	75
Figure 12. Modeled $\delta^2\text{H}$ -excess vs. humidity, temperature, and rainout .....	76
Figure 13. Ka‘ala precipitation and spring chemistry time series.....	79
Figure 14. Ka‘ala summit rainfall-spring-fog mixing model analysis .....	80

### Chapter 4

Figure 1. Map of soil and meteorological data collection sites .....	92
Figure 2. Uluakupu study site .....	93
Figure 3. Lower Manana study site .....	94

Figure 4. Upper Manana study site .....	95
Figure 5. Uluakupu soil water retention curves .....	107
Figure 6. Soil water column height calculation diagram.....	108
Figure 7. Upper Manana time series of soil tension and potential gradient ....	112
Figure 8. Lower Manana time series of soil tension and potential gradient.....	113
Figure 9. Upper Manana water budget time series .....	114
Figure 10. Lower Manana water budget time series .....	115
Figure 11. Time series of $\delta^{18}\text{O}$ of precipitation and meteoric water lines.....	117
Figure 12. Upper Manana soil moisture vs. precipitation analysis .....	123
Figure 13. Lower Manana soil moisture vs. precipitation analysis.....	124
Figure 14. Regression analysis of infiltration vs. precipitation .....	125

## CHAPTER 1: INTRODUCTION

### 1. Relevance

This dissertation is essentially a study of the inorganic chemistry of rainfall on the Island of O‘ahu, Hawai‘i. Rainfall is the primary source of groundwater recharge on O‘ahu, and groundwater supplies more than 90% of the island’s freshwater needs (Gingerich & Oki, 2000; Hawaii, 2019; Nichols, Shade, & Hunt, Jr., 1997). Many other Pacific Island Communities (PIC) are similarly dependent on groundwater (Sharan, Lal, & Datta, 2021). This resource is limited, and vulnerable. Many PICs struggle with freshwater supplies due to limited rainfall, contamination from saltwater intrusion (SWI) or other prior human activities. For example, on Wake Island US military activity has created multiple groundwater contamination hazards from fuels, polychlorinated biphenyl (PCB), and per- and polyfluoroalkyl substances (PFAS) (Engineering-Science, 1984). Similarly, on Kwajalein, US military activity has contaminated much of the limited, shallow, unconfined aquifers with fuel and solvents (Hunt, 1996). The United States Environmental Protection Agency (US EPA) established “Superfund” sites on Guam and Saipan to remediate groundwater contamination, which has cost US taxpayers millions of dollars, and only partially addressed the issues (US EPA, 2023a; US EPA, 2023b). On O‘ahu, as recently as 2021, fuel contamination of groundwater from the Red Hill Fuel Storage Facility impacted more than 90,000 residents and forced the US Department of Defense to divert critical funds and labor away from operational requirements to address the contamination (US EPA, 2023c). These and many other cases demonstrate the vulnerability of groundwater resources in the Pacific and highlight some of the costs associated with mismanagement. Sadly, history has shown that without deliberate, careful management, groundwater resources are likely to be tarnished, and the most societally vulnerable will bear the worst of the consequences.

O‘ahu exemplifies the water resource challenges facing PICs in several respects. It is unlikely that any other location in the world offers such a compact blend of ecohydrological diversity and climactic variability, while housing one of the world’s most prolific and

strategically important military-industrial hubs. These dynamics will intensify in the future. Urbanization and population growth are projected to increase demand for freshwater on O‘ahu (Hawaii, 2019), while simultaneously encroaching on critical groundwater recharge areas. Long-term drying trends will further strain water resources (Frazier & Giambelluca, 2017). Pacific Islands are also highly sensitive to hydrologic fluctuations associated with climate change (Vernon et al., 2019). Coupled with the island’s accessibility and diverse physiography, these factors make O‘ahu an ideal location to carry out research aimed at solving PIC-focused water resource management challenges.

Analysis of inorganic chemistry in precipitation offers several advantageous tools that can be applied to water resource challenges in the Pacific. The inorganic constituents of precipitation include those ions and molecules that do not incorporate carbon into their chemical structure. Nitrogen-based compounds are commonly included in this category but are excluded from the analysis presented here. In this study, the term “inorganics” encompasses four major cations ( $\text{Ca}^{2+}$ ,  $\text{Mg}^{2+}$ ,  $\text{K}^+$ ,  $\text{Na}^+$ ), two major anions ( $\text{Cl}^-$  and  $\text{SO}_4^{2-}$ ), and two stable isotopes of water ( $^{18}\text{O}$  and  $^2\text{H}$ ). Analysis of the inorganic chemical constituents in precipitation can provide a chemical “fingerprint” for water, including information about season, moisture source, transport path, and precipitation elevation. These chemical markers can be connected to groundwater drawn from wells to establish connectivity between points of recharge, and points of withdrawal, and even to identify the periods when most recharge occurs. Knowing the origins, transport path, and timing of groundwater recharge is necessary to ensure sustainable replenishment. Since these chemical constituents are ubiquitous in nature, and since some are biologically conservative, they offer an economical, universally available, and simple option to address many important water resource challenges.

## 2. Dissertation Overview

This research was carried out in three parts, each exploring one facet of precipitation inorganic chemistry. Precipitation was sampled at 20 locations across the Island of O‘ahu approximately quarterly between December 2018 and August 2021, and integrated with similar,

already-existing O‘ahu data to create the most spatially and topographically diverse precipitation collector network on O‘ahu to date. In the first study, we examined the sources and evolution of six major ions in O‘ahu’s rainfall:  $\text{Na}^+$ ,  $\text{Cl}^-$ ,  $\text{Ca}^{2+}$ ,  $\text{K}^+$ ,  $\text{Mg}^{2+}$ ,  $\text{SO}_4^{2-}$ . Ocean sea spray emerged as the dominant driver of precipitation inorganic chemistry, with marine sea salt aerosols constituting over 90% of the total ion load in rainfall. The study also unveiled the influence of diverse weather patterns and nutrient sources impacting precipitation chemistry, including long range atmospheric transport of Asian continental dust, local sedimentary deposits, and anthropogenic contributions from agricultural activity.

In the second study we examined the controls, and influences on, the amounts of  $^{18}\text{O}$  and  $^2\text{H}$  in rainfall, with a particular focus on the extent to which elevation impacts stable isotope composition. The findings from this study revealed strong influences on  $^{18}\text{O}$  and  $^2\text{H}$  composition from geographical location, season, and precipitation source. While altitude and isotopic composition exhibited strong correlations along specific elevation transects, microclimate effects prevented extrapolation to broader regions of the island. Notably, the findings from this study suggest that  $^2\text{H}$ -excess may be a reliable proxy for precipitation elevation in groundwater tracer studies. Analysis of water samples from a high-elevation spring near Mount Ka‘ala’s summit indicate that fog could constitute up to 45% of total groundwater recharge at the summit. The findings from this study cumulatively point to strong, intricate connections between O‘ahu’s microclimates and the isotopic composition of rainfall.

In the last study, we explored the chemical evolution of rainfall during the process of soil infiltration. This study introduces a method to investigate how factors like soil moisture, soil water potential, precipitation, temperature, and humidity affect the stable isotope composition of precipitation during infiltration. To evaluate this method, we present and interpret soil tension, soil moisture, water chemistry, and atmospheric data from three sites in a montane subtropical forest on O‘ahu. The results indicate the method developed can produce reasonable estimates of infiltration which may be used to semi-quantitatively weight precipitation chemistry by infiltration amount. Our findings also indicate a chemical partitioning of soil water, with

precipitation following dry periods that effectively replenish upper soil capillary water until field capacity is reached, and subsequent rainfall dominating deep soil water chemistry.

The findings from these three complimentary studies reveal many important meteorological and physiographic dynamics that impact precipitation inorganic chemistry on O'ahu. They help to establish a baseline from which to assess future fluctuations in precipitation chemistry, and they open several avenues for further research. Notably, the strong influence exerted by microclimates and precipitation source on the composition of rainfall highlights a need for more spatially diverse, event-based precipitation sampling in connection with basic meteorological data collection. Fog sampling in both the Ko‘olau and Wai‘anae Ranges is also warranted. The soil tension, soil moisture, water chemistry, and atmospheric data presented in the third study indicate further work needs to be done to understand the chemical changes in precipitation during the process of infiltration. In sum, the findings from these three studies highlight the importance of understanding the source and evolution of inorganic water chemistry, and of developing methodologies to quantify these changes through the hydrologic cycle, which are important preliminary steps in utilizing natural geochemical tracers to elucidate groundwater flow paths and recharge processes on O'ahu.

### 3. Chapter 1 References

- Engineering-Science. (1984). *Installation Restoration Program Phase 1: Records Search Wake Island Airfield; A report prepared for United States Air Force AFESC/DEV and HQ PACAF/DEEV*. Atlanta, GA. Retrieved from <https://apps.dtic.mil/sti/tr/pdf/ADA147764.pdf>
- Frazier, A., & Giambelluca, T. (2017). Spatial trend analysis of Hawaiian rainfall from 1920 to 2012. *International Journal of Climatology*, 37(5), 2522–2531.  
doi:<https://doi.org/10.1002/joc.4862>
- Gingerich, S., & Oki, D. (2000). *Groundwater in Hawai‘i*. U.S. Geological Survey.
- Hawaii, S. o. (2019). *Water Resource Protection Plan 2019 Update: Report prepared by Townscape Inc. for the State of Hawai‘i, Commission on Water Resource Management*.
- Hunt, C. (1996). *Ground-water resources and contamination at Kwajalein Island, Republic of the Marshall Islands, 1990-91*. Map, U.S. Department of the Interior, U.S. Geological Survey. Retrieved from <https://pubs.usgs.gov/publication/wri944248>
- Nichols, W. D., Shade, P. J., & Hunt, Jr., C. D. (1997). *Summary of the Oahu, Hawaii, regional aquifer-system analysis*. U.S. Geological Survey Professional Paper 1412-A. Retrieved from <https://pubs.usgs.gov/pp/1412a/report.pdf>
- Sharan, A., Lal, A., & Datta, B. (2021). A review of groundwater sustainability crisis in the Pacific Island countries: Challenges and solutions. *Journal of Hydrology*, 603.  
doi:<https://doi.org/10.1016/j.jhydrol.2021.127165>
- US EPA. (2023a). *Superfund Site: PCB Warehouse Garapan, MP*. Retrieved from epa.gov: <https://cumulis.epa.gov/supercpad/cursites/csitiinfo.cfm?id=0902806>
- US EPA. (2023b). *Superfund Site: Ordot Landfill Agana, GU*. Retrieved from epa.gov: <https://cumulis.epa.gov/supercpad/cursites/csitiinfo.cfm?id=0902814>
- US EPA. (2023c). *About Red Hill Fuel Releases*. Retrieved from epa.gov: <https://www.epa.gov/red-hill/about-red-hill-fuel-releases>
- Vernon, S., Mouchet, M., Govaerts, R., Haevermans, T., & Pellens, R. (2019). Vulnerability to Climate Change of Islands Worldwide and its Impacts on the Tree of Life. *Scientific Reports*, 9(1), 14471. doi:<https://doi.org/10.1038/s41598-019-51107-x>

CHAPTER 2: UNDERSTANDING THE ORIGINS OF AND INFLUENCES ON  
PRECIPITATION MAJOR ION CHEMISTRY ON THE ISLAND OF O‘AHU, HAWAI‘I

Published as: Brennis, T., Lautze, N., Whitter, R., Giuseppe, T., & Thomas, D. (2023).  
Understanding the origins of and influences on precipitation major ion chemistry on the Island of  
O‘ahu, Hawai‘i. *Environmental Monitoring and Assessment*, 195(11). doi:  
<https://doi.org/10.1007/s10661-023-11887-2>

## CHAPTER 2 ABSTRACT

Precipitation is the primary groundwater source for the Island of O‘ahu, Hawai‘i, USA, and is an important source of terrestrial nutrients. Since Pacific Islands are particularly vulnerable to the impacts of climate change, they are important venues for studying the controls on and fluctuations in precipitation chemistry. Spatial variations in some of the dissolved rainfall ions can also be of value as natural geochemical tracers in examining surface and groundwater flow. This study collected and chemically analyzed bulk precipitation from 20 sites across the Island of O‘ahu approximately quarterly between April 2018 and August 2021. The new precipitation chemistry data were integrated with previously published precipitation data to characterize major ion composition and examine the atmospheric processes controlling inorganic ion deposition. Linear regression and multivariate analysis were used to quantify the relationships among major ions and to assess the impacts of various environmental and meteorological factors on precipitation chemistry. Ordinary kriging, and inverse distance weighted interpolations were conducted to help visualize spatial variations in major ion deposition. The results clearly indicate that ocean sea spray is the primary driver of precipitation inorganic chemistry, with marine sea salt aerosols accounting for more than 90% of the measured ion load. However, they also show that various weather patterns and nutrient sources impact inorganic deposition. Most notably, upper atmospheric transport of Asian continental dust during Hawaiian wet seasons,  $\text{Ca}^{2+}$  from local sedimentary deposits, and anthropogenic  $\text{K}^+$  from agricultural activity appear to be substantial non-marine deposition sources. This study synthesizes data from multiple sources into the most spatially and topographically diverse precipitation collector network on O‘ahu to date. The findings from this effort help establish a baseline for assessing future fluctuations in inorganic ion deposition and lay important groundwork for examining connections between precipitation and groundwater chemistry within the study area.

## 1. Introduction

Precipitation chemistry is linked to environmental and atmospheric processes and as such has been the focus of much research over the last several decades (Keresztesi et al., 2020; Ghahremaninezhad et al., 2016; Shi et al., 2009; Pearson & Fisher 1971; Hutchinson 1954). Evaporated moisture is chemically pure H<sub>2</sub>O such that any additional chemical constituents in precipitation reflect its journey through the atmosphere (Lewis 1981; Xiao 2016; Mphepya et al., 2004). The analysis of precipitation chemistry not only reflects current atmospheric processes but also provides a baseline from which we can gauge future changes due to natural processes, climate change or anthropogenic activity.

Precipitation chemistry studies abound in scientific literature, but such Hawai‘i-focused research is sparser and predominantly focused on O and H isotopologues or as related to volcanic influences on the Island of Hawai‘i (Tachera et al., 2021; Scholl & Ingebritsen 1995; Harding & Miller 1982; Miller & Yoshinaga 1981). Precipitation chemistry studies on the more populous Hawaiian Islands have largely focused on using stable isotopologues of water to explore moisture cycling in the atmosphere, surface waters, and subsurface hydrogeology (Scholl et al., 2002; Dores et al., 2020; Booth et al., 2021; Torri et al., 2023; Glenn et al., 2013). In the greater Pacific region, precipitation chemistry studies have been an effective tool to isolate nutrient contributions from anthropogenic, marine, and terrestrial sources (Li et al., 2007; Lu et al., 2011) and to illuminate key atmospheric processes, such as atmospheric wind regimes (Darzi & Winchester 1982; Saltzman et al., 1986; Torri et al., 2023), and acid rain production (Satake & Yamane 1992; Scholl & Ingebritsen 1995; Lee et al., 2000). These and many other studies demonstrate the utility of assessing the relative abundances of chemical constituents in precipitation and stimulate a desire for more precipitation chemistry research in Hawai‘i.

This paper presents inorganic ion data from bulk precipitation samples collected at 20 sites in and around the Pearl Harbor Aquifer, on the island of O‘ahu, Hawai‘i, USA, approximately quarterly between April 2018 and August 2021. We incorporate data from previous work (Dores et al., 2020) to increase sample point density (Table 1; Figure 1). Inorganic constituents in precipitation include ions that do not incorporate carbon into their chemical structure. While nitrogen-based compounds are commonly included in this category, we exclude them from the analysis due to source differentiation and biochemical reactivity uncertainties. In this study, the

term “inorganics” refers to four major cations ( $\text{Ca}^{2+}$ ,  $\text{Mg}^{2+}$ ,  $\text{K}^+$ ,  $\text{Na}^+$ ) and two major anions ( $\text{Cl}^-$  and  $\text{SO}_4^{2-}$ ).

The objective of this paper is to investigate inorganic ion deposition variability to characterize precipitation chemistry in and around the Pearl Harbor Aquifer and to consider the atmospheric processes impacting changes in compositions over our collection period. Results from this study will lay groundwork for analyses of future fluctuations in precipitation chemistry in response to evolving climate change processes occurring in the North Pacific basin.

There are three dominant sources of inorganic ions in precipitation: terrestrial (crustal) dust, marine sea-salt aerosols (SSA), and anthropogenic activity. Terrestrial dust particles accumulate in the atmosphere through weathering of rocks and aeolian transport (Pearson & Fisher 1971; Keresztesi et al., 2020); sea-salt aerosols are formed when bubbles produced by breaking waves rise to the surface and burst, releasing microscopic aerosol particles which are transported by air currents (Keene et al., 1986; Lewis & Schwartz 2004; Laskin et al., 2012); anthropogenic sources of atmospheric inorganic particulates include a great variety of activities with the most massive sources being combustion of fossil fuels, industrial processes, and agriculture (Keresztesi et al., 2020; Pearson & Fisher 1971; Lu et al., 2011). Hawai‘i is one of a relatively small number of regions in which volcanic aerosols can also make substantial, localized contributions to the ion content of rainfall (Tachera et al., 2021). Chemical constituents can be delivered to the surface through both wet and dry deposition (Manahan 2017); wet deposition occurs when chemically laden moisture precipitates and falls to the surface, where it can infiltrate the soil, be stored in the canopy, or be transported through runoff and throughfall processes; dry deposition occurs when suspended solid particulate matter settles on the surface. Dry deposition migrates along the ground surface through aeolian transport until it is arrested through either chemical, hydrologic, or physical means. Many processes can further impact both the speciation and concentration of inorganic ions in atmospheric moisture during transport, such as biogenic activity (Ghahremaninezhad et al., 2016; Norman et al., 1999; Nightingale et al., 2000), acid-base reactions (Laskin et al., 2012 and references therein), and hygroscopicity (Hu et al., 2011; Hu et al., 2010). A more detailed review of these and other processes is included in the supplemental materials (Appendix A, Tab A.1.). Simply put, no major ion is completely conservative, and the strength of the various processes that can change concentrations is not spatially or temporally uniform. Our aim in analyzing precipitation chemistry is, therefore, to

identify which sources and processes are the most significant and, and to understand how they are distributed within the study area.

## 2. Methods

### 2.1. Study Area

This study focuses on the Pearl Harbor Aquifer on the Island of O‘ahu, Hawai‘i, USA, the most populous, and third largest island of the Hawaiian Archipelago (Figure 1). O‘ahu lies between 21° and 22°N and 157° and 159°W. The island is composed of two extinct shield volcanoes, Wai‘anae and the younger Ko‘olau (Sherrod et al., 2021). The physiography of O‘ahu is severe and highly variable, characterized by thick rainforests, dramatic elevation gradients, broad, flat, semi-arid regions, and highly urbanized areas, all contained within a 1600 km<sup>2</sup> area (Sherrod et al., 2021).

The climate of O‘ahu is diverse: mean annual rainfall can vary from 500-6,500 mm/year over fewer than 30 km (Giambelluca et al., 2013). There are two distinct seasons: a wet season, from November to April, and a dry season, from May to October. The Hawaiian Islands sit in the path of the northeast trade winds, which are a circulation pattern associated with the North Pacific High (Giambelluca 1983). The trade winds persist more than 90% of the time during summer and approximately 50% during winter, leading to orographic precipitation at high elevations and windward areas (Noguchi 1979). A variety of weather patterns regulate the wet season climate, including cold fronts, upper-level lows, Kona lows, and subtropical storms (Longman et al., 2021). Although sporadic, these events can often individually supply more than half the annual rainfall in the drier areas of O‘ahu (Giambelluca 1983; Dores et al., 2020).

Twenty precipitation collectors were deployed throughout the study region to assess rainfall chemistry. Collectors were grouped into several zones, consisting of two to four collectors each. Sampling occurred approximately quarterly. Three collector groups were aimed at assessing elevation transects in key areas of the island. The first elevation transect was deployed along the Manana Ridge trail within the ‘Ewa Forest Reserve. It consisted of four collectors distributed between the trailhead (MT1) at 291m above mean sea level (amsl) and progressing up to the trail summit (MTS) at 806m amsl. The second elevation transect was deployed along Mount Ka‘ala Road and included four collectors progressing from 290m amsl (K1) up to the highest point on O‘ahu at 1212m amsl (KS). The third transect was deployed along the Schofield Plateau, with

four collectors distributed generally east-to-west connecting the Wai‘anae Range at Kolokole Pass (KK) to the foot of the Ko‘olau Range at the East Range Military Training Area (ER). Two collectors were deployed in southwest O‘ahu at Makakilo (M) and Ewa Beach (EB). Six collectors were deployed across southcentral O‘ahu: Aiea (A), Department of Health (DOH), Tripler Ridge Trail (TR), upper Waimanu Trail (WU), Pu‘u Wai‘awa (PW), and Mililani High School (MHS). Two collectors were only sampled once due to access constraints related to the COVID-19 pandemic (PW and MHS).

Table 1. Summary of precipitation collector locations sampled between March 2017 and August 2021 on O‘ahu, Hawai‘i, USA. Universal Transverse Mercator (UTM) zone is 4Q. Collectors with abbreviations beginning with “D” are from Dores et al., (2020).

Location Description	Abbreviation	n	Sample Window	UTM Easting	UTM Northing	Latitude	Longitude	Elevation (ft)	Elevation (m)
Kaala Gate 3	K1	11	12/18 - 4/21	586972	2382274	21.54118	-158.16010	953	290
Kaala Milepost 3	K2	9	7/19 - 4/21	586483	2381009	21.52963	-158.16487	1813	553
Kaala Culvert 49	K3	9	7/19 - 4/21	587231	2379032	21.51185	-158.15778	3051	930
Kaala Summit	KS	11	12/18 - 4/21	588665	2378648	21.50827	-158.14395	3975	1212
Manana Trailhead	MT1	15	6/17 - 4/21	610053	2370120	21.43008	-157.93803	956	291
Manana Trail 2	MT2	9	5/19 - 4/21	612935	2371499	21.44235	-157.91015	1483	452
Manana Trail 3	MT3	9	5/19 - 4/21	614505	2372110	21.44780	-157.89497	1801	549
Manana Trail Summit	MTS	7	7/19 - 4/21	616531	2373121	21.45677	-157.87535	2644	806
Ewa Beach	EB	12	7/19 - 5/21	600025	2357418	21.31592	-158.03555	24	7
Tripler Ridge	TR	12	7/19 - 4/21	617134	2363592	21.37067	-157.87018	1247	380
Mililani High School	MHS	1	10/19 - 1/20	602746	2372839	21.45508	-158.00838	727	222
Makakilo	M	10	10/19 - 5/21	594714	2363528	21.37140	-158.08641	1099	335
Puu Waiawa LZ	PW	1	10/19 - 1/20	614537	2374421	21.46866	-157.89450	2222	677
Kolekole Pass	KK	6	2/20 - 4/21	592178	2374817	21.47352	-158.11030	1827	557
Schofield Barracks	SB	4	2/20 - 1/21	593399	2376482	21.48850	-158.09840	1216	371
Wheeler Army Airfield	WAAF	5	2/20 - 4/21	599238	2375874	21.48269	-158.04210	886	270
East Range	ER	5	2/20 - 4/21	603095	2376433	21.48753	-158.00480	1004	306
Aiea	A	22	3/19 - 6/21	610581	2364529	21.37949	-157.93322	43	13
Dept. of Health	DOH	33	4/18 - 8/21	609043	2368670	21.41723	-157.94814	505	154
Waimanu Upper	WU	25	6/19 - 8/21	610936	2369743	21.42663	-157.92957	1083	330
Kamehameha Hwy	D1	2	10/17 - 3/18	621325	2373115	21.45642	-157.82910	20	6
Ewa Waimano	D3	5	4/17 - 7/18	610052	2370111	21.43000	-157.93810	955	291
Haleiwa Wells	D4	2	10/17 - 3/18	593961	2386342	21.57754	-158.09240	210	64
Hawai‘i Ag. Center	D6	5	4/17 - 7/18	628197	2362396	21.35911	-157.76360	364	111
HIG UH Mānoa	D7	5	4/17 - 7/18	622760	2355609	21.29818	-157.81650	72	22
Honolulu F.R.	D8	1	4/17 - 6/17	618954	2365377	21.38667	-157.85250	617	188
Ho‘omaluhia B.G.	D9	5	4/17 - 7/18	623417	2365502	21.38750	-157.80940	213	65
Kahalu‘u Ridge	D10	6	3/17 - 7/18	619516	2371546	21.44236	-157.84660	328	100
Ka‘ena Point	D11	4	4/17 - 7/18	577713	2383945	21.55667	-158.24940	36	11
Kunia III Wells	D12	2	10/17 - 3/18	601295	2366681	21.39953	-158.02280	322	98
Lyon Arboretum	D13	5	4/17 - 7/18	624183	2359481	21.33306	-157.80250	500	152
Mokuleia F.R.	D14	5	4/17 - 7/18	585481	2383615	21.55333	-158.17440	548	167
Mokuleia F.R. 2	D15	2	1/18 - 7/18	583448	2382783	21.54591	-158.19410	2001	610
Nanakuli F.R.	D16	1	4/17 - 6/17	589090	2365463	21.38917	-158.14060	167	51
Wahiawa B.G.	D17	5	4/17 - 7/18	602113	2378146	21.50306	-158.01420	1010	308
Waiāhole F.R.	D18	6	3/17 - 7/18	616351	2375013	21.47389	-157.87690	623	190
Waianae Kai	D19	4	4/17 - 3/18	587481	2375570	21.48056	-158.15560	860	262
Waimea Valley	D20	5	4/17 - 7/18	597896	2392848	21.63611	-158.05400	13	4

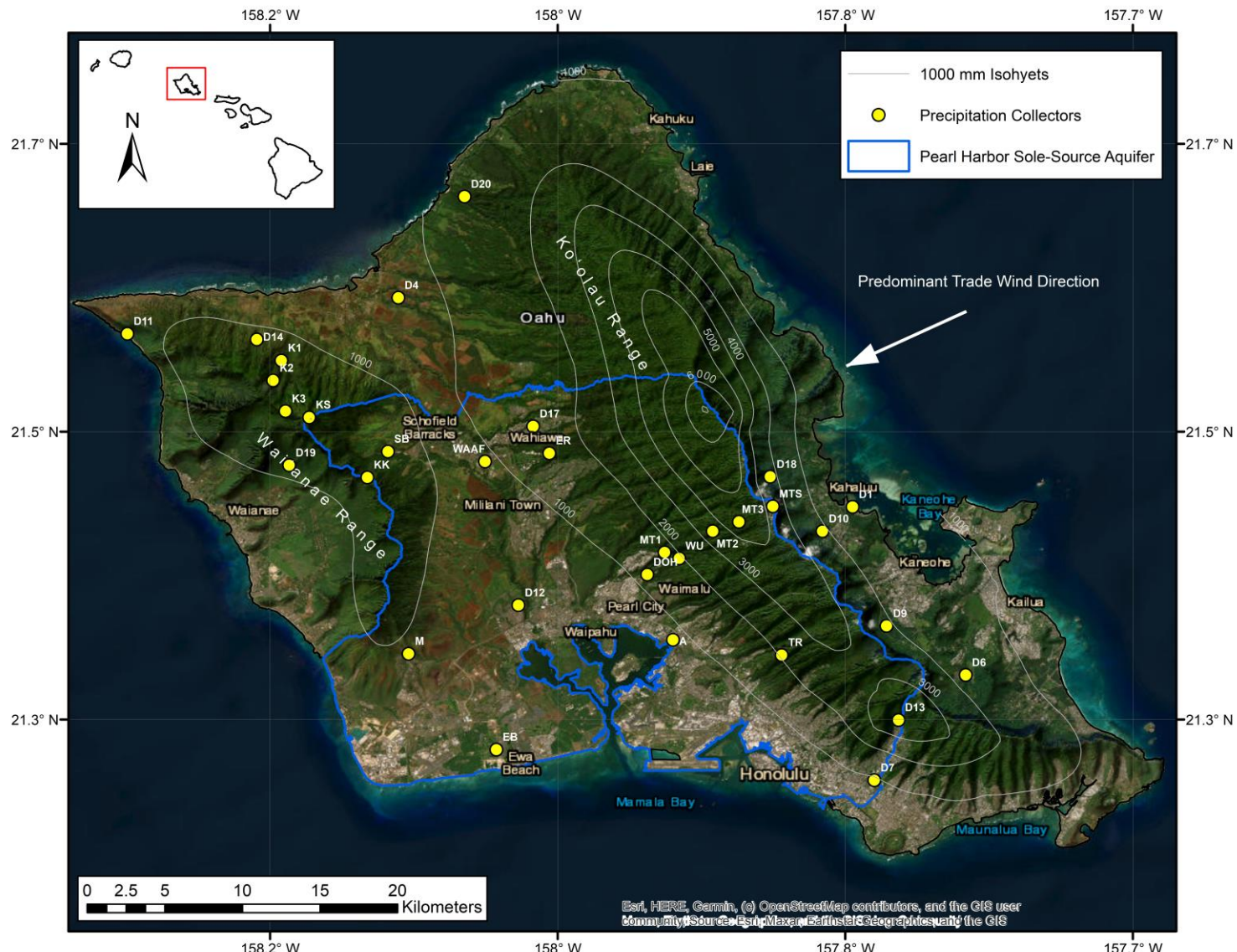


Figure 1. Map of the study area showing the locations of precipitation collectors and long-term average 1000 mm rainfall contours (isohyets). Collectors from Dores et al., (2020) are included and shown by the designation “D”.

## 2.2. Precipitation Collection

The precipitation collectors that were used for this study allowed us to assess bulk rainfall chemistry, which includes both wet and dry deposition. Most precipitation collectors were of the design used in previous studies (Fackrell et al., 2020, Scholl et al., 1995, 2002, Dores et al., 2020, Booth et al., 2021, Tachera et al., 2021). These collectors consisted of a 5-gal HPDE bucket with a 76- or 110-mm Buchner funnel affixed to the lid. Collectors had an O-ring-sealed spigot installed on the bottom for sample collection. The precipitation collectors were installed in the field on a base with three or four metal support legs for stabilization and ground clearance. A two-centimeter-thick layer of high-purity mineral oil in each collector prevented the evaporation of the collected precipitation. Collectors were covered with black polyethylene bags to reduce biologic productivity in the collectors, which could impact ion compositions. This method also protects against ultraviolet light damage to the plastic buckets. Samples were collected in a triple-deionized-rinsed 500 mL or 60 mL HPDE bottle. The sample bottles were filled completely, forming a convex meniscus at the container mouth to minimize air bubbles, and were refrigerated within six hours of collection to minimize chemical reactions.

## 2.3. Chemical Analysis

Preparation for chemical analyses involved collecting an aliquot of each sample from the HPDE field bottles using a syringe. Each sample aliquot was passed through a 0.45  $\mu\text{m}$  filter into a 40 mL vial with a septum or similar container. The vials were filled to the shoulder and then sealed with thin plastic film to minimize evaporation and atmospheric interactions. Samples were analyzed for concentration of major inorganic ions by the Water Resources Research Center laboratory at the University of Hawai‘i at Mānoa. Some samples were analyzed for pH and conductivity, but analysis of this sample subset is not included here. Major inorganic ions were determined using dual Dionex ICS-1100 Ion Chromatographs operated at ambient temperature following the US EPA Method 300.1 (Hautman & Munch 1997). Anions were separated on a Dionex IonPac AS14A column with 9 mM  $\text{Na}_2\text{CO}_3$  and 1 mM  $\text{NaHCO}_3$  eluent. Cations were separated on a Dionex IonPacCS12A column with 20 mM  $\text{CH}_3\text{SO}_3\text{H}$  eluent. The flow rate was 1.0 mL/min, with detection by suppressed conductivity. Duplicate sampling was conducted as part of routine lab procedures and indicates relative standard deviations of  $\pm 0.06 \text{ mg L}^{-1}$  ( $\text{F}^-$ ),  $\pm 0.26 \text{ mg L}^{-1}$  ( $\text{Cl}^-$ ),  $\pm 0.28 \text{ mg L}^{-1}$  ( $\text{Br}^-$ ),  $\pm 0.28 \text{ mg L}^{-1}$  ( $\text{SO}_4^{2-}$ ),  $\pm 0.06 \text{ mg L}^{-1}$  ( $\text{Na}^+$ ),  $\pm 0.15 \text{ mg L}^{-1}$

( $K^+$ ),  $\pm 0.08$  mg L<sup>-1</sup> ( $Mg^{2+}$ ), and  $\pm 0.14$  mg L<sup>-1</sup> ( $Ca^{2+}$ ). Sample precision from the results of similar previous research completed using the same facility and equipment indicate variances among duplicate sample pairs of  $\pm 0.03$  mg L<sup>-1</sup> ( $F^-$ ),  $\pm 1.01$  mg L<sup>-1</sup> ( $Cl^-$ ),  $\pm 0.03$  mg L<sup>-1</sup> ( $Br^-$ ),  $\pm 1.82$  mg L<sup>-1</sup> ( $SO_4^{2-}$ ),  $\pm 0.57$  mg L<sup>-1</sup> ( $Na^+$ ),  $\pm 0.05$  mg L<sup>-1</sup> ( $K^+$ ),  $\pm 0.32$  mg L<sup>-1</sup> ( $Mg^{2+}$ ), and  $\pm 0.66$  mg L<sup>-1</sup> ( $Ca^{2+}$ ) (Tachera et al., 2021). Field blanks were analyzed to assess sample contamination during sampling procedures, and from the practice of recycling of mineral oil. Analysis of the variance between field blanks and reference deionized water indicate potential contamination of up to 0.04 mg L<sup>-1</sup> ( $Cl^-$ ), 0.03 mg L<sup>-1</sup> ( $Na^+$ ), 0.01 mg L<sup>-1</sup> ( $K^+$ ), 0.01 mg L<sup>-1</sup> ( $Mg^{2+}$ ), and 0.07 mg L<sup>-1</sup> ( $Ca^{2+}$ ), which, at maximum, constituted less than 3% of the mean sample concentration for each species.

#### 2.4. Weather Trend Analysis

Seasonal precipitation trends were differentiated by analyzing weather data from the International Global Radiosonde Archive (IGRA; Durre et al., 2006; 2016), and observations from monthly weather summaries provided by the National Oceanic and Atmospheric Administration (NOAA/NWS 2023). The IGRA contains meteorological measurements from daily weather balloon launches at Līhue, on the Island of Kauai. These include elevation profiles of wind direction and speed for each launch. The IGRA data were sifted by selecting measurements below 2500m amsl, which is generally considered to be the maximum height of the trade wind regime over Hawai‘i (Cao et al., 2007). Days when the average wind direction below 2500m amsl was between 22° and 112° from North were categorized as trade wind days. These assignments were compared with observations in the monthly NOAA summaries. The NOAA summaries were also used to identify periods when cold fronts, Kona lows, upper-level lows, and tropical cyclones delivered rainfall to O‘ahu. The results from this analysis were overlaid on the precipitation chemistry data utilizing “rug” plots. (Wickam et al., 2016).

#### 2.5. Data Analysis

The overarching goal of our data analyses was to identify the contributions of terrestrial, marine SSA, and anthropogenic inputs to the bulk precipitation chemistry within and around the Pearl Harbor aquifer, and to observe how they vary in time and space. A review of relevant precipitation chemistry studies highlighted several methods which guided the analyses of the

data presented herein. We computed a rainfall volume-weighted-average (VWA) chemistry for each collector location and major ion to highlight the long-term spatial trends in the inorganic ion deposition (Lu et al., 2011; Keresztesi et al., 2020; Lee et al., 2000; Akpo et al., 2015; Scholl & Ingebritsen 1995). We calculated total and wet deposition to give a sense of the differing masses of chemical constituents entering the nutrient cycle in each sampling interval (Akpo et al., 2015; Lee et al., 2000). Wet deposition was calculated by multiplying the VWA ion concentration by long term average annual precipitation (Frazier & Giambelluca 2017). Total deposition was measured by multiplying each sample concentration by the measured precipitation and summing these values over a year. We used correlation analysis to quantify the relationships among different ions and to assess the impacts of various environmental and meteorological factors on precipitation chemistry (Li et al., 2007; Keene et al., 1986; Akpo et al., 2015; Keresztesi et al., 2020; Lu et al., 2011; Kroopnick 1977). We conducted principal component analysis (PCA) to parse out different sources of precipitation inorganic constituents (Li et al., 2007; Keresztesi et al., 2020; Lee et al., 2000; Shi et al., 2009). To assess crustal and anthropogenic inorganic sources more closely we completed a SSA correction, which is a procedure that differentiates chemical contributions from marine SSAs by correcting bulk chemistry based on a reference species (Scholl & Ingebritsen 1995; Satake & Yamane 1992; Saltzman et al., 1986; Keene et al., 1986; Akpo et al., 2015; Lee et al., 2000; Lu et al., 2011). Finally, we completed spatial interpolations via ordinary kriging and inverse distance weighting (power two) to aid in visualizing spatial variations of nutrient deposition (Scholl & Ingebritsen 1995; Pearson & Fisher 1971; Keresztesi et al., 2020). Several calculations warrant a more detailed explanation, as described in the sections below.

### 2.5.1. Sea Salt Aerosol Correction

The non-sea salt (NSS) fraction of each chemical species in precipitation was calculated by completing SSA corrections. This procedure removed the estimated SSA fraction of each species from bulk precipitation. The SSA fraction of a chemical species was calculated by selecting a reference species and multiplying the concentration of the reference species in the sample by the seawater ratio of that chemical species to the reference species, such that

$$C_{ssa} = \frac{C_{sw}}{R_{sw}} \cdot R_s \quad (1)$$

, where  $C_{ssa}$  is the sea salt fraction of each chemical species  $C$ ,  $C_{sw}/R_{sw}$  is the seawater ratio of each chemical species  $C$  to the reference species  $R$ , and  $R_s$  is the concentration of the reference species in the sample. The NSS fraction of the chemical species  $C_{nss}$  was calculated by subtracting the SSA fraction from the total concentration of that species,

$$C_{nss} = C_s - C_{ssa} \quad (2)$$

, where  $C_s$  is the concentration of each chemical species  $C$  in the sample. The accuracy of this procedure depends on two assumptions: to begin with, the reference species must be sourced solely from SSAs; additionally, there should not be significant fractionation of that species relative to the other sea salt constituents during mobilization, transport, and deposition (Keene et al., 1986).

### 2.5.2. Crustal & Marine Enrichment Factors

Crustal and marine enrichment factors (EF) were calculated to compare precipitation chemistry with the average compositions of seawater (Wilson 1975; Keene et al., 1986; Pilson 1998) and continental crust (Kring 1997) according to the expressions

$$EF_{sw} = \frac{\frac{C_s}{R_s}}{\frac{C_{sw}}{R_{sw}}} \quad (3)$$

$$EF_{cr} = \frac{\frac{C_s}{R_s}}{\frac{C_{cr}}{R_{cr}}} \quad (4)$$

, where  $C_s$  is the concentration of species  $C$  in the sample,  $R_s$  is the concentration of the reference species  $R$  in the sample,  $C_{sw}/R_{sw}$  is the average ratio of species  $C$  to reference species  $R$  in seawater, and  $C_{cr}/R_{cr}$  is the average ratio of species  $C$  to reference species  $R$  in the continental crust. The accuracy of marine and crustal EFs depend on the same assumptions as SSA corrections.

### 2.5.3. Regression Analysis

Regression analysis was used to determine the SSA origin for inorganic ions in precipitation (Keene et al., 1986; Khemani et al., 1985; Akpo et al., 2015). This procedure is based on the observation that, though the composition of ocean water varies across the globe, the relative ratios of inorganic ions in seawater are consistent (Keene et al., 1986; Lewis & Schwartz 2004; Table 3). If the regression coefficients of meteoric chemical ratios were not significantly

different from those of seawater (within the 95% confidence intervals), we assessed that both species originated primarily from SSAs (Keene et al., 1986). Regression analysis was also used to parse bulk deposition into dry and wet deposition following Pearson & Fisher (1971).

Following this work, wet deposition was assessed to be the most probable deposition mode if regression analysis of rainfall rates ( $\text{mm d}^{-1}$ ) vs. bulk deposition ( $\text{g ha}^{-1} \text{d}^{-1}$ ) produced  $p \leq 0.05$ ,  $r^2 \geq 0.5$ , and a positive slope. When these conditions were not met, dry deposition, or a combination of both dry and wet deposition, were assumed to be the dominant deposition modes.

#### 2.5.4. Principal Component Analysis

Principal component analysis (PCA) is a common statistical technique that can be used to simplify multivariate datasets (Abdi & Williams, 2010). The goal of PCA is to reduce the dimensionality of a dataset by analyzing the structure of the data and the interrelationships among variables. The principal components are displayed in a loading matrix. Each column in the loading matrix contains the eigenvector of each variable for a particular principal component. The total eigenvalue for that component is usually added as an additional row at the bottom of the loading matrix. The eigenvectors communicate the weight or loading each variable gives within that principal component. The eigenvalue, often called inertia, reflects the importance of that principal component in the overall dataset. The inertia of each component is usually displayed as a percentage of the total inertia of the dataset (the sum of all eigenvalues). The inertia of a component communicates the amount of variance within the dataset that is explained by that component. The principal components can be viewed as the primary sources of variability within the dataset. In studies of bulk precipitation chemistry, principal components are interpreted to be the principal sources of chemical constituents (Li et al., 2007; Keresztesi, et al., 2020; Lee et al., 2000; Shi et al., 2009).

### 3. Results & Discussion

The following consists of four sections grouped by major ions which contain results and discussion subsections.

#### 3.1. Sodium & Chloride

##### 3.1.1. Results

Sodium and  $\text{Cl}^-$  were the most abundant constituents in bulk precipitation, exceeding other ions by an order of magnitude in most samples. Volume-weighted average concentrations ranged from  $4.5 \pm 1.0 \text{ mg L}^{-1}$   $\text{Cl}^-$  and  $3.2 \pm 0.8 \text{ mg L}^{-1}$   $\text{Na}^+$  at Ka‘ala Summit to  $39.7 \pm 2.3 \text{ mg L}^{-1}$   $\text{Cl}^-$  and  $22.9 \pm 1.8 \text{ mg L}^{-1}$   $\text{Na}^+$  at Ka‘ena Point (Table 2; Figure 2). The highest sample concentrations of  $\text{Na}^+$  and  $\text{Cl}^-$ , excluding samples taken from the Ka‘ena Point collector (D11), were detected between 5/10/2019 and 7/11/2019 along the Manana Ridge transect at the two lowest-elevation collectors (290 m and 450 m amsl). Sample concentrations were  $60.8 \text{ mg L}^{-1}$   $\text{Cl}^-$  and  $40.8 \text{ mg L}^{-1}$   $\text{Cl}^-$  at MT1 and MT2, respectively. Sample contamination was ruled out due to proportional enrichment in those samples of both  $\text{SO}_4^{2-}$  and  $\text{Mg}^{2+}$  consistent with marine sea salt origin, and similar enrichment at other collectors in the vicinity.

Concentrations of  $\text{Na}^+$  and  $\text{Cl}^-$  were strongly correlated, indicating a predominantly marine SSA origin for these species. Reduced major axis (RMA) regression analysis of precipitation  $\text{Na}^+$  vs.  $\text{Cl}^-$  produced a slope of  $0.878 \pm 0.35$ , an intercept of  $10.101 \pm 11.31$ , a Spearman correlation coefficient of 0.99, and  $p < 0.01$  (Table 3). The results of the RMA regression are consistent with SSA origin (Keene et al., 1986). The principal component analysis further corroborates SSA origin for meteoric  $\text{Na}^+$  and  $\text{Cl}^-$ . The PCA loading matrix shows that approximately 90% of the variability in the major ions in precipitation is related to a parameter weighted heavily by  $\text{Na}^+$  and  $\text{Cl}^-$  concentrations (Table 4; Abdi & Williams 2010).

Table 2. Precipitation volume weighted average chemistry and uncertainty calculated from samples collected on O‘ahu, HI, USA between March 2017 and June 2021.

Precipitation Volume-Weighted Average Concentration (mg L <sup>-1</sup> )													
Location Description	Abbreviation	Cl <sup>-</sup>	ΔCl <sup>-</sup>	Na <sup>+</sup>	ΔNa <sup>+</sup>	Ca <sup>2+</sup>	ΔCa <sup>2+</sup>	K <sup>+</sup>	ΔK <sup>+</sup>	SO <sub>4</sub> <sup>2-</sup>	ΔSO <sub>4</sub> <sup>2-</sup>	Mg <sup>2+</sup>	ΔMg <sup>2+</sup>
Kaala Gate 3	K1	6.69	1.10	4.44	0.85	0.70	0.82	0.50	0.28	0.86	1.34	0.49	0.57
Kaala Milepost 3	K2	4.70	1.07	3.25	0.83	2.36	0.87	0.38	0.28	0.56	1.19	0.34	0.57
Kaala Culvert 49	K3	4.77	1.06	3.37	0.82	0.90	0.82	0.69	0.30	0.35	0.91	0.39	0.57
Kaala Summit	KS	4.48	1.03	3.16	0.79	0.50	0.81	0.27	0.25	0.60	1.26	0.32	0.57
Manana Trailhead	MT1	11.31	1.17	6.87	0.89	2.30	0.83	0.42	0.24	1.82	1.33	1.01	0.58
Manana Trail 2	MT2	12.34	1.18	7.46	0.90	1.03	0.82	0.36	0.25	1.80	1.30	0.93	0.58
Manana Trail 3	MT3	6.87	1.04	4.50	0.79	1.31	0.82	0.24	0.24	0.96	1.35	0.54	0.57
Manana Trail Summit	MTS	7.63	1.13	5.09	0.88	1.34	0.83	0.45	0.27	0.86	1.35	0.44	0.57
Ewa Beach	EB	5.50	1.21	3.53	0.93	5.08	1.13	0.26	0.27	0.93	1.29	0.50	0.58
Tripler Ridge	TR	10.25	1.18	6.33	0.91	1.25	0.82	0.40	0.26	1.46	1.30	0.63	0.57
Makakilo	M	7.85	1.24	5.09	0.97	2.27	0.90	0.36	0.28	1.85	1.36	0.57	0.58
Kolekole Pass	KK	7.02	1.15	3.40	0.84	3.98	0.91	1.06	0.39	0.88	1.25	0.94	0.58
Schofield Barracks	SB	6.26	1.29	4.04	1.00	2.64	0.97	0.84	0.44	0.77	1.06	0.57	0.59
Wheeler Army Airfield	WAAF	11.18	1.31	6.01	0.96	2.34	0.85	2.59	0.62	1.59	1.32	1.16	0.59
East Range	ER	10.53	1.30	5.99	0.98	2.43	0.86	0.51	0.31	1.23	1.35	0.68	0.58
Aiea	A	11.55	1.60	6.55	1.21	0.91	0.84	0.36	0.31	2.12	1.37	0.77	0.61
Dept. of Health	DOH	14.90	1.57	8.53	1.19	0.75	0.84	1.24	0.47	2.56	1.34	0.87	0.60
Waimanu Upper	WU	9.55	1.28	5.36	0.96	0.32	0.81	0.28	0.26	1.66	1.35	0.58	0.58
Kamehameha Hwy	D1	12.87	1.35	6.98	1.01	1.02	0.82	0.80	0.33	2.45	1.36	0.80	0.58
Haleiwa Wells	D4	16.70	1.96	9.59	1.49	3.42	0.98	4.86	1.01	2.11	1.39	1.62	0.69
Hawai‘i Ag. Center	D6	9.84	1.13	6.18	0.87	3.19	0.85	0.34	0.21	1.93	1.35	0.93	0.57
HIG UH Mānoa	D7	15.89	1.58	10.19	1.25	5.19	1.08	0.44	0.27	3.20	1.37	1.32	0.61
Ho‘omaluhia B.G.	D9	7.17	1.08	4.92	0.84	4.27	0.87	0.24	0.18	1.36	1.23	0.83	0.57
Kahalu‘u Ridge	D10	7.47	1.07	4.73	0.82	2.72	0.84	0.30	0.21	1.49	1.35	0.92	0.57
Ka‘ena Point	D11	39.70	2.33	22.93	1.77	5.65	1.03	1.37	0.43	7.02	1.45	2.96	0.73
Kunia III Wells	D12	10.10	1.63	5.55	1.21	4.07	1.09	5.47	1.15	3.16	1.41	1.30	0.67
Lyon Arboretum	D13	10.37	1.09	6.17	0.83	3.26	0.83	0.22	0.18	2.16	1.35	1.19	0.57
Mokuleia F.R.	D14	8.00	1.22	5.23	0.96	3.36	0.90	0.82	0.35	1.69	1.35	1.06	0.60
Wahiawa B.G.	D17	12.79	1.34	8.06	1.05	5.73	0.98	1.35	0.40	1.81	1.20	1.42	0.60
Waiāhole F.R.	D18	10.23	1.12	6.48	0.87	4.37	0.85	0.31	0.20	1.64	1.35	0.95	0.57
Waianae Kai	D19	10.24	1.33	6.13	1.02	5.73	1.03	1.39	0.45	2.53	1.36	1.07	0.60
Waimea Valley	D20	10.80	1.20	6.66	0.92	7.82	1.01	0.64	0.25	1.58	1.35	1.31	0.59

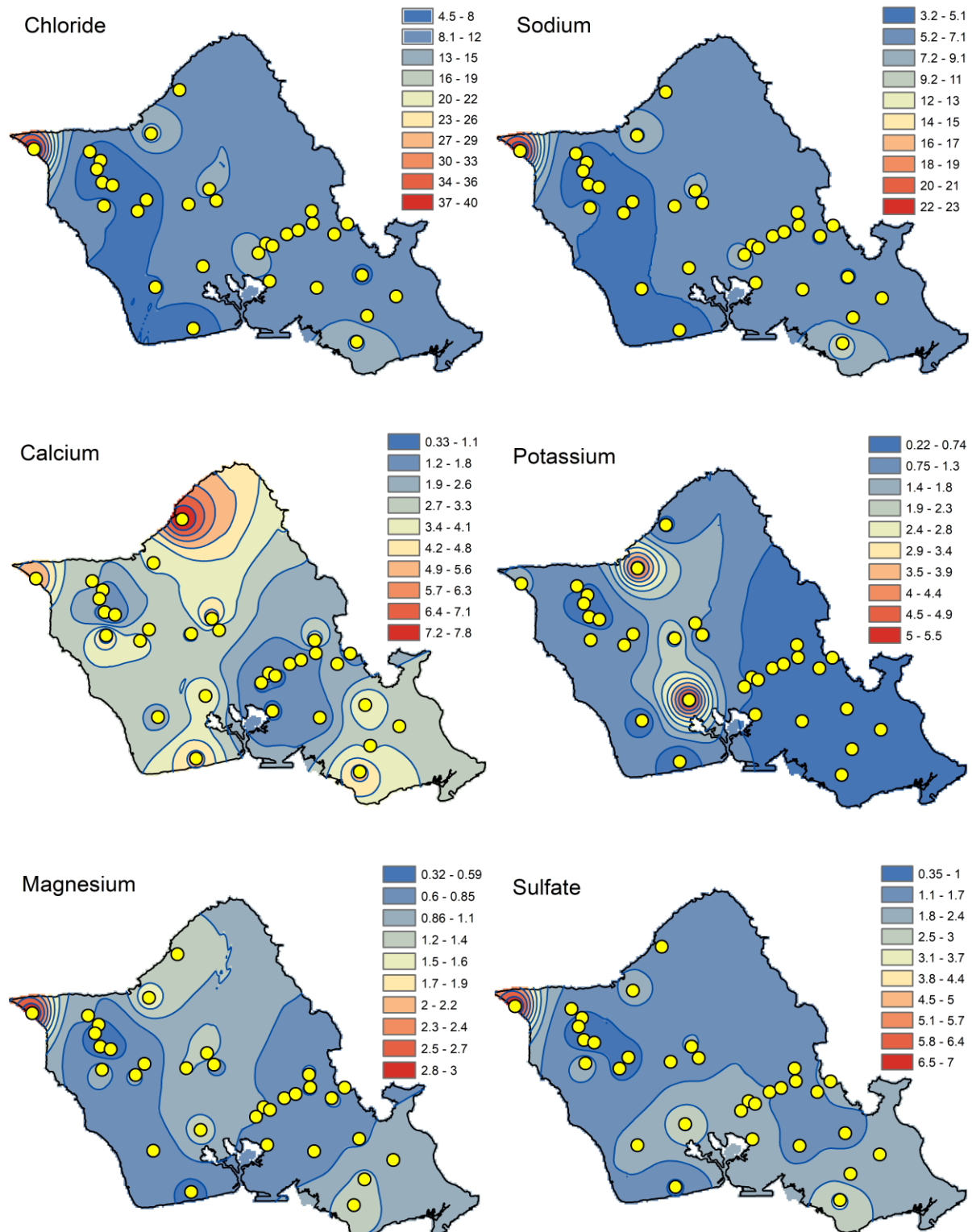


Figure 2. Interpolated precipitation volume-weighted average chemistry of six major ions on the island of O'ahu, HI, USA. Interpolation method was inverse distance weighted, power two. Coverages were interpolated from the precipitation collector locations represented by yellow circles. Data from Dores et al., (2020) is included. Units are mg L<sup>-1</sup>.

Table 3. Regression analysis of seawater (SW) and bulk precipitation major ion molar ratios. A reduced major axis (RMA) regression was used due to uncertainty in both variables. Ninety-five percent confidence intervals (CI) were calculated to assess agreement with the seawater ratios. Seawater molar ratios were taken from Pilson (1998). Shaded cells identify regression slopes and intercepts that fall within the 95% CI for the SW molar ratios, indicating predominantly sea salt aerosol origin. P-values for all regressions were less than 0.01.

Ions	Seawater Ratios	RMA Slope	RMA Intercept	Correlation Coefficient
Na/Cl	0.859	0.878 ± 0.35	10.101 ± 11.31	0.99
Mg/Cl	0.097	0.108 ± 0.01	2.595 ± 3.67	0.90
SO <sub>4</sub> /Cl	0.052	0.076 ± 0.01	-4.473 ± 3.64	0.79
Ca/Cl	0.019	0.331 ± 0.08	-40.955 ± 25.38	0.19
K/Cl	0.019	0.237 ± 0.04	-49.976 ± 11.31	0.29
Mg/Na	0.113	0.123 ± 0.01	1.351 ± 3.93	0.89
SO <sub>4</sub> /Na	0.060	0.086 ± 0.01	-5.345 ± 3.59	0.81
Ca/Na	0.022	0.377 ± 0.09	-44.764 ± 26.34	0.18
K/Na	0.022	0.270 ± 0.06	-52.703 ± 18.62	0.24
SO <sub>4</sub> /Mg	0.534	0.700 ± 0.10	-6.289 ± 3.85	0.79
Ca/Mg	0.195	3.061 ± 0.69	-48.899 ± 25.68	0.38
K/Mg	0.193	2.192 ± 0.50	-55.663 ± 18.46	0.37

Table 4. Rotation matrix displaying the results from principal component analysis completed on bulk precipitation chemistry. The principal components (PC) can be viewed as the primary sources of variability within the dataset. In studies of bulk precipitation chemistry, the principal components are interpreted to be the principal sources of chemical constituents (Li et al., 2007; Keresztesi et al., 2020; Lee et al., 2000; Shi et al., 2009).

	PC1	PC2	PC3	PC4	PC5	PC6
Chloride	-0.75	-0.03	0.09	0.65	-0.04	-0.07
Sulfate	-0.05	0.01	0.01	-0.16	-0.81	-0.56
Sodium	-0.65	-0.06	-0.17	-0.72	0.15	0.03
Potassium	-0.05	0.15	0.97	-0.18	0.07	-0.02
Magnesium	-0.07	0.07	0.04	-0.03	-0.56	0.82
Calcium	-0.05	0.98	-0.16	0.00	0.05	-0.05
% of Total Variance Explained	91.14	5.50	2.65	0.53	0.11	0.06

### 3.1.2 Discussion

Another important control on  $\text{Na}^+$  deposition may be related to atmospheric dust: many of our samples showed an apparent excess of  $\text{Na}^+$  relative to the seawater molar sodium-chloride ratio of 0.86. Long-range atmospheric dust transport is a reasonable explanation for this excess  $\text{Na}^+$ , suggesting  $\text{Cl}^-$  is a more appropriate reference species to use in sea salt corrections. However, due to the possibility of  $\text{Cl}^-$  depletion from SSAs through reaction with weak organic and inorganic acids (Laskin et al., 2012), it was not possible to differentiate the apparent enrichment in  $\text{Na}^+$  from the depletion of  $\text{Cl}^-$  without comparing  $\text{Na}^+$  and  $\text{Cl}^-$  concentrations to other major SSA constituents. Sulfate and  $\text{Mg}^{2+}$  were therefore plotted against  $\text{Cl}^-$  and  $\text{Na}^+$  to assess whether the apparent  $\text{Na}^+$  excess was due to depletion of  $\text{Cl}^-$  or a true NSS  $\text{Na}^+$  source. Chloride fractionation would manifest as a regression slope greater than the magnesium- and sulfate-to-chloride seawater ratio slopes when compared to the magnesium- and sulfate-to-sodium seawater ratio slopes. Sodium enrichment from an atmospheric source would manifest as a regression slope generally parallel to the seawater ratio slopes but with a negative y-intercept. Results from this analysis (Figure 4) indicate  $\text{Cl}^-$  depletion was negligible. The reduced major axis regression slopes on Figures 4B and 4C ( $\text{Mg}^{2+}$  vs.  $\text{Cl}^-$  and  $\text{Mg}^{2+}$  vs.  $\text{Na}^+$ ) vary indistinguishably from the seawater ratios, as do those on Figures 4D and 4E ( $\text{SO}_4^{2-}$  vs.  $\text{Cl}^-$  and  $\text{SO}_4^{2-}$  vs.  $\text{Na}^+$ ). Samples with excess  $\text{Na}^+$  also plotted more consistently below the seawater ratio slopes which suggests a NSS  $\text{Na}^+$  source, though uncertainties were too great to definitively say either species produced a negative y-intercept (Table 3). Chloride was therefore selected as the reference species for the SSA correction.

Sea salt aerosol correction results corroborate a non-marine source of  $\text{Na}^+$ . The propagated error for NSS  $\text{Na}^+$  was  $\pm 0.80 \text{ mg L}^{-1}$ . This uncertainty was large due to the compounding effect of instrumental uncertainty for both  $\text{Cl}^-$  ( $\pm 1.01 \text{ mg L}^{-1}$ ) and  $\text{Na}^+$  ( $\pm 0.66 \text{ mg L}^{-1}$ ). Even with the higher uncertainty, there was a strong trend in NSS  $\text{Na}^+$  across most collectors throughout the dataset. Excluding samples from two collectors where there were overcorrections producing negative NSS  $\text{Na}^+$  values (WAAF and KK), NSS  $\text{Na}^+$  concentrations for all collectors and all samples were within a narrow range of  $1.15 \text{ mg L}^{-1}$ . This uniformity is striking and necessitates a NSS  $\text{Na}^+$  source that is evenly distributed across the entire sample area, with atmospheric dust being a more plausible mechanism than local dust transport, which would be expected to be more spatially variable. Analysis of wind patterns from International

Global Radiosonde Archive (IGRA) data taken at Līhue (Durre et al., 2006; 2016), and monthly weather summaries provided by the National Oceanic and Atmospheric Administration (NOAA/NWS 2023), show an inverse relationship between trade winds and NSS Na<sup>+</sup> deposition (Figure 3). During dry seasons, when trade winds were more consistent, NSS Na<sup>+</sup> deposition was low. During wet seasons, when the trades were inconsistent and disturbance-based weather events were more frequent, NSS Na<sup>+</sup> was consistently elevated. These elevated NSS Na<sup>+</sup> deposition periods coincided with seasonal shifts in atmospheric wind source trajectories to more remote, north-northwesterly locations and higher-altitudes (Torri et al., 2023), suggesting Asian continental dust as a likely source of NSS Na<sup>+</sup>.

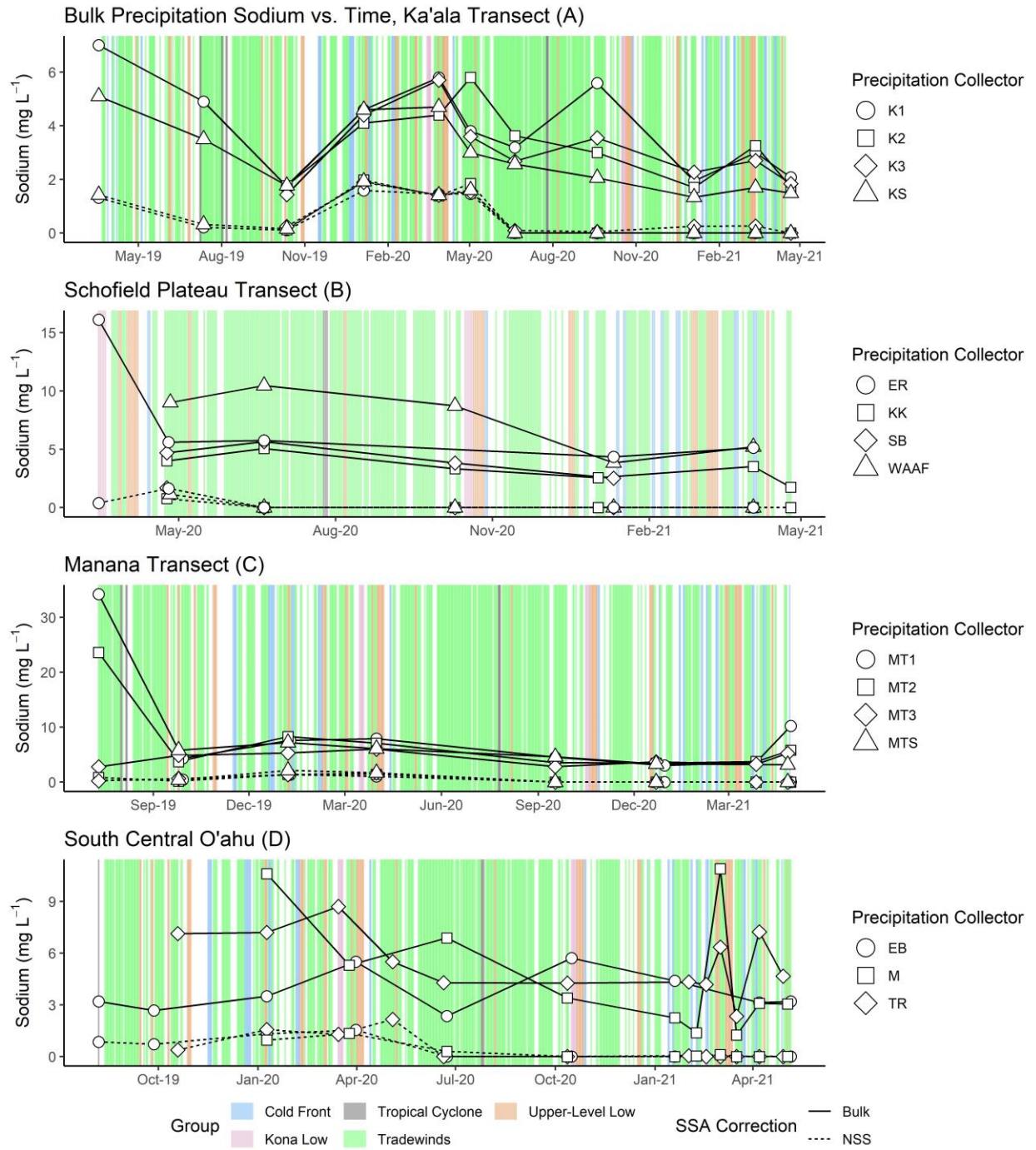


Figure 3. Time series of bulk precipitation  $\text{Na}^+$  concentrations taken on O'ahu, HI, USA. Ka'ala Transect (A), Schofield Plateau Transect (B), Manana Transect (C), and South-Central O'ahu collectors (D). Non-sea salt (NSS) contributions are displayed in dotted lines. Non-sea salt uncertainty was  $\pm 0.80 \text{ mg L}^{-1}$ . Weather trend data derived from International Global Radiosonde Archive (IGRA) weather balloon launches at Lihue, Kauai (Durre et al., 2006; 2016), and from monthly weather summaries provided by the National Oceanic and Atmospheric Administration (NOAA/NWS 2023) are shown in the background.

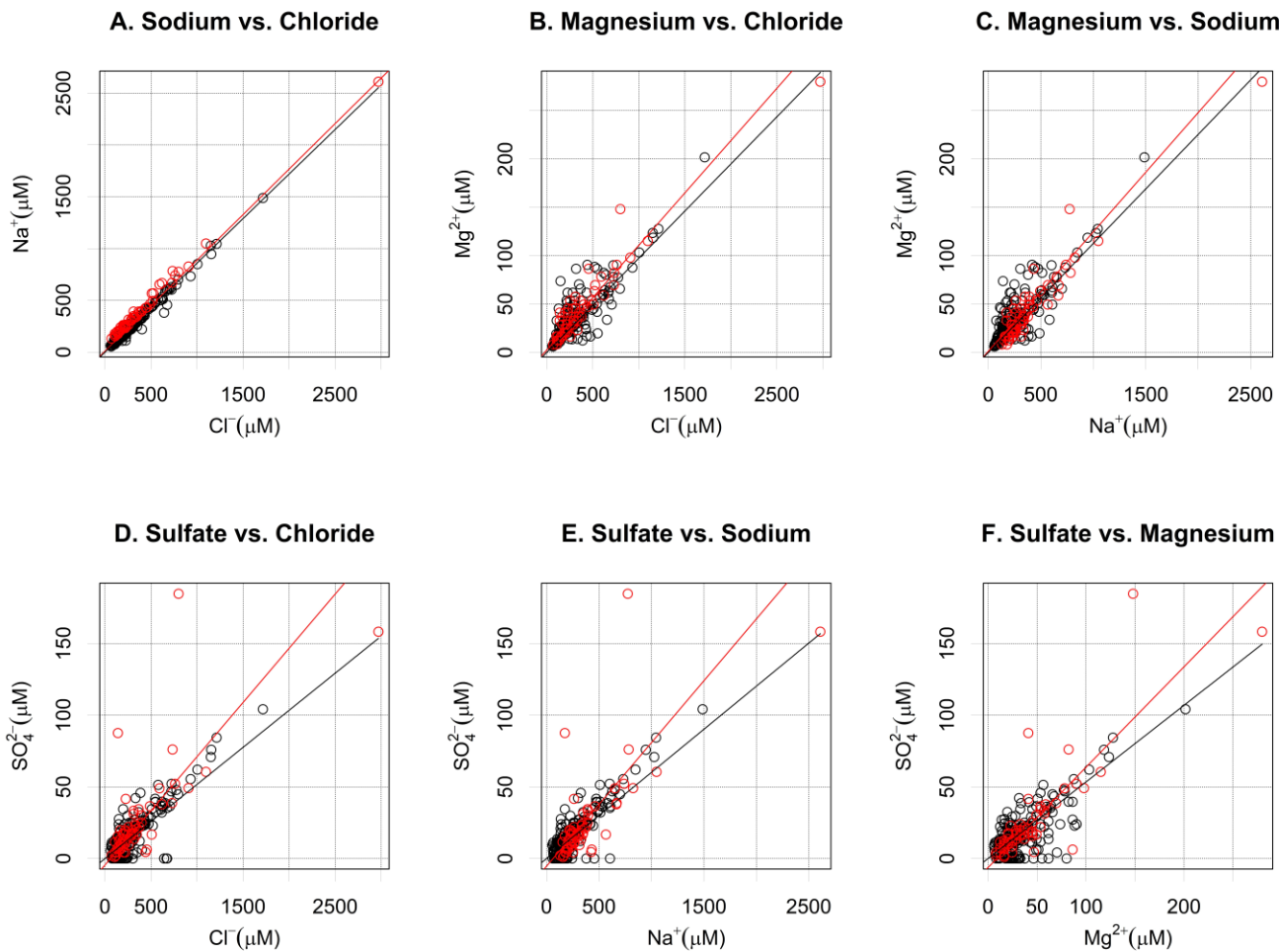


Figure 4. Plots of major sea-salt constituents ( $\text{Cl}^-$ ,  $\text{Na}^+$ ,  $\text{Mg}^{2+}$ , and  $\text{SO}_4^{2-}$ ) relative to seawater ratios in bulk precipitation from O'ahu, HI, USA. The red line displays reduced major axis regression fits for each plot. The black lines display the seawater ratios for each major ion pair (Pilson 1998). Red points display samples with  $>40 \mu\text{mol L}^{-1}$   $\text{Na}^+$  excess relative to the chloride:sodium seawater ratio.

## 3.2. Calcium

### 3.2.1. Results

Calcium was the third most abundant constituent in bulk precipitation, below chloride and sodium. Volume-weighted average  $\text{Ca}^{2+}$  and propagated uncertainty ranged from  $0.32 \pm 0.81 \text{ mg L}^{-1} \text{ Ca}^{2+}$  at Waimano Trail (WU) to  $7.82 \pm 1.00 \text{ mg L}^{-1} \text{ Ca}^{2+}$  at Waimea Valley (D20) (Table 2). Individual sample uncertainty based on duplicates was  $0.66 \text{ mg L}^{-1} \text{ Ca}^{2+}$  (Tachera et al., 2021). The highest single sample concentration was  $39.74 \text{ mg L}^{-1}$  collected at Ewa Beach between 6/23/2020 and 10/16/2020. Results from the SSA correction indicate most precipitation  $\text{Ca}^{2+}$  was non-marine; the propagated NSS uncertainty was low, at  $\pm 0.66 \text{ mg L}^{-1} \text{ NSS Ca}^{2+}$ .

### 3.2.2. Discussion

Bulk precipitation chemistry data suggest at least one NSS  $\text{Ca}^{2+}$  source. Calcium in precipitation is often attributed to crustal dust transport (Niu et al., 2014; Szép et al., 2018; Xiao 2016; Zhang et al., 2003; Loyer-Pilot et al., 1986; Brahney et al., 2013). Long-range transport is possible; however, a more spatially uniform distribution of NSS  $\text{Ca}^{2+}$  would be expected across all precipitation collectors, as was observed with NSS  $\text{Na}^+$ . This trend was not apparent in  $\text{Ca}^{2+}$  concentrations, which were generally higher in coastal areas and lower at high elevations (Figure 2). Regression analysis of rainfall rates ( $\text{mm d}^{-1}$ ) vs.  $\text{Ca}^{2+}$  bulk deposition ( $\text{g ha}^{-1} \text{ d}^{-1}$ ) suggests that  $\text{Ca}^{2+}$  is delivered primarily through dry deposition, though there were no obvious correlations to weather or location (Table 5).

There are two probable local sources of NSS  $\text{Ca}^{2+}$ . The first is O‘ahu’s coastal alluvial deposits, mainly composed of calcite-cemented shallow marine sediments (Sherrod et al., 2021; Fletcher et al., 2008). Volume-weighted average  $\text{Ca}^{2+}$  exceeded  $5 \text{ mg L}^{-1}$  at five locations that resided on or close to such deposits: Ka‘ena Point (D11), the University of Hawai‘i at Mānoa (UHM) campus (D7), Wai‘anae Kai (D19), Waimea Valley (D20) and Ewa Beach (EB) (Figure 5). Marine enrichment factors of  $\text{Ca}^{2+}$  were also elevated near these deposits (Figure 5). The Ewa Beach collector is notable in that it also resided within a high-growth suburban area where there was extensive vegetation stripping and excavation during the study period. Such activity has been connected with increased mineral dust transport elsewhere (Neff et al., 2005; Brahney et al., 2013). The other probable source for NSS  $\text{Ca}^{2+}$  is cement production operations, which also tend to be concentrated in O‘ahu’s southern coastal plains. Dominant wind direction links these

potential calcite sources with areas showing elevated NSS Ca<sup>2+</sup> deposition. Weather data show that Ca<sup>2+</sup> deposition generally increased during periods of persistent trade winds (Figure 6). The principal component analysis also implicates calcium-rich dust transport. Principal component 2 accounted for approximately 6% of the variability in the major ions and was strongly weighted by Ca<sup>2+</sup> concentrations (Table 4; Abdi & Williams 2010). These spatiotemporal trends indicate that mineral dust transport from local alluvial deposits and cement production activity are the two most probable NSS sources for Ca<sup>2+</sup> in bulk precipitation chemistry.

Table 5. Regression analysis of rainfall rates ( $\text{mm d}^{-1}$ ) vs. bulk deposition ( $\text{g ha}^{-1} \text{d}^{-1}$ ). Cells colored blue are those that met three conditions:  $p \leq 0.05$ ,  $r^2 \geq 0.5$ , and positive slope, indicating wet deposition as the most probable deposition mode. Red colored cells represent collectors where these conditions were not met, and thus where dry deposition, or a combination of both dry and wet deposition, were assumed to be the dominant deposition modes (Pearson & Fisher 1971).

	Ion	Chloride				Sodium				Calcium				Sulfate				Magnesium				Potassium			
Collector	n	b	m	r	p	b	m	r	p	b	m	r	p	b	m	r	p	b	m	r	p	b	m	r	p
K1	11	1.00	0.01	0.77	0.00	1.38	0.02	0.70	0.00	1.44	0.09	0.47	0.02	2.25	0.06	0.42	0.03	0.67	0.17	0.84	0.00	0.83	0.17	0.37	0.05
K2	9	0.72	0.02	0.80	0.00	1.00	0.02	0.66	0.01	2.68	0.01	0.37	0.08	2.62	0.07	0.40	0.07	0.67	0.17	0.84	0.00	3.77	0.01	0.00	0.94
K3	9	1.50	0.01	0.76	0.00	1.87	0.02	0.62	0.01	0.95	0.09	0.71	0.00	4.32	0.03	0.08	0.46	1.49	0.18	0.56	0.02	0.69	0.13	0.73	0.00
KS	11	1.97	0.02	0.62	0.00	3.06	0.02	0.45	0.02	0.27	0.19	0.72	0.00	3.63	0.09	0.50	0.02	1.94	0.24	0.62	0.00	6.61	0.01	0.00	0.95
MT1	12	3.58	0.00	0.32	0.05	3.40	0.01	0.36	0.04	4.68	0.01	0.08	0.37	4.03	0.02	0.22	0.12	2.98	0.05	0.32	0.06	5.33	0.04	0.09	0.33
MT2	8	7.90	0.00	0.19	0.28	7.73	0.00	0.23	0.23	8.48	0.01	0.04	0.63	8.14	0.01	0.19	0.29	7.86	0.02	0.19	0.28	8.23	0.03	0.13	0.37
MT3	8	3.10	0.01	0.89	0.00	5.14	0.01	0.88	0.00	14.85	-0.01	0.03	0.68	3.71	0.07	0.84	0.00	3.78	0.13	0.53	0.04	9.34	0.10	0.17	0.31
MTS	6	0.92	0.01	0.78	0.02	1.90	0.01	0.67	0.05	4.86	-0.01	0.03	0.72	1.24	0.08	0.92	0.00	1.15	0.16	0.73	0.03	2.24	0.11	0.34	0.22
EB	9	0.04	0.02	0.93	0.00	-0.12	0.03	0.96	0.00	0.31	0.02	0.48	0.04	0.47	0.08	0.86	0.00	0.12	0.21	0.84	0.00	0.59	0.19	0.78	0.00
TR	12	1.68	0.01	0.64	0.00	1.80	0.01	0.59	0.00	7.40	0.01	0.01	0.73	2.39	0.05	0.62	0.00	1.01	0.16	0.63	0.00	0.18	0.29	0.62	0.00
M	10	1.58	0.01	0.38	0.06	1.86	0.01	0.39	0.05	3.25	0.01	0.02	0.70	0.46	0.06	0.60	0.01	1.82	0.12	0.33	0.09	2.09	0.17	0.33	0.08
KK	6	0.46	0.01	0.94	0.00	0.60	0.03	0.93	0.00	0.73	0.02	0.92	0.00	1.96	0.07	0.82	0.01	0.68	0.09	0.97	0.00	-2.29	0.14	0.83	0.01
SB	4	-0.47	0.02	0.99	0.00	0.28	0.02	0.96	0.02	1.38	0.01	0.02	0.87	0.74	0.07	0.84	0.08	-0.84	0.26	0.85	0.08	1.18	0.04	0.05	0.78
WAAF	5	-0.50	0.01	0.97	0.00	-0.33	0.02	0.92	0.01	-0.19	0.05	0.99	0.00	0.40	0.06	0.95	0.01	-0.20	0.09	1.00	0.00	-2.21	0.06	0.33	0.31
ER	5	3.04	0.00	0.31	0.33	2.91	0.01	0.31	0.33	1.21	0.04	0.45	0.21	4.18	0.01	0.12	0.57	2.35	0.07	0.43	0.23	5.23	0.01	0.01	0.87
D6	4	0.84	0.01	0.95	0.03	1.97	0.01	0.62	0.21	30.44	-0.06	0.57	0.24	4.55	0.03	0.42	0.35	3.71	0.07	0.39	0.37	7.42	0.08	0.66	0.19
D7	4	-0.71	0.01	0.80	0.11	0.05	0.01	0.63	0.21	4.59	-0.01	0.25	0.50	0.07	0.03	0.67	0.18	0.05	0.07	0.65	0.19	2.04	0.08	0.86	0.07
D9	4	1.67	0.01	0.91	0.05	3.24	0.01	0.91	0.05	5.69	0.01	0.64	0.20	4.86	0.04	0.77	0.12	3.06	0.08	0.98	0.01	9.71	-0.01	0.01	0.91
D10	5	5.02	0.01	0.68	0.09	5.96	0.01	0.64	0.10	17.03	-0.02	0.26	0.38	4.16	0.04	0.90	0.01	4.89	0.07	0.95	0.00	9.86	0.05	0.26	0.38
D11	4	2.96	0.00	0.04	0.80	3.12	0.00	0.02	0.85	-2.31	0.03	0.18	0.57	1.88	0.01	0.10	0.69	1.52	0.02	0.24	0.51	2.67	0.02	0.22	0.53
D13	4	9.80	0.00	0.59	0.23	8.11	0.01	0.83	0.09	13.39	0.01	0.39	0.38	6.71	0.03	0.92	0.04	7.83	0.05	0.90	0.05	15.77	0.04	0.11	0.67
D14	4	1.64	0.01	0.89	0.05	1.12	0.01	0.99	0.01	-3.32	0.06	0.69	0.17	0.84	0.04	0.97	0.01	0.75	0.07	0.75	0.14	3.31	0.00	0.00	0.99
D17	4	2.88	0.00	0.60	0.23	2.99	0.00	0.70	0.16	4.28	0.00	0.03	0.82	4.26	0.00	0.25	0.50	3.81	0.01	0.27	0.48	4.59	0.00	0.01	0.90
D18	5	7.88	0.00	0.29	0.35	10.13	0.00	0.08	0.65	4.67	0.01	0.56	0.15	9.71	0.01	0.07	0.67	3.52	0.07	0.74	0.06	11.77	0.01	0.01	0.86
D19	4	0.95	0.01	0.49	0.30	0.84	0.01	0.41	0.36	1.54	0.01	0.55	0.26	1.28	0.02	0.80	0.10	-7.34	0.31	0.84	0.08	3.39	0.00	0.03	0.82
D20	4	-0.99	0.01	0.96	0.02	0.73	0.01	0.93	0.03	-6.62	0.02	0.94	0.03	-0.77	0.07	0.95	0.03	-2.70	0.10	0.92	0.04	7.79	-0.01	0.02	0.87
A	22	1.24	0.01	0.46	0.00	1.31	0.01	0.45	0.00	-0.21	0.15	0.52	0.00	0.38	0.05	0.62	0.00	0.50	0.13	0.42	0.00	0.63	0.27	0.46	0.00
DOH	33	0.30	0.01	0.92	0.00	0.14	0.01	0.92	0.00	-0.12	0.22	0.42	0.00	-0.01	0.05	0.93	0.00	-0.44	0.16	0.78	0.00	0.55	0.12	0.32	0.00
WU	25	2.51	0.01	0.72	0.00	2.51	0.01	0.72	0.00	1.29	0.25	0.84	0.00	1.70	0.04	0.78	0.00	-0.16	0.20	0.65	0.00	2.35	0.21	0.69	0.00

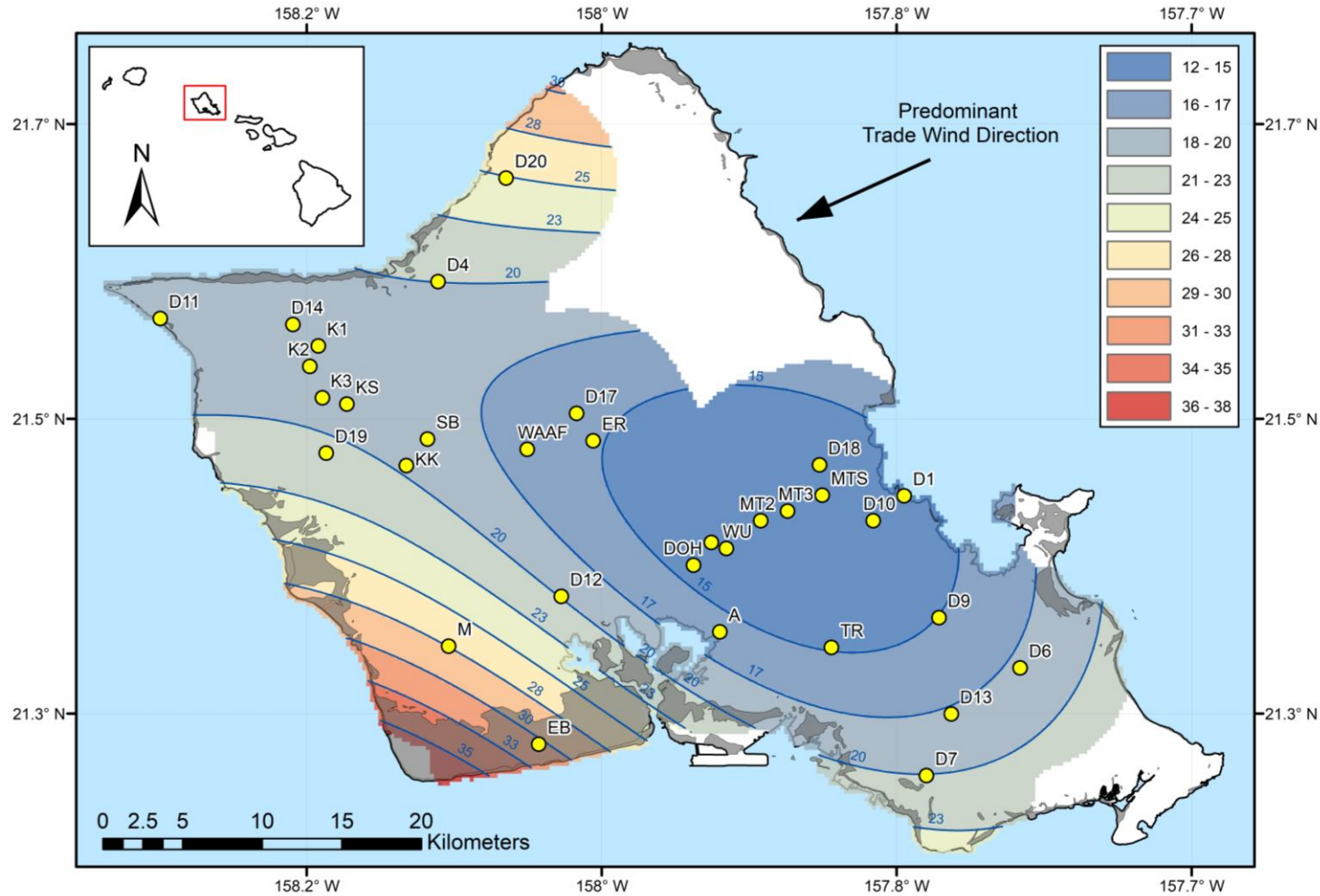


Figure 5. Calcium marine enrichment factor map for O'ahu, HI, USA interpolated from bulk precipitation chemistry data collected between March 2017 and June 2021. Data from Dores et al., (2020) are included. The interpolation method was ordinary kriging. Enrichment factor contour intervals are shown in blue. Exposures of calcite-cemented, shallow marine sediments are shown in dark gray. The coverage was interpolated from data at the collector locations displayed. Points were given a 6 km buffer to limit the extent of interpolation.

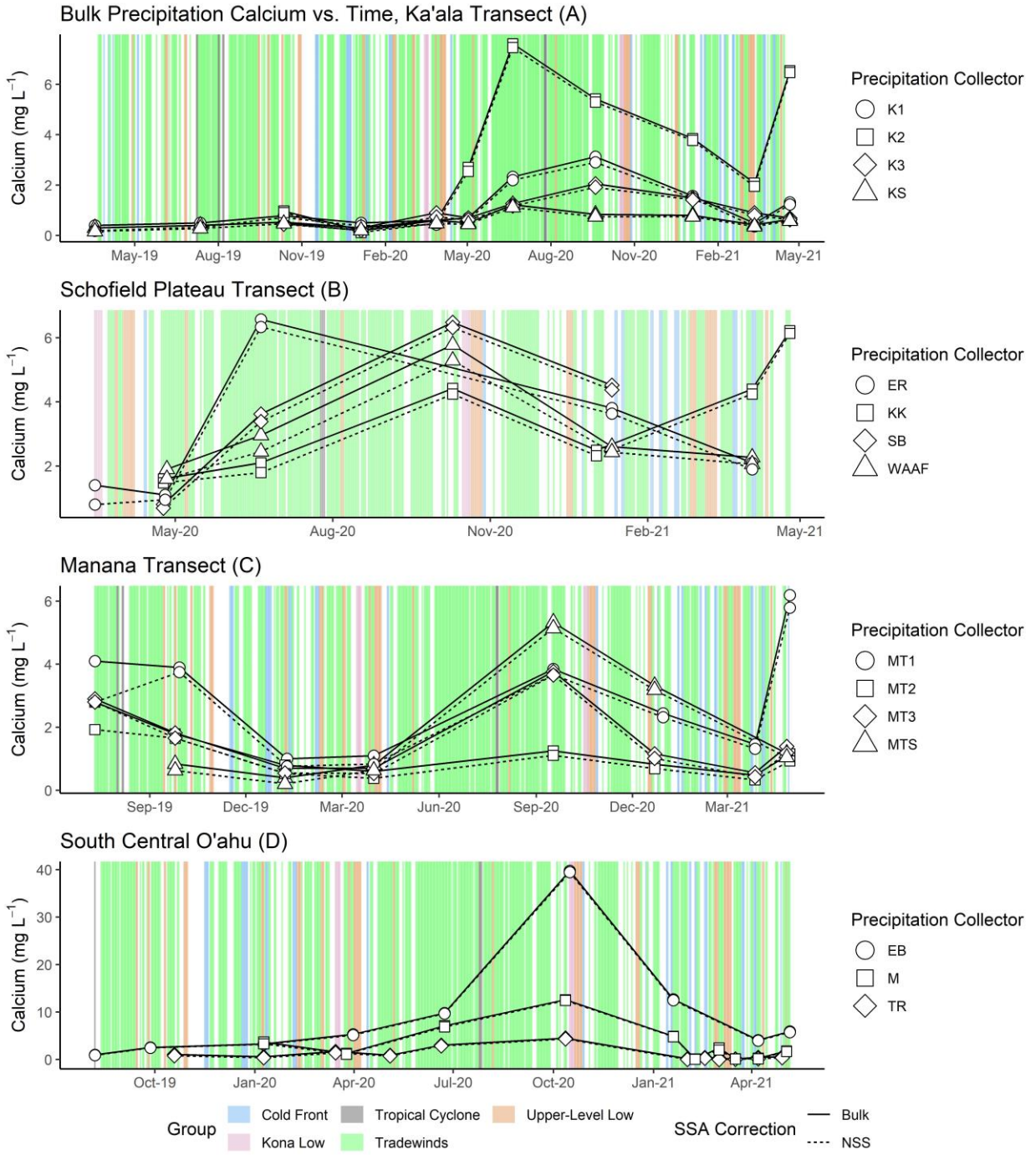


Figure 6. Time series of bulk precipitation  $\text{Ca}^{2+}$  concentrations taken on O'ahu, HI, USA. Ka'ala Transect (A), Schofield Plateau Transect (B), Manana Transect (C), and South-Central O'ahu collectors (D). Non-sea salt (NSS) contributions are displayed in dotted lines. Non-sea salt uncertainty was  $\pm 0.66 \text{ mg L}^{-1}$ . Weather trend data derived from International Global Radiosonde Archive (IGRA) weather balloon launches at Lihue, Kauai (Durre et al., 2006; 2016), and from monthly weather summaries provided by the National Oceanic and Atmospheric Administration (NOAA/NWS 2023) are shown in the background.

### 3.3. Potassium

#### 3.3.1. Results

Potassium concentrations in samples were generally low, constituting less than 3% of the measured ion load on average. Volume-weighted average  $K^+$  ranged from  $0.22 \pm 0.18 \text{ mg L}^{-1} K^+$  at Lyon Arboretum (D13) to  $5.47 \pm 1.15 \text{ mg L}^{-1} K^+$  at Kunia III Wells (D12). The ratio of potassium-to-chloride in bulk precipitation exceeded the seawater molar ratio of 0.02 in nearly all samples. Instrumental precision based on duplicate sampling was  $\pm 0.05 \text{ mg L}^{-1} K^+$  (Tachera et al., 2021), which rules out uncertainty as the sole culprit for excess NSS  $K^+$ . Sea-salt aerosol correction results confirm that NSS sources of  $K^+$  dominated, whereas propagated error through the SSA correction was low ( $\pm 0.06 \text{ mg L}^{-1}$  NSS  $K^+$ ).

The data suggest local, NSS  $K^+$  sources contribute to bulk precipitation chemistry. There were notable spikes in NSS  $K^+$  at select locations. Concentrations of NSS  $K^+$  exceeded  $1.95 \text{ mg L}^{-1}$  in one or more samples at Kolekole Pass (KK), Schofield Barracks (SB), Wheeler Army Airfield (WAAF), East Range (ER), Hale‘iwa (D4), Ka‘ena Point (D11), Kunia (D12), Mokulē‘ia (D14), Wahiawa (D17), Wai‘anae Kai (D19) and Waimano Ridge (DOH) (Figure 2). Excluding Ka‘ena Point, the proximity of these collectors to populated and/or agricultural areas suggests a possible connection with fertilizer use, which is consistent with findings in other precipitation chemistry studies (Keresztesi et al., 2020; Lu et al., 2011). Interpolated coverages of average annual bulk deposition and crustal and marine enrichment factors show elevated  $K^+$  deposition in central O‘ahu, near the island’s main agricultural areas (Figure 7). Regression analysis of rainfall rates ( $\text{mm d}^{-1}$ ) vs.  $K^+$  bulk deposition ( $\text{g ha}^{-1} \text{ d}^{-1}$ ) indicates that dry deposition is the most likely delivery mode (Table 5).

#### 3.3.2. Discussion

There are several plausible processes that could connect potential anthropogenic  $K^+$  sources to precipitation collectors. Elevated  $K^+$  in the Kolekole and Schofield Barracks collectors during the 2020 trade wind season could have been sourced from pineapple cultivation areas approximately 8 km to the northeast. These areas are aligned with the predominant trade wind direction. The Hale‘iwa and Mokulē‘ia collectors, likewise, are situated southwest of agricultural areas and subject to persistent northeasterly trade winds for much of the year, which could explain elevated NSS  $K^+$  in several samples at these locations (Figure 7). The Wai‘anae Kai

collector (D19) is isolated from trades by Mount Ka‘ala, so dust transport from agricultural areas in central and north O‘ahu is unlikely. Non-sea salt K<sup>+</sup> deposition at this site could have been caused by sea breeze wind patterns transporting dust particles from diversified crop areas to the southwest (Figure 7). Direct contamination was also a possibility at several sites. The Wheeler Army Airfield, Wahiawa, East Range, and Waimano Ridge collectors were all located close to residential or manicured areas. Elevated K<sup>+</sup> at these locations could be due to hand fertilization associated with groundskeeping. Potassium enrichment from non-agricultural sources, such as bird feces or algal residue, is also possible, although this potentiality was not explored in detail. Altogether, the spatiotemporal trends in bulk precipitation chemistry suggest local agricultural dust transportation is a plausible mechanism for non-marine K<sup>+</sup> deposition within the study area.

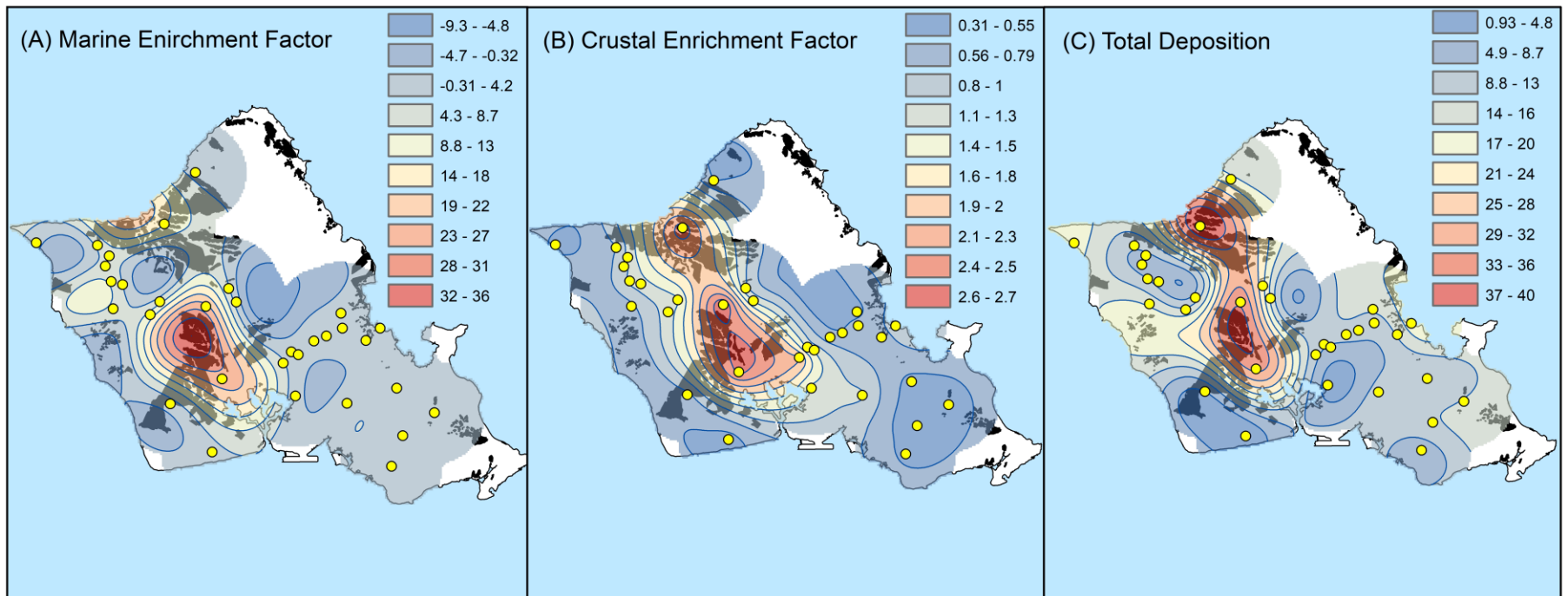


Figure 7. Interpolated coverages of  $K^+$  marine enrichment factor (A),  $K^+$  crustal enrichment factor (B), and average annual bulk deposition of  $K^+$  in  $\text{kg ha}^{-1}$  (C). The interpolation method was ordinary kriging. Interpolation points are shown in yellow. The interpolated coverages were limited to a 6 km buffer around each point. Data from Dores et al., (2020) are included. The crustal enrichment factor was calculated using  $\text{Ca}^{2+}$  as the reference species and was based on average crustal composition (Kring 1997). The marine enrichment factor was calculated using  $\text{Cl}^-$  as the reference species and was based on average seawater composition (Wilson 1975). Agricultural areas are shown in black.

### 3.4. Sulfate & Magnesium

#### 3.4.1. Results

On average,  $Mg^{2+}$  and  $SO_4^{2-}$  constituted less than 5% and 3% of the measured ion load in bulk precipitation samples. Volume-weighted average  $SO_4^{2-}$  ranged from  $0.35 \pm 0.91 \text{ mg L}^{-1}$  at Ka‘ala Culvert 49 (K3) to  $7.02 \pm 1.45 \text{ mg L}^{-1}$  at Ka‘ena Point (D11). Volume-weighted average  $Mg^{2+}$  ranged from  $0.34 \pm 0.57 \text{ mg L}^{-1}$  at Ka‘ala Milepost 3 (K2) to  $2.96 \pm 0.73 \text{ mg L}^{-1}$  at Ka‘ena Point (D11). Instrumental uncertainties based on duplicate sampling were  $\pm 1.82 \text{ mg L}^{-1} SO_4^{2-}$ , and  $\pm 0.32 \text{ mg L}^{-1} Mg^{2+}$  (Tachera et al., 2021). Sea-salt correction propagated uncertainty was  $\pm 0.33 \text{ mg L}^{-1} NSS Mg^{2+}$ , and  $\pm 1.83 \text{ mg L}^{-1} NSS SO_4^{2-}$ . Marine enrichment factors showed a slight elevation of  $SO_4^{2-}$  compared to  $Mg^{2+}$ , though both constituents were close to marine major ion ratios.

#### 3.4.2. Discussion

Differentiating  $Mg^{2+}$  and  $SO_4^{2-}$  sources in bulk precipitation was difficult due to low concentrations, relatively high uncertainty, and irregular spatiotemporal patterns. Samples with excess  $SO_4^{2-}$  and  $Mg^{2+}$  were found most frequently in collectors at lower elevations or in more urbanized areas. Collectors in high elevation and pristine settings had minor  $SO_4^{2-}$  and  $Mg^{2+}$ , and negligible NSS contributions. Regression analysis of rainfall rates ( $\text{mm d}^{-1}$ ) vs.  $Mg^{2+}$  and  $SO_4^{2-}$  bulk deposition ( $\text{g ha}^{-1} \text{ d}^{-1}$ ) indicates that both dry and wet deposition occurred (Table 5). Samples from the Ewa Beach (EB) collector showed the most substantial component of NSS  $Mg^{2+}$ , accounting for approximately 20% of the total  $Mg^{2+}$  ion load. This is potentially related to the collector’s downwind proximity to the heavy military and aviation activity centered on Pearl Harbor, which includes Joint Base Pearl Harbor Hickam, and the Daniel K. Inouye International Airport. Elevated NSS  $Mg^{2+}$  at Ewa Beach could also be due to dust transport of dolomitized soils. This phenomenon has been observed in semi-arid settings on O‘ahu in the past (Sherman et al., 1947). However, it is unclear why similar trends were not observed in other semi-arid locations, including Wai‘anae Kai (D19) and Ka‘ena Point (D11). Samples from the Makakilo collector (M) showed the most substantial component of NSS  $SO_4^{2-}$ , with an average of 40% of the ion load coming from NSS sources. The Kahe Power Plant, approximately 5 km to the east, is a potential source of combustion particulate byproducts. However, there was no clear correlation between wind patterns and excess  $SO_4^{2-}$  at Makakilo. Volcanic emissions from

Kīlauea have been associated with elevated  $\text{SO}_4^{2-}$  in precipitation on O‘ahu in the past (Dugan & Ekern 1984), but this trend was not observed in this study, likely due to low volcanic activity during the sampling period.

At some locations,  $\text{Mg}^{2+}$  and  $\text{SO}_4^{2-}$  had an apparent inverse relationship. Following the 2020 trade wind season, bulk precipitation samples showed elevated  $\text{Mg}^{2+}$ , and roughly proportional depletion of  $\text{SO}_4^{2-}$  at Ewa Beach (EB), Tripler Ridge (TR), Wheeler Army Airfield (WAAF), Kolekole Pass (KK), and all collectors along the Ka‘ala transect (K1, K2, K3, and KS) (Figure 8). This inverse relationship was also visible in the PCA. Principal component 6, which accounted for 0.5% of the total variance in the dataset, shows an eigenvector of -0.56 for  $\text{SO}_4^{2-}$  and 0.82 for  $\text{Mg}^{2+}$ , indicating strong inverse loading for these two constituents (Table 4; Abdi & Williams 2010). The cause of this relationship is unclear but could indicate chemical reactions involving both species, whereby one is enriched relative to the other through a reaction pathway involving both. The trends in  $\text{Mg}^{2+}$  and  $\text{SO}_4^{2-}$  concentrations in bulk precipitation do not definitively point to any single source or process for non-marine deposition. Particulate from combustion emissions and marine biogenic activity are the most likely sources of NSS  $\text{SO}_4^{2-}$ . Aviation activity, leaflitter decay and local dust transport are the most likely sources of NSS  $\text{Mg}^{2+}$ .

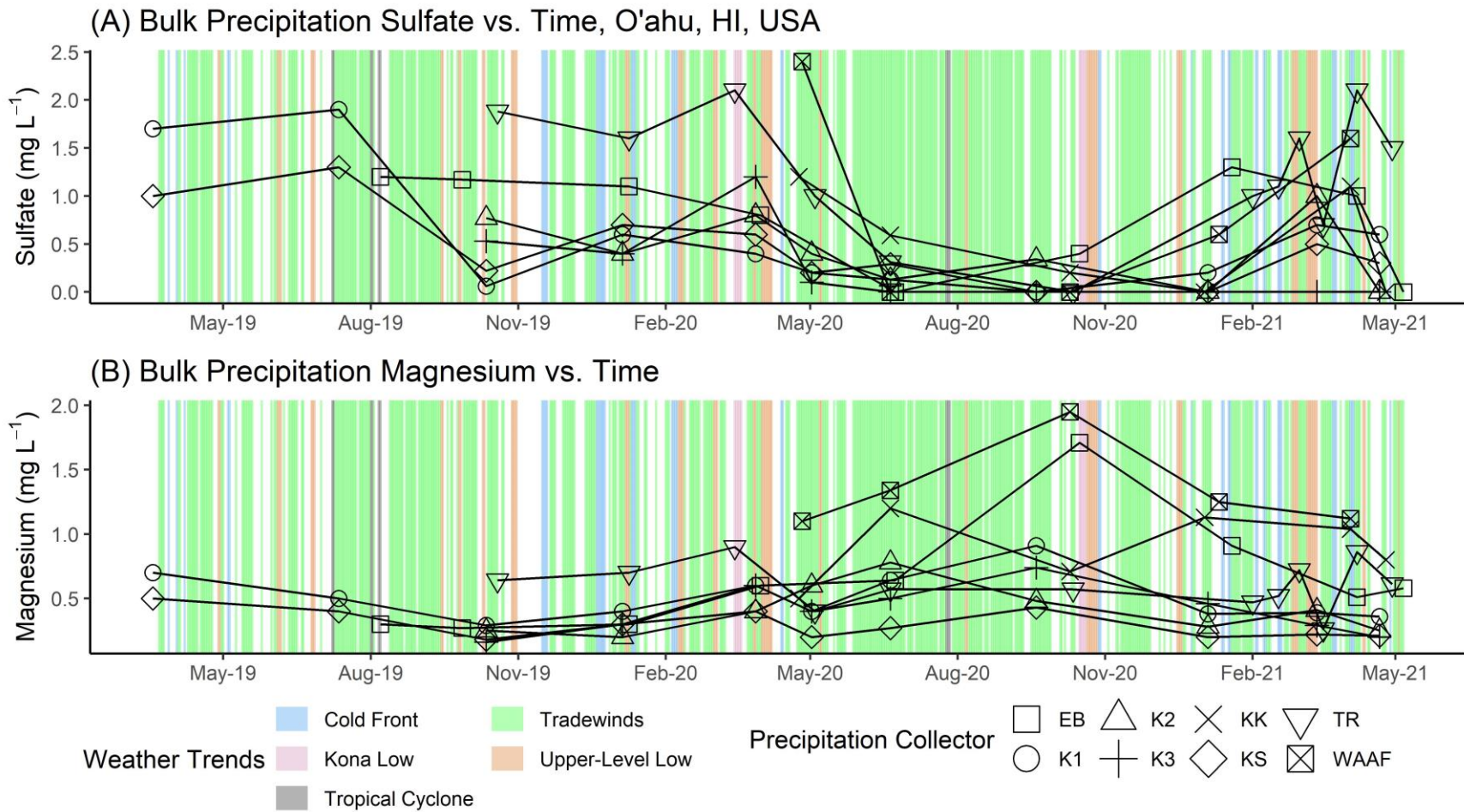


Figure 8. Time series of bulk precipitation  $\text{Mg}^{2+}$  and  $\text{SO}_4^{2-}$  concentrations in bulk precipitation taken on O'ahu, HI, USA between June 2018, and May 2021. Abbreviations: EB is Ewa Beach, TR is Tripler Ridge, WAAF is Wheeler Army Airfield, KK is Kolekole Pass, and K is Ka'ala. Weather trend data derived from International Global Radiosonde Archive (IGRA) weather balloon launches at Līhue, Kauai (Durre et al., 2006; 2016), and from monthly weather summaries provided by the National Oceanic and Atmospheric Administration (NOAA/NWS 2023) are shown in the background.

#### 4. Conclusions

Analysis of inorganic constituents in precipitation confirms that marine-origin SSAs exert the strongest influence on precipitation major ion chemistry throughout the study area. However, it also illuminates several interesting NSS deposition sources and atmospheric processes that impact precipitation chemistry. The strong correlation between precipitation chloride-to-sodium ratios and the seawater chloride-to-sodium ratio indicates that these ions are sourced almost exclusively from marine-origin SSAs. Sodium concentrations suggest at least one NSS source that is most likely terrestrial dust transported from the Asian continent above the trade-wind regime. Chloride was selected as the reference species for SSA corrections due to measurable excess in  $\text{Na}^+$  relative to seawater composition. Spatially variable NSS  $\text{Ca}^{2+}$  concentrations in precipitation suggest that local dust transport, most likely from calcite-rich sedimentary deposits and/or cement production, is the dominant source of NSS  $\text{Ca}^{2+}$  deposition. Potassium concentrations were generally low, but a number of collectors close to agricultural areas showed accumulations of NSS potassium-rich dust through dry deposition. Sulfate and  $\text{Mg}^{2+}$  concentrations were low, highly variable, and often inversely related, suggesting a chemical reaction involving both species and making source differentiation difficult. Lastly, the cumulative effect of summing and squaring uncertainties in the volume-weighting calculations produced large errors in some VWA chemical concentrations, indicating increased instrumental precision may be necessary for more comprehensive analysis using this procedure. These findings illuminate some of the key atmospheric processes governing precipitation chemistry in and around the Pearl Harbor Aquifer and help to establish a baseline for assessing future fluctuations. Future work will examine spatiotemporal changes in water stable isotopologue concentrations (oxygen-18 and deuterium) within precipitation over the same sampling period and collector distribution. These two efforts aim to characterize precipitation chemistry within the Pearl Harbor region and postulate its primary controlling factors. These two efforts will culminate in an examination of groundwater chemistry within the study area with the ultimate goal of constraining groundwater flow paths by means of natural geochemical tracers.

## 5. Chapter 2 References

- Abdi, H., & Williams, L. (2010). Principal Component Analysis. *Wiley Interdisciplinary Reviews. Computational Statistics*, 2(4), 433-459. doi:<https://doi.org/10.1002/wics.101>
- Akpo, A., Galy-Lacaux, C., Laouali, D., Delon, C., Liousse, C., Adon, M., . . . Darakpa, C. (2015). Precipitation chemistry and wet deposition in a remote wet savanna site in West Africa: Djougou (Benin). *Atmospheric Environment*, 115, 110–123. <https://doi.org/10.1016/j.atmosenv.2015.04.064>.
- Booth, H., Lautze, N., Tachera, D., & Dores, D. (2021). Event-Based Stable Isotope Analysis of Precipitation Along a High Resolution Transect on the South Face of O'ahu, Hawai'i. *Pacific Science*, 75(3), 421–. <https://doi.org/10.2984/75.3.9>.
- Brahney, J., Ballantyne, A., Sievers, C., & Neff, J. (2013). Increasing Ca<sup>2+</sup> deposition in the wester US: The role of mineral aerosols. *Aeolian Research* (10), 77-87. doi:<https://dx.doi.org/10.1016/j.aeolia.2013.04.003>
- Cao, G., Giambelluca, T., Stevens, D., & Schroeder, T. (2007). Inversion Variability in the Hawaiian Trade Wind Regime. *Journal of Climate*, 20(7), 1145-1160. doi:10.1175/JCLI4033.1
- Charlson, R., Lovelock, J., Andreae, M., & Warren, S. (1987). Oceanic phytoplankton, atmospheric sulphur, cloud albedo and climate. *Nature*, 326, 655-661.
- Chung, K., & Park, S. (1998). A numerical study on the size and deposition of Yellow Sand events. *Journal of Korea Air Pollution Research Association*, 10, 64-72.
- Darzi, M., & Winchester, J. (1982). Resolution of Basaltic and Continental Aerosol Components During Spring and Summer Within the Boundary Layer of Hawaii. *Journal of Geophysical Research*, 87(C9), 7262-7272.
- Dores, D., Glenn, C. R., Torri, G., Whittier, R. B., & Popp, B. (2020). Implications for groundwater recharge from stable isotopic composition of precipitation in Hawai'i during the 2017–2018 La Niña. *Hydrological Processes*, 34(24), 4675–4696. <https://doi.org/10.1002/hyp.13907>.
- Dugan, G., & Ekern, P. (1984). *Chemical Constituents of Rainfall at Different Locations on O'ahu, Hawai'i*. University of Hawai'i at Mānoa . Honolulu: Water Resources Research Center.
- Durre, I., Vose, R., & Wuertz, D. (2006). Overview of the Integrated Global Radiosonde Archive. *Journal of Climate*, 19(1), 53-68. doi:<https://doi.org/10.1175/JCLI3594.1>
- Durre, I., Xungang, Y., Vose, R., Applequist, S., & Arnfield, J. (2016). Integrated Global Radiosonde Archive (IGRA), Version 2. *Subset USM00091165, Lihue, HI, USA*. NOAA National Centers for Environmental Information. doi:10.7289/V5X63K0Q

- Fackrell, J. K., Glenn, C. R., Thomas, D., Whittier, R., & Popp, B. (2020). Stable isotopes of precipitation and groundwater provide new insight into groundwater recharge and flow in a structurally complex hydrogeologic system: West Hawai'i, USA. *Hydrogeology Journal*, 28(4) 1191-1207. <https://doi.org/10.1007/s10040-020-02143-9>.
- Fletcher, C., Bochicchio, C., Conger, C., Engels, M., Feirstein, E., Frazier, N., . . . Vitousek, S. (2008). Geology of Hawaii Reefs. In B. Reigl, R. Dodge, , & R. Appledoorn, *Coral Reefs of the USA* (pp. 435-487). Netherlands: Springer.
- Frazier, A. & Giambelluca, T. (2017). Spatial trend analysis of Hawaiian rainfall from 1920 to 2012. *International Journal of Climatology*, 37(5), 2522-2531. <https://doi.org/10.1002.joc.4862>
- Ghahremaninezhad, R., Norman, A.-L., Abbatt, J., Levasseur, M., & Thomas, J. (2016). *Biogenic, anthropogenic and sea salt sulfate size-segregated aerosols in the Arctic summer*. Atmospheric Chemistry and Physics, 16(8), 5191–5202. <https://doi.org/10.5194/acp-16-5191-2016>.
- Giambelluca, T. (1983). *Water balance of the Pearl Harbor-Honolulu Basin, Hawai'i, 1946-1975*. Water Resources Research Center, University of Hawai'i at Manoa.
- Giambelluca, T., Chen, Q., Frazier, A., Price, J., Chen, Y.-L., Chu, P.-S., . . . Delparte, D. (2013). Online Rainfall Atlas of Hawai'i: Bulletin of the American Meteorological Society. v. 94, p. 313-316. doi:<https://doi.org/10.1175/BAMSD-11-00228.1>
- Glenn, C., Whittier, R., Dailer, M., El-Kadi, A., Fackrell, J., Kelly, J., . . . Sevadjian, J. (2013). *Lahaina Groundwater Tracer Study - Lahaina, Maui, Hawaii*. Final Report prepared for the State of Hawaii Department of Health, the U.S. Environmental Protection Agency, and the U.S. Army Engineer Research and Development Center.
- Harding, D., & Miller, J. (1982). The Influence on Rain Chemistry of the Hawaiian Volcano Kilauea. *Journal of Geophysical Research*, 87(C2), 1225-1230.
- Hautman, D., & Munch, D. (1997). *Method 300.1, Revision 1-0: Determination of Inorganic Anions in Drinking Water by Ion Chromatography*. U.S. Environmental Protection Agency, National Exposure Research Laboratory, Office of Research and Development, Cincinnati OH.
- Hu, D., Chen, J., Ye, X., Li, L., & Yang, X. (2011). Hygroscopicity and evaporation of ammonium chloride and ammonium nitrate: Relative humidity and size effects on the growth factor. *Atmospheric Environment* (1994), 45(14), 2349–2355. <https://doi.org/10.1016/j.atmosenv.2011.02.024>.
- Hu, D., Qiao, L., Chen, J., Ye, X., Yang, X., Cheng, T., & Fang, W. (2010). Hygroscopicity of inorganic aerosols: size and relative humidity effects on the growth factor. *Aerosol and Air Quality Research*, 10, 255-264.

- Hutchinson, G. (1954). The Solar System: The biochemistry of the terrestrial atmosphere. In G. Kuiper (Ed.), *The Earth as a Planet* (Vol. 2, pp. 371-433). Chicago, IL: University of Chicago Press.
- Junge, C. (1972). Our Knowledge of the Physico-Chemistry of Aerosols in the Undisturbed Marine Environment. *Journal of Geophysical Research*, 77(27), 5183-5200. doi:<https://doi.org/10.1029/JC077i027p05183>
- Keene, W., Pszenny, A. A., Galloway, J., & Hawley, M. (1986). Sea-salt corrections and interpretation of constituent ratios in marine precipitation. *Journal of Geophysical Research*, 91(D6), 6647–6658. <https://doi.org/10.1029/JD091iD06p06647>.
- Keresztesi, Á., Nita, I.-A., Boga, R., Birsan, M.-V., Bodor, Z., & Szép, R. (2020). Spatial and long-term analysis of rainwater chemistry over the conterminous United States. *Environmental Research*, 188, 109872–109872. <https://doi.org/10.1016/j.envres.2020.109872>.
- Khemani, L., Momin, G., Naik, M., Prakasa Rao, P., Kumar, R., & Ramana Murty, B. (1985). Trace Elements and Sea Salt Aerosols over the Sea Areas Around the Indian Sub-Continent. *Atmospheric Environment*, 19(2), 277-284. doi:[https://doi.org/10.1016/0004-6981\(85\)90095-2](https://doi.org/10.1016/0004-6981(85)90095-2)
- Kring, D. A. (1997). Composition of Earth's continental crust as inferred from the compositions of impact melt sheets. *Lunar and Planetary Science XXVIII; 28th Lunar and Planetary Science Conference*, (pp. 763-). Houston, TX.
- Kroopnick, P. (1977). The SO<sub>4</sub>:Cl Ratio in Oceanic Rainwater. *Pacific Science*, 31(1), 91-106.
- Laskin, A., Moffet, R. C., Gilles, M. K., Fast, J. D., Zaveri, R. A., Wang, B., . . . Shutthanandan, J. (2012). Tropospheric chemistry of internally mixed sea salt and organic particles: Surprising reactivity of NaCl with weak organic acids. *Journal of Geophysical Research. D. (Atmospheres)*, 117(D15). <https://doi.org/10.1029/2012JD017743>.
- Lee, B., Hong, S., & Lee, D. (2000). Chemical composition of precipitation and wet deposition of major ions on the Korean peninsula . *Atmospheric Environment*, (34) 563-575.
- Lewis, E., & Schwartz, S. (2004). *Sea Salt Aerosol Production: Mechanisms, Methods, Measurements, and Models - A Critical Review*. Washington D.C.: American Geophysical Union.
- Lewis, W. M. (1981). Precipitation chemistry and nutrient loading by precipitation in a tropical watershed. *Water Resources Research (United States)*, 17(1), 169–181. <https://doi.org/10.1029/WR017i001p00169>.
- Li, C., Kang, S., Zhang, Q., & Kaspari, S. (2007). Major ionic composition of precipitation in the Nam Co region, Central Tibetan Plateau. *Atmospheric Research*, 85(3), 351–360. <https://doi.org/10.1016/j.atmosres.2007.02.006>.

- Longman, R., Ellison, T., Giambelluca, T., & Kaiser, L. (2021). A 20-year analysis of disturbance-driven rainfall on O'ahu, Hawai'i. *Monthly Weather Review*. doi:<https://doi.org/10.1175/MWR-D-20-0287.1>
- Loye-Pilot, M., Martin, J., & Morelli, J. (1986). Influence of Saharan dust on the rain acidity and atmospheric input to the Mediterranean. *Nature*, 321, 427-428.
- Lu, X., Li, L. Y., Li, N., Yang, G., Luo, D., & Chen, J. (2011). Chemical characteristics of spring rainwater of Xi'an city, NW China. *Atmospheric Environment* (1994), 45(28), 5058–5063. <https://doi.org/10.1016/j.atmosenv.2011.06.026>.
- Manahan, S. (2017). *Environmental Chemistry*. (10, Ed.) Boca Raton, FL: CRC Press.
- Miller, J., & Yoshinaga, A. (1981). The pH of Hawaiian Precipitation: A Preliminary Report. *Geophysical Research Letters*, 8(7), 779-782.
- Mphepya, J., Pienaar, J., Galy-Lacaux, C., Held, G., & Turner, C. (2004). Precipitation chemistry in semiarid areas of Southern Africa: a case study of a rural and an industrial site. *Journal of Atmospheric Chemistry*, 47 (1), 1-24.
- Neff, J., Belnap, R., & Lamothe, P. (2005). Multi-decadal impacts of grazing on soil physical and biogeochemical properties in southeast Utah. *Ecological Applications*, 15(1), 87-95.
- Nightingale, P., Liss, P., & Schlosser, P. (2000). Measurements of air-sea gas transfer during an open ocean algal bloom. *Geophysical Research Letters*, 27, 2117-2120.
- Niu, H., He, Y., Lu, X., Shen, J., Du, J., Zhang, T., . . . Chang, L. (2014). Chemical composition of rainwater in the yulong snow mountain region, southwestern China. *Atmospheric Reserach*, 144, 195-206. doi:<https://doi.org/10.1016/j.atmosres.2014.03.010>
- NOAA/NWS. (2023). *Hawaii Monthly Weather Summaries*. Retrieved from [https://www.hawaii.edu/climate-data-portal/publications-list/?collection\\_id=PZN8C7R9&collection\\_name=%2520NOAA%252FNWS%2520Monthly%2520Precipitation%2520Summaries](https://www.hawaii.edu/climate-data-portal/publications-list/?collection_id=PZN8C7R9&collection_name=%2520NOAA%252FNWS%2520Monthly%2520Precipitation%2520Summaries)
- Noguchi, Y. (1979). Deformation of trees in Hawaii and its relation to wind. *The Journal of Ecology*, 67(2), 611-628. doi:<https://doi.org/10.2307/2259116>
- Norman, A., Barrie, L., Toom-Sauntry, D., Sirois, A., Krouse, H., Li, S., & Sharma, S. (1999). Sources of aerosol sulfate at Alert: apportionment using stable isotopes. *Journal of Geophysical Research*, 104, 11619-11631.
- Pearson, F., & Fisher, D. W. (1971). *Chemical composition of atmospheric precipitation in the Northeastern United States*. U.S. Geological Survey, U.S. Department of the Interior. doi:[10.3133/wsp1535P](https://doi.org/10.3133/wsp1535P)
- Pilson, M. E. (1998). *An Introduction to the Chemistry of the Sea* (2 ed.). Cambridge, NY: Cambridge University Press.

- Saltzman, E., Savoie, D., Prospero, J., & Zika, R. (1986). Methanosulfonic Acid and Non-Sea-Salt Sulfate in Pacific Air: Regional and Seasonal Variations. *Journal of Atmospheric Chemistry*, 277-240.
- Satake, H., & Yamane, T. (1992). Deposition of non-sea salt sulfate observed at Toyama facing the Sea of Japan for the period of 1981-1991. *Geochemical Journal*, 26, 299-305.
- Scholl, M. A., Gingerich, S. B., & Tribble, J. W. (2002). The influence of microclimates and fog on stable isotope signatures used in interpretation of regional hydrology: East Maui, Hawaii. *Journal of Hydrology (Amsterdam)*, 264(1), 170–184.  
doi:[https://doi.org/10.1016/S0022-1694\(02\)00073-2](https://doi.org/10.1016/S0022-1694(02)00073-2)
- Scholl, M., & Ingebritsen, S. (1995). *Total and non-seasalt sulfate and chloride measured in bulk precipitation samples from the Kilauea Volcano area, Hawaii*. U.S. Geological Survey, U.S. Department of Interior. Retrieved from <https://pubs.usgs.gov/wri/1995/4001/report.pdf>
- Sherman, G., Kanehiro, Y., & Fujimoto, C. (1947). Dolomitization in Semi-arid Hawaiian Soils. *Pacific Science*.
- Sherrod, D., Sinton, J., Watkins, S., & Brunt, K. (2021). *Geologic map of the State of Hawai‘i: U.S. Geological Survey Scientific Investigations Map 3143, pamphlet 72 p., 5 sheets, scales 1:100,000 and 1:250,000*. doi:<https://doi.org/10.3133/sim3143>
- Shi, G.-L., Li, X., Feng, Y.-C., Wang, Y.-Q., Wu, J.-H., Li, J., & Zhu, T. (2009). Combined source apportionment, using positive matrix factorization–chemical mass balance and principal component analysis/multiple linear regression–chemical mass balance models. *Atmospheric Environment* (1994), 2929–2937.  
<https://doi.org/10.1016/j.atmosenv.2009.02.054>.
- Szép, R., Mateescu, E., Niță, I.-A., Birsan, M.-V., Bodor, Z., & Keresztesi, Á. (2018). Effects of the Eastern Carpathians on atmospheric circulations and precipitation chemistry from 2006 to 2016 at four monitoring stations (Eastern Carpathians, Romania). *Atmospheric Research*, 214, 311-328. doi:<https://doi.org/10.1016/j.atmosres.2018.08.009>
- Tachera, D., Lautze, N., Torri, G., & Thomas, D. (2021). Characterization of the isotopic composition and bulk ion deposition of precipitation from Central to West Hawai‘i Island between 2017 and 2019. *Journal of Hydrology. Regional Studies*, 34, 100786.  
<https://doi.org/10.1016/j.ejrh.2021.100786>.
- Torri, G., Nugent, A., & Popp, B. (2023). The Isotopic Composition of Rainfall on a Subtropical Mountainous Island. *Journal of Hydrometeorology*. doi:<https://doi.org/10.1175/JHM-D-21-0204.1>
- Wickam, H., Chang, W., Henry, L., Pedersen, T., Takahashi, K., Wilke, C., . . . Dewey, H. (2016). *Rug plots in the margins*. (S.-V. N. York, Producer) Retrieved from ggplot2: Elegant Graphics for Data Analysis:  
[https://ggplot2.tidyverse.org/reference/geom\\_rug.html](https://ggplot2.tidyverse.org/reference/geom_rug.html)

- Wilson, T. (1975). Salinity and the major elements of sea water. In J. Riley, & G. Skirrow, *Chemical Oceanography* (2 ed., Vol. 1, pp. 365-413). Orlando: Academic.
- Xiao, J. (2016). Chemical composition and source identification of rainwater constituents at an urban site in Xi'an. *Environmental Earth Sciences*, 75, 1-12.  
doi:<https://doi.org/10.1007/s12665-015-4997-z>
- Zhang, D., Peart, M., Jim, C., He, Y., Li, B., & Chen, J. (2003). Precipitation chemistry of Lhasa and other remote towns, Tibet. *Atmospheric Environment*, 37 (2), 231-240.

CHAPTER 3: UNDERSTANDING THE SOURCE AND EVOLUTION OF  
PRECIPITATION STABLE ISOTOPE COMPOSITION ACROSS O‘AHU, HAWAI‘I, USA

Submitted on 11/6/2023 as: Brennis, T., Lautze, N., Whitter, R., Kagawa-Viviani, A., Tseng, H., Torri, G., & Thomas, D. (*in review*). Understanding the source and evolution of precipitation stable isotope composition across O‘ahu, Hawai‘i, USA. *Journal of Hydrometeorology*

## CHAPTER 3 ABSTRACT

Pacific Islands present unique challenges for water resource management due to their environmental vulnerability, dynamic climates, and heavy reliance on groundwater resources. Quantifying the connections between meteoric, ground-, and surface waters is critical for effective water resource management on Pacific Islands. Analyses of the stable isotopes of oxygen and hydrogen in the hydrosphere can help illuminate such connections. This study investigates the stable isotope composition of rainfall on the Island of O‘ahu, Hawai‘i, USA, with a particular focus on the extent to which altitude impacts stable isotope composition. Rainfall chemistry was sampled at 20 locations across the island approximately quarterly from March 2018 to August 2021. The new precipitation chemistry data were integrated with previously published precipitation data to create the most spatially and topographically diverse precipitation collector network on O‘ahu to date. Results show that  $^{18}\text{O}$  and  $^2\text{H}$  concentrations in precipitation varied greatly across the study region, displaying distinct isotopic signatures influenced by geographical location, season, and precipitation source. Altitude and volume-weighted average isotopic compositions were strongly correlated along certain elevation transects, but these relationships could not be extrapolated to larger regions due to microclimate influences. Altitude and deuterium-excess (d-excess) were strongly correlated across the entire study region, suggesting d-excess may be a reliable proxy for precipitation elevation in ground- and surface water tracer studies. Analysis of high-elevation spring, rainfall, and fog chemistry from the summit of Mount Ka‘ala suggests fog may contribute up to 45% of total groundwater recharge at the summit. These findings highlight the strong influence of microclimates on the stable isotope composition of rainfall and underscore the need for further investigation into fog's role in the water budget on O‘ahu. They also demonstrate the importance of stable isotope analysis for comprehending hydrologic dynamics in environmentally sensitive regions.

## 1. Introduction

Analyses of the stable isotopes of oxygen (O) and hydrogen (H) in the hydrosphere can illuminate hydrologic connections between precipitation, ground-, and surface waters (Kendall & McDonnell, 1998) and references therein; (Gat, 1996) and references therein. The stable isotope composition of meteoric waters is governed by kinetic and equilibrium fractionation processes (Dansgaard, 1964; Craig, 1961; Gat, 1996), including the continental effect, the rainout effect, the amount effect, and the altitude effect (Kendall & McDonnell, 1998) which results in semi-predictable spatial patterns across the globe. Local variations in water chemistry can be established through long-term (years to decades) point sampling and analyses of precipitation, ground-, and surface waters, which can then enable the creation of spatial models that can be used to extrapolate precipitation chemistry for larger regions where rainfall sampling may not be feasible. Regional understanding of stable isotope chemistry in water can allow the tracing of surface and groundwater back to source regions and thus illuminate water flow paths and residence times.

Pacific Islands are an important venue for such research as these areas are particularly sensitive to hydrologic fluctuations associated with climate change (Vernon et al., 2019) and are overwhelmingly reliant on groundwater for freshwater needs. The island of O‘ahu, Hawai‘i, USA, is emblematic of these issues in several respects. Groundwater is a critical resource on O‘ahu, where it supplies more than 90% of freshwater needs and is replenished primarily from precipitation (Gingerich & Oki, 2000, State of Hawai‘i, 2019; Nicols et al., 1997). Urbanization and population growth are projected to increase the demand for freshwater on O‘ahu (State of Hawai‘i, 2019) while simultaneously encroaching on critical groundwater recharge areas. O‘ahu is also experiencing a long-term drying trend (Frazier & Giambelluca, 2017). Coupled with the island’s accessibility, diverse physiography, and dynamic climate, these factors make O‘ahu an ideal location for stable isotope hydrology research.

The Hawaiian Islands have a rich history of stable isotope research going back to the 1950’s (Friedman & Woodcock, 1956). One of the earliest efforts was undertaken by the International Atomic Energy Agency, which sampled precipitation monthly at a station in Hilo, Hawai‘i Island from 1963-1970 (IAEA/WMO, 2023). Scholl et al. (1995) utilized precipitation and well water stable isotope compositions to reveal groundwater flow paths, recharge areas, and residence times near the Kīlauea Volcano. Similar results were found on Maui, where isotope tracer

methods were used to differentiate fog and rainfall contributions to recharge (Scholl et al., 2002; 2007).

Findings from these works have spurred several more recent studies on Hawai‘i Island (Tillman et al., 2015; Kelly & Glenn, 2015; Fackrell et al., 2020; Tachera et al., 2021) and O‘ahu (Dores et al., 2020; Booth et al., 2021; Torri et al., 2023). Of note, Dores et al. (2020) found that the drier, leeward areas of O‘ahu received most precipitation from synoptic storms, which partially accounted for disparities between precipitation and groundwater isotopic compositions. Following this work, Booth et al. (2022) and Torri et al. (2023) both identified systematic isotopic differences between orographic trade wind-derived rainfall and rainfall from synoptic, disturbance-based storms. Findings from these recent works on O‘ahu have highlighted the importance of the moisture source on the isotopic composition of precipitation (i.e., rainout effect) but have largely left questions related to the altitude effect open to further exploration.

The establishment of reliable elevation stable isotope lapse rates was a critical step in connecting ground- and surface water to recharge areas on Maui and Hawai‘i Island. Such relationships have not been definitively established on O‘ahu. Recent research has also established a connection between deuterium excess (d-excess) and precipitation altitude (Natali et al., 2022), which has yet to be explored on O‘ahu. These recent works indicate a need for more expansive, longer-term precipitation sampling to fully characterize O‘ahu’s isotopic landscape (isoscape; Bowen, 2010).

The goal of this paper is to explore the source and evolution of precipitation stable isotope composition on O‘ahu, with a particular focus on the extent to which the altitude effect impacts precipitation chemistry. We propose that although the atmospheric and physiographic dynamics impacting O‘ahu’s isoscape are complex, they are semi-predictable. We support this claim by presenting, analyzing, and interpreting new stable isotope data from bulk precipitation and high elevation spring water collected on O‘ahu, Hawai‘i. This work supports a larger, long-term effort to establish a predictive model that can be used to estimate the isotopic composition of precipitation in unmonitored or inaccessible sites, which would be a valuable tool in exploring the connections between precipitation and groundwater and in understanding the complex Earth system processes governing precipitation chemistry.

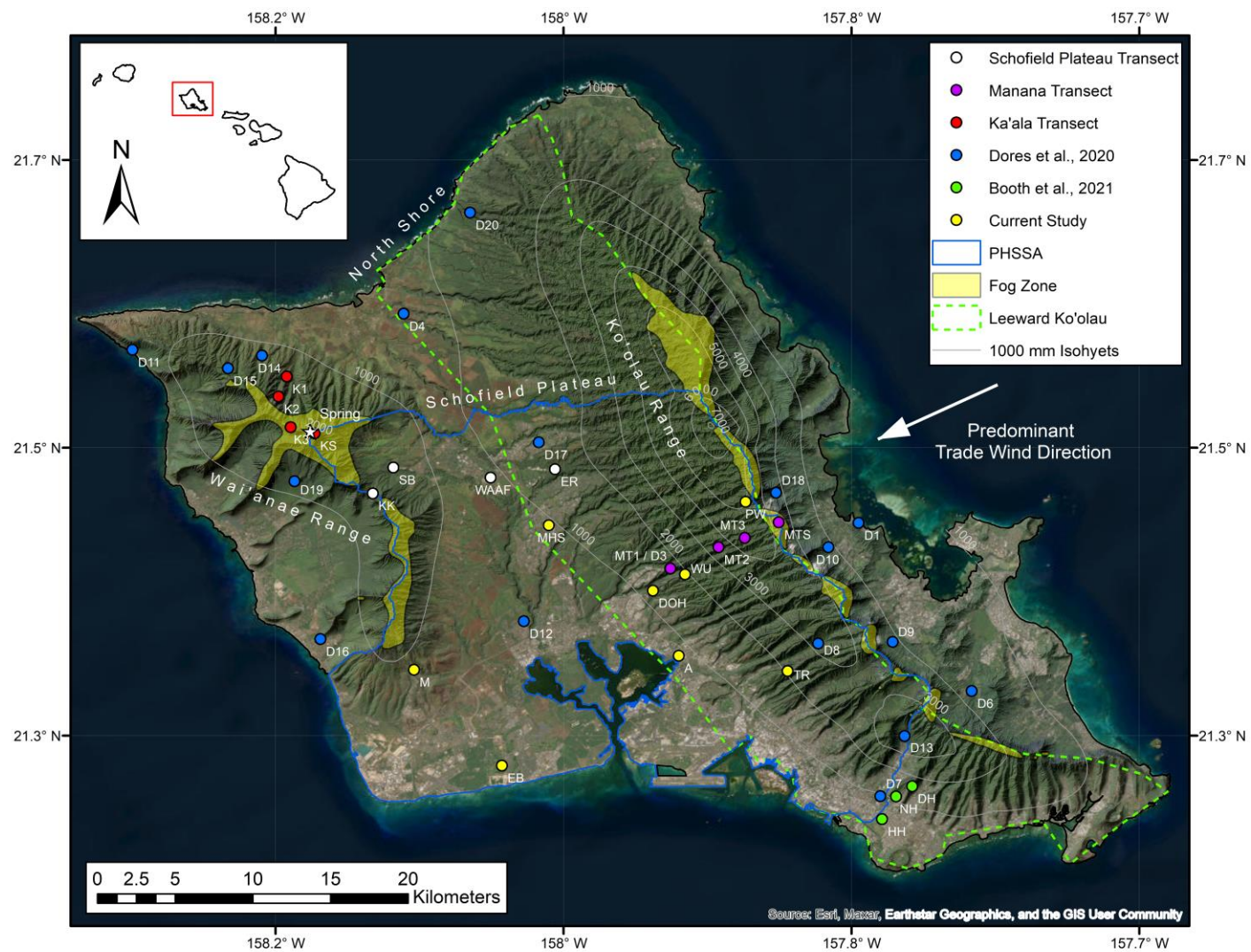


Figure 1. Bulk precipitation chemistry collector locations on the island of O'ahu, HI, USA sampled from March 2018 to August 2021. Collectors are colored by study source and by elevation transect. The boundaries of the Pearl Harbor Sole-Source Aquifer (PHSSA) are outlined in red. 1000 mm rainfall isohyets are shown in gray. Fog zones were identified by highlighting areas above 600m amsl. Collectors D3 and MT1 were co-located but sampled at different periods. The datum is NAD 1983.

## 2. Methods

### 2.1. Water Stable Isotope Fundamentals

There are three stable isotopes of oxygen and two of hydrogen. The heavy isotopologues  $^{18}\text{O}$  and  $^2\text{H}$ , or deuterium, have natural abundances high enough to allow reliable detection. Abundances are typically expressed in delta-notation, which relates  $^{18}\text{O}$  and  $^2\text{H}$  concentrations to standard mean ocean water (SMOW) following (Craig, 1961) and others, according to the expression:

$$\delta(\text{in } \text{\textperthousand}) = \frac{R_x}{R_s - 1} \cdot 1000 \quad (1)$$

, where  $R$  denotes the ratio of the heavy to light isotope, and the subscripts  $x$  and  $s$  denote the sample and standard (SMOW), respectively. The  $\delta^{18}\text{O}$  and  $\delta^2\text{H}$  of meteoric waters are strongly correlated in precipitation globally (Dansgaard, 1964). This linear relationship is expressed as the Global Meteoric Water Line (GMWL) according to the expression:

$$\delta^2\text{H} = 8 \cdot \delta^{18}\text{O} + 10 \quad (2)$$

The meteoric water line relation also varies locally. The establishment of a local meteoric water line (LMWL) usually precedes the application of stable isotope tracer methods (Scholl et al., 1995; Davis et al., 1970). Deuterium excess (d-excess) is the composition of  $^2\text{H}$  in water relative to the 8-to-1 permille ratio of  $\delta^2\text{H}$  and  $\delta^{18}\text{O}$ . Deuterium excess can be calculated by rearranging the GMWL and LMWL expressions to solve for the y-intercept, such that:

$$d = \delta^2\text{H} - 8 \cdot \delta^{18}\text{O} \quad (3)$$

, where  $d$  represents d-excess. Deuterium excess fluctuates in meteoric waters due to the different mass-dependent diffusivities of  $^1\text{H}^2\text{H}^{16}\text{O}$  (molar mass = 19 g mol $^{-1}$ ) and  $^1\text{H}_2^{18}\text{O}$  (molar mass = 20 g mol $^{-1}$ ), which impacts kinetic fractionation processes (Kendall & McDonnell, 1998).

Deuterium excess production is strongly governed by temperature and relative humidity. Many studies have documented seasonal patterns in the d-excess of precipitation, finding lower d-excess values during warm seasons due to increased relative humidity (Natali et al., 2022; Dores et al., 2020; Booth et al., 2021; Guan et al., 2013).

### 2.2. Study Region Isoscape

Strong seasonal weather trends, severe physiography, and marine atmospheric influences create a dynamic isoscape with semi-predictable seasonal and spatial patterns. The study area is centered on the Pearl Harbor Sole Source Aquifer (PHSSA), which occupies the southern third

of O‘ahu and encompasses the majority of the island’s urban sprawl (Figure 1). Two steep volcanic ranges dominate the physiography, the older Wai‘anae Range in the west reaching approximately 1200m above mean sea level (amsl), and the Ko‘olau Range in the east reaching 900m amsl (Sherrod et al., 2021). These volcanic ranges are connected by a central saddle called the Schofield Plateau. O‘ahu’s topography has created a rain shadow effect that divides the island into distinct windward and leeward regions. Northeast-facing windward slopes receive abundant rainfall and are characterized by deep amphitheater valleys with steep intervening ridgelines, abundant streams and waterfalls, and thick vegetation. The drier leeward regions in south-central and southwest O‘ahu generally receive less than 500mm of rainfall a year and are characterized by semi-arid, mesquite forest scrub lands.

Elevation gradients on O‘ahu are severe, and the topography exerts a strong influence on weather patterns and, thus, precipitation isotopic composition. Persistent northeasterly trade winds bring warm, humid air to the island, which is lifted and cooled as it passes over the Ko‘olau and Wai‘anae Ranges, lowering atmospheric vapor pressure and causing condensation (Wahl & Urey, 1935). The trade winds persist approximately 90% of the time during the dry season (May – October) and 50% of the time during the wet season (November – April) (Giambelluca, 1983), and generally bring precipitation with an isotopic signature in the 0 to -5 ‰  $\delta^{18}\text{O}$  range (Torri et al., 2023; Booth et al., 2021; Dores et al., 2020). Trade wind-driven orographic precipitation is thought to constitute approximately 70% of O‘ahu’s total annual precipitation (Longman et al., 2021).

Synoptic, disturbance-based weather patterns generate the remaining 30% of O‘ahu’s precipitation. Synoptic storms, which tend to be highly depleted in heavy isotopes (Booth et al., 2021; Torri et al., 2023), supply most of the precipitation to leeward areas (Dores et al., 2020). Synoptic systems include cold fronts, upper-tropospheric troughs, Kona lows, and tropical cyclones, and, excepting tropical cyclones, occur more frequently in the wet season (Torri et al., 2023). The systematic differences between orographic and synoptic precipitation stable isotope compositions present a challenge in defining regional isoscapes. Since these rainfall sources are not spatially or temporally uniform, they influence regional isoscapes to varying degrees at different times throughout the year. A moisture parcel’s origin and evolution must, therefore, be considered when using stable isotope tracer methods to examine connections between rainfall and groundwater.

### 2.3. Water Chemistry Data Collection

Twenty precipitation collectors were deployed throughout the study region to assess bulk precipitation chemistry (Figure 1; Table 1). Sampling for stable isotope composition occurred approximately quarterly. This is the same sample collection location, sampling period, and frequency as described by (Brennis et al., 2023), where major ions (not stable isotopes) are the focus. Three elevation transects with four collectors each were sampled to evaluate the impacts of the altitude effect on stable isotope composition (Figure 1). The first elevation transect was deployed along the Manana Ridge trail within the ‘Ewa Forest and had collectors distributed between 291 m (MT1) and 806 m amsl (MTS). The second elevation transect was deployed along Mount Ka‘ala Road and had collectors distributed between 290 m amsl (K1) and the summit of Mount Ka‘ala, which is the highest point on O‘ahu at 1212 m amsl (KS). A high-elevation perennial spring just below the summit of Mount Ka‘ala was also sampled from October 2019 to April 2021 (Figure 2). A third transect was deployed along the Schofield Plateau, with four collectors distributed generally east-to-west, connecting the Wai‘anae Range to the foot of the Ko‘olau Range. Precipitation collectors were of the same design used by Fackrell et al. (2020), Scholl et al. (1995; 2002), Dores et al. (2020), Booth et al. (2021) and Tachera et al. (2021) (Figure 3). Samples were collected in a triple-deionized-rinsed 500 mL or 60 mL HPDE bottle. The sample bottles were filled completely, forming a convex meniscus at the container mouth to minimize air bubbles, and were refrigerated within six hours of collection to minimize chemical reactions.

### 2.4. Chemical Analysis

Samples were analyzed at one of two laboratories: the Isotope Biogeochemistry Laboratory at the University of Hawai‘i at Mānoa or the Stable Isotope Ratio Facility for Environmental Research (SIRFER) at the University of Utah. Both facilities determined hydrogen and oxygen isotopic composition of rainwater using a Picarro L2130-I cavity ring-down spectrometer equipped with a high-precision vaporizer (V1102-I, Picarro, Inc., Santa Clara, CA, USA) and autosampler (HTC PAL, Leap Technologies, Carrboro, NC, USA) with Chem-Correct acquisition software that monitors for interference of isotopologues of water by organic compounds (Gupta et al., 2009). All measurements were performed in the nitrogen carrier mode, using ultra-high-purity nitrogen (< 10 ppm H<sub>2</sub>O, > 99.99% N<sub>2</sub>; Matheson, Irving, TX, USA)

using eight 1.2  $\mu\text{L}$  injections. Analytical precision determined through duplicate sampling indicates variances of  $\pm 0.35 \text{ ‰}$   $\delta^{18}\text{O}$  and  $\pm 1.32 \text{ ‰}$   $\delta^2\text{H}$ .

## 2.5. Local Meteoric Water Line

A LMWL was determined by combining the precipitation stable isotope data from this study with the data from Dores et al. (2020), and Booth et al. (2022) into one dataset, which we refer to hereafter as the combined dataset, and testing two different linear regressions: reduced major axis (RMA), and precipitation-weighted reduced major axis (PW-RMA). These were compared using three difference measures: root mean square error (RMSE), mean absolute error (MAE), and index of agreement (IA) following (Wilmott & Wicks, 1980) and (Wilmott, 1981; Wilmott, 1982a; Wilmott, 1982b). The regression with the lowest RMSE and MAE, and the highest IA was assumed to be the closest representation of O‘ahu’s LMWL.

## 2.6. Statistical Analysis: Amount and Altitude Effect

Regression analysis was performed to quantify the impact of the amount and altitude effects on precipitation stable isotope composition in the study area. To test the amount effect, individual sample precipitation  $\delta^{18}\text{O}$  was plotted against sample rainfall rates. This procedure was carried out on the combined dataset and on subsets of the dataset where we speculate that there may be distinct isotopic microclimate regimes. The dataset was subdivided by season (dry, wet, or split) and collector location. Samples were categorized as “split season” if the sample period covered a month or more in both the dry and wet seasons. Collectors were grouped into one of eight regions based on geographic location and general climate trends. Regression fits were scored by the Spearman correlation coefficient and p-test. Subsets with p-tests less than or equal to 0.05 and Spearman scores greater than 0.5 were assumed to represent non-negligible correlations. Due to wide variability in rainfall rates and similar cumulative distribution functions, rainfall rates were normalized and given a percentile score between 0 and 1, following Torri et al. (2023). The intent of examining these subsets was to explore whether the amount effect influenced precipitation chemistry more strongly in certain regions and in certain seasons. Similarly, we assessed the altitude effect by plotting precipitation volume-weighted average (VWA) isotopic composition against collector elevation. Precipitation volume-weighted averages were used because of our interest in the hydrologic connectivity between precipitation

and groundwater, since precipitation amount and recharge volume tend to be strongly correlated on O‘ahu (Engott et al., 2017).

## 2.7. Weather Trend Analysis

Weather trend analysis was used to differentiate orographic and synoptic precipitation events, which allowed us to examine the origin and evolution of meteoric water more closely. Distinctions between orographic and synoptic precipitation were made by i) using observations from monthly weather summaries provided by the National Oceanic and Atmospheric Administration (NOAA/NWS, 2023), and ii) analyzing weather data from the International Global Radiosonde Archive (IGRA; Durre et al., 2016). The NOAA summaries identify instances of rainfall associated with cold fronts, Kona lows, upper-level lows, and tropical cyclones impacting O‘ahu. The IGRA contains meteorological measurements collected from daily weather balloon launches at Līhue, Kauai. These measurements include elevation profiles detailing wind direction and speed for each launch. The IGRA data were filtered by isolating readings below 2500 meters amsl, a height typically associated with the upper limit of the trade wind regime over Hawai‘i (Cao et al., 2007). Days in which the average wind direction below 2500m amsl ranged from 22° to 112° from North were categorized as trade wind days. These categorizations were cross-referenced with data from monthly NOAA summaries. The results from this analysis were overlaid on the precipitation chemistry data utilizing “rug” plots, which are a plot enhancement that display variable frequency as tick marks along an axis (Wickam, et al., 2016)



Figure 2. Perennial high elevation spring along Mount Ka‘ala Road at 945m amsl. Sunglasses are shown at the bottom for scale.

Figure 3. Left. Design of HPDE bucket style bulk precipitation collectors deployed throughout the study region. Right: Collector deployed along the Tripler Ridge hiking trail (TR) within the ‘Ewa Forest Reserve, O‘ahu, HI, USA.

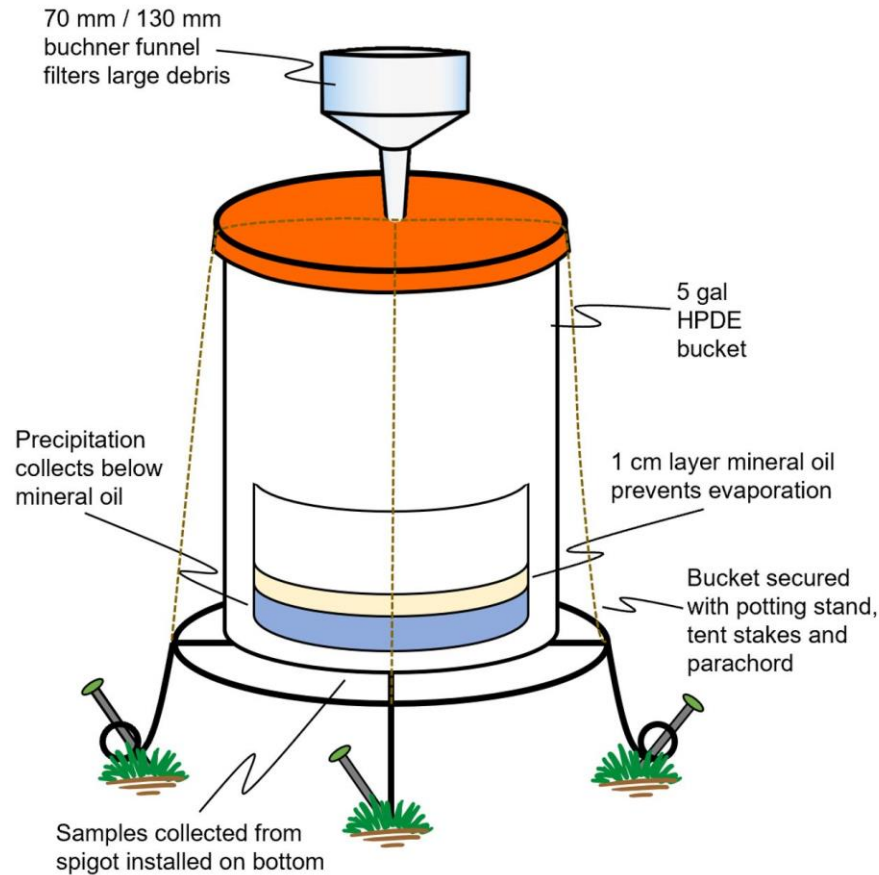


Table 1. Rainfall volume-weighted average H and O composition from precipitation collectors sampled between March 2018 and August 2021. Collectors beginning with the letter “D” are from Dores et al. (2020). The three Honolulu collectors are from Booth et al. (2021). Deuterium excess uncertainty is  $\pm 3.1\text{\textperthousand}$  for all collectors.

Collector	Location	Region	Elev. (m)	Longitude	Latitude	$\delta^{18}\text{O}$	$\delta^2\text{H}$	$\delta^2\text{H-Excess}$
K1	Ka'ala Base	Windward Wai'anae	290	-158.1601	21.5412	-3.41 $\pm$ 0.69	-14.56 $\pm$ 1.40	12.73
K2	Ka'ala #2	Windward Wai'anae	553	-158.1649	21.5296	-4.05 $\pm$ 0.76	-17.20 $\pm$ 1.54	15.19
K3	Ka'ala #3	Windward Wai'anae	930	-158.1578	21.5119	-4.14 $\pm$ 0.74	-16.59 $\pm$ 1.46	16.50
KS	Ka'ala Summit	Windward Wai'anae	1212	-158.1440	21.5083	-4.52 $\pm$ 0.70	-19.67 $\pm$ 1.43	16.48
MT1	Manana Base	Leeward Ko'olau	291	-157.9380	21.4301	-2.39 $\pm$ 0.62	-7.51 $\pm$ 1.17	11.64
MT2	Manana #2	Leeward Ko'olau	452	-157.9102	21.4424	-2.70 $\pm$ 0.63	-7.38 $\pm$ 1.20	14.18
MT3	Manana #3	Leeward Ko'olau	549	-157.8950	21.4478	-2.92 $\pm$ 0.62	-8.58 $\pm$ 1.19	14.74
MTS	Manana Summit	Leeward Ko'olau	806	-157.8754	21.4568	-3.56 $\pm$ 0.71	-13.25 $\pm$ 1.38	15.26
EB	'Ewa Beach	Leeward	7	-158.0355	21.3159	-4.23 $\pm$ 0.92	-22.88 $\pm$ 2.09	10.94
TR	Tripler Ridge	Leeward Ko'olau	380	-157.8702	21.3707	-2.45 $\pm$ 0.65	-7.88 $\pm$ 1.23	11.69
M	Makakilo	Leeward	335	-158.0864	21.3714	-4.15 $\pm$ 0.82	-20.61 $\pm$ 1.78	12.62
KK	Kolekole Pass	Windward Wai'anae	557	-158.1103	21.4735	-3.12 $\pm$ 0.72	-11.10 $\pm$ 1.39	13.83
SB	Schofield Barracks	Windward Wai'anae	371	-158.0984	21.4885	-3.69 $\pm$ 0.90	-17.37 $\pm$ 1.94	12.18
WAAF	Wheeler Army Airfield	Central	270	-158.0421	21.4827	-2.99 $\pm$ 0.70	-12.01 $\pm$ 1.38	11.93
ER	East Range	Leeward Ko'olau	306	-158.0048	21.4875	-2.67 $\pm$ 0.69	-8.64 $\pm$ 1.27	12.71
HH	Kapahulu	Honolulu	3	-157.8155	21.2850	-2.65 $\pm$ 0.81	-12.92 $\pm$ 1.70	8.24
NH	Lower Wa'ahila Ridge	Honolulu	148	-157.8074	21.2980	-3.02 $\pm$ 0.83	-14.41 $\pm$ 1.73	9.77
DH	Upper Wa'ahila Ridge	Honolulu	311	-157.7981	21.3040	-3.01 $\pm$ 0.78	-13.10 $\pm$ 1.56	10.98
D1	Kamehameha Hwy	Windward Ko'olau	6	-157.8291	21.4564	-3.40 $\pm$ 0.73	-14.47 $\pm$ 1.47	12.76
D3	Manana Base	Leeward Ko'olau	291	-157.9381	21.4300	-2.73 $\pm$ 0.68	-9.14 $\pm$ 1.29	12.69
D4	Hale'iwa Wells	Central	291	-158.0924	21.5775	-2.75 $\pm$ 0.72	-10.10 $\pm$ 1.42	11.92
D6	Hawai'i Ag. Center	Windward Ko'olau	111	-157.7636	21.3591	-2.51 $\pm$ 0.62	-6.46 $\pm$ 1.18	13.61
D7	UHM	Honolulu	22	-157.8165	21.2982	-2.72 $\pm$ 0.70	-11.50 $\pm$ 1.41	10.27
D9	Ho'omaluhia B.G.	Windward Ko'olau	65	-157.8094	21.3875	-2.34 $\pm$ 0.63	-5.19 $\pm$ 1.19	13.51
D10	Kahalu'u Ridge	Windward Ko'olau	100	-157.8466	21.4424	-2.75 $\pm$ 0.63	-8.08 $\pm$ 1.21	13.88
D11	Ka'ena Point	Leeward	11	-158.2494	21.5567	-2.49 $\pm$ 0.69	-8.23 $\pm$ 1.34	11.72
D12	Kunia III Wells	Central	98	-158.0228	21.3995	-3.55 $\pm$ 0.96	-16.95 $\pm$ 2.07	11.42
D13	Lyon Arboretum	Leeward Ko'olau	152	-157.8025	21.3331	-1.91 $\pm$ 0.60	-4.07 $\pm$ 0.86	11.22
D14	Mokuleia F.R. #1	Waianae	167	-158.1744	21.5533	-3.21 $\pm$ 0.73	-12.88 $\pm$ 1.44	12.78
D15	Mokuleia F.R. #2	Waianae	610	-158.1941	21.5459	-3.51 $\pm$ 0.77	-13.09 $\pm$ 1.49	14.99
D17	Wahiawa B.G.	Leeward Ko'olau	308	-158.0142	21.5031	-2.52 $\pm$ 0.66	-7.99 $\pm$ 1.26	12.21
D18	Waiāhole F.R.	Windward Ko'olau	190	-157.8769	21.4739	-2.67 $\pm$ 0.62	-6.91 $\pm$ 1.19	14.48
D19	Wai'anae Kai	Leeward	262	-158.1556	21.4806	-2.06 $\pm$ 0.62	-7.52 $\pm$ 1.21	8.95
D20	Waimea Valley	Central	4	-158.0540	21.6361	-2.04 $\pm$ 0.63	-4.76 $\pm$ 1.19	11.54
A	Aiea	Leeward Ko'olau	13	-157.9332	21.3795	-3.05 $\pm$ 0.79	-14.82 $\pm$ 1.64	9.59
DOH	DOH	Leeward Ko'olau	154	-157.9481	21.4172	-2.67 $\pm$ 0.71	-10.59 $\pm$ 1.33	10.73
WU	Waimano Upland	Leeward Ko'olau	330	-157.9296	21.4266	-2.75 $\pm$ 0.71	-9.86 $\pm$ 1.32	12.11

### 3. Results

#### 3.1. Rainfall H and O isotopic composition

The isotopic composition of rainfall in the study area showed strong spatial and seasonal trends and was generally consistent with the narrow isotopic range of marine precipitation (Gat, 1996). Precipitation VWA  $\delta^{18}\text{O}$  varied narrowly from -4.5 ‰ at Ka‘ala Summit (KS) to -1.9 ‰ at Lyon Arboretum (D13). Precipitation VWA  $\delta^2\text{H}$  varied from -22.9 ‰ at Ewa Beach (EB) to -4.1 ‰ at Lyon Arboretum (D13). Excluding storm samples taken by Booth et al. (2021), individual sample composition ranged from -5.9 ‰  $\delta^{18}\text{O}$  at Ewa Beach (EB) to -1.1 ‰  $\delta^{18}\text{O}$  at Manana Trail (MT1), and  $\delta^2\text{H}$  composition ranged from -35.7 ‰ at Ewa Beach (EB) to -3.7 ‰ at Tripler Ridge (TR). Figure 4 displays an interpolated coverage of the VWA  $\delta^{18}\text{O}$  composition of rainfall. Rainfall tended to be more enriched in heavy isotopes in the Ko‘olau Range and in valleys and isotopically lighter in leeward O‘ahu and the Wai‘anae Range (Figure 4). Figure 5 displays a time series of precipitation  $\delta^{18}\text{O}$  with weather patterns derived from the NOAA and IGRA data overlain. Figure 5 shows that wet seasons tended to bring isotopically lighter rainfall and higher rainfall rates, particularly during periods when there were disruptions to the trade wind regime. Dry seasons tended to produce isotopically heavy rainfall (i.e., closer to SMOW) and lower rainfall amounts, which is consistent with weather patterns reported by Longman et al. (2021) and other studies.

#### 3.2. Local Meteoric Water Line

The RMA regression produced the best results, with a RMSE of 3.02, a MAE of 2.24, an IA of 0.98, a Spearman correlation of 0.91,  $p < 0.001$ , a slope of  $7.21 \pm 0.45$ , and an intercept of  $9.58 \pm 1.16$  (Figure 6; Table 2), resulting in the following LMWL:

$$\delta^2\text{H} = 7.2 \cdot \delta^{18}\text{O} + 9.6 \quad (4)$$

The PW-RMA regression also produced strong results (Table 2), resulting in a similar LMWL:

$$\delta^2\text{H} = 7.1 \cdot \delta^{18}\text{O} + 9.9 \quad (5)$$

All O‘ahu LMWLs considered, including ones from previous studies, had slopes below the 8-to-1  $\delta^2\text{H}$ - $\delta^{18}\text{O}$  ratio in the GMWL, indicating a generally higher composition of  ${}^1\text{H}_2{}^{18}\text{O}$  vs.  ${}^1\text{H}^2\text{H}{}^{16}\text{O}$ . There was an observable seasonal impact on the LMWL, with the wet season LMWL showing a 1.4 ‰ increase in  $\delta^2\text{H}$  (Figure 7).

### 3.3. Amount Effect

Regression analysis of  $\delta^{18}\text{O}$  vs. rainfall rates shows that rainfall isotopic composition did not vary appreciably with rainfall rate, which indicates the amount effect was not a major factor controlling the stable isotope composition of rainfall on O‘ahu. Excluding individual storm samples, regression analysis on the combined dataset produced poor results ( $r^2 = 0.11$ ,  $p < 0.001$ ). Table 3 summarizes the results of regression analysis on subsets of the combined dataset broken down by collector region and by sample season. The results from this analysis show that for all subsets of collector region and sample season, only two met the Spearman and p-test criteria: the dry season windward sample group and the spilt season North Shore sample group. Interestingly, the North Shore split season subset showed a positive correlation between rainfall rate and  $\delta^{18}\text{O}$ , which is the opposite of what would be expected in samples impacted by the amount effect. Overall, the regression analysis results show that the amount effect was weak and localized, if not negligible, within the dataset.

### 3.4. Altitude Effect

Figure 8 shows the key trends observed in elevation- $\delta^{18}\text{O}$  lapse rates within the study area. The  $\delta^{18}\text{O}$ -elevation relationships were similar to those found in other parts of the Hawaiian Islands (Tachera et al., 2021; Dores et al., 2020; Fackrell et al., 2020; Scholl et al., 1996; Booth et al., 2022; Torri et al., 2023), and to the average global lapse rate of  $-0.28\text{‰}/100\text{m}$  (Poage & Chamberlain, 2011). Of the three elevation transects sampled in this study, the Manana Ridge transect showed the strongest lapse rate, with a depletion of approximately  $0.23\text{‰} \delta^{18}\text{O}$  for every  $100\text{m}$  of elevation gain, and a 0.99 Spearman correlation coefficient. Several other collectors located in the leeward Ko‘olau Range plotted close to the Manana elevation lapse rate line (Figure 8). The Ka‘ala transect produced a depletion rate of  $0.11\text{‰} \delta^{18}\text{O}$  for every  $100\text{m}$  of elevation gain, and a 0.82 Spearman correlation coefficient. The Ka‘ala lapse rate was  $0.5\text{--}1.0\text{‰}$  depleted in  $^{18}\text{O}$  relative to the Manana transect. The Schofield Plateau transect did not produce a discernable lapse rate but rather seemed to straddle those of the Manana and Ka‘ala, possibly representing a transition zone between two distinct regimes. Within the Schofield Plateau transect, the Kolekole collector (KK) produced an unexpectedly enriched VWA  $\delta^{18}\text{O}$  value, which created a dramatic kink in the elevation lapse rate, giving it a “U” shape (Figure 8). No clear regional or island-wide elevation lapse rates could be established. Regression analysis of all

leeward Ko‘olau collectors (MT1, MT2, MT3, MTS, A, DOH, WU, D3, D17, ER) produced a poor fit, with a Spearman correlation coefficient of 0.17 and  $p = 0.11$ .

### 3.5. Deuterium Excess

There was a strong correlation between VWA d-excess and elevation for collectors in several regions of the study area (Figure 9). The strongest correlations were found among collectors in the leeward Ko‘olau and windward Wai‘anae ranges. For the leeward Ko‘olau collectors, regression analysis produced a Spearman correlation coefficient of 0.85,  $p < 0.01$ , and a d-excess enrichment rate of 0.76 ‰ per 100m of elevation gain (Figure 10B). For the Wai‘anae collectors, regression analysis produced a Spearman correlation coefficient of 0.78,  $p < 0.002$ , and a d-excess enrichment rate of 0.45 ‰ per 100m of elevation gain (Figure 10B). There is a moderately strong correlation between island-wide VWA d-excess and collector elevation, with regression analysis producing a Spearman correlation coefficient of 0.51,  $p < 0.01$ , and a d-excess enrichment rate of 0.52 ‰ per 100m of elevation gain (Figure 10A). Deuterium excess also varied semi-predictably with season, with wet seasons bringing higher d-excess in rainfall.

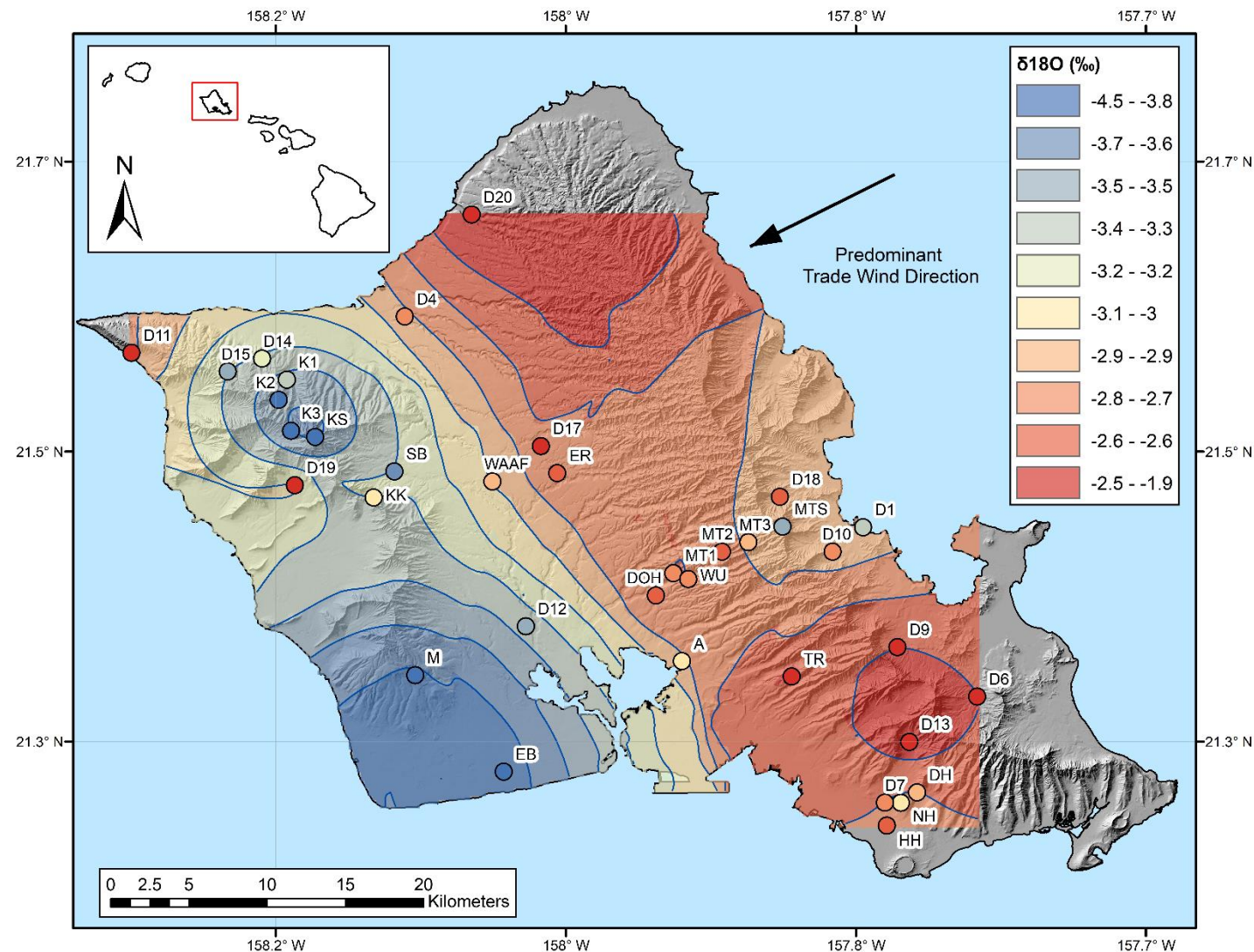


Figure 4. Precipitation volume-weighted average  $\delta^{18}\text{O}$  (‰) map for O'ahu, HI, USA interpolated from bulk precipitation chemistry data collected between March 2017 and August 2021, plus data from Dores et al. (2020) and Booth et al. (2021). Contour intervals are shown in blue. The interpolation method was ordinary kriging, with coverage interpolated from data at the collector locations displayed. MT1 and D3 were collocated.

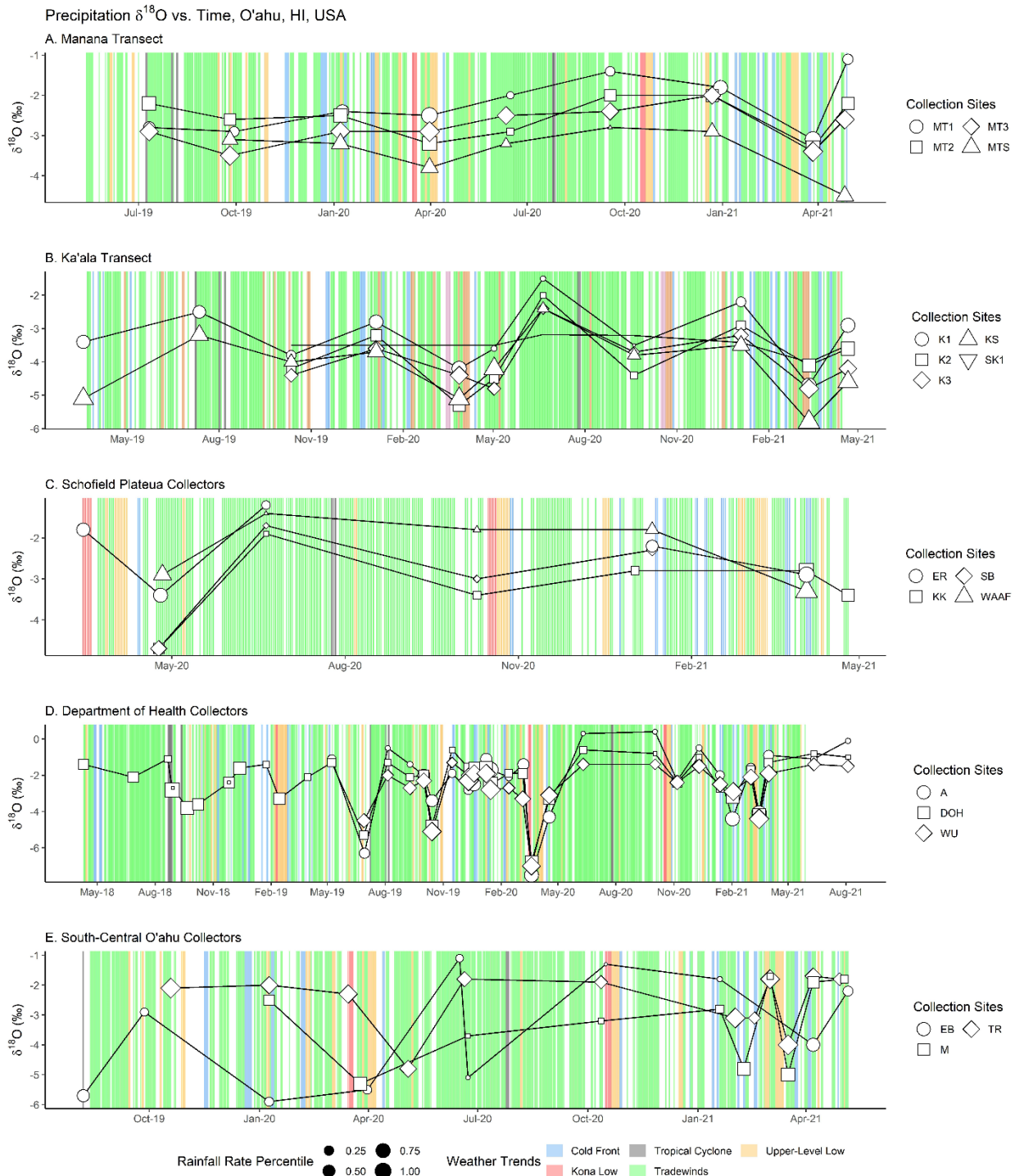


Figure 5. Time series of precipitation  $\delta^{18}\text{O}$  composition for 18 precipitation collectors sampled across the island of O'ahu, HI, USA from March 2018 to August 2021. Precipitation collectors are identified by shape and sample points are sized by normalized rainfall rate over the sample period. Weather trend data derived from International Global Radiosonde Archive (IGRA) weather balloon launches at Līhue, Kauai (Durre et al., 2016), and from monthly weather summaries provided by the National Oceanic and Atmospheric Administration (NOAA/NWS, 2023) are shown in the background.

## Local Meteoric Water Lines, O'ahu, HI, USA

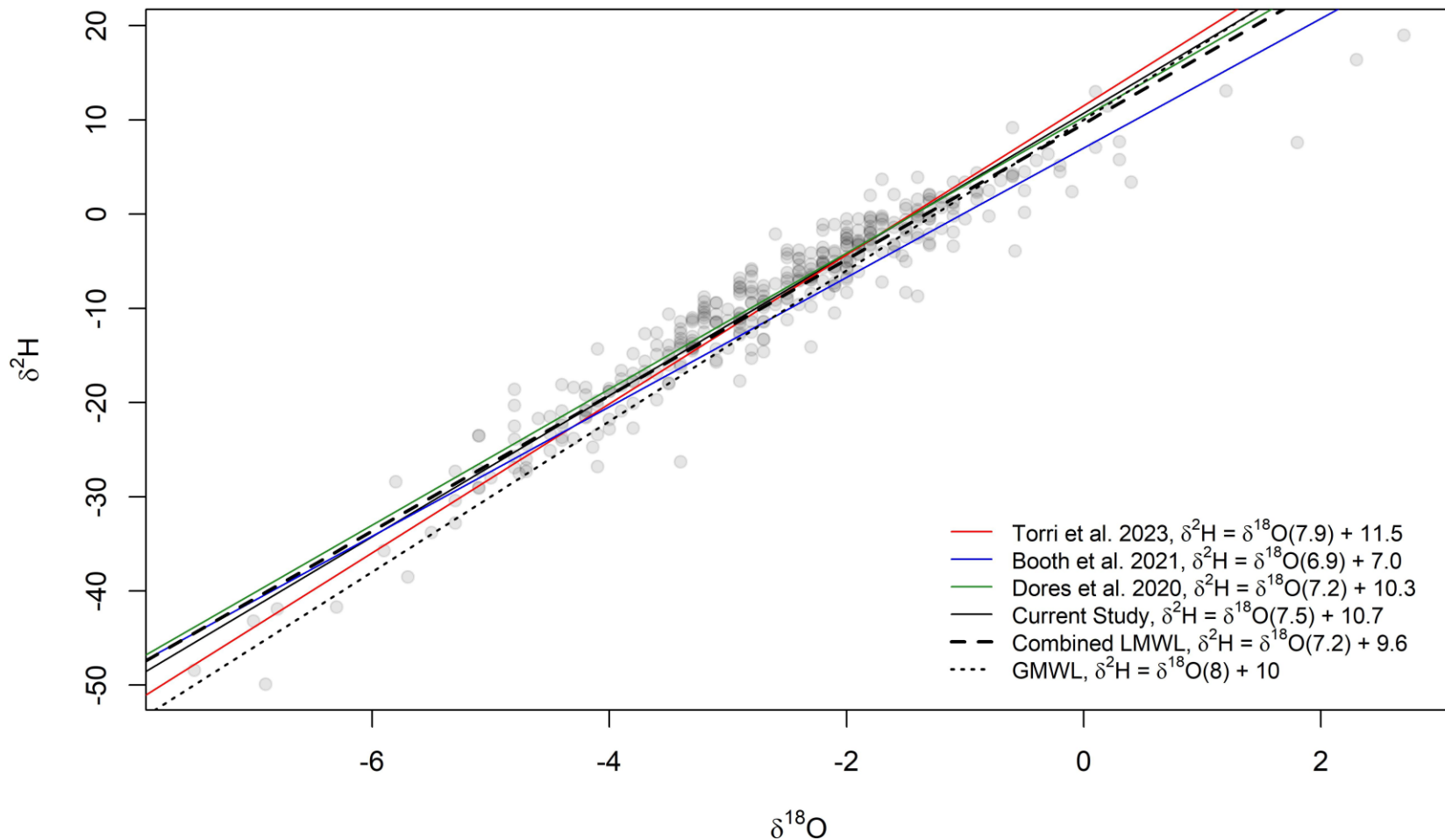


Figure 6. Local Meteoric Water Lines (LMWL) for O'ahu, HI, USA, derived from four different datasets compared to the Global Meteoric Water Line (GMWL). The combined LMWL presented in this study is not significantly different from those of other studies on O'ahu or from the GMWL.

Table 2. Results from regression analysis performed on two different methods for determining the Local Meteoric Water Line for O‘ahu, HI, USA from bulk precipitation chemistry data. Methods were compared in terms of Spearman correlation coefficient ( $R^2$ ), p-test, root mean square error (RMSE), mean absolute error (MAE), and index of agreement (IA), following Wilmott (1981, 1982a, 1982b) and Wilmott & Wicks (1980). Data from two other studies (Dores et al., 2020; Booth et al., 2021) were included in these analyses. P-test values for all regressions were less than 0.001.

	$R^2$	RMSE	MAE	IA
Reduced Major Axis	0.914	3.020	2.240	0.978
Precipitation Weighted Reduced Major Axis	0.859	3.045	2.221	0.977

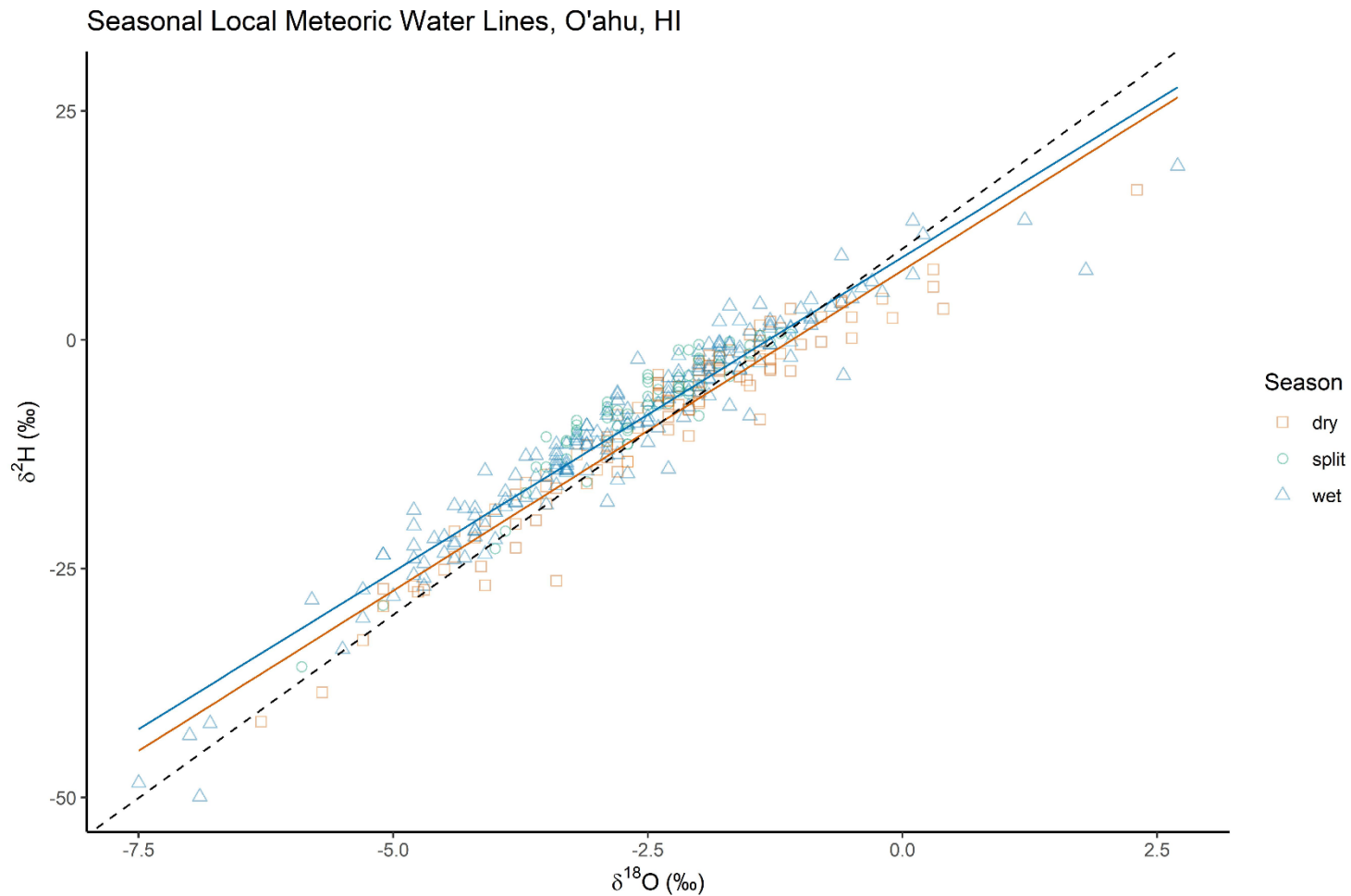


Figure 7. Seasonal Local Meteoric Water Lines (LMWL) for O'ahu, HI, USA, derived from the combined dataset. The wet season occurs from November – April. The dry season occurs May – October. Samples with more than 30 days in both wet and dry seasons were classified as split and removed from the seasonal LMWL calculation. The dashed line shows the GMWL. The blue and orange lines show the wet and dry season LMWLs, respectively.

Table 3. Amount effect regression analysis on the combined dataset. The windward dry season is the only data subset that shows a significant amount effect. The North Shore has two subsets showing strong positive correlations between rainfall rate percentile and rainfall isotopic composition, which counters what is expected. Abbreviations: n = sample group size; S = Spearman correlation coefficient; p = p-test score.

Location	Ka'ala			Manana			South Central			Central			Honolulu			Windward			North Shore			Leeward		
Season	n	S	p	n	S	p	n	S	p	n	S	p	n	S	p	n	S	p	n	S	p	n	S	p
Wet	24	0.12	0.06	13	-0.03	0.41	75	0.21	0.00	14	-0.04	0.49	19	0.20	0.03	7	-0.07	0.46	2	NA	NA	2	NA	NA
Split	10	0.32	0.05	15	-0.08	0.99	8	0.03	0.31	3	-0.80	0.79	6	-0.20	0.71	13	0.05	0.23	4	0.98	0.01	5	-0.33	0.95
Dry	13	0.31	0.03	12	-0.06	0.53	43	0.31	0.00	8	-0.16	0.91	10	-0.12	0.80	4	0.88	0.04	1	NA	NA	2	NA	NA
Combined	47	0.25	0.00	40	0.03	0.14	126	0.20	0.00	25	0.15	0.03	35	0.02	0.18	24	-0.03	0.57	7	0.57	0.03	9	0.12	0.19

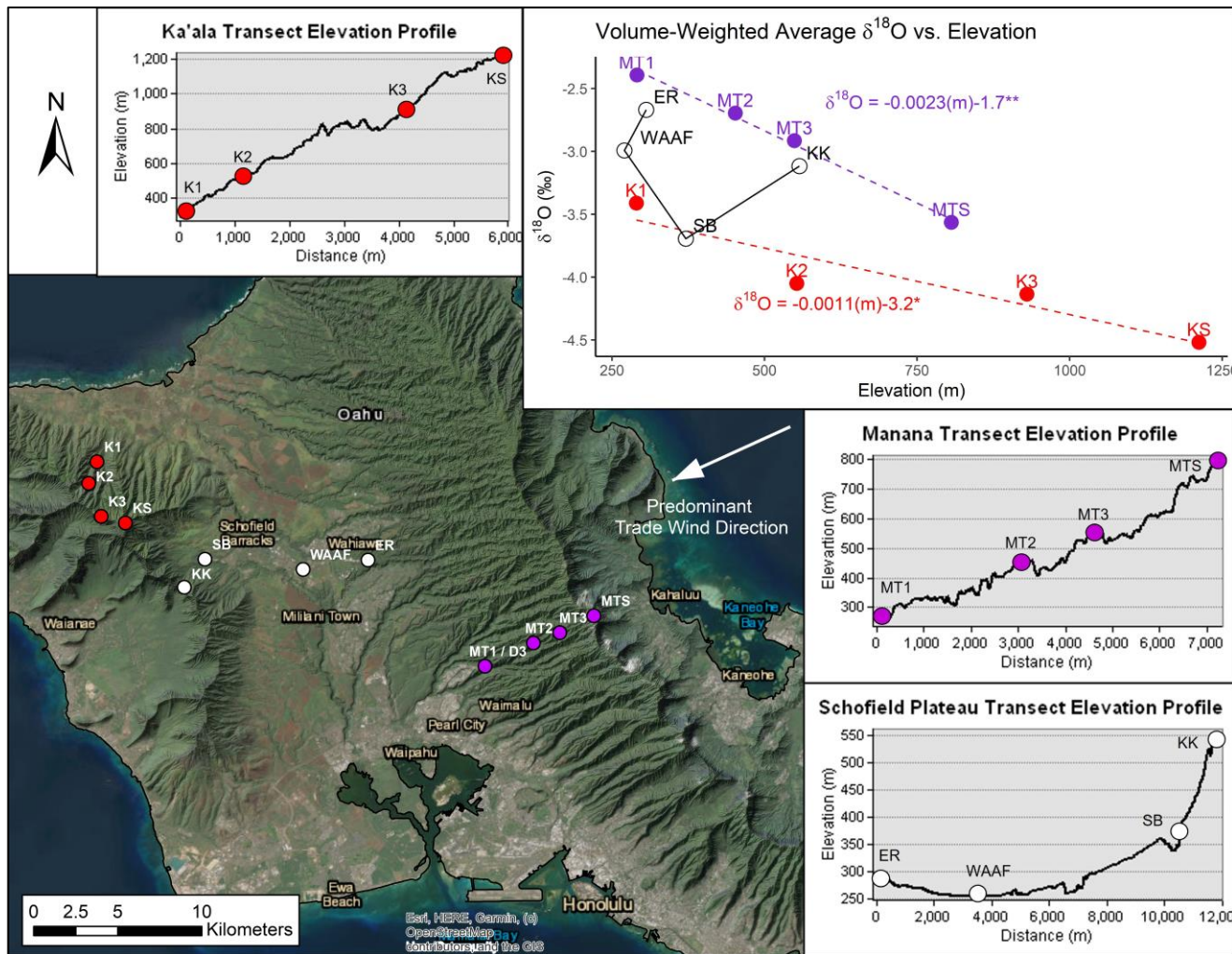


Figure 8. Precipitation volume-weighted average  $\delta^{18}\text{O}$ -elevation lapse rates from bulk precipitation samples on the island of O'ahu, HI, USA taken from March 2017 to August 2021. Three elevation transects are shown. The Manana transect is shown in purple and represents the leeward Ko'olau Range, where trade wind-driven precipitation dominates stable isotope composition. The Ka'ala transect is shown in red and represents the windward Wai'anae Range, where synoptic storms have a stronger influence on stable isotope composition. The Schofield Plateau transect is shown in white and shows traits intermediate between the Ko'olau and Wai'anae isotopic regimes. The dashed lines show ordinary least squares regressions for each transect.

Key: \* = P-value < 0.05; \*\* = 0.05 < P-value < 0.10.

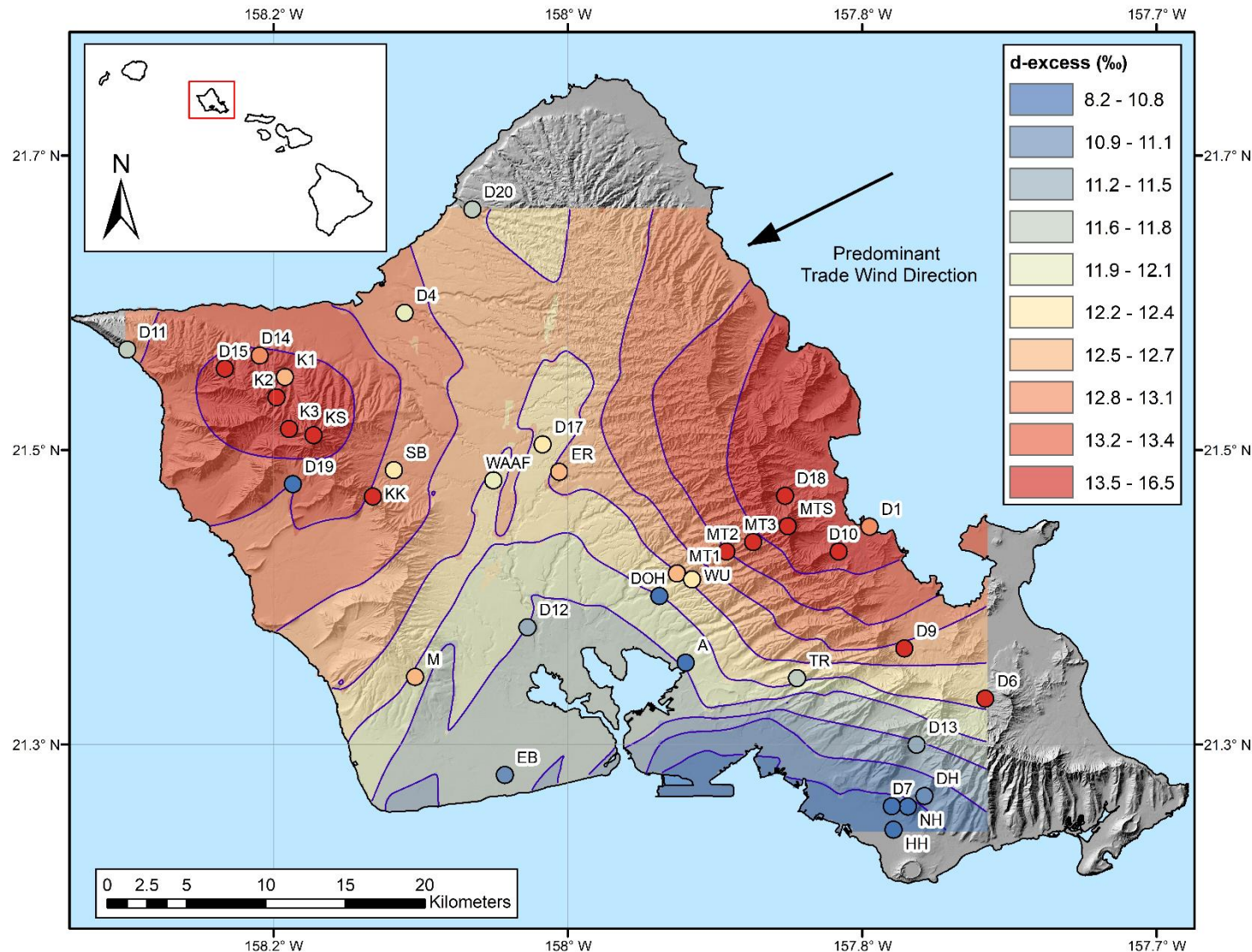


Figure 9. Precipitation volume-weighted average  $^2\text{H}$ -excess (‰) map for O'ahu, HI, USA interpolated from the combined bulk precipitation chemistry dataset, collected between March 2017 and August 2021. Contour intervals are shown in blue. The interpolation method was ordinary kriging. The coverage was interpolated from data at the collector locations displayed. MT1 and D3 were collocated.

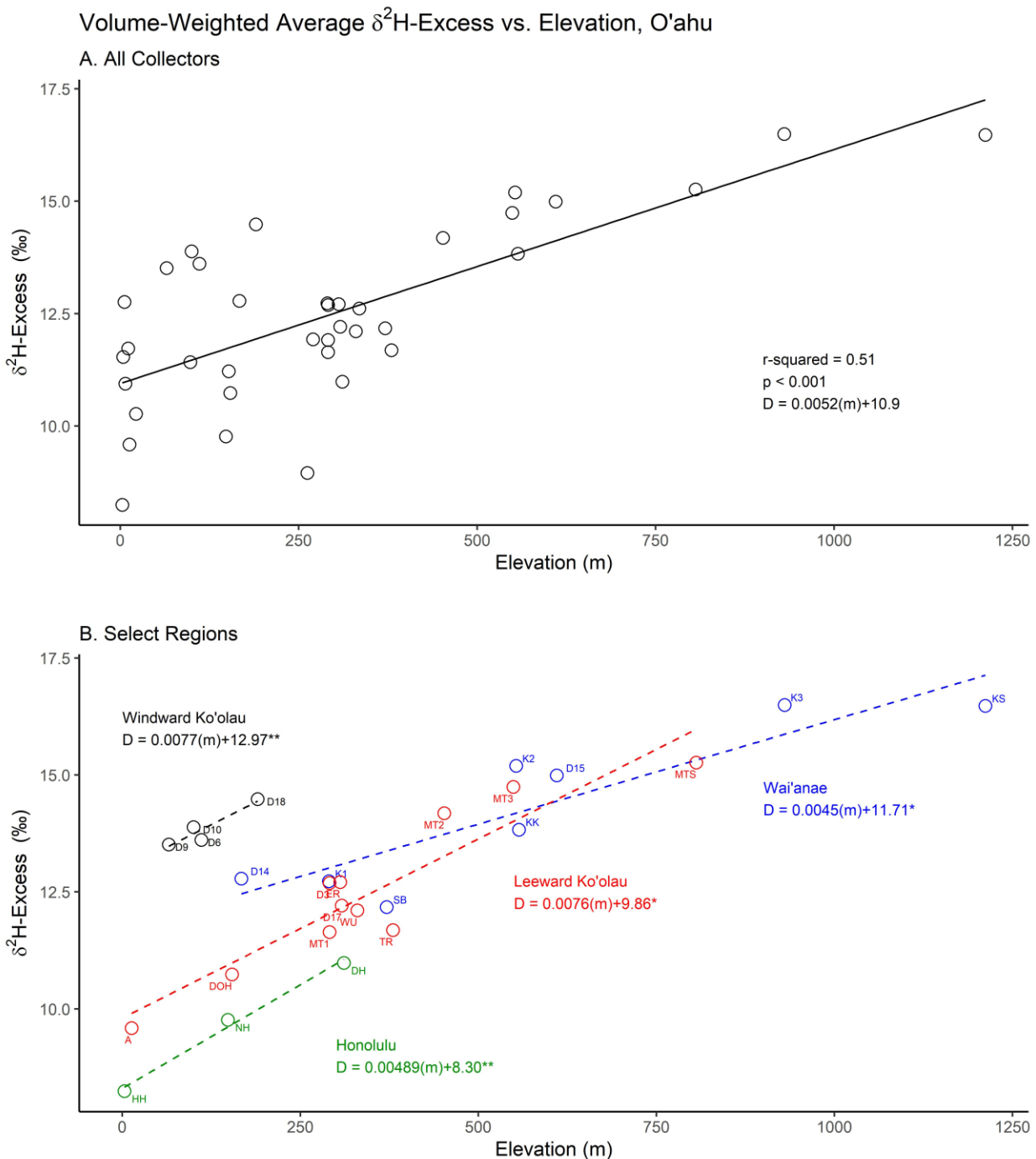


Figure 10. Precipitation volume-weighted average  $^2\text{H}$ -excess plotted against elevation for O‘ahu, HI, USA, from the combined bulk precipitation chemistry dataset collected between March 2017 and August 2021. A (top) = island-wide collectors. B (bottom) = select collectors located in key regions of the island. Key: \* = P-value <0.05; \*\* = 0.05 < P-value < 0.10.

## 4. Discussion

### 4.1. Altitude Effect

Our results show that the altitude effect exerts a strong influence on precipitation stable isotope composition on O‘ahu. In examining the strength of the various isotopic fractionation processes, it is important to isolate the ones that may be competing or pulling the isotopic composition in opposite directions. The previous examination of the relationship between sample rainfall rates and stable isotope compositions provides convincing evidence that the amount effect had a negligible influence on precipitation isotopic composition over the study period, which points to the altitude and rainout effects as the primary relations impacting O‘ahu’s isoscapes. Proceeding from this, several elevation transects produced strong linear regression fits, confirming that the altitude effect was observed in certain regions of the island. One of the key regions where a predictable  $\delta^{18}\text{O}$ -elevation lapse rate would be useful is the leeward portion of the Ko‘olau Range, which supplies more than half of O‘ahu’s groundwater recharge (Engott et al., 2017). Ten precipitation collectors resided within this region: the Department of Health (DOH), Aiea (A), Waimano Upland (WU), the Manana Transect (MT1/D3, MT2, MT3, MTS), Tripler Ridge (TR), East Range (ER), and Wahiawa Botanical Gardens (D17). These collectors produce poor fits when subjected to linear regression analysis, which does not, in our estimation, support the establishment of a leeward Ko‘olau  $\delta^{18}\text{O}$ -elevation lapse rate (Figure 11).

We speculate that the variable performance of the regional  $\delta^{18}\text{O}$ -elevation regressions is due to the seasonally dependent interactions between topography and the trade wind weather regime. At lower elevations on the leeward flank of the Ko‘olau Range, rainfall contributions from synoptic, disturbance-based storms are proportionally greater than the contributions from orographic precipitation. This is supported by isotope data from three locations within the leeward Ko‘olau region: Aiea (A, 13 m amsl), Department of Health (DOH, 154 m amsl), and Waimano Trail (WU, 330 m amsl) span an important transition zone where orographic precipitation begins to dominate local rainfall contributions. From sea level to approximately 100m amsl, long-term average annual precipitation increases gradually from 600mm per year to about 1000mm per year (Frazier & Giambelluca, 2017). Above 100m amsl, long-term average precipitation increases steeply, climbing to more than 5000mm per year over less than 400m of elevation gain (Frazier & Giambelluca, 2017). These three collectors represent a transition zone where synoptic versus orographic rainfall processes dominate the stable isotope composition of precipitation.

Figure 11 depicts the interplay between these two precipitation zones. Figure 11A shows the leeward Ko‘olau  $\delta^{18}\text{O}$ -elevation lapse rate before and after a correction for synoptic storm rainfall contributions. Figure 11A shows that the Aiea (A) and DOH collectors had unexpectedly low VWA  $\delta^{18}\text{O}$  compositions, which distorted the regional lapse rate. These collectors were set apart as being more heavily influenced by synoptic rainfall events. Figure 11B displays a time series of  $\delta^{18}\text{O}$  composition with weather patterns overlain. This plot shows that the deviation from the regional lapse rate was due to five individual samples, all of which were taken after a period of disturbance-based precipitation. These samples also stood out in that they generally had higher rainfall rate, and volume, and mirrored each other in terms of chemistry, which all point to a strong influence from synoptic rainfall events. Removing these samples from the VWA calculations produced a strong linear regression fit and a lapse rate nearly identical to that of the Manana transect (Figure 11A). These findings indicate that precipitation sources must be considered when estimating elevation lapse rates from raw  $\delta^{18}\text{O}$  and  $\delta^2\text{H}$  composition.

We suggest that d-excess may be a more reliable proxy to elevation on O‘ahu than  $\delta^{18}\text{O}$  or raw  $\delta^2\text{H}$  composition. Figure 10 shows that d-excess increased with elevation island-wide and that correlations were stronger when divided by region. We speculate that this correlation is related to temperature and humidity elevation gradients. The process of isotope fractionation is sensitive to temperature and humidity. This can be demonstrated by using the Craig-Gordon model for isotopic fractionation to predict the d-excess of vapor evaporated from the ocean surface at a range of temperatures and humidities, and then using the Rayleigh law to simulate rainout. Following Gat (1996), the  $\delta^{18}\text{O}$  and  $\delta^2\text{H}$  composition of vapor can be approximated as:

$$\delta_E = (\delta_w - h\delta_a - \epsilon)/(1 - h) \quad (6)$$

, where  $\delta_E$  is the isotopic composition of vapor evaporated from surface water,  $\delta_w$  and  $\delta_a$  are the isotopic compositions of surface water and atmospheric water vapor, respectively,  $h$  is relative humidity, and  $\epsilon$  is the kinetic isotope fractionation factor (Kendall & McDonnell, 1998, p.68). The kinetic isotope fractionation factor takes the form:

$$\epsilon = (1 - \alpha) \cdot 10^3 + (1 - h) \cdot \theta \cdot n \cdot \epsilon_k \quad (7)$$

, where  $\theta$  is a weighting term that has been shown to be equal to 0.5 for the Eastern Mediterranean Sea (Gat, et al., 1996) ,  $n$  is another weighting term that was set equal to 0.5 by Gat (1996), and  $\epsilon_k$  is a kinetic constant with values of 25.1 ‰ and 28.5 ‰ for  $\delta^2\text{H}$  and  $\delta^{18}\text{O}$ , respectively (Merlivat, 1978; Kendall & McDonnell, 1998, p.68). The term  $\alpha$  is the equilibrium

isotope fractionation factor, which is a temperature-dependent ratio of isotopic compositions (Friedman & O'Neil, 1977). The evolution of d-excess in a moisture system subject to rainout fractionation can be calculated by using the Rayleigh law formulated in approximate differential form:

$$\delta \approx \delta_E + (1 - \alpha) \cdot 10^3 \cdot \ln f \quad (8)$$

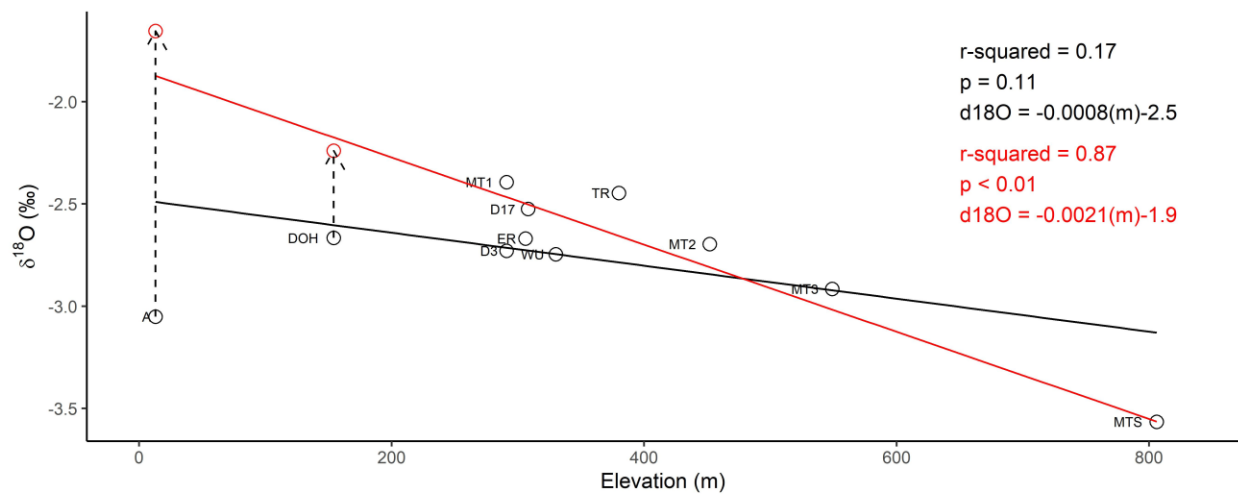
, where  $f$  is a number between 0 and 1 representing the remaining fraction of the original vapor mass (Kendall & McDonnell, 1998, p.66). This expression can be used to calculate the  $\delta^{18}\text{O}$  and  $\delta^2\text{H}$  composition of the residual vapor at each stage in the rainout process. The d-excess content of the vapor can then be calculated using the GMWL relation (Expression 3).

Figure 12 displays the results of this analysis. Figure 12A shows d-excess change vs. fraction of rainout with temperature changes denoted by color. This figure shows that d-excess change is most pronounced at higher temperatures and in the initial stages of rainout ( $0 < f < 0.15$ ). Storms originating in cooler regions could theoretically experience minimal d-excess change as they progress towards Hawai'i. Figure 12B shows that d-excess production is more sensitive to temperature and humidity changes than rainout. Intuitively, higher temperature and lower humidity result in higher d-excess.

We suggest a pseudo-orographic control on the values of d-excess within the study area. On O'ahu the mean annual temperature at sea level fluctuates between 25°C and 29°C. Orographic temperature gradients can be steeper (~1°C per 100m of elevation gain) and can thus exert a stronger influence on isotope fractionation processes (Gat, 1996; Natali et al., 2022). In other words, if a storm's history has not caused a dramatic departure from the GMWL, a depleted air parcel from a synoptic storm could produce precipitation with a nearly identical d-excess signature to that of a more enriched parcel delivered by trade wind orographic processes. As the air parcel progresses up the Ko'olau Range, temperature drops, which increases sub-cloud evaporation of rainfall and increases d-excess. One of the shortcomings of this model is that the Rayleigh equation assumes equilibrium conditions during the rainout process (i.e., 100% relative humidity), which is not always true. This model also does not account for moisture that is recycled back into a storm system during transit. Despite these simplifications, the results provide insight into the stronger dependence of d-excess on temperature and humidity as opposed to rainout. These dynamics could be explored further by event-based precipitation

sampling coupled with meteorological data collection and storm trajectory analysis, following Torri et al. (2023) and others.

A. Volume-Weighted Average  $\delta^{18}\text{O}$  vs. Elevation, Leeward Ko'olau Range



B. Department of Health Collectors

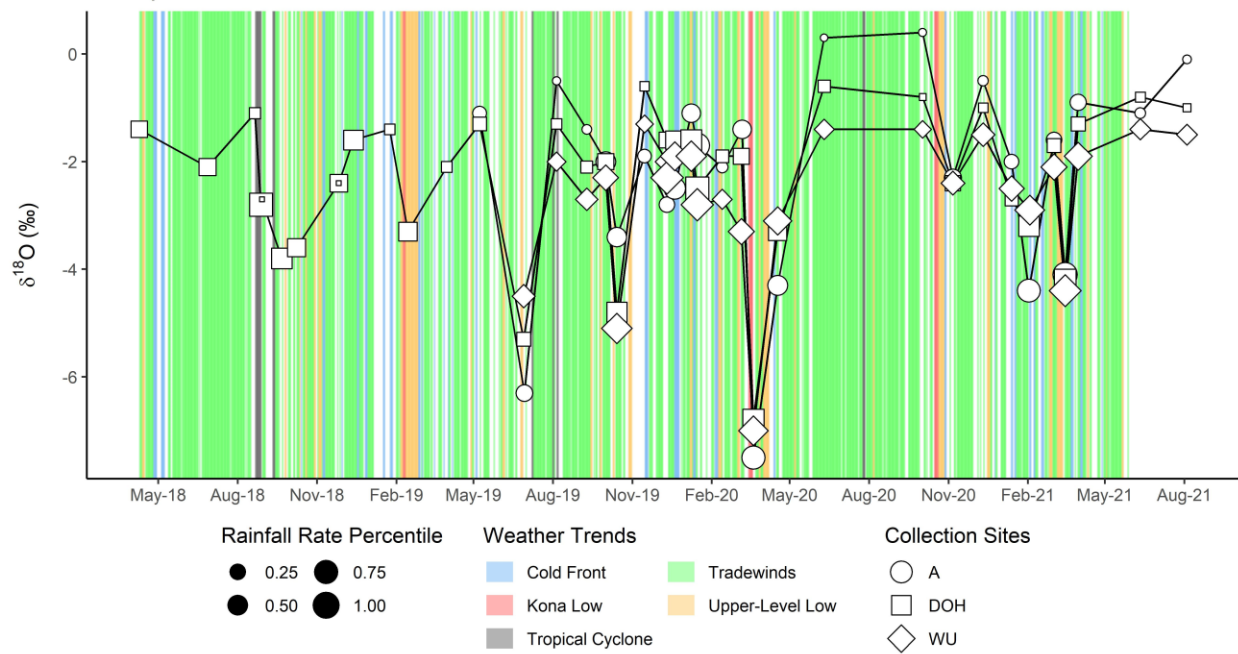


Figure 11. (A) Comparison of the VWA  $\delta^{18}\text{O}$ -elevation lapse rate from precipitation collectors located in the leeward Ko'olau Range before and after a correction for synoptic storm contributions. The black regression line shows the raw, unadjusted  $\delta^{18}\text{O}$ -elevation lapse rate. The red regression line shows the model performance after 5 samples determined to be impacted by synoptic storms were removed from the calculations. Data for collectors D17 and D3 were taken from Dores et al. (2020). (B) Time series of precipitation  $\delta^{18}\text{O}$  compositions for three precipitation collectors sampled on the island of O'ahu, HI, USA from March 2018 to August 2021.

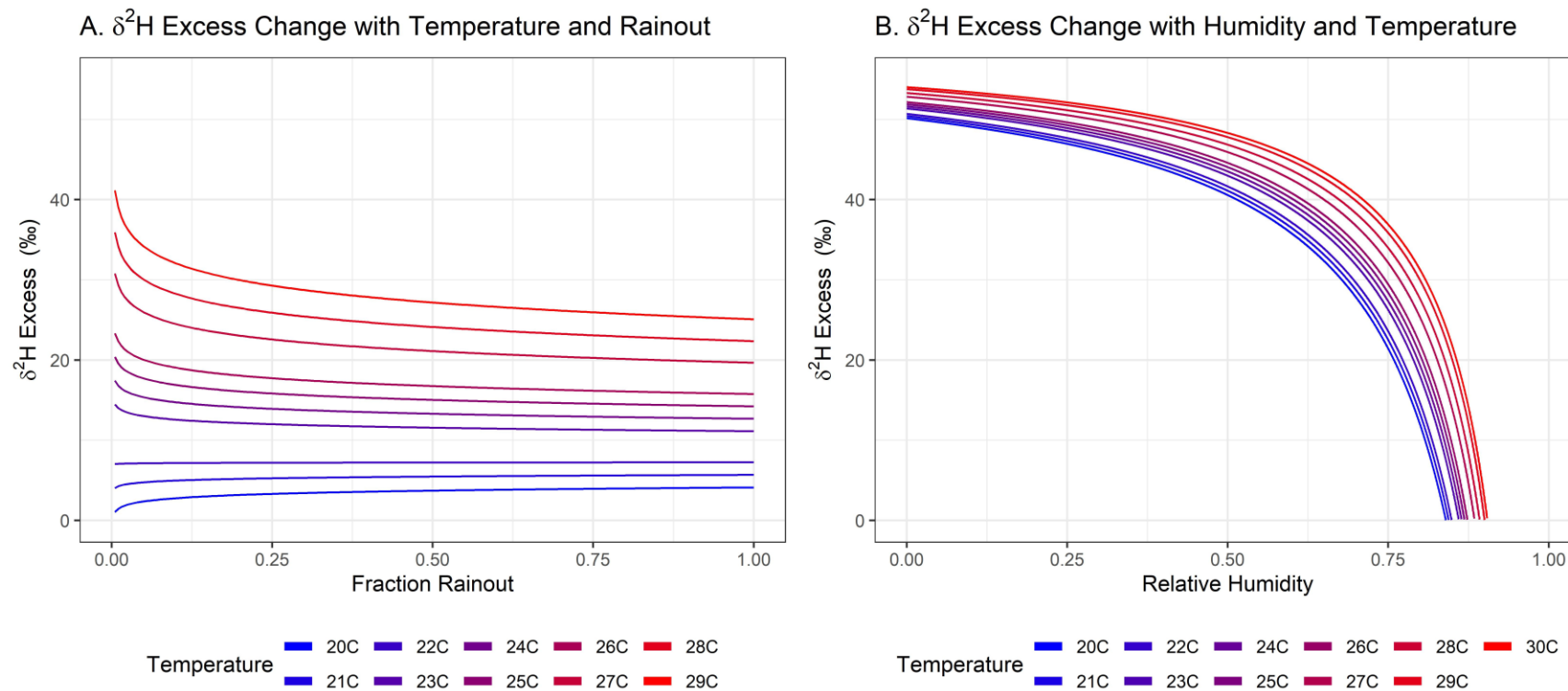


Figure 12. Modeled  $\delta^2\text{H}$ -excess (d-excess) production due to kinetic and equilibrium isotope fractionation. (A) D-excess production vs. fraction of rainout with temperature changes denoted by color. (B) D-excess production vs. relative humidity with temperature changes denoted by color. Figures were derived from equations given in (Kendall & McDonnell, 1998, p.66-68) using equilibrium isotope fractionation factors from (Friedman & O'Neil, 1977).

## 4.2. Fog

Precipitation and high-elevation spring chemistry data collected along the Ka‘ala transect presented an opportunity to explore fog contributions to the Wai‘anae Range water budget. Previous work has established that fog is an important component of the hydrologic cycle on O‘ahu (Ekern, 1983; Tseng, 2021). Given that fog is enriched in heavy isotopes relative to precipitation (Ingraham & Matthews, 1988; 1990), the chemistry of the spring sampled at 945 m amsl near the Ka‘ala summit, along with its perennial flow indicates a connection to high-elevation groundwater. The spring’s chemical signal was damped and enriched in heavy isotopes compared to summit rainfall chemistry, and it maintained steady flow through three dry seasons (Figure 13). The chemical signal from a spring sourced exclusively from surface runoff would more closely match that of local precipitation, and the flow would be measurably reduced after dry periods. If we assume the spring is replenished primarily by a well-mixed, high-elevation groundwater reservoir and that fog is the source of the spring’s enrichment relative to rainfall chemistry, we can treat the spring chemistry as the product of a two-component mixing model, given by the expression:

$$\delta S = f_R \cdot \delta R + f_F \cdot \delta F \quad (9)$$

, where  $S$ ,  $R$ , and  $F$  stand for spring, rainfall, and fog, respectively, and  $f$  is a number between 0 and 1 representing an end member’s contribution to the total precipitation at the Ka‘ala summit. Rearranging this expression to solve for  $f_F$  allows an analysis of the fraction of the fog contribution to the summit’s water budget:

$$\frac{\delta S - \delta R}{\delta F - \delta R} = f_F \quad (10)$$

This expression presents two unknowns: the fog contribution to the overall water budget at the summit ( $f_F$ ), which is the target variable, and the isotopic composition of fog from the summit ( $\delta F$ ). An intersecting research endeavor carried out by the University of Hawai‘i at Mānoa Department of Geography and Environment (Tseng et al., 2018) provided fog stable isotope chemistry data from the Ka‘ala summit. Average Ka‘ala fog chemistry was calculated from six samples collected between April and July 2018 during a research effort exploring ecological and climactic dynamics in Hawaiian forests (Tseng et al., 2018). These fog isotopic chemistry data are presented in Table 4.

Figure 14 displays the results of the mixing model analysis. The mixing line passes through the VWA summit spring composition and extends to the average fog composition. Confidence

intervals were added to the mixing line to account for the observational and instrumental uncertainty in both the spring and VWA rainfall composition measurements. The summit VWA rainfall chemistry was  $-4.5 \pm 0.7\text{\textperthousand}$   $\delta^{18}\text{O}$  and  $-19.7 \pm 1.4\text{\textperthousand}$   $\delta^2\text{H}$ . The average isotopic composition of the high elevation spring was  $-3.50 \pm 0.02\text{\textperthousand}$   $\delta^{18}\text{O}$  and  $-10.4 \pm 0.6\text{\textperthousand}$   $\delta^2\text{H}$ . The average isotopic composition of fog at the Ka‘ala summit was  $-2.00 \pm 0.01\text{\textperthousand}$   $\delta^{18}\text{O}$  and  $1.00 \pm 0.06\text{\textperthousand}$   $\delta^2\text{H}$ . These values agree reasonably well with fog isotopic compositions presented by Scholl et al. (2002) from the eastern flank of Haleakalā on the Island of Maui. Scholl et al (2002) presented the fog isotopic data as raw fog composition, and as the relative enrichment of fog compared to VWA rainfall isotopic composition. Figure 14 depicts the Ka‘ala VWA rainfall isotopic composition enriched by  $2.9\text{\textperthousand}$   $\delta^{18}\text{O}$  and  $21\text{\textperthousand}$   $\delta^2\text{H}$ , which was the relative enrichment of Maui fog from Maui VWA rainfall chemistry (Scholl et al., 2002).

The mixing model produced fog fractions of 0.41 – 0.45, which exceed regional fog drip estimates extrapolated from Ekern (1983). Other researchers have also noted that fog is a major component of the summit water budget. Tseng (2021) measured fog input due to interception by vegetation at the Ka‘ala summit and found that fog accounted for approximately 33.5% of precipitation. The findings presented here are preliminary but do suggest more research is needed to fully understand the fog contributions to the water budget on Ka‘ala. Particularly of interest are temporal changes to fog contributions and chemistry, and the isotopic behavior of moisture in the canopy and soil during the infiltration process. Mount Ka‘ala is an ideal place to carry out such research due to its pristine ecology, high elevation, and accessibility.

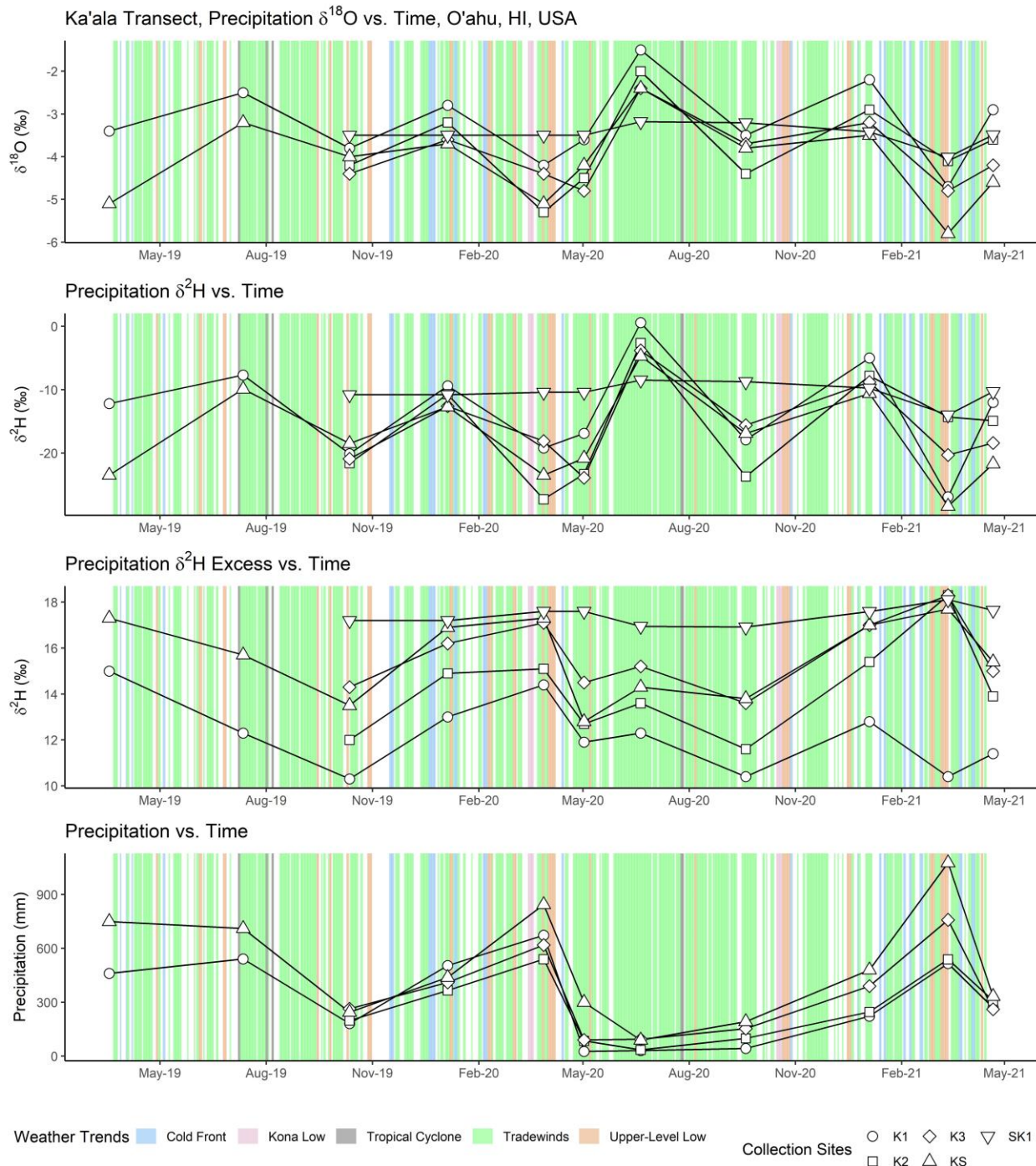


Figure 13. Ka‘ala transect precipitation and high elevation spring chemistry time series data with weather trends overlaid. Data were collected between December 2018 and April 2021. The high-elevation spring chemistry is depicted by the inverted triangle labeled SK1. Weather trend data derived from International Global Radiosonde Archive (IGRA) weather balloon launches at Līhue, Kauai (Durre et al., 2016), and from monthly weather summaries provided by the National Oceanic and Atmospheric Administration (NOAA/NWS, 2023) are shown in the background.

## Mount Ka'ala Rainfall-Spring-Fog Mixing Model

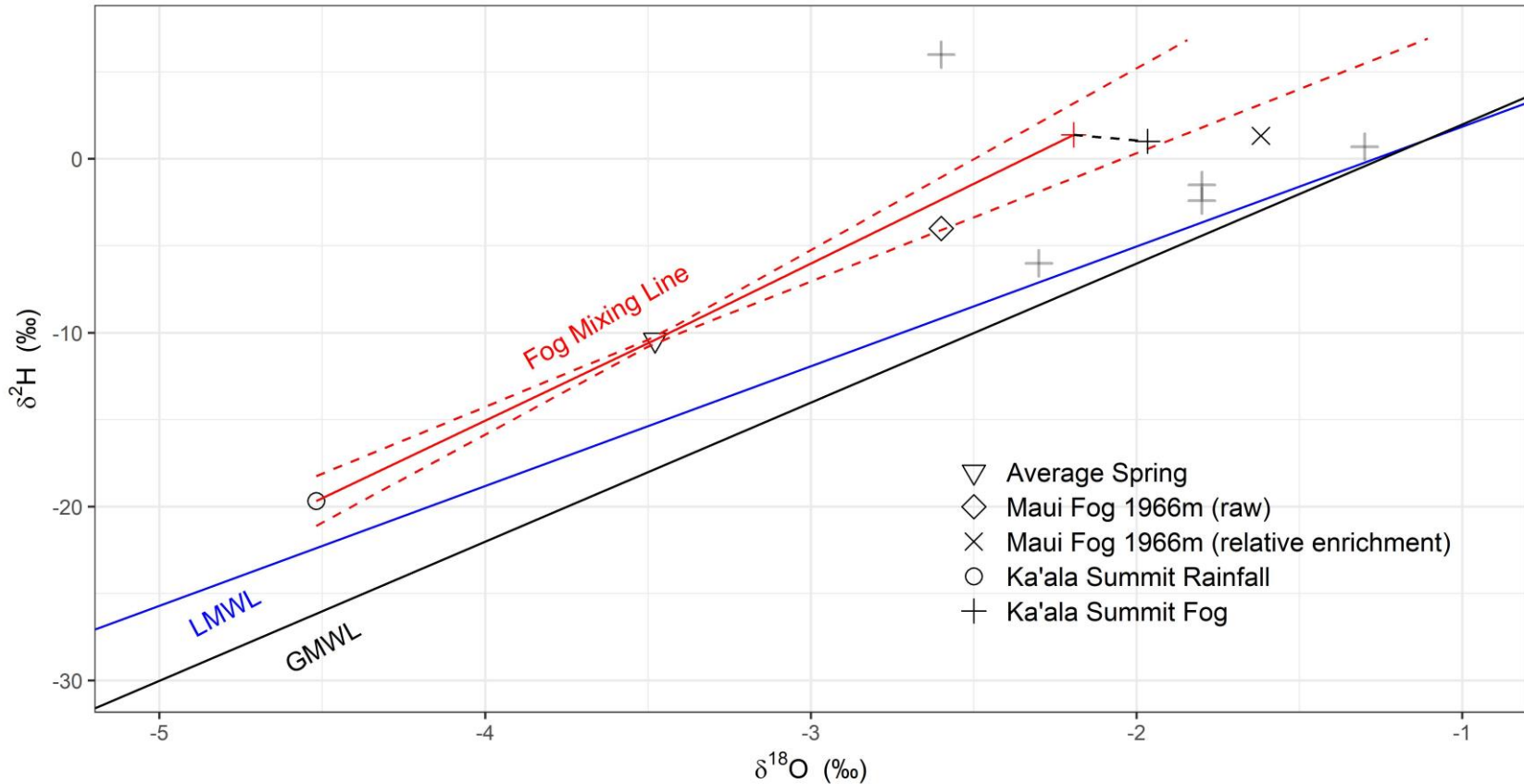


Figure 14. Ka'ala summit rainfall-spring-fog mixing model analysis. The Ka'ala summit (KS) VWA rainfall chemistry is  $-4.5 \pm 0.7 \delta^{18}\text{O}$  and  $-19.7 \pm 1.4 \delta^2\text{H}$ . The average Ka'ala high elevation spring composition is  $-3.5 \pm 0.3 \delta^{18}\text{O}$  and  $-10.4 \pm 2.4 \delta^2\text{H}$ . The average isotopic composition of fog at the Ka'ala summit was  $-2.0 \delta^{18}\text{O}$  and  $1.0 \delta^2\text{H}$  (Tseng et al. 2018). The fog average composition was derived from the fog samples shown in light gray. Maui fog samples are taken from Scholl et al. (2002). Raw Maui fog composition was  $-2.6 \delta^{18}\text{O}$  and  $-4 \delta^2\text{H}$ . Relative enrichment depicts the departure from VWA precipitation at that location. The mixing model produced fog fractions of 0.41 – 0.45.

Table 4. Stable isotope composition of six fog samples collected on Mount Ka‘ala between April and July 2018 (Tseng et al. 2018). Samples were analyzed in the Isotope Biogeochemistry Laboratory at the University of Hawai‘i at Mānoa.

Sample Date	$\delta^{18}\text{O}$	$\delta^2\text{H}$	$\delta^{18}\text{O SD}$	$\delta^2\text{H SD}$	D-Excess
4/28/2018	-2.6	6.0	0.01	0.10	26.8
4/28/2018	-2.0	9.3	0.01	0.13	25.3
6/27/2018	-1.8	-1.5	0.07	0.28	12.9
7/14/2018	-2.3	-6.0	0.02	0.06	12.4
7/14/2018	-1.8	-2.4	0.02	0.10	12.0
7/14/2018	-1.3	0.7	0.02	0.08	11.1

#### 4.3. Influence of Microclimates

The findings cumulatively point to strong, locale-specific connections between microclimates and the isotopic composition of rainfall; we identify six potentially distinct isotopic microclimate regimes. In high-elevation, high-rainfall areas in the leeward Ko‘olau Range, topographic influences on condensation during trade wind periods represent one regime, as evidenced by the strong  $\delta^{18}\text{O}$ -elevation lapse rate along the Manana Transect (Figure 8). In lower elevation, leeward areas, synoptic storms influence rainfall stable isotope composition in a fundamentally different way (i.e., the rainout effect), producing an isoscape characterized by higher depletion and moderate d-excess. Collectors D11 and D19 reveal another potential isoscape in the leeward Wai‘anae Range. These collectors produced distinctly higher VWA  $\delta^{18}\text{O}$  and  $\delta^2\text{H}$  composition and moderate d-excess, possibly signaling the incorporation of vapor carried in-land by land-sea breeze cycles (Figures 4 and 9). The strong influence of fog on Mount Ka‘ala points to another isotopic regime in high-elevation, fog-impacted areas. The Schofield Plateau and the Honolulu Transect present two more potentially distinct isoscapes (Figure 8). Lastly, we speculate that there may be a Ko‘olau valley effect. Collectors D13 and D20 produced isotopically light precipitation and moderate d-excess (Figures 4 and 9). Persistent trade wind-driven precipitation, along with cooler, more humid conditions in Ko‘olau Range valleys, would intuitively reduce sub-cloud rainfall evaporation, which we would expect to dampen the d-excess and produce isotopically light rainfall. Understanding the strength and consistency of these microclimate stable isotope regimes will be an important step in examining connectivity between meteoric, ground- and surface water. We propose that focused sampling in the Ko‘olau Range, particularly in valleys and high-elevation fog-impacted areas would provide valuable insights into these dynamics.

### 5. Conclusions

The data and findings presented here illuminate some key processes controlling the stable isotope composition of precipitation on O‘ahu. Analysis of bulk precipitation chemistry data indicates that the altitude effect exerts a distinct influence on precipitation stable isotope composition. However, systematic differences between orographic and synoptic precipitation values coupled with strong microclimate influences on rainfall stable isotope composition necessitate accounting for synoptic storm influences to establish reliable regional precipitation

$\delta^{18}\text{O}$ -elevation lapse rates. The data also reveal that rainfall d-excess is strongly connected to elevation, potentially more reliably than either  $\delta^{18}\text{O}$  or raw  $\delta^2\text{H}$  composition. This connection is likely due to the strong correlation between elevation and temperature and humidity, which are the key parameters controlling d-excess in meteoric waters. The exploration of a montane spring enabled the assessment of fog contribution to the Ka‘ala summit’s water budget. These results suggest that fog drip could constitute as much as 45% of the total groundwater recharge at the summit. Cumulatively, these findings indicate the stable isotopic composition of rainfall strongly reflects the regional microclimates on O‘ahu.

The findings of this study highlight a need for more event-based precipitation sampling in connection with basic meteorological data collection to examine local controls on stable water isotope composition and d-excess. Fog sampling in both the Ko‘olau and Wai‘anae Ranges is also warranted. This study, along with previous work examining the major ion composition of precipitation in the same region and over the same timespan (Brennis et al., 2023), lays the groundwork for future research aimed at understanding the chemical connections between precipitation and groundwater recharge. Our ultimate goal is to constrain groundwater flow paths by means of natural, conservative geochemical tracers.

## 6. Chapter 3 References

- Booth, H., Lautze, N., Tachera, D., & Dores, D. (2021). Event-Based Stable Isotope Analysis of Precipitation Along a High Resolution Transect on the South Face of O'ahu, Hawai'i. *Pacific Science*, 75(3), 421–441. doi:<https://doi.org/10.2984/75.3.9>
- Bowen, G. (2010). Isoscapes: Spatial Pattern in Isotopic Biogeochemistry. *Annual Review of Earth and Planetary Sciences*, 38(1), 161-187.
- Brennis, T., Lautze, N., Whitter, R., Giuseppe, T., & Thomas, D. (2023). Understanding the origins of and influences on precipitation major ion chemistry on the Island of O'ahu, Hawai'i. *Environmental Monitoring and Assessment*, 195(11). doi:<https://doi.org/10.1007/s10661-023-11887-2>
- Cao, G., Giambelluca, T., Stevens, D., & Schroeder, T. (2007). Inversion Variability in the Hawaiian Trade Wind Regime. *Journal of Climate*, 20(7), 1145-1160. doi:[10.1175/JCLI4033.1](https://doi.org/10.1175/JCLI4033.1)
- Craig, H. (1961). Isotopic Variations in Meteoric Waters. *Science*, 133(3465), 1702-1703. doi:<https://doi.org/10.1126/science.133.3465.1702>
- Dansgaard, W. (1964). Stable Isotopes in Precipitation. *Tellus*, 16, 436-468.
- Davis, H., Lee, C., Bradley, E., & Payne, B. (1970). Geohydrologic Interpretations of a Volcanic Island from Environmental Isotopes. *Water Resources Research*, 6(1), 99-109. doi:<https://doi.org/10.1029/WR006i001p00099>
- Dores, D., Glenn, C. R., Torri, G., Whittier, R. B., & Popp, B. (2020). Implications for groundwater recharge from stable isotopic composition of precipitation in Hawai'i during the 2017–2018 La Niña. *Hydrological Processes*, 34(24), 4675–4696. <https://doi.org/10.1002/hyp.13907>.
- Durre, I., Xungang, Y., Vose, R., Applequist, S., & Arnfield, J. (2016). Integrated Global Radiosonde Archive (IGRA), Version 2. *Subset USM00091165, Lihue, HI, USA*. NOAA National Centers for Environmental Information. doi:[10.7289/V5X63K0Q](https://doi.org/10.7289/V5X63K0Q)
- Ekern, P. (1983). *WRRCTR No.156 Measured Evaporation in High Rainfall Areas, Leeward Ko'olau Ranges, O'ahu, Hawai'i*. Water Resources Research Center, University of Hawaii at Manoa.
- Engott, J. A., Johnson, A. G., Bassiouni, M., Izuka, S. K., & Rotzoll, K. (2017). *Spatially distributed groundwater recharge for 2010 land cover estimated using a water-budget model for the Island of O'ahu, Hawai'i (ver 2.0, December 2017)*. U.S. Geological Survey Scientific Investigations Report 2015–5010, 49 p. doi:<https://doi.org/10.3133/>
- Fackrell, J. K., Glenn, C. R., Thomas, D., Whittier, R., & Popp, B. (2020). Stable isotopes of precipitation and groundwater provide new insight into groundwater recharge and flow in

a structurally complex hydrogeologic system: West Hawai‘i, USA. *Hydrogeology Journal*, 28(4), 1191–1207. <https://doi.org/10.1007/s10040-020-02143-9>.

Frazier, A., & Giambelluca, T. (2017). Spatial trend analysis of Hawaiian rainfall from 1920 to 2012. *International Journal of Climatology*, 37(5), 2522–2531.  
doi:<https://doi.org/10.1002/joc.4862>

Friedman , I., & Woodcock, A. (1956). Determination of Deuterium-Hydrogen Ratios in Hawaiian Waters. *Tellus*, 9(4), 553-556.

Friedman, I., & O'Neil, J. (1977). *Compilation of stable isotope fractionation factors of geochemical interest*. Reston, VA: U.S. Geological Survey.

Gat, J. (1996). Oxygen and Hydrogen Isotopes in the Hydrologic Cycle. *Annu. Rev. Earth Planet. Sci.*, 24, 225-262.

Gat, J., Shemesh, A., Tziperman, E., Hecht, A., Georgopoulos, D., & Basturk, O. (1996). The stable isotope composition of waters of the eastern Mediterranean Sea. *Journal of Geophysical Research*, 101(C3), 6441-6451. doi:<https://doi.org/10.1029/95JC02829>

Giambelluca, T. (1983). *Water balance of the Pearl Harbor-Honolulu Basin, Hawai‘i, 1946-1975*. Water Resources Research Center, University of Hawai‘i at Manoa.

Gingerich, S., & Oki, D. (2000). *Groundwater in Hawai‘i*. U.S. Geological Survey.

Guan, H., Zhang, X., Skrzypek, G., Sun, Z., & Xu, X. (2013). Deuterium excess variations of rainfall events in a coastal area of South Australia and its relationship with synoptic weather systems and atmospheric moisture sources. *Journal of Geophysical Research: Atmospheres*, 118, 1123-1138. doi:<https://doi.org/10.1002/jgrd.50137>

Gupta, P., Noone, D., Galewski, J., Sweeney, C., & Vaughn, B. (2009). Demonstration of high-precision continuous measurements of water vapor isotopologues in laboratory and remote field deployments using wavelength-scanned cavity ring-down. *Rapid Communications in Mass Spectrometry*, 23, 2534-2542.

IAEA/WMO. (2023). Retrieved from Global Network of Isotopes in Precipitation. The GNIP Database: <https://nucleus.iaea.org/wiser>

Ingramam, N., & Matthews, R. (1988). Fog Drip as a Source of Groundwater Recharge in Northern Kenya. *Water Resources Research*, 24(8), 1406-1410.

Ingramam, N., & Matthews, R. (1990). A Stable Isotope Study of Fog: The Point Reyes Peninsula, California, U.S.A. *Chemical Geology (Isotope Geoscience Section)*(80), 281-290.

Kelly, J., & Glenn, C. (2015). Chlorofluorocarbon Apparent Ages of Groundwaters from West Hawai‘i. *Jounral of Hydrology*, 527, 355-366.  
doi:<https://dx.doi.org/10.1016/j.jhydrol.2015.04.069>

Kendall, C., & McDonnell, J. J. (1998). *Isotope Tracers in Catchment Hydrology*. Elsevier.

- Longman, R., Ellison, T., Giambelluca, T., & Kaiser, L. (2021). A 20-year analysis of disturbance-driven rainfall on O'ahu, Hawai'i. *Monthly Weather Review*. doi:<https://doi.org/10.1175/MWR-D-20-0287.1>
- Merlivat, L. (1978). Molecular Diffusivities of H<sub>2</sub><sup>16</sup>O, HD<sub>16</sub>O, and H<sub>2</sub><sup>18</sup>O in gases. *Journal of Chemical Physics*, 69(6), 2864-2871. doi:<https://doi.org/10.1063/1.436884>
- Natali, S., Doveri, M., Giannecchini, R., & Baneschi, I. (2022). Is the deuterium excess in precipitation a reliable tracer of moisture sources and water resources fate in the western Mediterranean? New insights from Apuan Alps (Italy). *Journal of Hydrology*, 614, 128497. doi:<https://doi.org/10.1016/j.jhydrol.2022.128497>
- Nichols, W. D., Shade, P. J., & Hunt, Jr., C. D. (1997). *Summary of the Oahu, Hawaii, regional aquifer-system analysis*. U.S. Geological Survey Professional Paper 1412-A. Retrieved from <https://pubs.usgs.gov/pp/1412a/report.pdf>
- NOAA/NWS. (2023). *Hawaii Monthly Weather Summaries*. Retrieved from [https://www.hawaii.edu/climate-data-portal/publications-list/?collection\\_id=PZN8C7R9&collection\\_name=%2520NOAA%252FNWS%2520Monthly%2520Precipitation%2520Summaries](https://www.hawaii.edu/climate-data-portal/publications-list/?collection_id=PZN8C7R9&collection_name=%2520NOAA%252FNWS%2520Monthly%2520Precipitation%2520Summaries)
- Poage, M., & Chamberlain, C. (2011). Empirical Relationships Between Elevation and the Stable Isotope Composition of Precipitation and Surface Waters: Considerations for the Studies of Paleoelevation Change. *American Journal of Science*, 1-15. doi:<https://doi.org/10.2475/ajs.301.1.1>
- Scholl, M. A., Gingerich, S. B., & Tribble, J. W. (2002). The influence of microclimates and fog on stable isotope signatures used in interpretation of regional hydrology: East Maui, Hawaii. *Journal of Hydrology (Amsterdam)*, 264(1), 170–184. doi:[https://doi.org/10.1016/S0022-1694\(02\)00073-2](https://doi.org/10.1016/S0022-1694(02)00073-2)
- Scholl, M., Giambelluca, T., Gingerich, S., Nullet, M., & Loope, L. (2007). Cloud water in windward and leeward mountain forests: The stable isotope signature of orographic cloud water. *Water Resources Research*, 43(12). doi:[10.1029/2007WR006011](https://doi.org/10.1029/2007WR006011)
- Scholl, M., Ingebritsen, S., Janik, C., & Kauahikaua, J. (1995). *An Isotope Hydrology Study of the Kilauea Volcano Area, Hawaii*. U.S. Geological Survey Water-Resources Investigations Report 95-4213. doi:<https://doi.org/10.3133/wri954213>
- Sherrod, D., Sinton, J., Watkins, S., & Brunt, K. (2021). *Geologic map of the State of Hawai'i: U.S. Geological Survey Scientific Investigations Map 3143, pamphlet 72 p., 5 sheets, scales 1:100,000 and 1:250,000*. doi:<https://doi.org/10.3133/sim3143>
- State of Hawai'i. (2019). *Water Resource Protection Plan 2019 Update: Report prepared by Townscape Inc. for the State of Hawai'i, Commission on Water Resource Management*.
- Tachera, D., Lautze, N., Torri, G., & Thomas, D. (2021). Characterization of the isotopic composition and bulk ion deposition of precipitation from Central to West Hawai'i Island

between 2017 and 2019. *Journal of Hydrology. Regional Studies*, 34, 100786.  
<https://doi.org/10.1016/j.ejrh.2021.100786>.

Tillman, F., Oki, D., Johnson , A., Barber, L., & Beisner, K. (2014). Investigation of Geochemical Indicators to Evaluate the Connection between Inland and Coastal Groundwater Systems near Kaloko-Honokohua National Historic Park, Hawaii. *Applied Geochemistry*, 51, 278-292. doi:<https://dx.doi.org/10.1016/j.apgeochem.2014.10.003>

Torri, G., Nugent, A., & Popp, B. (2023). The Isotopic Composition of Rainfall on a Subtropical Mountainous Island. *Journal of Hydrometeorology*. doi:<https://doi.org/10.1175/JHM-D-21-0204.1>

Tseng, H. (2021). Cloud Water Interception in Hawai'i. Retrieved from <https://hdl.handle.net/10125/81641>

Tseng, H., Kagawa-Viviani, A., Beilman, D., & Giambelluca, T. (2018, April, June, July). Fog Stable Isotope Data from Mount Ka'ala, O'ahu, HI, USA. *Unpublished Data*.

Vernon, S., Mouchet, M., Govaerts, R., Haevermans, T., & Pellens, R. (2019). Vulnerability to Climate Change of Islands Worldwide and its Impacts on the Tree of Life. *Scientific Reports*, 9(1), 14471. doi:<https://doi.org/10.1038/s41598-019-51107-x>

Wahl, M., & Urey, H. (1935). The Vapor Pressures of the Isotopic Forms of Water. *Journal of Chemical Physics*, 3(7), 411-414. doi:<https://doi.org/10.1063/1.1749690>

Wickam, H., Chang, W., Henry, L., Pedersen, T., Takahashi, K., Wilke, C., . . . Dewey, H. (2016). *Rug plots in the margins*. (S.-V. N. York, Producer) Retrieved from ggplot2: Elegant Graphics for Data Analysis: [https://ggplot2.tidyverse.org/reference/geom\\_rug.html](https://ggplot2.tidyverse.org/reference/geom_rug.html)

Wilmott, C. (1981). On the Validation of Models. *Physical Geography*, 2(2), 184-194. doi:<https://doi.org/10.1080/02723646.1981.10642213>

Wilmott, C. (1982a). On the Climatic Optimization of the Tilt and Azimuth of Flat-plate Solar Collectors. *Solar Energy*, 28(3), 205-216. doi:[https://doi.org/10.1016/0038-092X\(82\)90159-1](https://doi.org/10.1016/0038-092X(82)90159-1)

Wilmott, C. (1982b). Some Comments on the Evaluation of Model Performance. *Bulletin of the American Meteorological Society*, 63(11), 1309-1313. doi:[https://doi.org/10.1175/1520-0477\(1982\)063<1309:SCOTEO>2.0.CO;2](https://doi.org/10.1175/1520-0477(1982)063<1309:SCOTEO>2.0.CO;2)

Wilmott, C., & Wicks, D. (1980). An Empirical Method for the Spatial Interpolation of Monthly Precipitation within California. *Physical Geography*, 1(1), 59-73. doi:<https://doi.org/10.1080/02723646.1980.10642189>

CHAPTER 4: A METHOD FOR EXPLORING THE IMPACTS OF SOIL MOISTURE  
DYNAMICS ON THE INORGANIC CHEMISTRY OF GROUNDWATER INFILTRATION

## CHAPTER 4 ABSTRACT

Pacific Islands face unique water resource management challenges due to their fragile environments, fluctuating climates, and heavy reliance on groundwater. To improve water resource management in these regions, it is crucial to comprehend the connections between meteoric, ground-, and surface waters. This study introduces a method that employs stable isotopes of oxygen and hydrogen to investigate how factors such as soil moisture, soil water potential, precipitation, temperature, and humidity affect groundwater chemistry during infiltration. This method involves the collection and interpretation of soil tension, soil moisture, water chemistry, and atmospheric data from three sites in a montane subtropical forest on the island of O‘ahu, Hawai‘i, USA. We determined the transfer function to convert soil dielectric constant values into soil water content, and then established a soil water retention curve using soil moisture and tension data. The soil water retention curve was used to estimate the soil water column height, and by combining this input with precipitation and evapotranspiration data, we estimated groundwater infiltration periods and amounts. We then compared precipitation and soil water chemistry with estimated infiltration to evaluate chemical changes during the infiltration process. Discrepancies between model results and long-term averages suggest refinement of the model may be needed, but overall, the results indicate the method developed can produce reasonable estimates of infiltration, which can in turn be used to semi-quantitatively weight precipitation chemistry by infiltration amount. Our results indicate a chemical partitioning of soil water, with precipitation following dry periods replenishing capillary water in the upper soil until field capacity is reached, and subsequent rainfall strongly controlling deep soil water chemistry. Understanding the source and evolution of soil water chemistry, and developing a methodology to estimate the chemistry of water that infiltrates the soil, are important preliminary steps in utilizing natural geochemical tracers in precipitation to determine groundwater recharge processes and flow paths on O‘ahu.

## 1. Introduction

Geochemical methods have been effectively used to explore the movement and distribution of groundwater in Hawai‘i (Fackrell et al., 2020; Scholl et al., 1995; Scholl et al., 2002; Glenn et al., 2013; Kelly & Glenn, 2015; Tachera et al., 2021) and elsewhere (Lee et al., 2007; Gat, 1996; Awaleh et al., 2017; Toulier et al., 2019; and others). Chemically tracing groundwater flow paths requires linking groundwater between two sample points, ideally the point of water infiltration and a location some distance downflow. Stable isotopes of water (oxygen-18 and hydrogen-2 or deuterium) are particularly useful in such efforts due to their conservative behavior through the process of infiltration (Kendall & McDonnell, 1998; Gat, 1996). Analysis of the stable isotope composition of water can provide linkage between the points of groundwater recharge and capture without the need to account for chemical fractionation due to biologic activity in the soil (Fackrell et al., 2020; Scholl et al., 2002). Such efforts also have the advantage of only requiring point measurements of precipitation and well chemistry.

A key assumption in groundwater studies that use precipitation chemistry to evaluate subsurface water processes is that the chemistry of precipitation at a point is the same as the chemistry of groundwater recharge at that point, and that there is no substantial chemical change during the process of soil infiltration. Here we pose the question as to whether factors such as soil moisture content, soil water potential, precipitation intensity, temperature, and humidity may cause a change in water chemistry by impacting when soil water infiltration occurs. To explore this question, we present and interpret soil tension, soil moisture, water chemistry, and atmospheric data from three sites in a montane subtropical forest.

This project complements a broader research effort aimed at constraining groundwater flow paths using natural, conservative geochemical tracers. This effort included extensive precipitation sampling and chemical analysis from across the island of O‘ahu, Hawai‘i, USA (Brennis et al., 2023, Booth et al., 2021, Dores et al., 2020). The initial intent was to determine the infiltration volume-weighted average (VWA) chemistry of precipitation in one or more key areas within the larger study region. Due to deployment delays, access limitations during the COVID-19 pandemic, and equipment malfunction, we were unable to obtain sufficient overlap between the soil, meteorological, and chemical data to calculate statistically valid volume-weighted averages. Consequently, the scope of this project was narrowed. The refined objectives are to 1) present new geochemical and meteorological data that may be of use to other

researchers, 2) present and evaluate a method to calculate infiltration VWA precipitation chemistry, and 3) identify, analyze and interpret the larger trends in the soil and precipitation chemistry data presented herein.

## 2. Methods

### 2.1. Study Area Overview

This study was focused on the Waimano Section of the ‘Ewa Forest Reserve, on the island of O‘ahu (Figure 1). The study sites are on the leeward flank of Ko‘olau Range, which is a critical groundwater recharge zone, supplying more than half of the total groundwater recharge for the island Engott et al., 2017). Instruments at the three study sites (Manana Lower, Manana Upper, and Uluakupu; Figures 2, 3, and 4) included a series of soil probes deployed at depths ranging from 30 to 122 cm below ground surface, a rain gauge, a temperature-humidity sensor, and a cumulative precipitation collector (Chapter 3, Figure 3). One site (Uluakupu) also included time domain reflectometry (TDR) soil moisture probes, soil lysimeters deployed at 30 and 90 cm below ground surface, and a weather station to collect meteorological data. Table 1 describes the key site characteristics for each station, including major hydrological fluxes and soil characteristics.

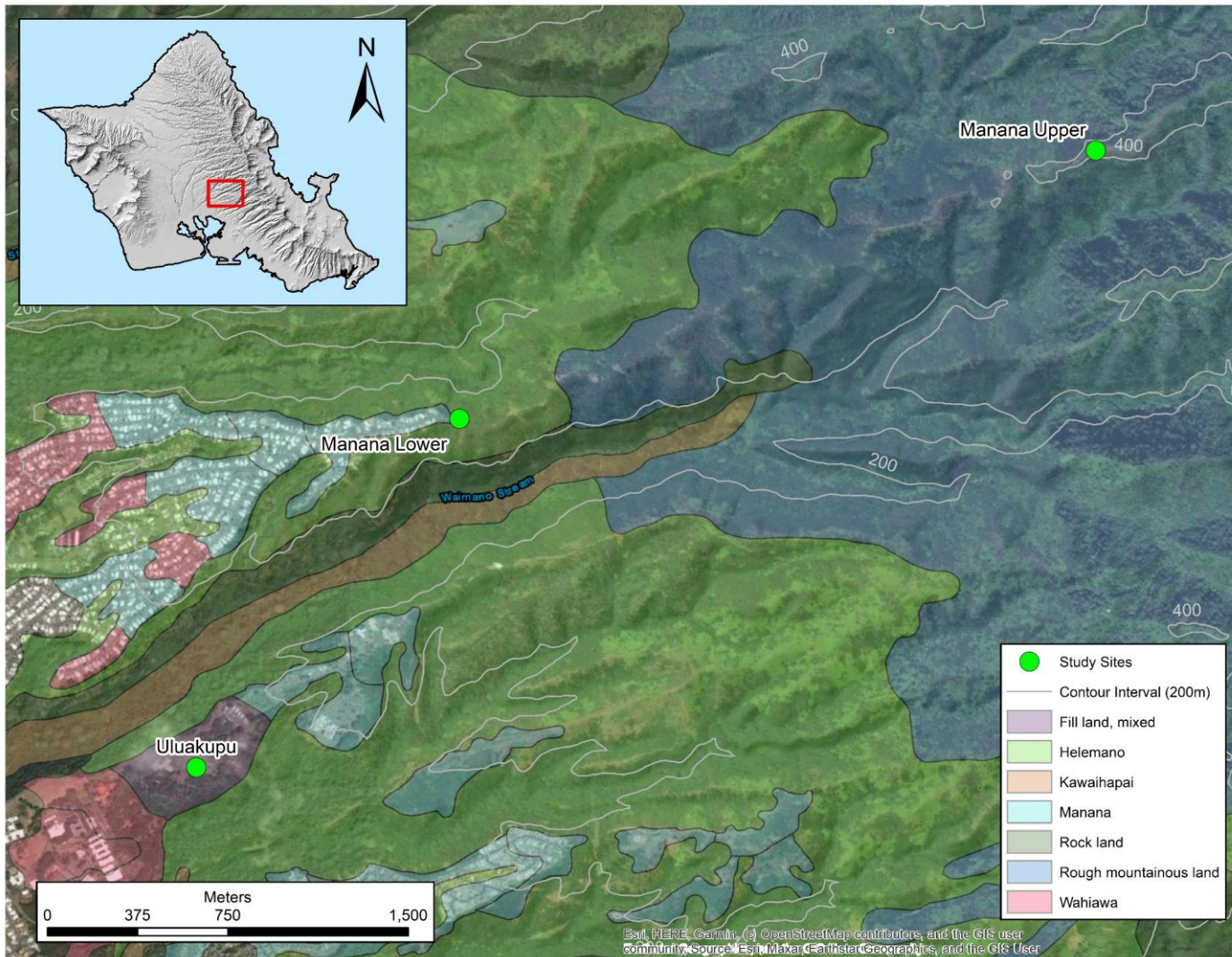


Figure 1. Soil and meteorological data collection sites within the Waimano Section of the 'Ewa Forrest Reserve on the island of O'ahu, HI, USA. Soil series from the USDA Gridded Soil Survey Geographic (gSSURGO) Database are overlain (Soil Survey, 2014). Two-hundred-meter contour intervals, shown in light gray, show elevation above mean sea level. The datum is NAD 1983.

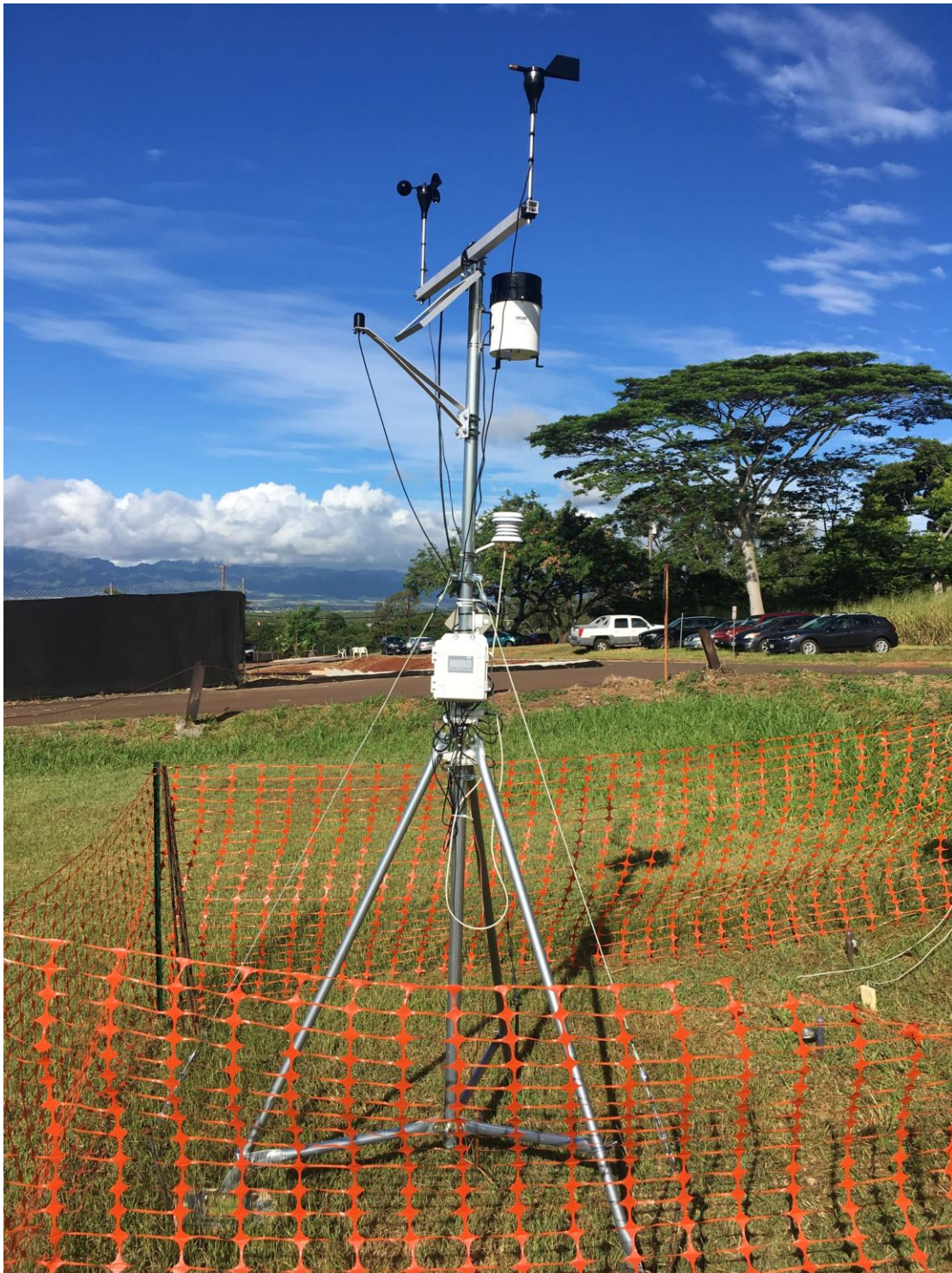


Figure 2. Uluakupu study site with three suction lysimeters, four TDR probes, four Watermark soil tensiometers, a soil temperature probe, a cumulative bulk precipitation collector, an Irrrometer 900M data logger, an OnSet portable weather station, a HOBO 2-RGx-M002 tip bucket rain gauge, a HOBO S-LIB-M003 silicon pyranometer, and a HOBO S-THB-M00X Temperature/Relative Humidity Sensor.



Figure 3. Lower Manana study site with four soil tension probes, a tipping bucket style rain gauge, a soil temperature probe, a cumulative bulk precipitation collector, an Irrometer 900M data logger, and an OnSet Computer Corporation HOBO U14-001 Temp/RH Data Logger.



Figure 4. Upper Manana study with five soil tension probes, a tipping bucket style rain gauge, a soil temperature probe, a cumulative bulk precipitation collector (not shown), an Irrometer 900M data logger, and an OnSet Computer Corporation HOBO U14-001 Temp/RH Data Logger.

Table 1. Study site characteristics and soil monitoring equipment information. Abbreviations: Elev. = elevation above mean sea level; Precip. = long term average annual precipitation taken from the Rainfall Atlas of Hawai‘i (Frazier & Giambelluca, 2017); ET = long term average annual actual evapotranspiration taken from (Giambelluca, et al., 2014); Rech. = long term average annual groundwater recharge taken from (Engott et al., 2017); TDR = time domain reflectometry. Soil order data was taken from the USDA Gridded Soil Survey Geographic (gSSURGO; (Soil Survey, 2014).

Site	Sample Period	Elev. (m)	Latitude	Longitude	Precip. (mm)	ET (mm)	Rech. (mm)	Soil Order	Watermark Probe Depths (cm)	TDR Probe Depths (cm)
Uluakupu	1/24/22 to 4/26/23	154	21.41723	-157.94814	1173	948	254	Entisol - land fill	30, 60, 90, 120	0-15, 0-30, 0-68, 90-105
Manana Lower	12/1/20 to 9/24/21	291	21.43008	-157.93803	1910	939	356	Entisol - rough, mountainous	52, 72, 91, 100	NA
Manana Upper	6/24/20 to 12/2/21	452	21.44235	-157.91015	3178	984	1676	Entisol - rough, mountainous	37, 57, 74, 92, 122	NA

## 2.2. Soil Moisture Dynamics Overview

Soil water can be generalized as existing in two interconnected reservoirs: Pore or gravitational water, which is water that exists in the larger spaces between soil particles, and capillary water, which is the water that clings to soil particles via capillary forces. Pore water drains away through gravitational forces at a rate determined by soil pore size, shape, and connectivity (Ward & Trimble, 2004; Dunne & Leopold, 1978). Capillary water content fluctuates more gradually depending on evaporation and transpiration (Ward & Trimble, 2004; Dunne & Leopold, 1978). Soil particles have a finite volume of water that they can hold via capillary forces. This volume can be measured indirectly by measuring capillary tension. When the capillary tension falls below a certain threshold soil particles are generally considered to be fully saturated with capillary water (Dunne & Leopold, 1978). This tension threshold corresponds to the maximum water content in the soil matrix called field capacity. Below field capacity tension, soil particles cannot hold on to any more capillary water and any remaining water in the soil matrix drains away as pore water at a rate determined by the soil's physical structure. Soil tension must be below the field capacity threshold for groundwater recharge to occur, that is soil particles must be sufficiently wetted for pore water to be able to drain away. For silty clays, which characterize the soils at the three study sites, field capacity water content is approximately  $0.40 \text{ cm}^3 \text{ cm}^{-3}$  (James, 1993, Table 1.2).

The direction and rate of pore water movement depends on the soil water potential gradient. Soil water potential is a measure of the cumulative potential energy of soil water due to gravitational, matric (capillary), and osmotic forces, and air pressure. Osmotic potential and air pressure are often negligible compared to gravitational and capillary potential. Soil water potential can thus be approximated as the sum of gravitational and matric potentials, both of which can be expressed as a length, or head, as follows:

$$\Psi_T = \Psi_G + \Psi_M = z + \rho_w gh = z + \frac{\Psi_M}{\rho_w g} \quad (1)$$

, where  $\psi_T$  is total soil water potential,  $\psi_G$  is gravitational potential,  $\psi_M$  is soil matric potential (Pa or  $\text{kg} \cdot \text{m}^{-1} \cdot \text{s}^{-2}$ ),  $z$  is elevation head (m),  $\rho_w$  is the density of water ( $\text{kg} \cdot \text{m}^{-3}$ ), and  $g$  is the acceleration due to gravity ( $\text{m} \cdot \text{s}^{-2}$ ). The elevation head ( $h$ ) is the elevation of the point of

interest in the soil in relation to a reference point, which is usually sea level or a known soil depth.

Water will move from high soil water potential to low potential. If we have multiple potential measurements in a soil column we can determine the change in soil water potential over soil depth. A negative slope indicates decreasing potential with depth or a downward potential gradient. Conversely, a positive slope indicates increasing potential with depth or an upward potential gradient. The soil water potential gradient must be negative (downward) for soil water to infiltrate and become groundwater recharge.

### 2.3. Soil Moisture Monitoring Methods Overview

Soil moisture can be measured directly or indirectly. Direct measurement can be accomplished by obtaining a soil core and measuring soil moisture change through drying and/or suction. Another direct method of measuring soil moisture is by using tensiometers, which directly measure the matric potential exerted by a soil matrix (Jones et al., 2022). Direct methods of measuring soil moisture have the advantage of precision, but tend to be more costly, labor intensive, and are less useful for obtaining continuous time-series data.

Two common indirect methods of soil moisture observation are time domain reflectometry (TDR) and frequency domain reflectometry (FDR). Both methods involve measuring the behavior of an electromagnetic signal as it passes through water saturated soil. Both TDR and FDR methods are based on the principle that the electrical permittivity of soil, expressed as the dielectric constant, changes as its water content changes (Jones et al., 2002). TDR probes are advantageous in that they can provide an integrated water content profile over the probe length (Jones et al., 2002). Granular matric sensors (GMS) are a widely used type of FDR probe that utilize an anode and a cathode separated by a porous material with a known dielectric constant (Thompson et al., 2006). Granular matrix sensors and most other types of FDR probes provide a more simplistic point estimate of soil water content and/or soil tension.

### 2.4. Stable Isotope Composition of Soil Water

The fundamentals of water stable isotopes were introduced in Chapter 3, Section 2.1, including delta notation, the Global Meteoric Water Line (GMWL) (Craig, 1961; Dansgaard, 1964), and the Local Meteoric Water Line (LMWL; Gat, 1996; Davis et al., 1970). Here we

expand on the concepts by briefly discussing water stable isotope behavior in the soil. Unsaturated soils can develop a stable isotope concentration profile due to several concurrent physical processes. Water stable isotopes in the soil can be modeled as simple solutes. In the liquid phase (the saturated portion of the soil) gravity drainage creates a downward advective flux. Evaporation of moisture from the upper soil preferentially depletes the lighter isotopes and causes enrichment in heavy isotopes, which creates an upward diffusive flux of lighter isotopes (Kendall & McDonnell, 1998). In the unsaturated level of the soil, stable isotopes diffuse as ideal gases according to Fick's law, which is driven by evaporation (Kendall & McDonnell, 1998). These processes can result in a stable isotope depth profile, characterized by a sharp increase in the concentration of heavy isotopes in the upper zones of the soil, followed by a sharp decrease, and then a gradual tapering, which brings soil water chemistry in line with precipitation chemistry (Kendall & McDonnell, 1998, Figure 5.3). In terms of isotopic fractionation, non-equilibrium (open system) conditions in the upper soil cause a preferential enrichment in  $^{18}\text{O}$  relative to  $^2\text{H}$ , which can manifest as a line sub-parallel to the LMWL that is called a Soil Evaporation Line (SEL). Evaporation Lines have a slope less than that of the LMWL, and they intersect the LMWL at a point that describes the general composition of precipitation for that location (Kendall & McDonnell, 1998).

## 2.5. Data Collection

### 2.5.1. Soil Tension

Soil tension was measured at each site using Watermark 200SS GMS probes (Irrometer, 2023). These were affixed to 12.7mm class-315 PVC pipe and inserted into holes of the same diameter augured to various depths at each site. Probes were submerged in water for 48 hours prior to deployment according to manufacturer specifications (Irrometer, 2023). The probes were connected to an Irrometer 900M data logger which recorded soil tension at 15- or 30-minute intervals. A temperature sensor was installed in the center of the PVC cylinders at each site for calibration. Probe holes were backfilled with a muddle slurry to ensure good contact with the soil and to prevent erroneous measurements from flooding. The probe readings were calibrated and converted to soil tension through Irrometer's proprietary software (WaterGraph). The first two days of recordings were discarded to allow the probes to equilibrate with the surrounding soil. Table 1 summarizes the probe depths and site characteristics. The probes at depths of 83 and 92

cm at the upper Manana station recorded spikes in soil tension, which were likely anomalies due to poor contact with the surrounding soil. The data from these probes were therefore not used in our study. Additionally, there were several periods when the data loggers failed at both Manana stations. These disruptions resulted in several gaps in the time series.

### 2.5.2. Soil Moisture Content

Soil water content was measured at the Uluakupu site using a TDR system consisting of a Tektronix 1052B Cable Tester and three TDR probes of various lengths. The TDR system works on the principle that as moisture content in the soil increases, the electrical permittivity of the soil increases, which changes the propagation speed of electromagnetic waves traveling through the soil. The soil moisture indicated by the TDR is a function of the actual probe length and the apparent probe length read by the cable tester, which is distorted by the changed wave speed. The difference between the two lengths can be used to calculate the dielectric constant of the soil according to the expression:

$$\epsilon_b = \left( \frac{x_2 - x_1}{V_p L} \right)^2 \quad (2)$$

, where  $\epsilon_b$  is the dielectric constant of the soil and water,  $x_2$  is the end TDR probe reflection distance,  $x_1$  is the beginning TDR probe reflection point distance,  $V_p$  is the relative propagation velocity (dimensionless), assumed to be 0.99 (Jones et al., 2002), and  $L$  is the actual probe length.

The transfer function to compute volumetric water from dielectric constant was found by incrementally adding water to oven dried soil from the Uluakupu site to increase volumetric water content by steps of approximately  $0.2 \text{ cm}^3 \text{ cm}^{-3}$ . The TDR probe was inserted into the soil and water mixture and the waveform parameters were recorded from the screen of the 1052B Cable Tester. The dielectric constant was computed, and a linear regression produced the transfer function between the dielectric constant and the volumetric soil moisture. The resulting transfer function to convert the dielectric constant ( $\epsilon_b$ ) to soil moisture ( $\theta$ ) is:

$$\theta = 0.055 \cdot \epsilon_b + 0.21 \quad (3)$$

Four TDR probes were installed at Uluakupu. Two Campbell Scientific CS610® 15 cm probes were installed, one at the surface and one buried at 90 cm. Another Campbell Scientific CS605® 30 cm probe was installed at the surface. Lastly, to measure a greater depth of the soil column we field constructed a 68 cm TDR probe to integrate the soil moisture through more of the rooting zone horizon (76 cm; Engott et al., 2017; Table 6). The field constructed TDR probe consisted of plastic block probe head made from a Powernail Large Tapping Block cut dimensions of 12 cm x 10 cm x 3 cm. Three 0.63 cm diameter rods with a length of 75 cm were inserted in the probe head with a spacing of 2.8 cm between them, extending 68 cm beyond the bottom of the block. The soil moisture content was measured at the Uluakupu site approximately three times per week with more frequent measurements taken during wet periods.

#### 2.5.3. Meteorological Data

At the Manana stations, temperature and relative humidity were recorded using OnSet Computer Corporation© (Bourne, Massachusetts) HOBO U14-001 Temp/RH Data Loggers, which have an operating temperature range and precision of -20°C to 50°C  $\pm 0.25^\circ\text{C}$  and an operating relative humidity range of 0 to 95% with an accuracy of  $\pm 2.5\%$  from 10 to 90% relative humidity (Onset, 2017). Precipitation was recorded at the Manana sites using an Irrometer 900RG Rain Gauge, which is a tipping bucket style rain gauge with integral bird spikes and a mounting base. The rain gauge was affixed to a 50 mm diameter PVC pipe installed in the center of the Watermark probes and connected to the Irrometer 900M data logger, which recorded precipitation every 15- to 30-minutes. The PVC pipe and the rain gauge were leveled prior to deployment to ensure proper tipping bucket performance.

Due to increased accessibility, a more extensive weather station was established at the Uluakupu site, which included measurements of temperature, humidity, precipitation, windspeed, and solar radiation. These data were collected using an OnSet Computer Corporation© portable weather station mounted on a 3 m M-TPA-KIT portable tripod, equipped with the OnSet Computer Corporation© HOBO series of sensors, and powered by a 5-watt solar panel and 12-volt storage battery. Data were averaged over 15-minute intervals using a HOBO U30 Remote Monitoring Station running HOBOware Pro 3.7.22 software. Rain was measured with a HOBO 2-RGx-M002 tipping bucket rain gauge that has a 15.4 cm receiving orifice and measures rainfall rates up to 20 mm hr<sup>-1</sup>. Solar radiation was measured with a HOBO S-LIB-M003 silicon

pyranometer with a measurement range of 0 to 1280 W m<sup>-2</sup>. Temperature and relative humidity were measured with a HOBO S-THB-M00X Temperature/Relative Humidity Sensor with a temperature range of -40°C to 75°C and an accuracy of ± 0.2°C.

#### 2.5.4. Soil Water Chemistry

Soil water samples were collected with Soil Moisture Equipment Corp. Model 190530 (30 cm) and Model 190590 (90 cm) Slim Tube Soil Water Sampler lysimeters installed at the Uluakupu station. Soil water samples were collected during periods when infiltration beneath the root zone was likely based on soil tension readings. When soil tension fell below 25 kPa a vacuum of about 60 to 80 kPa was created in the lysimeters using a hand vacuum pump. The lysimeters were then sealed and allowed to equilibrate with the surrounding soil moisture for several hours, usually overnight. Soil water was extracted using a 60 ml syringe with 0.3 cm diameter plastic tubing of sufficient length to reach the bottom of the lysimeter. Samples were collected in triple-deionized-rinsed HPDE bottles. The sample bottles were filled completely, forming a convex meniscus at the container mouth to minimize air bubbles, and were refrigerated immediately to minimize chemical reactions.

Samples were analyzed at one of two laboratories: the Isotope Biogeochemistry Laboratory at the University of Hawai‘i at Mānoa, or the Stable Isotope Ratio Facility for Environmental Research (SIRFER) at the University of Utah. Both facilities determined hydrogen and oxygen isotopic composition of rainwater using a Picarro L2130-I cavity ring-down 221 spectrometer equipped with a high-precision vaporizer (V1102-I, Picarro, 222 Inc., Santa Clara, CA, USA) and autosampler (HTC PAL, Leap Technologies, Carrboro, NC, 223 USA) with Chem-Correct acquisition software that monitors for interference of isotopologues of 224 water by organic compounds (Gupta et al., 2009). All measurements were performed in the nitrogen 225 carrier mode, using ultra-high-purity nitrogen (< 10 ppm H<sub>2</sub>O, > 99.99% N<sub>2</sub>; Matheson, Irving, 226 TX, USA) using eight 1.2 μL injections. Analytical precision determined through duplicate sampling indicates variances of ±0.35 ‰ δ<sup>18</sup>O and ±1.32 ‰ δ<sup>2</sup>H (Chapter 3, Section 2.4).

## 2.6. Data Analysis

### 2.6.1. Soil Water Retention Curve

Soil tension and soil water content data obtained at the Uluakupu site were used to create a soil water retention curve (SWRC), which enables the estimation of soil water content for a given soil tension measurement (Dunne & Leopold, 1978). Soil water content values for the 30 cm, 68 cm, and 90 cm TDR probes were plotted against the soil tension measurements at 30 cm, 60 cm, and 90 cm, respectively. Logarithmic regressions (base  $e$ ) were fitted through each tension-moisture data set to be used to estimate soil water content at the sites where TDR probes were not installed. The SWRC generated from this procedure was then used to estimate field capacity tension (Figure 5).

### 2.6.2. Soil Water Column Height

Figure 6 displays the methodology used to calculate soil water column height for each day in the time series. Soil water column height was calculated by summing soil volumetric water content along the tensiometer probe depth profile of for each station and then multiplying this value by the average porosity of the soil (Figure 6). Each station had tension readings from multiple depths which were converted to soil volumetric water content ( $\text{cm}^3 \text{ cm}^{-3}$ ) using the SWRC. For each station, readings from the shallowest probe were assumed to represent soil conditions from the ground surface down to the depth of that probe. Soil volumetric water content was extended step-wise down to the lowest depth sampled (Figure 6). Integrating soil volumetric water content over the soil depth profile produced measurements of dimension length which represent the height of water saturation within the soil column. This saturated height includes the soil matrix. Soil porosity was determined by finding the maximum soil water content on the 30 cm TDR probe – 30 cm Watermark tensiometer SWRC. This produced a soil porosity of 0.55, which is close to the value expected in silty clays (James, 1993). Multiplying the height of water saturation within the soil column by the average porosity of the soil gives the water column height with only pore spaces. The water column height provides an estimate of the total volume of water available within the soil for groundwater recharge at each time increment. The change in soil water column height was calculated for each time step to measure soil water flux.

### 2.6.3. Evapotranspiration

Evapotranspiration (ET) was calculated at each site using the Penman-Monteith equation (Penman, 1948; Monteith, 1965; Dunne & Leopold, 1978). Several forms of the Penman-Monteith equation exist. The one used in this study follows the American Society of Civil Engineers (Allen, et al., 2005), and is given by the expression:

$$PET = \frac{0.408\Delta(R_n - G) + \gamma \frac{C_n}{T+273} u_2(e_s - e_a)}{\Delta + \gamma(1 + C_d \cdot u_2)} \quad (4)$$

, where:

- $PET$  is the reference evapotranspiration for short grass surfaces given in  $\text{mm d}^{-1}$ ,
- $R_n$  is calculated net radiation at the crop surface given in  $\text{MJ m}^{-2} \text{d}^{-1}$ ,
- $G$  is soil heat flux density at the soil surface given in  $\text{MJ m}^{-2} \text{d}^{-1}$ ,
- $T$  is mean daily temperature at 1.5 to 2.5-m height ( $^{\circ}\text{C}$ ),
- $u_2$  is mean daily wind speed at 2-m height given in  $\text{m s}^{-1}$ ,
- $e_s$  is saturation vapor pressure at 1.5 to 2.5-m height (kPa),
- $e_a$  is mean actual vapor pressure at 1.5 to 2.5-m height (kPa),
- $\Delta$  is the slope of the saturation vapor pressure-temperature curve given in  $\text{kPa } ^{\circ}\text{C}^{-1}$ ,
- $\gamma$  is the psychrometric constant given in  $\text{kPa } ^{\circ}\text{C}^{-1}$ ,
- $C_n$  is a numerator constant that changes with crop reference type and time step, and
- $C_d$  is the denominator constant that changes with reference type and calculation time step.

The Penman-Monteith formula is an energy-balance which expresses the net energy accumulation at the soil surface as a measurement of potential evapotranspiration (PET). The amount of moisture this accumulated energy can remove from soil depends on vegetation, soil characteristics and available moisture. The soil and vegetation physical characteristics are captured in a parameter called the crop coefficient curve ( $C_n/C_d$ ), which varies by land cover and time timestep, and can be multiplied by the Penman-Monteith PET to convert to actual evapotranspiration (AET; Monteith, 1965; Allen et al., 2005).

At the two Manana stations, AET was calculated by taking the temperature and relative humidity data recorded on each site's HOBO Temp/RH Data Logger, solar radiation data measured at the Uluakupu site, and wind data taken from the Uluakupu site. A crop coefficient for turf grass warm season was selected for the Manana upper station (Allen, Pereira, Raes, & Smith, 1998) Table 17). The lower station resided in a sub-tropical forested area, with sparse ground cover and strawberry guava in the immediate vicinity (Figure 3). A crop coefficient of 1.00 was selected as an intermediate value between the crop coefficients for tropical fruits and trees listed in FAO 56 (Allen et al., 1998, Table 17). The AET calculations were carried out at an hourly time step and then aggregated to a daily resolution for plotting and visualization.

#### 2.6.4. Water Budget Calculations

The amount of water that infiltrated through the soil column was estimated at a daily time step by passing the soil, precipitation, and ET data through a water budget algorithm that accounted for periods when soil conditions were favorable for recharge. For all days, if either the soil water potential gradient was positive (upward) or the lowest probe tension was above field capacity tension, infiltration was set to zero. All time steps that had both a negative (downward) soil water potential gradient and a bottom probe tension reading below field capacity were tagged as infiltration periods. For these infiltration periods, if there was measured precipitation and a net loss of soil moisture from the previous time step, infiltration was calculated by adding precipitation to the change in soil moisture and then subtracting ET. For periods when there was no measured precipitation and a net loss of soil moisture, infiltration was calculated by subtracting ET from the soil moisture change. For periods when there was measured precipitation and a net increase in soil moisture from the previous time step, infiltration was calculated by subtracting the soil moisture gain and ET from precipitation. For periods when there was no measured precipitation and a net increase in soil moisture from the previous time step, infiltration was set to zero. Runoff was considered in each scenario by calculating the saturated hydraulic conductivity of soils characteristic of each site and determining if the rainfall intensity ever exceeded this threshold. This condition was not met within the time series presented here. If this condition had been met, runoff would have been calculated by subtracting the saturated hydraulic conductivity of stony alluvial land (musym rSM), which is  $7 \mu\text{m s}^{-1}$  (Soil

Survey, 2014), from the rainfall intensity of the time step, and then subtracting the resulting water amount from precipitation.

### 2.6.5. Limitations

The overall purpose of the data analysis was to develop and evaluate a method to determine an infiltration volume weighted average chemistry for water stable isotopes that considers local soil and meteorological conditions over the sampling interval. The goal was to quantitatively weight precipitation chemistry for periods when groundwater recharge was most likely to occur, versus to develop a rigorous water balance approach. Consequently, the methodology presented above has several uncertainties that limit its precision. The transform function to convert the soil dielectric constant to soil water content was determined using two soil samples. A more rigorous approach would require an assessment of all major soil types in the high recharge areas of the island. Uncertainties also arise from utilizing a single soil tension measurement to represent a depth profile of water content derived from a TDR probe in the SWRC calculations. A more rigorous approach here would require a TDR probe that spanned the entire soil rooting zone with multiple soil tensiometers deployed along the profile. The application of solar irradiation and wind data from another location created additional uncertainties in the ET calculations. Instrumental uncertainties from the devices used to collect data should also be considered. Of particular importance, while Watermark probes have been shown to reliable tools in assessing soil water content, some researchers have noted that they can be slow in responding to changes in soil moisture (Nolz et al., 2016; Thompson et al., 2006), and can be affected by poor soil contact caused by soil cracking and interaction with roots (Peries & Enciso, 2009). Given these constraints, we consider the calculated recharge to be semi-qualitative approach aimed at identifying those periods when recharge occurs to use the stable isotope composition of precipitation during those periods to estimate the composition of deep infiltration.

### Uluakupu Soil Water Retention Curves

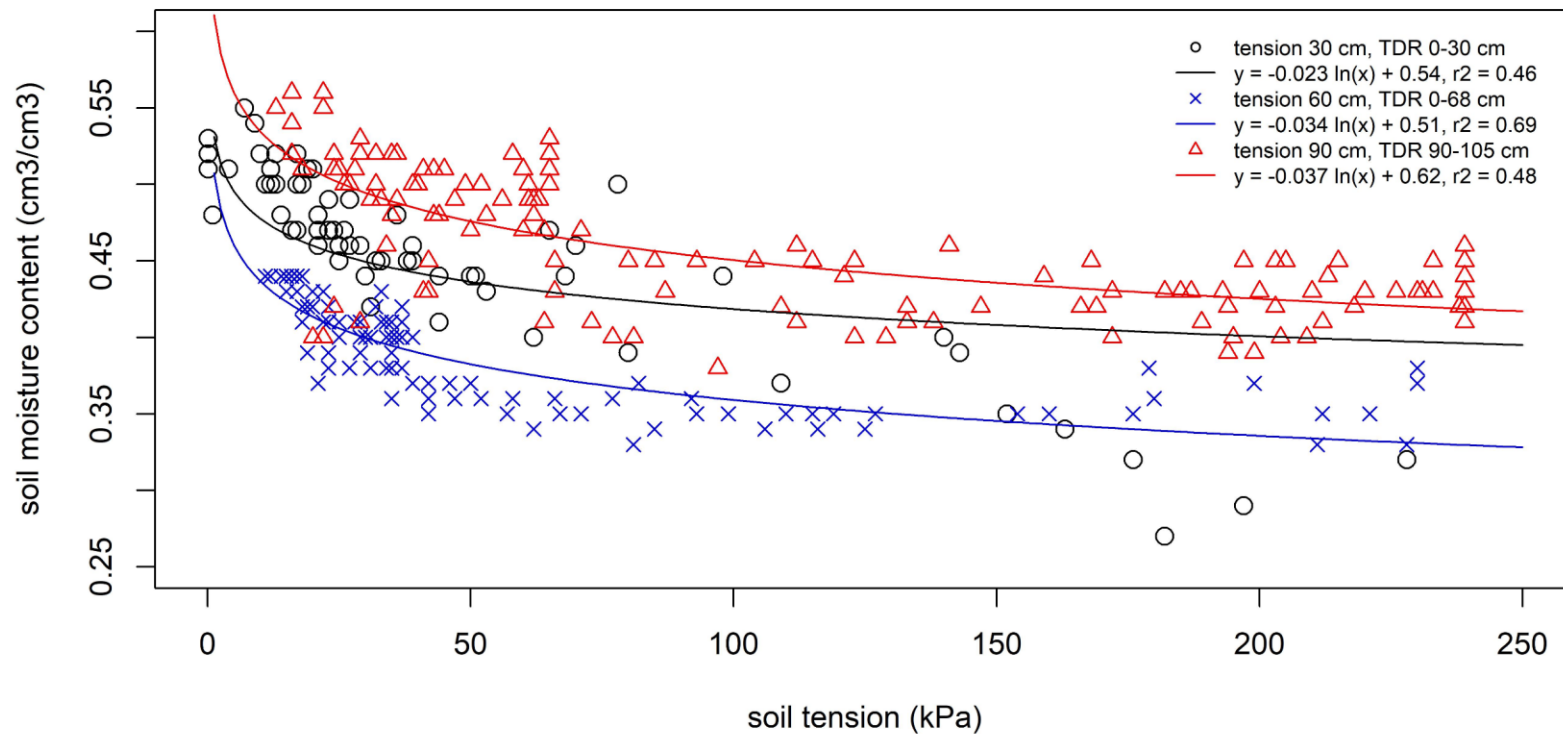


Figure 5. Soil Water Retention Curves (SWRC) developed using soil tension and soil water content data from the Uluakupu study site, O'ahu, HI, USA. Data from three time-domain reflectometry (TDR) probes and three Watermark 200SS granular matric sensor (GMS) probes. The three sets of data were plotted against one another to produce three SWRCs. The 60 cm tension, 0-68 cm TDR probe pairing (shown in blue) was selected because of the greater depth of the TDR probe, the better regression fit through the data, the intermediate depth of the 60 cm tension probe relative to the TDR probe, and the more reliable performance of the 60 cm tension probe over the sampling period.

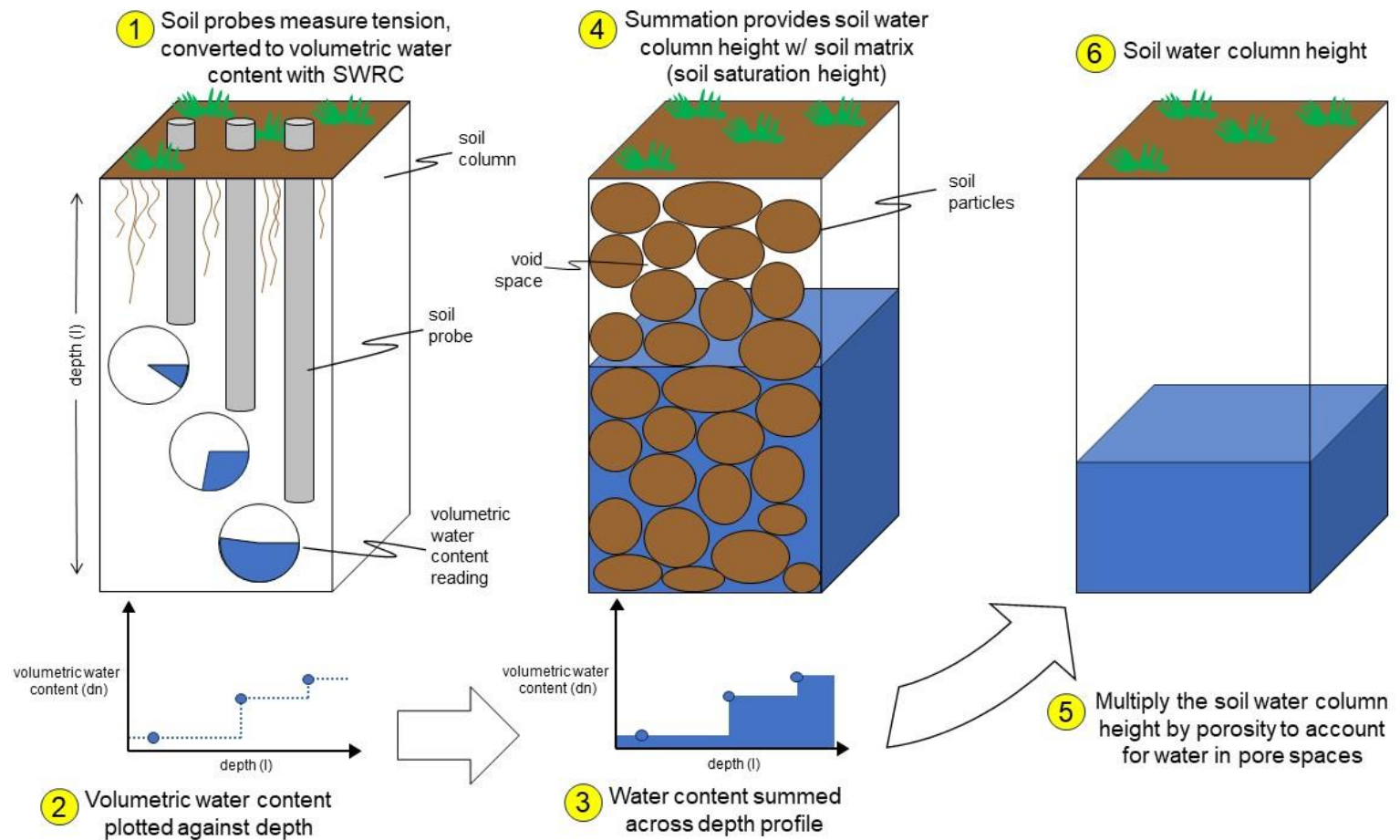


Figure 6. Graphical depiction of the method developed for calculating soil water column height and daily soil water flux in the water budget calculations.

### 3. Findings

#### 3.1. Soil Water Retention Curve

Figure 5 shows the performance of the three SWRCs calculated from the Uluakupu soil tension and TDR data. Of the three tension-TDR probe pairings discussed in section 2.6.1, the 60 cm tension – 68 cm TDR probe SWRC produced the best fit through the data ( $r^2 = 0.69$ ,  $p < 0.001$ ). We selected this SWRC to convert the Manana station tension readings to soil water content. Appendix C, Tabs C.1 and C.2 provide the results of the SWRC conversion at a daily resolution for both Manana stations. This SWRC was also used to generate the soil field capacity tension, which we determined to be 33 kPa.

#### 3.2. Infiltration Periods

Figures 7 and 8 display the changes in calculated soil water potential gradient and measured deep probe soil tension for both the upper and lower Manana stations. Deep soil tension did not exceed field capacity at any point in the sampling period for either site, indicating that deep soils below the rooting-zone maintained water content sufficient to allow infiltration through the soil column to occur. The calculated soil water potential gradient at the upper Manana station was downward for the entire sampling period, fluctuating between -0.4 and -3.2. These data suggest that the upper Manana station was continuously in recharge conditions from October 2020 to April 2021. The calculated soil water potential gradient at the lower Manana station was downward during 47% of the sampling period, with the longest continuous downward period occurring from mid-February to early-April 2021. The lower station shifted to an upward soil water potential gradient in April, corresponding to the beginning of the dry season. There were intermittent showers in April that lowered the soil water potential gradient, but these did not provide sufficient moisture to shift the overall gradient downward, suggesting that all infiltration went to replenishing shallow capillary soil water in the rooting zone during this period.

#### 3.3. Water Budget Amounts

Appendix C, Tabs C.1 and C.2 provide the results of the water budget calculations at a daily resolution for both Manana stations. Figures 9 and 10 provide a visual summary of these results. The top portions of Figures 9 and 10 show measured precipitation, estimated AET, modeled soil water content change, and modeled infiltration through the soil column. The bottom portions of

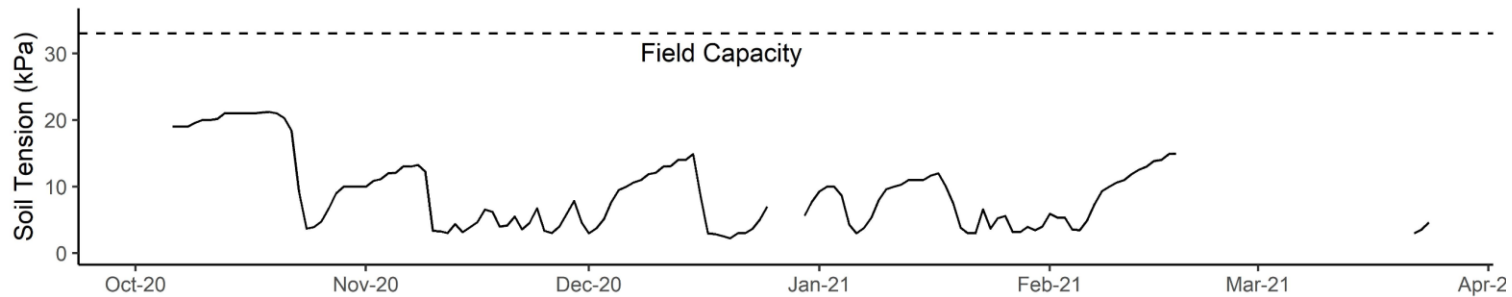
Figures 9 and 10 show stacked area charts with cumulative water amounts of precipitation, AET, and infiltration. Daily soil water content changes fluctuated between 13 mm of water loss and 22 mm water gain at the lower Manana station, and 38 mm of water loss and 48 mm of water gain at the upper station. The water budget results generally showed a logical sequence of events for periods of soil water loss. Large precipitation events were accompanied by a sharp increase in soil water content, and then followed by a period of soil water loss, likely from gravity drainage of pore water. This progression is consistent with the observed behavior of unsaturated soils during wetting events (Figures 8 and 9). Total modeled infiltration through the soil column over the sampling period at the upper Manana station was 635 mm, which is 30% lower than the long-term average (LTA) annual recharge expected over the same period (Table 2; Engott et al., 2017). Total modeled infiltration through the soil column at the lower Manana station was 322 mm, which exceeds the LTA annual recharge expected over the same period at that location by 86% (Table 2; Engott et al., 2017). Actual evapotranspiration calculated using the Penman-Montieth equation was greater than the LTA annual AET reported by (Giambelluca, et al., 2014) at both stations (Table 2). Measured precipitation at each site was lower than the LTA annual rainfall amounts reported by (Table 2; Frazier et al., 2016).

### 3.4. Soil and Precipitation H and O isotopic composition

The isotopic composition of rainfall and soil water collected at the three stations was depleted in heavy water isotopes relative to Standard Mean Ocean Water (SMOW) (Figure 11) (Kendall & McDonnell, 1998). Oxygen-18 and  $\delta^2\text{H}$  concentrations were strongly correlated, producing a LMWL of  $\delta^2\text{H} = 7.3 \delta^{18}\text{O} + 8.6$  ( $r^2 = 0.92$ ,  $p < 0.001$ ), which is similar to ones from previous studies on O‘ahu (Dores et al., 2020; Booth et al., 2021; Torri et al., 2023). The range of isotopic compositions in rainfall samples was consistent with marine precipitation (Gat, 1996), varying from  $-7.9 \text{ ‰ } \delta^{18}\text{O} / -52.0 \text{ ‰ } \delta^2\text{H}$  to  $-0.6 \text{ ‰ } \delta^{18}\text{O} / 4.3 \text{ ‰ } \delta^2\text{H}$  at the Uluakupu station. The deep soil water samples taken from the 90 cm depth lysimeter closely matched the Uluakupu precipitation chemistry, varying from  $-4.5 \text{ ‰ } \delta^{18}\text{O} / -25.2 \text{ ‰ } \delta^2\text{H}$  to  $-1.9 \text{ ‰ } \delta^{18}\text{O} / -6.2 \text{ ‰ } \delta^2\text{H}$  (Figure 11). Deep soil water response was somewhat dampened and delayed with respect to precipitation chemistry (Figure 11). Soil water sampled from the 30 cm depth lysimeter at the Uluakupu station was consistently enriched in heavy water isotopes relative to precipitation at that location, suggesting fractionation due to evaporative processes in the shallow soil (Figure

11). Shallow soil water samples plotted along a SEL of  $\delta^2\text{H} = 6.6 \delta^{18}\text{O} + 5.0$  ( $r^2 = 0.93$ ,  $p < 0.001$ ). The SEL is semi-parallel to the LMWL, so determining a starting precipitation chemistry from this relationship did not produce realistic results. Using only the Uluakupu precipitation data produced a LMWL of  $\delta^2\text{H} = 7.6 \delta^{18}\text{O} + 9.7$  ( $r^2 = 0.96$ ,  $p < 0.001$ ). The SEL intersected the Uluakupu LMWL at  $-4.7 \text{‰ } \delta^{18}\text{O} / -26.0 \text{‰ } \delta^2\text{H}$ . The volume weighted average isotopic composition of precipitation from the Uluakupu station is  $-2.7 \pm 0.7 \text{‰ } \delta^{18}\text{O} / -10.6 \pm 1.3 \text{‰ } \delta^2\text{H}$ , which is substantially enriched in heavy water isotopes relative to the SEL-LMWL intersection (Figure 11).

Manana Upper Station, Dec. 2020 - April 2021, O'ahu, HI, USA  
Soil Tension at 122cm Depth



Soil Hydraulic Gradient 0-122cm Depth

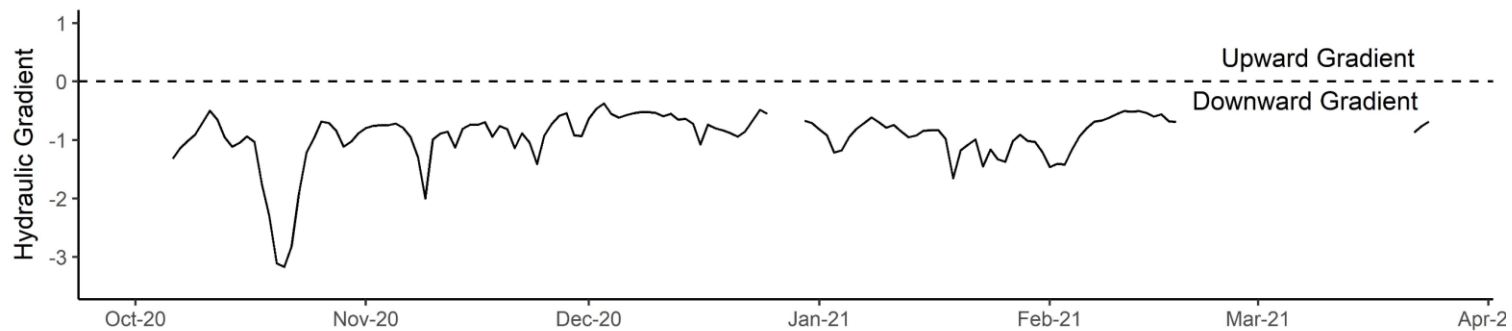


Figure 7. Time series of deep soil tension (top) and soil water potential gradient (bottom) for the upper Manana station. Field capacity was set at 33 kPa.

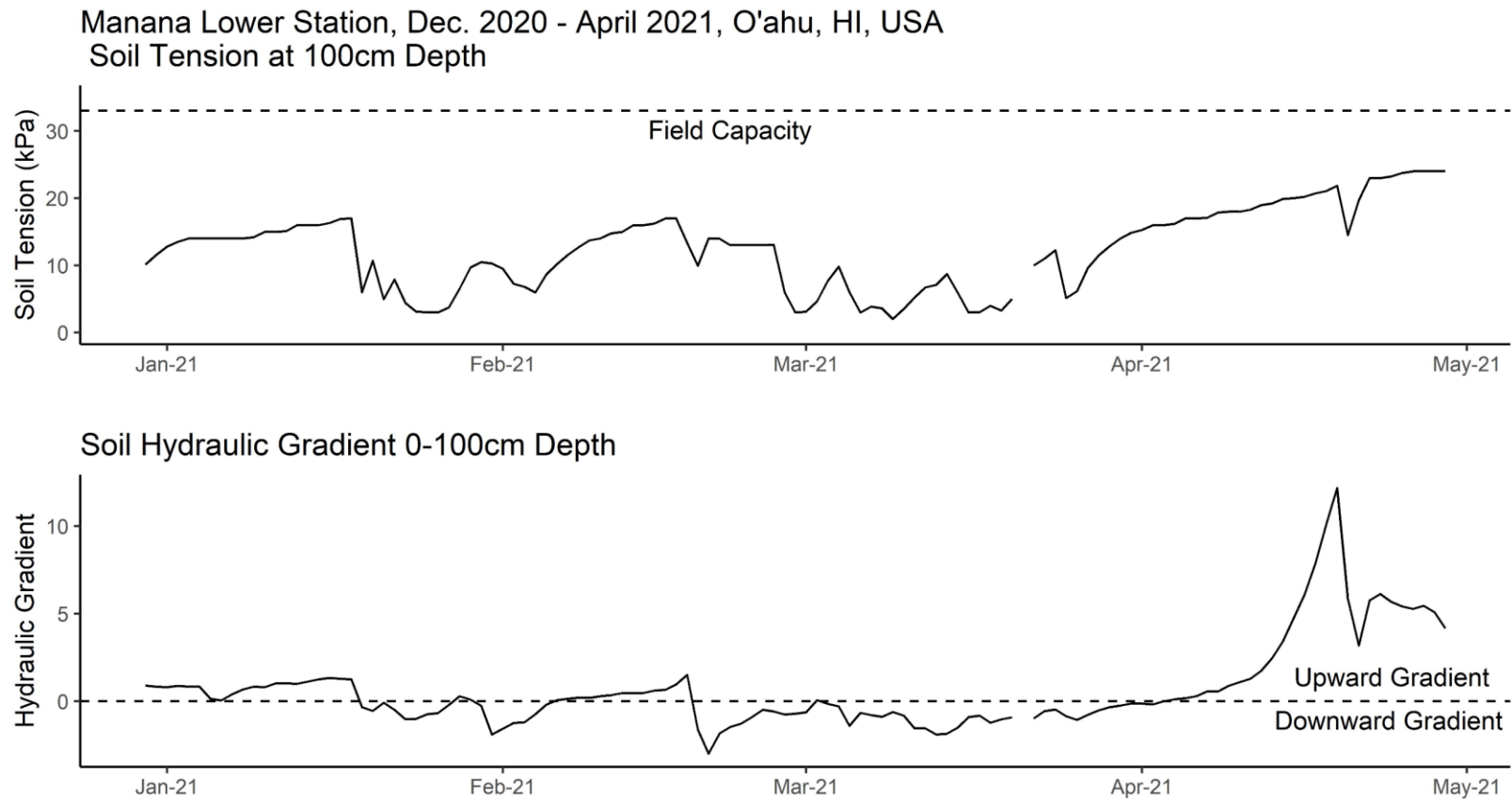


Figure 8. Time series of deep soil tension (top) and soil water potential gradient (bottom) for the lower Manana station. Field capacity was set at 33 kPa.

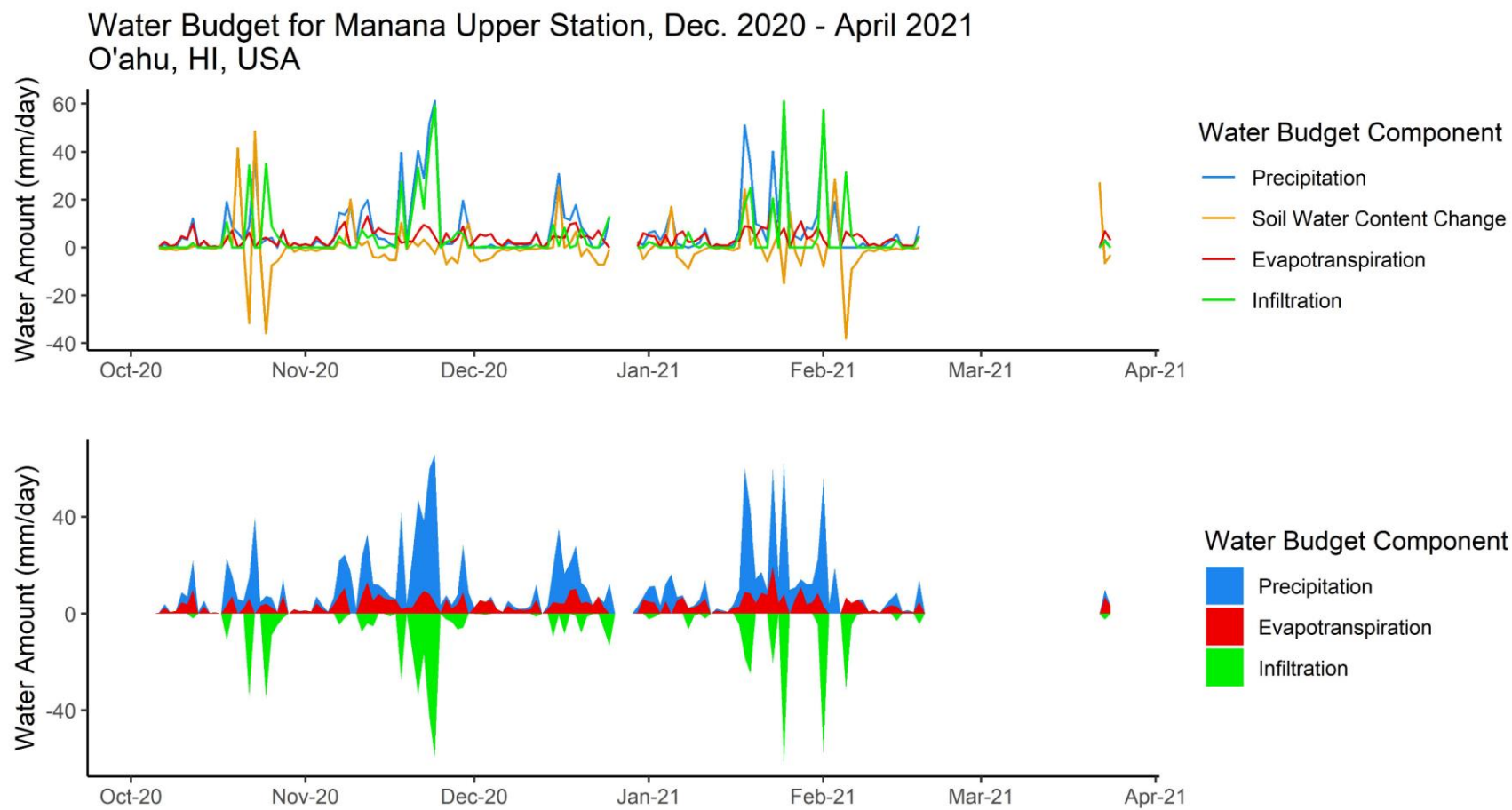


Figure 9. Time series of water budget components for the upper Manana study site. Top: Line plot of precipitation soil water content change, evapotranspiration, and infiltration. Bottom: Stacked area plot of water budget components. Infiltration is shown in green and inverted relative to precipitation and evapotranspiration to aid in visualization.

Water Budget for Manana Base Station, Dec. 2020 - April 2021  
O'ahu, HI, USA

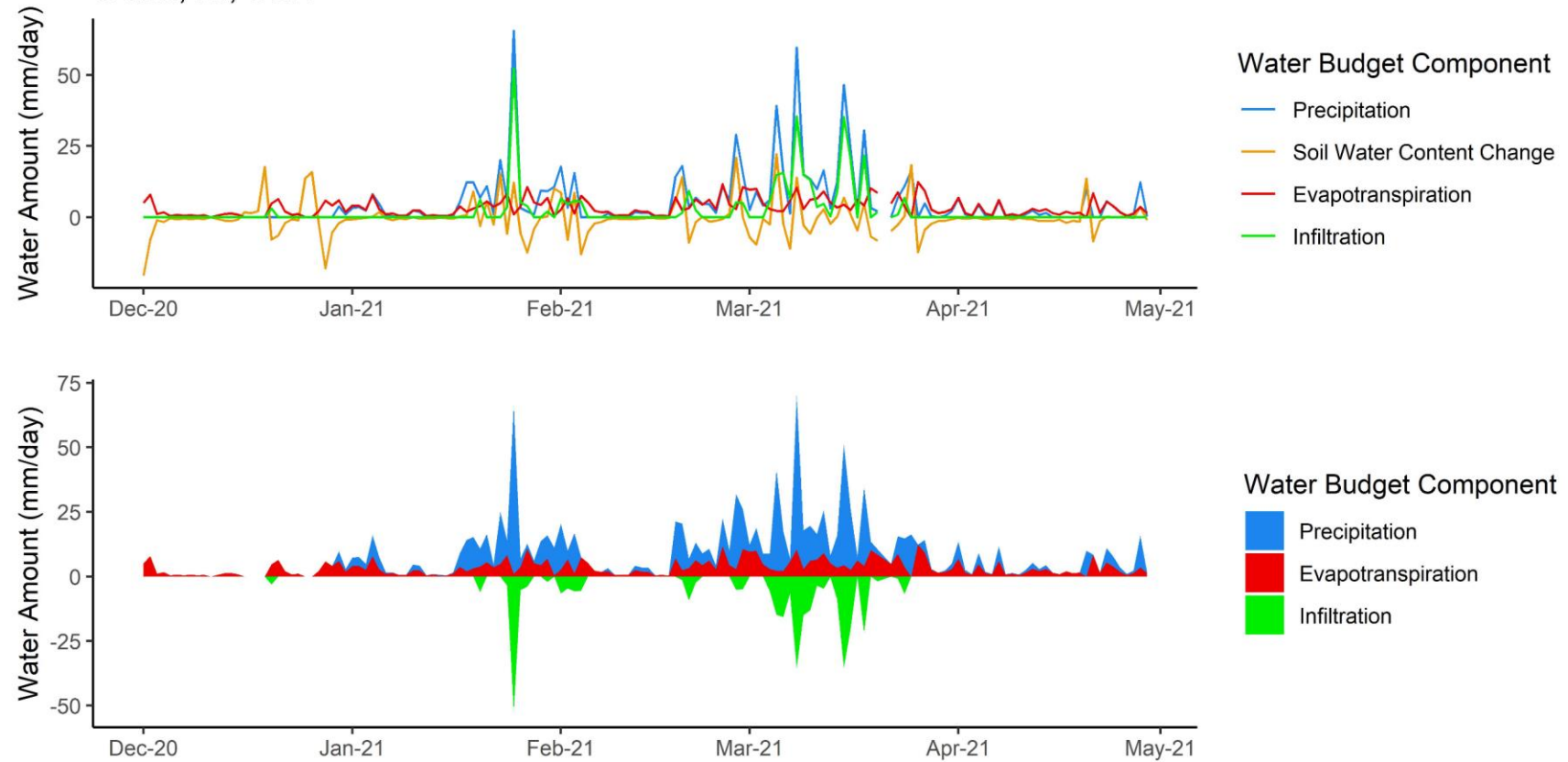


Figure 10. Time series of water budget components for the lower Manana study site. Top: Line plot of precipitation soil water content change, evapotranspiration, and infiltration. Bottom: Stacked area plot of water budget components. Infiltration is shown in green and inverted relative to precipitation and evapotranspiration to aid in visualization.

Table 2. Summary of water budget model results for the upper and lower Manana study sites. Abbreviations: long-term average (LTA); point precipitation (Precip.); percent difference (% Diff.); actual evapotranspiration (AET); Penman-Montieth evapotranspiration (P-M AET); long-term average recharge (LTA Rech.); change in soil water content ( $\Delta$ SW). Long-term average precipitation values were taken from Frazier et al. (2016). Long-term average AET values were taken from Giambelluca et al. (2014). Long-term average groundwater recharge values were taken from Engott et al. (2017) and derived by weighting annual recharge according to monthly LTA precipitation expected over the study period.

Site	LTA Precip.	Measured Precip.	% Diff.	LTA AET	P-M AET	% Diff.	LTA Rech.	Modeled Infil.	% Diff.	Cumulative soil water change	Anomaly (P - ET - I - $\Delta$ SW)
Manana Lower	653	610	-7%	350	489	40%	173	322	86%	-42	-116
Manana Upper	1658	937	-43%	444	514	16%	913	635	-30%	19	490

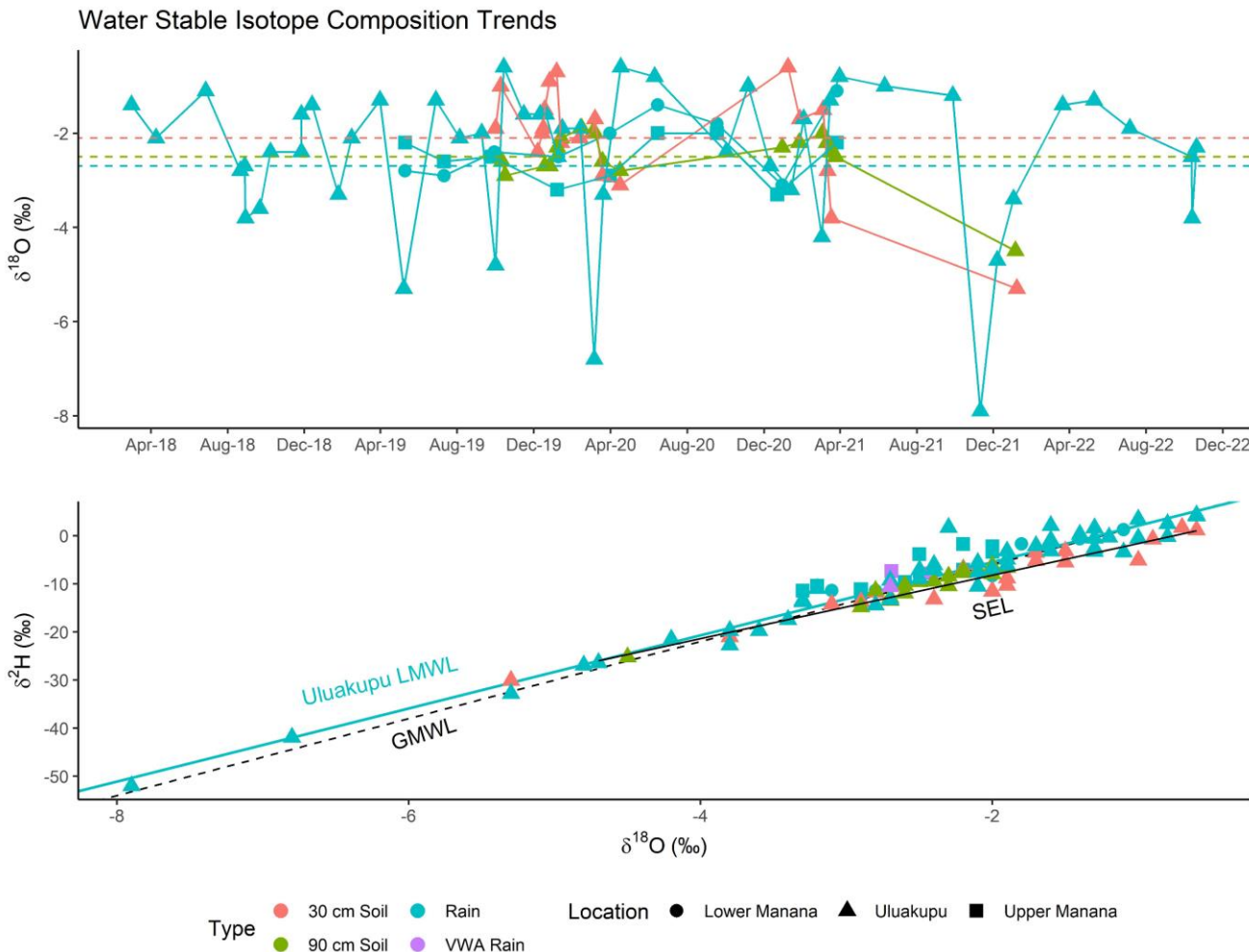


Figure 11. Top: Time series of  $\delta^{18}\text{O}$  of precipitation from the Uluakupu, Upper Manana and Lower Manana study sites, and of soil water from the Uluakupu site. Volume-weighted average precipitation chemistry from the Uluakupu station is shown as a dashed line in blue. Average soil chemistry for the 30 cm and 90 cm lysimeters are shown as dashed lines in coral and green, respectively. Bottom: Plot of  $\delta^2\text{H}$  vs.  $\delta^{18}\text{O}$  of precipitation and soil water from all three study sites. The local meteoric water line (LMWL) was calculated using precipitation collected only at the Uluakupu site. The global meteoric water line (GMWL) was set as  $\delta^2\text{H} = 8 \cdot \delta^{18}\text{O} + 10$  (Gat, 1996). The soil evaporation line (SEL) was calculated by using only soil water chemistry from the 30 cm probe.

## 4. Discussion

### 4.1. Soil Water Retention Curve Performance

Our results indicate the Uluakupu SWRC provides a reasonable approximation of soil water content at the Manana stations. Of the three tension-TDR probe pairings discussed in section 2.6.1, the 60 cm tension – 68 cm TDR probe pairing was selected to generate the SWRC to for converting the Manana station tension readings to soil water content (Figure 5). This selection was made because of the greater depth of the 68 cm TDR probe, the better regression fit through the data, the intermediate depth of the 60 cm tension probe relative to the TDR probe, and the more reliable performance of the 60 cm tension probe over the sampling period. The 30 cm depth Watermark probe would have been a better pairing, as this was approximately halfway down the length of the TDR probe and thus a better representative value for integrated soil water content along the entire probe length. This probe produced anomalously high tension readings for several long stretches from February to October 2022. These irregularities suggest there was some constriction of water movement near the probe during this period, possibly due to an aquitard or the muddy-clay-rich slurry that was added to the probe shaft during installation. After October 2022, approximately halfway through the time series, the 30 cm probe signal became more regular, showing readings that tracked along with the 60 cm and 90 cm probes. We speculate that this was due to the soil settling, which resulted in better contact with the probe and more realistic readings. The 60 cm depth Watermark probe provided consistent, gradual tension readings throughout the sampling interval, consistent with the expected changes in soil moisture.

The SWRC was tested by observing its performance responding to precipitation events at the Manana stations, the theory being that the soil moisture content change should approximately mirror the amount of precipitation received at that site. This test ignores changes due to runoff, ET, and infiltration so its precision is limited, but we propose that it serves as a good first pass test to check that soil moisture changes are generally proportional to and synchronized with precipitation events. Figures 12 and 13 displays the results of this analysis for both Manana stations. Regression analysis of soil water column height change vs. point precipitation at each site did not produce strong results (Figures 12 and 13). We speculate that the precision of the Irrrometer 900RG Rain Gauge, which recorded precipitation amount to the nearest 0.25 mm, might have contributed to the poor regression performance (Figures 12 and 13). The results could also have been impacted by delayed responses from the Watermark probes. Though there

was not a strong quantitative agreement between soil water content change and precipitation amount, there is a noticeable qualitative correspondence that can be observed in the bottom portions of Figures 12 and 13. Soil water column height change and precipitation amount generally tracked together within approximately 5-10 mm, which is within the error range that would be expected from ignoring ET and runoff (Figures 12 and 13). This performance justified the application of the Uluakupu SWRC to the Manana station soil tension readings, which enabled us to estimate soil water flux using the water budget algorithm approach previously described.

#### 4.2. Water Budget Model Performance

Overall, we assess that the water budget model did a good job predicting relative infiltration amounts, but we note that discrepancies between predicted infiltration and long-term average recharge suggest this method may have limited precision. The modeled infiltration through the soil column at the upper Manana station produced an anomaly of +490 mm when ET, infiltration, and cumulative soil water change were subtracted from precipitation (Table 2). In other words, 490 mm of water was added to the system but not accounted for through either soil water content change, ET, or infiltration. The most likely culprits for this discrepancy are unaccounted-for runoff, and uncertainties in the soil water content, and ET calculations. It is well established that streams draining from the Ko‘olau Range are sensitive to intense rainfall (Lau & Mink, 2006) so runoff and shallow subsurface flow are important components of water budgets in these regions. It is possible that local irregularities in the soil structure and composition at the upper Manana station caused variances in soil saturated hydraulic conductivity ( $K_{sat}$ ), which was a key parameter used to screen rainfall intensity in the water budget algorithm. Locations with lower saturated hydraulic conductivity, either due to higher clay content, or other chemical and structural features, would have a lower rainfall intensity threshold, and would generate surface runoff more quickly than soils where  $K_{sat} \approx 7 \mu\text{m s}^{-1}$ . Unaccounted-for runoff due to lower  $K_{sat}$  could thus explain at least a portion of the positive anomaly at the upper Manana station.

Interpreting the data from the lower Manana station is more challenging, but the deviations from long term averages are likely due to similar factors. The modeled infiltration at the lower station was 86% greater than long term average recharge expected over the same period (Table 2). Modeled AET was higher, measured precipitation was lower, and the soil moisture sensors

showed a net loss of 43 mm of soil moisture over the sampling period. With less water entering the system, and more water leaving the system through ET and soil drainage, the expectation would be reduced infiltration, yet the lower Manana station produced an anomaly of -116 mm. It is possible that these deviations from the long-term averages were due to some specific aspects of the water budget calculations. At each time step, ET was screened to limit it to the moisture available from precipitation and soil moisture change. During some time-steps, ET was artificially set to zero or limited below the Penman-Montieth ET to constrain it to available moisture. It is possible that in these instances, the true ET was higher, drawing on deeper or adjacent soil moisture. This would have artificially increased the modeled infiltration and could explain part of the deviation. Discrepancies between soil water flux, ET and precipitation also could have been caused by delayed responses in the Watermark sensors. Lastly, we reiterate that several assumptions were made in the calculations for ET and soil moisture change, and all of these could have contributed to uncertainty in the modeled infiltration at both sites. Despite uncertainties, we assess that this method serves as a usable framework for estimating infiltration volume-weighted average precipitation. Due deployment delays, equipment malfunctions, and COVID-19 related complications, we were unable to obtain more than two overlapping precipitation chemistry samples for either of the Manana sites which prevented us from obtaining meaningful infiltration volume weighted averages for those sites.

#### 4.3. Soil Moisture Dynamics Impacting Groundwater Chemistry

The infiltration model results and the chemical data both support the contention that soil moisture dynamics play an important role in determining the stable isotope composition of infiltration. Comparison of infiltration and precipitation time series data shows that after extended periods of low precipitation, precipitation events were generally not accompanied by infiltration (Figures 9 and 10). We speculate that during these initial events, precipitation was replenishing soil capillary water, which is consistent with the observed behavior of unsaturated soils during wetting (Jones et al., 2002; Or & Tuller, 1999; 2002; Tuller et al., 1999; Phillips, 2010; Brooks, 2015). Extended or voluminous precipitation events following dry periods created a delayed infiltration response. Subsequent precipitation events generally produced proportional infiltration (Figure 13). In terms of chemistry, we speculate that initial soil wetting precipitation events minimally impacted the chemistry of infiltrating water as this moisture would have been

bound up into the soil as capillary water. Lending further support to this, at the Uluakupu site we observed enriched shallow soil water that tracked along a SEL, while deep soil water mirrored precipitation chemistry and plotted along a LMWL (Figure 11). Shallow soil water in the rooting zone is subject to evaporation, which is a kinetic fractionation process that we would expect to cause a departure from the LMWL (Gat, 1996). Soil water from the 30 cm depth lysimeter was enriched in  $\delta^{18}\text{O}$  by 0.4 ‰ relative to the 90 cm depth lysimeter. These trends suggest a physical separation of shallow pore water and deep gravitational water, which has been observed in other ecohydrological stable isotope studies (Brooks et al., 2010; Herve-Fernandez et al., 2016). If true, this would imply that precipitation immediately following dry periods goes almost exclusively to replenishing soil capillary water, and that the chemistry of water that infiltrates through the soil column is dominated by subsequent precipitation events that occur while soil moisture conditions remain favorable for recharge.

These findings raise several questions and indicate a need for more research. If the chemistry of precipitation immediately following dry periods does not impact recharge chemistry, and by extension groundwater chemistry, this begs the question as to whether dry season precipitation can be ignored in assessing groundwater chemistry, and whether recharge chemistry can be inferred without continuous soil moisture monitoring and precipitation chemistry sampling. Though there is an observable seasonal variation in the stable isotope composition of precipitation (Chapter 3, Figure 7), the chemistry and impact of initial soil wetting precipitation events may be highly variable. For example, the most heavily depleted rainfall sample at Uluakupu was collected from 9/27/2021 – 11/10/2021, which marks the transition between dry and wet seasons. Uluakupu received low rainfall over the preceding period, so soil conditions were dry. The depleted rainfall received during this period saturated the shallow capillary water reservoir and drained to the deeper soil water, as evidenced by the soil water samples from this period (Figure 11). In this instance the distinct chemistry of precipitation received during this period extended to deep soil water, and likely to groundwater recharge. This would seem to agree with the observations of Dores et al (2021), who found that large, isotopically depleted, synoptic storms provided most of the groundwater recharge in the dryer, leeward areas of O‘ahu. Complicating matters further, it should be noted that seasons do not necessarily correspond to soil moisture conditions. There can be long periods of reduced precipitation during the wet season which dry the soil sufficiently to change the soil water potential gradient.

The impacts of elevation and runoff also need to be explored more thoroughly. The depth of the soil horizon pinches out as the elevation on O‘ahu increases, giving way to rocky cliffs and steep ridgelines in the upper Ko‘olau Range. Soil moisture dynamics may be irrelevant above a certain elevation, where most precipitation becomes runoff. Stream dynamics and shallow subsurface hydrology in the intervening valleys between ridgelines then become the critical areas for exploring the evolution of precipitation chemistry. These findings and questions indicate that great care should be taken in inferring infiltration chemistry from precipitation chemistry, and they clearly indicate that more stable isotope research is needed to fully understand the connections between soil moisture dynamics and the stable isotope composition of infiltration on O‘ahu.

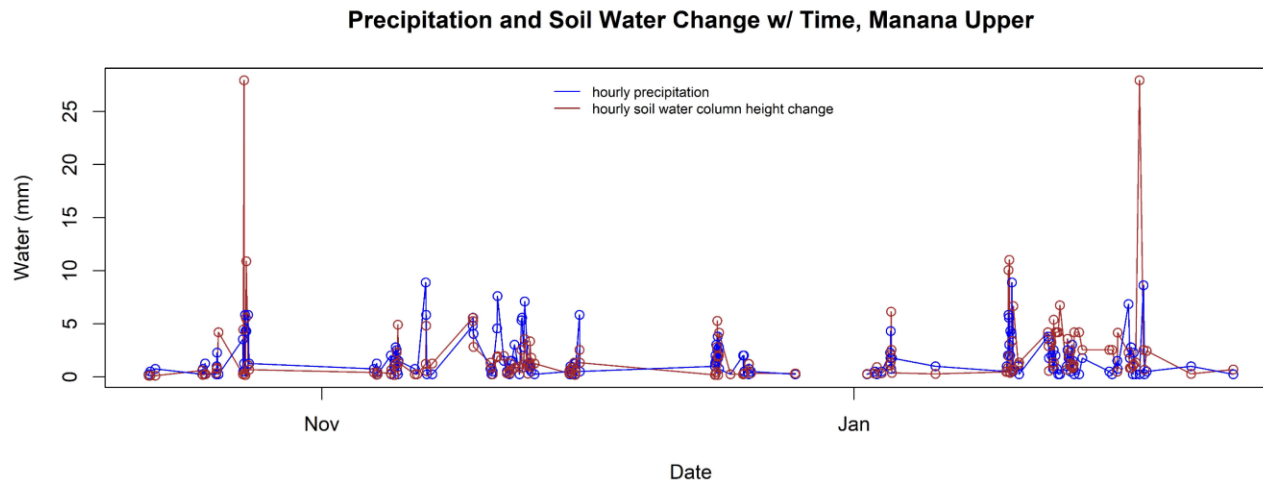
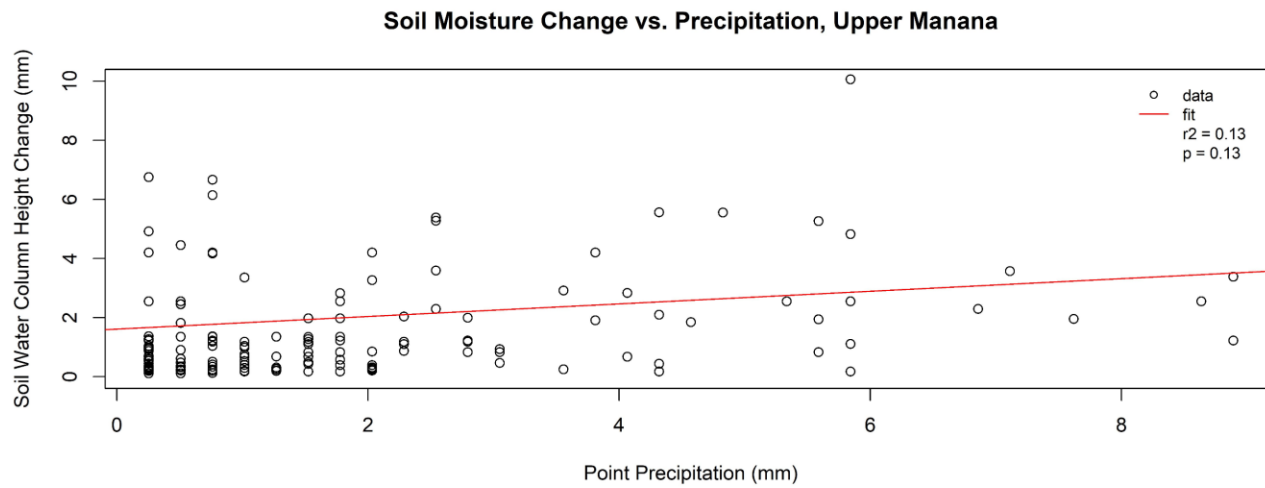


Figure 12. Top: Hourly soil water column height change vs. hourly point precipitation from the upper Manana study site. Bottom: Time series of hourly soil water content change and hourly measured precipitation. For both plots, only timesteps with measured point precipitation and infiltration were plotted.

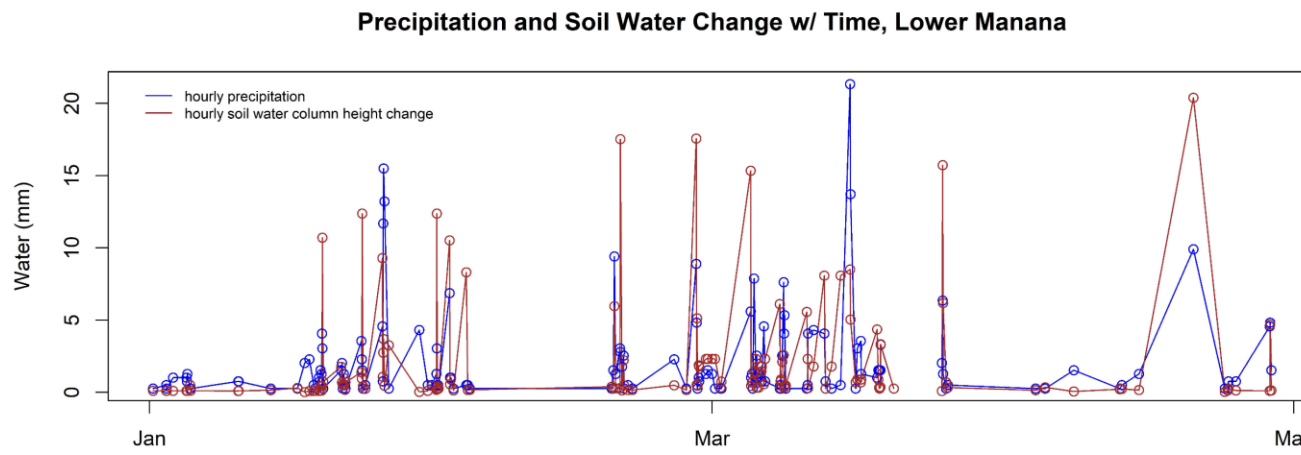
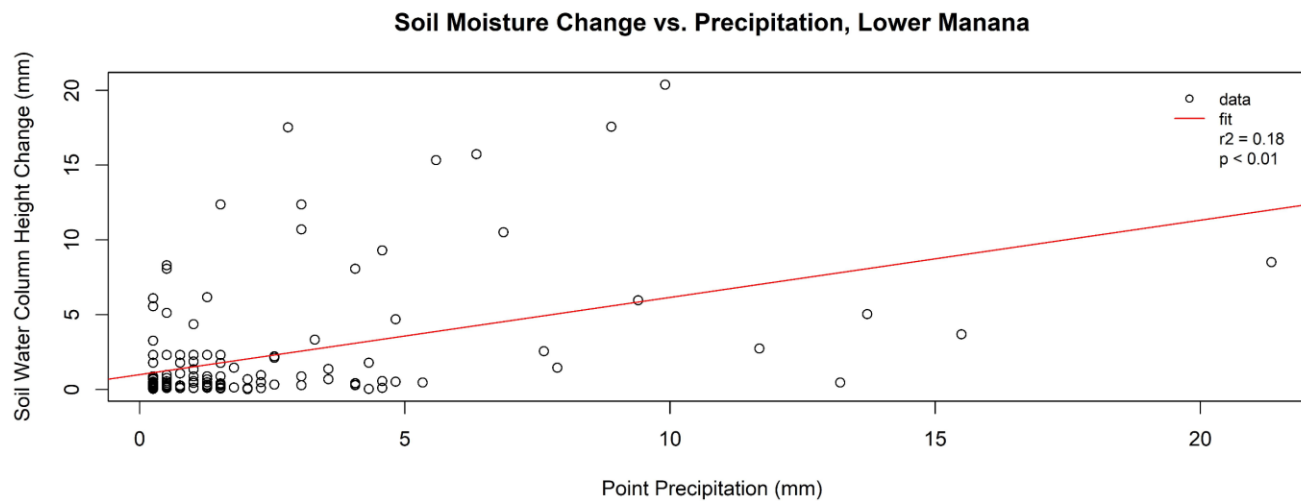


Figure 13. Top: Hourly soil water column height change vs. hourly point precipitation from the lower Manana study site. Bottom: Time series of hourly soil water content change and hourly measured precipitation. For both plots, only timesteps with measured point precipitation and infiltration were plotted.

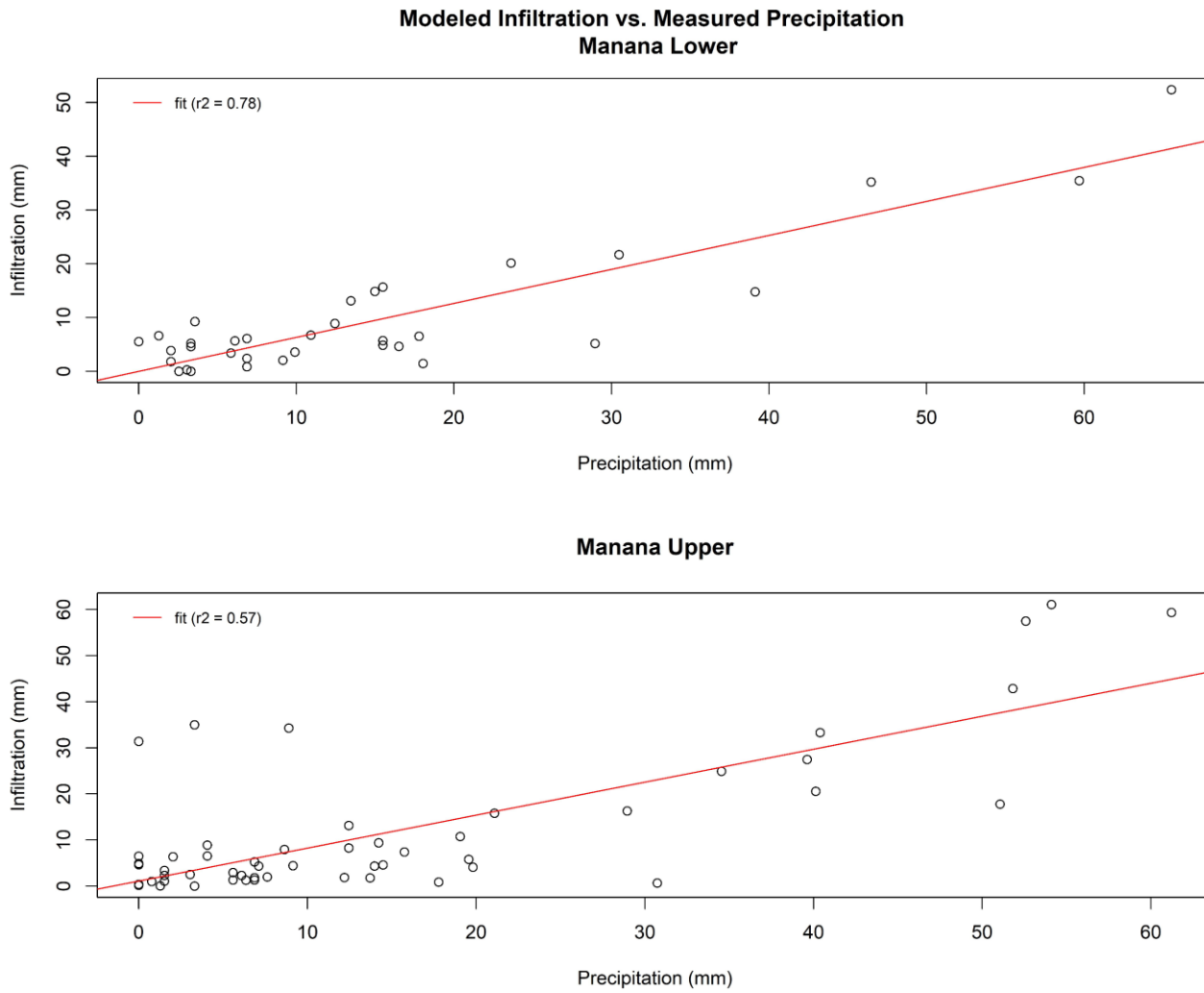


Figure 14. Regression analysis of daily modeled infiltration vs. measured precipitation for both upper and lower Manana study sites. Both linear fits produced p-values less than 0.001.

## 5. Conclusion

In this study we analyzed soil moisture, meteorological, and chemical data from three stations in the Waimano Section of the ‘Ewa Forrest Reserve on the island of O‘ahu. The initial intent of this effort was to calculate the infiltration volume-weighted average chemistry of precipitation to explore the chemical connectivity between groundwater and precipitation. In other words, our intent was to weight precipitation chemistry according to the periods and amount of infiltration to trace local groundwater chemistry to points of recharge up gradient. Several factors complicated research efforts, and the scope was narrowed to focus on presenting new geochemical and meteorological data, while evaluating the methodology developed to estimate infiltration amount, and discussing the major trends observed in the data. As an initial step we created a transfer function to convert TDR probe readings to soil water content in native soil. Soil tension and soil water content measurements at the Uluakupu station were used to develop a soil water retention curve, which was subsequently used to convert tension readings at the two Manana stations to soil water content. Soil water content at the two Manana stations was integrated along the soil profile to calculate soil water column height and soil water flux. We used meteorological data from the Uluakupu station to calculate evapotranspiration at the two Manana stations using the Penman-Monteith equation. This allowed us to estimate infiltration while factoring in soil conditions, precipitation, evapotranspiration, and runoff. Infiltration estimates confirmed that latent soil conditions and precipitation trends play important roles in determining when infiltration occurs. Discrepancies between model results and long-term averages suggest refinement of the model may be needed but could also represent the normal variability in long term averages. Comparison of the trends in modeled infiltration, measured precipitation and soil chemistry suggest a portioning of soil water. Shallow soil water plotted along a SEL, indicating kinetic fractionation likely from evaporation, whereas deep soil plotted along a LMWL. We assess that these chemical trends indicate precipitation immediately following dry periods is sequestered in the shallow soil as capillary water, while subsequent precipitation moves deeper into the soil as gravitational water. Understanding the source and evolution of soil water chemistry, and developing a methodology to compute infiltration chemistry, are important preliminary steps in utilizing natural geochemical tracers in precipitation to explore groundwater flow paths and recharge processes on O‘ahu. The work

presented here contributes to those goals and opens several avenues for future complimentary research.

## 6. Chapter 4 References

- Allen, R., Pereira, L., Raes, D., & Smith, M. (1998). *Crop Evapotranspiration - Guidelines for Computing Crop Water Requirements - FAO Irrigation and Drainage Paper 56*. Rome: Food and Agricultural Organization of the United Nations.
- Allen, R., Walter, I., Elliott, R., Howell, T., Itenfisu, D., Jensen, M., & Snyker, R. (2005). *The ASCE Standardized Reference Evapotranspiration Equation*. American Society of Civil Engineers. doi:<https://doi.org/10.1061/9780784408056>
- Awaleh, M., Baudron, P., Soubaneh, Y., Boschetti, T., Hoch, F., Egueh, N., . . . Gassani, J. (2017). Recharge, groundwater flow pattern and contamination processes in an arid volcanic area: Insights from isotopic and geochemical tracers (Bara aquifer system, Republic of Djibouti). *Journal of Geochemical Exploration*, 175, 82-98. doi:<https://doi.org/10.1016/j.gexplo.2017.01.005>
- Booth, H., Lautze, N., Tachera, D., & Dores, D. (2021). Event-Based Stable Isotope Analysis of Precipitation Along a High Resolution Transect on the South Face of O'ahu, Hawai'i. *Pacific Science*, 75(3), 421–441. doi:<https://doi.org/10.2984/75.3.9>
- Brooks, J. (2015). Water, bound and mobile. *Science*, 349(6244), 138-139. doi:<https://doi.org/10.1126/science.aac4742>
- Brooks, J., Barnard, H., Coulombe, R., & McDonnell, J. (2010). Ecohydrologic separation of water between trees and streams in a Mediterranean climate. *Nature Geoscience*, 3(2), 100-104. doi:<https://doi.org/10.1038/ngeo722>
- Craig, H. (1961). Isotopic Variations in Meteoric Waters. *Science*, 133(3465), 1702-1703. doi:<https://doi.org/10.1126/science.133.3465.1702>
- Dansgaard, W. (1964). Stable Isotopes in Precipitation. *Tellus*, 16, 436-468.
- Davis, H., Lee, C., Bradley, E., & Payne, B. (1970). Geohydrologic Interpretations of a Volcanic Island from Environmental Isotopes. *Water Resources Research*, 6(1), 99-109. doi:<https://doi.org/10.1029/WR006i001p00099>
- Dores, D., Glenn, C. R., Torri, G., Whittier, R. B., & Popp, B. (2020). Implications for groundwater recharge from stable isotopic composition of precipitation in Hawai'i during the 2017–2018 La Niña. *Hydrological Processes*, 34(24), 4675–4696. <https://doi.org/10.1002/hyp.13907>.
- Dunne, T., & Leopold, L. B. (1978). *Water in Environmental Planning*. W.H. Freeman.
- Engott, J. A., Johnson, A. G., Bassiouni, M., Izuka, S. K., & Rotzoll, K. (2017). *Spatially distributed groundwater recharge for 2010 land cover estimated using a water-budget*

*model for the Island of O‘ahu, Hawai‘i (ver 2.0, December 2017).* U.S. Geological Survey Scientific Investigations Report 2015–5010, 49 p. doi:<https://doi.org/10.3133/>

Fackrell, J. K., Glenn, C. R., Thomas, D., Whittier, R., & Popp, B. (2020). Stable isotopes of precipitation and groundwater provide new insight into groundwater recharge and flow in a structurally complex hydrogeologic system: West Hawai‘i, USA. *Hydrogeology Journal*, 28(4), 1191–1207. <https://doi.org/10.1007/s10040-020-02143-9>.

Frazier, A., & Giambelluca, T. (2017). Spatial trend analysis of Hawaiian rainfall from 1920 to 2012. *International Journal of Climatology*, 37(5), 2522–2531. doi:<https://doi.org/10.1002/joc.4862>

Frazier, A., Giambelluca, T., Diaz, H., & Needham, H. (2016). Comparison of Geostatistical Approaches to Spatially Interpolate Month-year Rainfall for the Hawaiian Islands. *International Journal of Climatology*, 36(3), 1459-1470. doi:<https://doi.org/10.1002/joc.4437>

Gat, J. (1996). Oxygen and Hydrogen Isotopes in the Hydrologic Cycle. *Annu. Rev. Earth Planet. Sci.*, 24, 225-262.

Giambelluca, T., Shuai, X., Barnes, M., Alliss, R., Longman, R., Miura, T., . . . Businger, A. (2014). *Evapotranspiration of Hawai‘i, Final Report: Submitted to U.S. Army Corps of Engineers-Honolulu District and Commission on Water Resource Management*. Honolulu: State of Hawai‘i.

Glenn, C., Whittier, R., Dailer, M., El-Kadi, A., Fackrell, J., Kelly, J., . . . Sevadjian, J. (2013). *Lahaina Groundwater Tracer Study - Lahaina, Maui, Hawaii*. Final Report prepared from the State of Hawaii Department of Health, the U.S. Environmental Protection Agency, and the U.S. Army Engineer Research and Development Center.

Gupta, P., Noone, D., Galewski, J., Sweeney, C., & Vaughn, B. (2009). Demonstration of high-precision continuous measurements of water vapor isotopologues in laboratory and remote field deployments using wavelength-scanned cavity ring-down. *Rapid Communications in Mass Spectrometry*, 23, 2534-2542.

Herve-Fernandez, P., Oyarun, C., Brumbt, C., Huygens, D., Bode, S., Verhoest, N., & Boeckx, P. (2016). Assessing the 'two water worlds' hypothesis and water sources for native and exotic evergreen species in south-central Chile. *Hydrological Processes*, 30, 4227-4241. doi:<https://doi.org/10.1002/hyp.10984>

Hildenbrand, A., Marlin, C., Conroy, A., Gillot, P., Filly, A., & Massault, M. (2005). Isotopic approach of rainfall and groundwater circulation in the volcanic structure of Tahiti-Nui (French Polynesia). *Journal of Hydrology*, 302(1-4), 187-208. doi:<https://doi.org/10.1016/j.jhydrol.2004.07.006>

Irrometer. (2023). Watermark Soil Moisture Sensor - Model 200SS. *Specification document*. Retrieved from Irrometer: [www.irrometer.com](http://www.irrometer.com)

James, L. (1993). *Principles of Farm Irrigation System Design*. Malabar, FL: Krieger Publishing Company.

Jones, S., Wraith, J., & Or, D. (2002). Time domain reflectometry measurement principles and applications. *Hydrological Processes*, 16, 141-153. doi:10.1002/hyp.513

Kelly, J., & Glenn, C. (2015). Chlorofluorocarbon Apparent Ages of Groundwaters from West Hawai'i. *Journal of Hydrology*, 527, 355-366.  
doi:<https://dx.doi.org/10.1016/j.jhydrol.2015.04.069>

Kendall, C., & McDonnell, J. J. (1998). *Isotope Tracers in Catchment Hydrology*. Elsevier.

Lau, L., & Mink, J. F. (n.d.). *Hydrology of the Hawaiian Islands*. 2006: University of Hawai'i Press.

Lee, K., Kim, J., Lee, D., Kim, Y., & Lee, D. (2007). Analysis of water movement through an unsaturated soil zone in Jeju Island, Korea using stable oxygen and hydrogen isotopes. *Journal of Hydrology*, 345(3-4), 199-211.  
doi:<https://doi.org/10.1016/j.jhydrol.2007.08.006>

Monteith, J. (1965). Evaporation and environment. G.E. Fogg (ed.) *Symposium of the Society for Experimental Biology, The State and Movement of Water in Living Organisms*. 19, pp. 205-234. NY, USA: Academic Press.

Nolz, R., Cepuder, P., Balas, J., & Loiskandl, W. (2016). Soil water monitoring in a vineyard and assessment of unsaturated hydraulic parameters as thresholds for irrigation management. *Agricultural Water Management*, 164, 235-242.  
doi:<https://dx.doi.org/10.1016/j.agwat.2015.10.030>

Onset. (2017). HOBO U14 Data Logger User Manual. Pocasset, MA: Onset Computer Corporation. Retrieved from <https://www.onsetcomp.com/sites/default/files/resources-documents/13416-E%20U14-00x%20Manual.pdf>

Or, D., & Tuller, M. (1999). Liquid retention and interfacial area in variably saturated porous media: Upscaling from single-pore to sample-scale model. *Water Resources Research*, 35(12), 3591-3605. doi:<https://doi.org/10.1029/1999WR900262>

Penman, H. (1948). Natural Evaporation from Open Water, Bare Soil and Grass. *Proceedings of the Royal Society of London, Series A, Mathematical and Physical Sciences*, 193, pp. 120-145. doi:<https://doi.org/10.1098.rspa.1948.0037>

Peries, X., & Enciso, J. (2009). Interpretation of Watermark Sensor Readings in Specific Soil Types. *Subtropical Plant Sciences*, 61, 6-14.

Phillips, F. (2010). Soil-water bypass. *Nature Geoscience*, 3(2), 77-78.  
doi:<https://doi.org/10.1038/ngeo762>

Scholl, M. A., Gingerich, S. B., & Tribble, J. W. (2002). The influence of microclimates and fog on stable isotope signatures used in interpretation of regional hydrology: East Maui,

Hawaii. *Journal of Hydrology (Amsterdam)*, 264(1), 170–184.  
doi:[https://doi.org/10.1016/S0022-1694\(02\)00073-2](https://doi.org/10.1016/S0022-1694(02)00073-2)

Scholl, M., Ingebritsen, S., Janik, C., & Kauahikaua, J. (1995). *An Isotope Hydrology Study of the Kilauea Volcano Area, Hawaii*. U.S. Geological Survey Water-Resources Investigations Report 95-4213. doi:<https://doi.org/10.3133/wri954213>

Soil Survey. (2014, February 22). National Value Added Look Up (valu) Table Database for the Gridded Soil Survey Geographic (gSSURGO) Database for the United States of America and the Territories, Commonwealths, and Island Nations served by the USDA-NRCS. United States Department of Agriculture, Natural Resources Conservation Service. Retrieved from <https://gdg.sc.egov.usda.gov/>

Tachera, D., Lautze, N., Torri, G., & Thomas, D. (2021). Characterization of the isotopic composition and bulk ion deposition of precipitation from Central to West Hawai‘i Island between 2017 and 2019. *Journal of Hydrology: Regional Studies*, 34, 100786. <https://doi.org/10.1016/j.ejrh.2021.100786>.

Thompson, R., Gallardo, M., & Aguera, T. (2006). Evaluation of the Watermark sensor for use with drip irrigated vegetable crops. *Irrigation Science*, 24, 185-202.

Torri, G., Nugent, A., & Popp, B. (2023). The Isotopic Composition of Rainfall on a Subtropical Mountainous Island. *Journal of Hydrometeorology*. doi:<https://doi.org/10.1175/JHM-D-21-0204.1>

Toulier, A., Baud, B., Montety, V., Lachassagne, P., Leonardi, V., Pistre, S., . . . Jourde, H. (2019). Multidisciplinary study with quantitative analysis of isotopic data for the assessment of recharge and functioning of volcanic aquifers: Case of Bromo-Tengger volcano, Indonesia. *Journal of Hydrology: Regional Studies*, 26. doi:<https://doi.org/10.1016/j.ejrh.2019.100634>

Tuller, M., Or, D., & Dudley, L. (1999). Adsorption and capillary condensation in porous media: Liquid retention and interfacial configurations in angular pores. *Water Resources Research*, 35(7), 1949-1964. doi:<https://doi.org/10.1029/1999WR900098>

Ward, A., & Trimble, S. (2004). Runoff and Subsurface Drainage. In *Environmental Hydrology* (pp. 119-160). Washington D.C.: Lewis Publishers.

## CHAPTER 5: CONCLUSION

### 1. Overview

This research delved into some of the intricacies of rainfall inorganic chemistry on the island of O‘ahu, Hawai‘i, and provided valuable insights into the sources, evolution, and controls on some key constituents in precipitation. This work contributes to a larger goal of utilizing natural geochemical tracers in rainfall to examine groundwater flow. Topographic and microclimate controls on precipitation chemistry were a particular focus because these relationships have been used elsewhere in Hawai‘i to understand groundwater flow and identify recharge areas. Findings from the three major science chapters in this dissertation revealed some key dynamics that influence the chemistry of meteoric waters as they progress through the hydrologic cycle on O‘ahu. This concluding chapter provides a synthesis of the major findings and offers some recommendations for further work in the field.

### 2. Synthesis of Key Findings

#### 2.1. Inorganic Chemistry of Rainfall

The first study confirmed that marine-origin sea salt aerosols (SSAs) are the primary source of dissolved ions in rainfall on O‘ahu. Through regression and principal component analysis we also identified substantial non-sea salt (NSS) sources of dissolved major ions, such as terrestrial dust from the Asian continent and local dust from sedimentary deposits, and agricultural activities. The spatial and seasonal variability of NSS sources underscores the complex interactions between humans, terrain, and climate, and reinforces the importance of considering multiple sources of dissolved ions in precipitation chemistry. The research helps to establish a baseline from which to understand future chemical changes to precipitation within the study area, thus setting the stage for further exploration.

## 2.2. Stable Isotope Composition of Rainfall

The second study provided important insights into the stable isotope composition of rainfall on O‘ahu. This research revealed that precipitation altitude exerts a strong control on stable isotope composition. Despite this strong connection, reliable regional and island-wide  $\delta^{18}\text{O}$ -elevation lapse rates could not be established due to microclimate and precipitation source related influences. Our research showed that deuterium-excess (d-excess) could supplement our understanding of elevation topographic controls on rainfall chemistry as these parameters were strongly correlated across the entire study region. Analysis of high-elevation spring, rainfall, and fog chemistry from the summit of Mount Ka‘ala suggests fog may contribute up to 45% of total groundwater recharge at the summit, underscoring need for further investigation into fog’s role in the water budget on O‘ahu. More broadly the findings from this study demonstrate the utility of stable isotope analysis for comprehending hydrologic dynamics in environmentally sensitive regions.

## 2.3. Chemical Evolution during Infiltration

The third study focused on examining how rainfall chemistry evolves during the process of soil infiltration, with the goal of connecting precipitation and groundwater recharge chemistry. We compared rainfall and soil water chemistry across multiple seasons and from multiple depths. We developed a methodology for estimating daily infiltration amount at two sites in the ‘Ewa Forest Reserve, using soil moisture, and meteorological data, which can be used to semi-quantitatively weight precipitation chemistry by soil infiltration amount. Our analysis show that rainfall chemistry does change measurably during the infiltration process, which indicates a chemical partitioning of soil water that is in general agreement with the “Two Water Worlds” hypothesis posited by Brooks (2015) and others. This final science chapter reinforces the importance of understanding the source and evolution of soil water chemistry, and of developing a methodology to estimate the chemistry of water that infiltrates the soil.

### 3. Recommendations for Future Work

#### 3.1. Spatially Diverse, Long-Term and Event-Based Sampling

Further examination of microclimate- and precipitation-source-related influences on inorganic chemistry is needed going forward. Synoptic storms contribute substantial rainfall to O‘ahu’s water budget, and our data analysis points to wide chemical variability in rainfall from these sources. Questions regarding the mechanisms contributing to the pseudo-altitude effect on d-excess also persist. Future research should focus on expanding the spatial distribution and temporal refinement of precipitation sampling, particularly during synoptic weather events. Capturing the dynamics of different weather patterns and their effects on precipitation composition island-wide will enhance our ability to predict fluctuations in water chemistry. We also need to continue expanding the temporal depth of O‘ahu’s rainfall chemistry record to examine how interannual and long-term climactic cycles, like the Pacific Decadal Oscillation and the El Nino Southern Oscillation, impact precipitation inorganic chemistry.

#### 3.2. Fog Sampling

The significance of fog as a contributor to groundwater recharge, as indicated by the findings from Chapter 3, warrants further investigation. High elevation areas on O‘ahu are known to be strongly impacted by fog and previous research has shown that fog chemistry is markedly different from rainfall chemistry. Greater fog contributions to groundwater recharge could help to explain abnormalities observed in groundwater chemistry. For example, on the Schofield Plateau, groundwater is known to be enriched in heavy isotopes relative to precipitation. Fog could account for some of this disparity. Sampling fog in both the Ko‘olau and Wai‘anae Ranges will help quantify these influences and refine the precision of geochemical tracer methods.

#### 3.3. Soil Water Chemical Sampling

Water infiltration below the soil horizon is the final linkage between precipitation and groundwater, and the findings from Chapter 4 reveal that water chemistry changes during this

process. These changes may be semi-predictable, but focused research on developing a model to account for this evolution should be undertaken. We need to build a longer record of soil water chemistry, soil moisture, and meteorological data to facilitate this objective.

### 3.4. Groundwater Flow Path Tracing

Building on the foundation laid in this dissertation, future research should aim to delineate or constrain groundwater flow paths on O‘ahu using natural geochemical tracers. We speculate that an effective spatial model for rainfall stable isotope composition could be developed from the data presented here. Outputs from this model could be fed into groundwater models for O‘ahu, and then compared with historical well chemistry data from the National Water Quality Assessment Program (Hunt C. , 2004). Examination of disparities between model results and well chemistry would provide valuable information that could be used to refine the prevailing conceptual models of groundwater flow and identify areas for further exploration.

## 4. Summary

In conclusion, this dissertation has illuminated some of the key dynamics impacting the inorganic chemistry of rainfall on O‘ahu and explored some of the implications for the island’s groundwater resources. The findings stimulate a desire for more research to further understand the complex interactions between microclimates, rainfall source, and topography that control the chemical evolution of water as it progresses through the hydrologic cycle. These complimentary studies lay groundwork for future research aimed at investigating groundwater flow paths and recharge processes using natural geochemical tracers. Understanding the source and evolution of water chemistry is essential for safeguarding O‘ahu’s groundwater resources, ensuring sustainable water management, and mitigating the environmental and societal costs associated with mismanagement.

## 5. Chapter 5 References

- Brooks, J. (2015). Water, bound and mobile. *Science*, 349(6244), 138-139.  
doi:<https://doi.org/10.1126/science.aac4742>
- Hunt, C. (2004). *Ground-Water Quality and its Relation to Land Use on Oahu, Hawaii, 2000-01: U.S. Geological Survey Water-Resources Investigations Report 03-4305*, 76 p.

## APPENDIX A: CHAPTER 2 SUPPLEMENTARY MATERIALS

### TAB A.1. PROCESSES IMPACTING PRECIPITATION INORGANIC CHEMISTRY

There are three dominant sources of inorganic ions in precipitation: terrestrial (crustal) dust, marine sea-salt aerosols (SSA), and anthropogenic activity. Terrestrial dust particles accumulate in the atmosphere through weathering of rocks and aeolian transport (Pearson & Fisher 1971; Keresztesi et al. 2020); sea-salt aerosols are formed when bubbles produced by breaking waves rise to the surface and burst, releasing microscopic aerosol particles which are transported by air currents (Keene et al. 1986; Lewis & Schwartz 2004; Laskin et al. 2012); anthropogenic sources of atmospheric inorganic particulates include a great variety of activities with the most massive sources being combustion of fossil fuels, industrial processes, and agriculture (Keresztesi et al. 2020; Pearson & Fisher 1971; Lu et al. 2011). Many processes can influence both the speciation and concentration of inorganics in the atmosphere, notably the formation and evolution of sea-salt aerosols, biogenic activity, acid-base reactions, hygroscopicity, and terrestrial dust transport, each of which will be discussed below.

Due to the study area's proximity to the ocean, marine processes must be considered carefully. Though the composition of ocean water varies across the globe, the relative ratios of inorganic ions in seawater are consistent (Keene et al. 1986; Lewis & Schwartz 2004). One fundamental assumption in assessing bulk precipitation chemistry in coastal and marine environments is that the chemistry of SSAs produced by wave action reflect the chemistry of seawater; that is, the relative ratios of inorganic ions are stable in the process of SSA formation. This assumption is well founded and supported by many years of research (Lewis 1981; Keene et al. 1986; Skartveit 1982; Hoffman & Duce 1972; Khemani et al. 1985; Junge 1972; Seto et al. 1969).

After SSA formation, there are three critical categories of chemical processes that can impact the relative ratios of inorganics in marine atmospheric moisture: biogenic activity, acid-base reactions, and variations in hygroscopicity among common inorganic salts. Among the ions examined here,  $\text{SO}_4^{2-}$  is the most important product of biogenic activity. Biogenic  $\text{SO}_4^{2-}$  is thought to be largely produced through the oxidation of dimethyl sulfide (DMS) into methanesulfonic acid (MSA) through reaction with free radicals (Norman et al. 1999; Ghahremaninezhad et al. 2016; Saltzman et al. 1986), though there are many other possible

reaction intermediaries and products. The sources of DMS, and the reaction pathways that connect algae with DMS, remain largely uncharacterized. Gaseous DMS is transported into the atmosphere through turbulent diffusion (Gahremaninezhad et al. 2016; Nightingale et al. 2000; Hu et al. 2011). Oxidized DMS compounds conglomerate on preexisting particles to become cloud condensation nuclei (CNN), which can then accumulate moisture and intermix with SSAs, enriching marine atmospheric moisture in  $\text{SO}_4^{2-}$  relative to the seawater ratios (Gahremaninezhad et al. 2016; Charlson et al. 1987).

Acid base reactions occurring on the surface of SSAs can also change the chemistry of marine moisture. Chloride is the ion most susceptible to these reactions. Many studies have reported measurable depletion of  $\text{Cl}^-$  in SSAs because of reaction with inorganic and weak organic acids (Laskin et al. 2012 and references therein). These acids tend to accumulate in the atmosphere near urbanized and industrialized areas similar to much of O‘ahu. Confusingly, the reactions driven forward by these acids can produce gaseous hydrochloric acid (HCl), which has been theorized to be a source of  $\text{Cl}^-$  enrichment in precipitation under certain atmospheric conditions (Keene et al. 1986). Acid-base reactions therefore have the potential to both increase and decrease  $\text{Cl}^-$  concentrations in SSAs. Neutralization of acidity in precipitation by reaction with terrestrially sourced alkaline species has also been observed (Keresztesi et al. 2020; Lee et al. 2000). These processes are particularly important in completing SSA corrections, which frequently use  $\text{Cl}^-$  concentrations as the basis for the correction.

The capacity of an aerosol particle to attract and retain moisture can impact the formation of CCN, which can affect when certain chemical species accumulate in precipitation. The tendency of a compound to absorb water on its surface is called hygroscopicity. The hygroscopicity of inorganic salts changes with temperature, humidity, particle size, and species (Hu et al. 2011). The general trend is that when relative humidity (RH) rises above a threshold, known as the deliquescence RH (DRH), the hygroscopicity of inorganic salts, particularly ammonium salts, increases with particle size (Hu et al. 2010; Hu et al. 2011). Conversely, below the DRH, evaporation of ammonium salts is enhanced as RH rises. This can result in measurable enrichment or depletion of major ions in precipitation depending on the specific atmospheric conditions. Chloride and  $\text{SO}_4^{2-}$  are the most susceptible to hygroscopic processes (Hu et al. 2011). The net effect of these three categories of marine-focused chemical processes is a tendency of  $\text{SO}_4^{2-}$  and  $\text{Cl}^-$  concentrations in bulk precipitation chemistry to depart from the

seawater ratios. Careful comparison must be made between bulk precipitation chemistry and seawater ratios to assess the magnitude of these effects in coastal and marine settings. This supports the conclusion of Keene et al. (1986) that selecting a reference species for sea-salt corrections must be done deliberately, based on objective criteria.

Dust transport of terrestrially, and anthropogenically derived inorganic constituents can also impact bulk precipitation chemistry. Magnesium,  $\text{Ca}^{2+}$ ,  $\text{Na}^+$ , and  $\text{K}^+$  are among the most abundant elements in the Earth's crust (Kring 1997). Rock and aeolian transport weathering can disperse substantial quantities of these constituents over vast distances (Chung & Park 1998). Many studies have linked the presence of  $\text{Ca}^{2+}$  and  $\text{Mg}^{2+}$  in precipitation to terrestrial dust transport (Niu et al. 2014; Szép 2019; Szép et al. 2018; Xiao 2016; Zhang et al. 2003; Loyer-Pilot et al. 1986; Brahney et al. 2013). Biomass burning and potash fertilization have also been linked to elevated  $\text{K}^+$  in bulk precipitation (Lu et al. 2011; Keresztesi et al. 2020). Potassium enrichment of coastal precipitation has also been attributed to high biogenic productivity in the North Sea and Norwegian Sea (Skartveit 1982).

Several studies have documented the effects of long-range dust transport in the Pacific. Suzuki & Tsunogai (1988) found that a large part of the non-sea-salt (NSS)  $\text{Ca}^{2+}$  in the troposphere over the western North Pacific originated from arid regions in Asia. Darzi & Winchester (1982) determined that local and continental soils were the only major sources of terrestrial elements in dust aerosols on Hawai'i Island, and likewise linked the origin of continental dust to arid regions in Asia. Using trajectory analysis, Shaw (1980) determined that an expansive atmospheric dust plume that passed over Hawai'i from late April to early May 1979 originated in the eastern deserts of Asia. Lee et al. (2000) attributed alkaline dust content in precipitation on the Korean peninsula to long-range transport from desert regions of Asia. They found that local aerosol transport derived from calcite and basalt exposure weathering contributed measurably to precipitation chemistry. Saltzman et al. (1986) studied bulk precipitation chemistry on Midway Atoll and observed significant seasonal trends in continental anthropogenic and marine biogenic NSS  $\text{SO}_4^{2-}$  deposition. Satake & Yamane (1992) analyzed NSS  $\text{SO}_4^{2-}$  deposition on central Japan's west coast and linked increased winter deposition to long-range transport from the Asian continent. These, and many other works, demonstrate that terrestrial dust can be a significant source of inorganic nutrients to precipitation in coastal and marine settings.

## Appendix A, Tab A.1. References

- Brahney, J., Ballantyne, A., Sievers, C., & Neff, J. (2013). Increasing Ca<sup>2+</sup> deposition in the wester US: The role of mineral aerosols. *Aeolian Research* (10), 77-87.  
doi:<https://dx.doi.org/10.1016/j.aeolia.2013.04.003>
- Charlson, R., Lovelock, J., Andreae, M., & Warren, S. (1987). Oceanic phytoplankton, atmospheric sulphur, cloud albedo and climate. *Nature*, 326, 655-661.
- Chung, K., & Park, S. (1998). A numerical study on the size and deposition of Yellow Sand events. *Journal of Korea Air Pollution Research Association*, 10, 64-72.
- Darzi, M., & Winchester, J. (1982). Resolution of Basaltic and Continental Aerosol Components During Spring and Summer Within the Boundary Layer of Hawaii. *Journal of Geophysical Research*, 87(C9), 7262-7272.
- Gahremaninezhad, R., Norman, A.-L., Abbatt, J., Levasseur, M., & Thomas, J. (2016). *Biogenic, anthropogenic and sea salt sulfate size-segregated aerosols in the Arctic summer*. Atmospheric Chemistry and Physics, 16(8), 5191–5202.  
<https://doi.org/10.5194/acp-16-5191-2016>.
- Hoffman, G., & Duce, R. (1972). Consideration of the chemical fractionation of alkali and alkaline earth metals in the Hawaiian marine atmosphere. *Journal of Geophysical Research*, 77(27), 5161-5169. doi:<https://doi.org/10.1029/JC077i027p05161>.
- Hu, D., Chen, J., Ye, X., Li, L., & Yang, X. (2011). Hygroscopicity and evaporation of ammonium chloride and ammonium nitrate: Relative humidity and size effects on the growth factor. *Atmospheric Environment* (1994), 45(14), 2349–2355.  
<https://doi.org/10.1016/j.atmosenv.2011.02.024>.
- Hu, D., Qiao, L., Chen, J., Ye, X., Yang, X., Cheng, T., & Fang, W. (2010). Hygroscopicity of inorganic aerosols: size and relative humidity effects on the growth factor. *Aerosol and Air Quality Research*, 10, 255-264.
- Junge, C. (1972). Our Knowledge of the Physico-Chemistry of Aerosols in the Undisturbed Marine Environment. *Journal of Geophysical Research*, 77(27), 5183-5200.  
doi:<https://doi.org/10.1029/JC077i027p05183>
- Keene, W., Pszenny, A. A., Galloway, J., & Hawley, M. (1986). Sea-salt corrections and interpretation of constituent ratios in marine precipitation. *Journal of Geophysical Research*, 91(D6), 6647–6658. <https://doi.org/10.1029/JD091iD06p06647>.
- Keresztesi, Á., Nita, I.-A., Boga, R., Birsan, M.-V., Bodor, Z., & Szép, R. (2020). Spatial and long-term analysis of rainwater chemistry over the conterminous United States. *Environmental Research*, 188, 109872–109872.  
<https://doi.org/10.1016/j.envres.2020.109872>.

- Khemani, L., Momin, G., Naik, M., Prakasa Rao, P., Kumar, R., & Ramana Murty, B. (1985). Trace Elements and Sea Salt Aerosols over the Sea Areas Around the Indian Sub-Continent. *Atmospheric Environment*, 19(2), 277-284. doi:[https://doi.org/10.1016/0004-6981\(85\)90095-2](https://doi.org/10.1016/0004-6981(85)90095-2)
- Kring, D. A. (1997). Composition of Earth's continental crust as inferred from the compositions of impact melt sheets. *Lunar and Planetary Science XXVIII; 28th Lunar and Planetary Science Conference*, (pp. 763-). Houston, TX.
- Laskin, A., Moffet, R. C., Gilles, M. K., Fast, J. D., Zaveri, R. A., Wang, B., . . . Shutthanandan, J. (2012). Tropospheric chemistry of internally mixed sea salt and organic particles: Surprising reactivity of NaCl with weak organic acids. *Journal of Geophysical Research. D. (Atmospheres)*, 117(D15). <https://doi.org/10.1029/2012JD017743>.
- Lee, B., Hong, S., & Lee, D. (2000). Chemical composition of precipitation and wet deposition of major ions on the Korean peninsula. *Atmospheric Environment*, (34) 563-575.
- Lewis, E., & Schwartz, S. (2004). *Sea Salt Aerosol Production: Mechanisms, Methods, Measurements, and Models - A Critical Review*. Washington D.C.: American Geophysical Union.
- Lewis, W. M. (1981). Precipitation chemistry and nutrient loading by precipitation in a tropical watershed. *Water Resources Research (United States)*, 17(1), 169–181. <https://doi.org/10.1029/WR017i001p00169>.
- Loye-Pilot, M., Martin, J., & Morelli, J. (1986). Influence of Saharan dust on the rain acidity and atmospheric input to the Mediterranean. *Nature*, 321, 427-428.
- Lu, X., Li, L. Y., Li, N., Yang, G., Luo, D., & Chen, J. (2011). Chemical characteristics of spring rainwater of Xi'an city, NW China. *Atmospheric Environment (1994)*, 45(28), 5058–5063. <https://doi.org/10.1016/j.atmosenv.2011.06.026>.
- Nightingale, P., Liss, P., & Schlosser, P. (2000). Measurements of air-sea gas transfer during an open ocean algal bloom. *Geophysical Research Letters*, 27, 2117-2120.
- Niu, H., He, Y., Lu, X., Shen, J., Du, J., Zhang, T., . . . Chang, L. (2014). Chemical composition of rainwater in the yulong snow mountain region, southwestern China. *Atmospheric Reserach*, 144, 195-206. doi:<https://doi.org/10.1016/j.atmosres.2014.03.010>
- Norman, A., Barrie, L., Toom-Sauntry, D., Sirois, A., Krouse, H., Li, S., & Sharma, S. (1999). Sources of aerosol sulfphate at Alert: apportionment using stable isotopes. *Journal of Geophysical Research*, 104, 11619-11631.
- Pearson, F., & Fisher, D. W. (1971). *Chemical composition of atmospheric precipitation in the Northeastern United States*. U.S. Geological Survey, U.S. Department of the Interior. doi:[10.3133/wsp1535P](https://doi.org/10.3133/wsp1535P)

- Saltzman, E., Savoie, D., Prospero, J., & Zika, R. (1986). Methanosulfonic Acid and Non-Sea-Salt Sulfate in Pacific Air: Regional and Seasonal Variations. *Journal of Atmospheric Chemistry*, 277-240.
- Satake, H., & Yamane, T. (1992). Deposition of non-sea salt sulfate observed at Toyama facing the Sea of Japan for the period of 1981-1991. *Geochemical Journal*, 26, 299-305.
- Seto, Y., Duce, R., & Woodcock, A. (1969). Sodium-to-Chlorine ratio in Hawaiian rains as a function of distance inland and of elevation. *Journal of Geophysical Research*, 74(4), 1101-1103. doi:<https://doi.org/10.1029/JB074i004p01101>
- Shaw, G. (1980). Transport of Asian Desert Aerosol to the Hawaiian Islands. *Journal of Applied Meteorology*, 19, 1254-1259.
- Skartveit, A. (1982). Wet Scavenging of sea-salts and acid compounds in a rainy, coastal area. *Atmospheric Environment*, 16(11), 2715-2724.
- Suzuki, T., & Tsunogai, S. (1988). Origin of Calcium in Aerosols over the Western North Pacific. *Journal of Atmospheric Chemistry*, 6, 363-374.
- Szép, R. B. (2019). Influence of peat fires on the rainwater chemistry in intra-mountain basins with specific atmospheric circulations (Eastern Carpathians, Romania). *Science of the Total Environment*, 647, 275-289. doi:<https://doi.org/10.1016/j.scitotenv.2018.07.462>
- Szép, R., Mphepya., Mateescu, E., Niță, I.-A., Birsan, M.-V., Bodor, Z., & Keresztesi, Á. (2018). Effects of the Eastern Carpathians on atmospheric circulations and precipitation chemistry from 2006 to 2016 at four monitoring stations (Eastern Carpathians, Romania). *Atmospheric Research*, 214, 311-328. doi:<https://doi.org/10.1016/j.atmosres.2018.08.009>
- Xiao, J. (2016). Chemical composition and source identification of rainwater constituents at an urban site in Xi'an. *Environmental Earth Sciences*, 75, 1-12. doi:<https://doi.org/10.1007/s12665-015-4997-z>
- Zhang, D., Peart, M., Jim, C., He, Y., Li, B., & Chen, J. (2003). Precipitation chemistry of Lhasa and other remote towns, Tibet. *Atmospheric Environment*, 37 (2), 231-240.

## APPENDIX A: CHAPTER 2 SUPPLEMENTARY MATERIAL

TAB A.2. MAJOR ION BULK DEPOSITION

Collector	From Date	To Date	Precipitation (mm)	Average Annual Bulk Deposition (kg · ha <sup>-1</sup> · d <sup>-1</sup> )								
				F <sup>-</sup>	Cl <sup>-</sup>	Br <sup>-</sup>	SO <sub>4</sub> <sup>2-</sup>	Li <sup>+</sup>	Na <sup>+</sup>	K <sup>+</sup>	Mg <sup>2+</sup>	Ca <sup>2+</sup>
K1	12/19/2018	3/18/2019	461	NA	0.53	NA	0.09	0.00	0.36	0.02	0.04	0.02
K1	3/18/2019	7/12/2019	541	NA	0.39	0.00	0.09	NA	0.23	0.03	0.02	0.02
K1	7/12/2019	10/12/2019	181	NA	0.06	NA	0.00	0.00	0.03	0.03	0.01	0.02
K1	10/12/2019	1/5/2020	504	NA	0.32	NA	0.04	0.00	0.27	0.02	0.02	0.03
K1	1/5/2020	3/28/2020	673	NA	0.63	NA	0.03	0.00	0.47	0.02	0.05	0.05
K1	3/28/2020	5/2/2020	26	NA	0.03	NA	0.00	0.00	0.03	0.00	0.00	0.01
K1	5/2/2020	6/20/2020	31	NA	0.04	NA	0.00	NA	0.02	0.01	0.00	0.01
K1	6/20/2020	9/19/2020	43	0.00	0.05	NA	0.00	NA	0.03	0.01	0.00	0.01
K1	9/19/2020	1/4/2021	222	NA	0.08	NA	0.00	NA	0.04	0.02	0.01	0.03
K1	1/4/2021	3/13/2021	516	NA	0.41	NA	0.05	NA	0.23	0.03	0.03	0.04
K1	3/13/2021	4/21/2021	270	NA	0.26	NA	0.04	NA	0.14	0.01	0.02	0.09
K2	7/12/2019	10/12/2019	198	NA	0.06	NA	0.02	0.00	0.04	0.03	0.01	0.02
K2	10/12/2019	1/5/2020	366	NA	0.16	NA	0.02	0.00	0.18	0.01	0.01	0.01
K2	1/5/2020	3/28/2020	540	NA	0.35	NA	0.05	0.00	0.29	0.01	0.03	0.04
K2	3/28/2020	5/2/2020	85	NA	0.17	NA	0.01	0.00	0.14	0.02	0.01	0.07
K2	5/2/2020	6/20/2020	35	NA	0.05	NA	0.00	NA	0.03	0.01	0.01	0.05
K2	6/20/2020	9/19/2020	99	NA	0.06	NA	0.00	0.00	0.03	0.00	0.01	0.06
K2	9/19/2020	1/4/2021	246	NA	0.08	NA	0.00	0.00	0.04	0.01	0.01	0.09
K2	1/4/2021	3/13/2021	539	NA	0.47	NA	0.08	0.00	0.26	0.02	0.03	0.16
K2	3/13/2021	4/21/2021	309	NA	0.25	NA	0.00	0.00	0.14	0.01	0.02	0.52
K3	7/12/2019	10/12/2019	264	NA	0.06	NA	0.02	0.00	0.04	0.01	0.00	0.01
K3	10/12/2019	1/5/2020	410	NA	0.22	NA	0.02	0.00	0.21	0.02	0.01	0.01
K3	1/5/2020	3/28/2020	619	NA	0.57	NA	0.09	0.00	0.42	0.05	0.04	0.07
K3	3/28/2020	5/2/2020	90	NA	0.09	NA	0.00	0.00	0.09	0.01	0.01	0.02
K3	5/2/2020	6/20/2020	94	NA	0.09	NA	0.00	NA	0.05	0.02	0.01	0.02
K3	6/20/2020	9/19/2020	153	NA	0.11	NA	0.00	NA	0.06	0.03	0.01	0.03
K3	9/19/2020	1/4/2021	390	NA	0.13	NA	0.00	NA	0.08	0.03	0.02	0.05
K3	1/4/2021	3/13/2021	759	NA	0.49	NA	0.00	0.00	0.30	0.08	0.03	0.10
K3	3/13/2021	4/21/2021	261	NA	0.22	NA	0.00	0.00	0.12	0.03	0.01	0.05
KS	12/19/2018	3/18/2019	750	NA	0.56	NA	0.08	0.00	0.43	0.04	0.04	0.03
KS	3/18/2019	7/12/2019	711	NA	0.35	0.00	0.08	NA	0.21	0.02	0.02	0.02
KS	7/12/2019	10/12/2019	244	NA	0.08	NA	0.01	0.00	0.05	0.01	0.00	0.01

KS	10/12/2019	1/5/2020	438	NA	0.25	NA	0.04	0.00	0.24	0.01	0.02	0.02
KS	1/5/2020	3/28/2020	844	NA	0.60	NA	0.06	0.00	0.48	0.02	0.04	0.06
KS	3/28/2020	5/2/2020	300	NA	0.21	NA	0.02	0.00	0.26	0.02	0.02	0.04
KS	5/2/2020	6/20/2020	89	NA	0.09	NA	0.01	NA	0.05	0.04	0.00	0.02
KS	6/20/2020	9/19/2020	192	NA	0.09	NA	0.00	NA	0.04	0.02	0.01	0.02
KS	9/19/2020	1/4/2021	480	NA	0.12	NA	0.00	NA	0.06	0.00	0.01	0.04
KS	1/4/2021	3/13/2021	1077	NA	0.50	NA	0.08	0.00	0.27	0.01	0.03	0.07
KS	3/13/2021	4/21/2021	333	NA	0.24	NA	0.03	0.00	0.13	0.01	0.02	0.05
MT1	5/10/2019	7/11/2019	255	0.00	2.50	0.01	0.41	0.00	1.41	0.12	0.20	0.17
MT1	7/11/2019	9/29/2019	216	NA	0.19	NA	0.00	0.00	0.12	0.01	0.02	0.11
MT1	9/29/2019	1/9/2020	592	NA	0.65	NA	0.08	0.00	0.44	0.03	0.05	0.06
MT1	1/9/2020	3/31/2020	1614	NA	2.42	NA	0.31	0.00	1.55	0.08	0.18	0.22
MT1	6/15/2020	9/17/2020	240	NA	0.22	NA	0.00	NA	0.12	0.01	0.02	0.10
MT1	9/17/2020	12/30/2020	753	NA	0.41	NA	0.08	0.00	0.22	0.02	0.05	0.18
MT1	12/30/2020	3/27/2021	1301	NA	0.99	NA	0.15	0.00	0.54	0.03	0.11	0.22
MT1	3/27/2021	4/29/2021	97	NA	0.54	NA	0.06	0.00	0.30	0.04	0.06	0.18
MT2	5/10/2019	7/11/2019	697	0.00	4.59	0.01	0.76	0.00	2.65	0.15	0.34	0.31
MT2	7/11/2019	9/25/2019	387	NA	0.32	NA	0.05	0.00	0.19	0.01	0.03	0.09
MT2	9/25/2019	1/7/2020	1041	NA	1.24	NA	0.20	0.00	0.83	0.03	0.10	0.08
MT2	1/7/2020	3/31/2020	1263	NA	1.53	NA	0.24	0.00	1.07	0.05	0.12	0.09
MT2	6/15/2020	9/17/2020	504	NA	0.35	NA	0.00	0.00	0.19	0.01	0.03	0.07
MT2	9/17/2020	12/22/2020	652	NA	0.44	NA	0.03	0.00	0.24	0.01	0.03	0.06
MT2	12/22/2020	3/27/2021	1416	NA	1.02	NA	0.13	0.00	0.56	0.02	0.07	0.07
MT2	3/27/2021	4/29/2021	249	NA	0.80	NA	0.13	0.00	0.44	0.03	0.06	0.09
MT3	5/10/2019	7/11/2019	597	NA	0.44	0.00	0.10	0.00	0.27	0.02	0.11	0.28
MT3	7/11/2019	9/25/2019	1064	NA	1.05	NA	0.16	0.00	0.68	0.05	0.09	0.25
MT3	9/25/2019	1/7/2020	1270	NA	0.87	NA	0.16	0.00	0.65	0.02	0.06	0.09
MT3	1/7/2020	3/31/2020	2032	NA	1.89	NA	0.24	0.00	1.45	0.05	0.12	0.17
MT3	6/11/2020	9/17/2020	712	NA	0.38	NA	0.01	0.00	0.20	0.02	0.03	0.27
MT3	9/17/2020	12/22/2020	684	NA	0.49	NA	0.06	0.00	0.26	0.01	0.03	0.08
MT3	12/22/2020	3/27/2021	1588	NA	1.01	NA	0.15	0.00	0.55	0.04	0.07	0.09
MT3	3/27/2021	4/26/2021	351	NA	1.11	NA	0.12	0.00	0.61	0.09	0.08	0.16
MTS	7/11/2019	9/25/2019	323	NA	0.41	0.00	0.04	0.00	0.25	0.03	0.01	0.04
MTS	9/25/2019	1/7/2020	605	NA	0.53	NA	0.05	0.00	0.42	0.03	0.02	0.02
MTS	1/7/2020	3/31/2020	479	NA	0.45	NA	0.06	0.00	0.35	0.02	0.03	0.05
MTS	6/11/2020	9/17/2020	92	NA	0.08	NA	0.00	NA	0.04	0.00	0.01	0.05
MTS	9/17/2020	12/22/2020	376	NA	0.24	NA	0.03	0.00	0.13	0.03	0.02	0.13
MTS	12/22/2020	4/26/2021	671	NA	0.31	NA	0.04	0.00	0.17	0.01	0.02	0.06
EB	7/13/2019	9/27/2019	83	0.00	0.04	NA	0.01	0.00	0.03	0.00	0.00	0.03

EB	9/27/2019	1/9/2020	169	NA	0.06	NA	0.02	0.00	0.06	0.00	0.00	0.05
EB	1/10/2020	3/31/2020	115	NA	0.10	NA	0.01	0.00	0.08	0.00	0.01	0.08
EB	3/31/2020	6/23/2020	23	NA	0.01	NA	0.00	NA	0.01	0.00	0.00	0.03
EB	6/23/2020	10/16/2020	13	NA	0.01	NA	0.00	0.00	0.01	0.00	0.00	0.04
EB	10/16/2020	1/19/2021	41	NA	0.04	NA	0.01	0.00	0.02	0.00	0.00	0.05
EB	1/19/2021	4/7/2021	404	NA	0.29	NA	0.05	0.00	0.16	0.01	0.03	0.21
EB	4/7/2021	5/6/2021	58	NA	0.12	NA	0.00	0.00	0.06	0.01	0.01	0.12
TR	7/26/2019	10/19/2019	1351	NA	1.92	0.01	0.30	0.00	1.13	0.07	0.10	0.17
TR	10/19/2019	1/9/2020	502	NA	0.62	NA	0.10	0.00	0.44	0.02	0.04	0.04
TR	1/9/2020	3/15/2020	537	NA	1.08	NA	0.17	0.00	0.71	0.03	0.07	0.14
TR	3/15/2020	5/4/2020	272	NA	0.33	NA	0.05	0.00	0.30	0.02	0.02	0.05
TR	5/4/2020	6/20/2020	183	NA	0.32	NA	0.01	NA	0.17	0.01	0.02	0.12
TR	6/20/2020	10/12/2020	280	NA	0.19	NA	0.00	NA	0.10	0.02	0.01	0.11
TR	1/20/2021	2/1/2021	211	NA	1.35	NA	0.18	NA	0.76	0.04	0.08	0.03
TR	2/1/2021	2/17/2021	31	NA	0.15	NA	0.02	NA	0.08	0.01	0.01	0.01
TR	2/17/2021	3/2/2021	138	NA	1.23	NA	0.17	0.00	0.67	0.04	0.08	0.02
TR	3/2/2021	3/17/2021	284	NA	0.82	NA	0.13	NA	0.44	0.03	0.05	0.03
TR	3/17/2021	4/7/2021	105	NA	0.67	NA	0.11	0.00	0.36	0.03	0.04	0.02
TR	4/7/2021	4/29/2021	48	NA	0.19	NA	0.03	NA	0.10	0.01	0.01	0.01
EB	8/5/2019	8/7/2019	8	0.00	0.17	NA	0.05	NA	0.13	0.02	0.01	0.04
MHS	10/18/2019	1/9/2020	243	NA	0.34	NA	0.07	0.00	0.23	0.02	0.02	0.05
M	10/23/2019	1/9/2020	262	NA	0.58	NA	0.12	0.00	0.36	0.02	0.04	0.12
M	1/9/2020	3/25/2020	731	NA	0.68	NA	0.15	0.00	0.51	0.04	0.05	0.12
M	3/25/2020	6/23/2020	38	NA	0.05	NA	0.02	NA	0.03	0.00	0.00	0.03
M	6/23/2020	10/12/2020	55	NA	0.03	NA	0.01	NA	0.02	0.00	0.00	0.06
M	10/12/2020	1/19/2021	140	NA	0.06	NA	0.02	NA	0.03	0.00	0.01	0.07
M	1/19/2021	2/8/2021	149	NA	0.18	NA	0.06	NA	0.10	0.01	0.01	0.01
M	2/8/2021	3/2/2021	20	0.00	0.18	NA	0.04	0.00	0.10	0.00	0.01	0.02
M	3/2/2021	3/17/2021	123	NA	0.20	NA	0.07	NA	0.10	0.01	0.01	0.01
M	3/17/2021	4/7/2021	101	NA	0.27	NA	0.08	NA	0.15	0.01	0.02	0.01
M	4/7/2021	5/3/2021	30	NA	0.06	NA	0.02	NA	0.04	0.01	0.01	0.02
PW	10/31/2019	1/29/2020	1086	NA	1.28	NA	0.23	0.00	0.92	0.04	0.10	0.08
KK	2/16/2020	4/24/2020	244	NA	0.21	NA	0.04	0.00	0.14	0.02	0.02	0.06
KK	4/24/2020	6/20/2020	27	NA	0.07	NA	0.00	NA	0.02	0.02	0.01	0.01
KK	6/20/2020	10/10/2020	142	NA	0.10	NA	0.00	NA	0.04	0.03	0.01	0.06
KK	10/10/2020	1/2/2021	148	NA	0.14	NA	0.00	0.00	0.05	0.05	0.02	0.04
KK	1/2/2021	4/3/2021	1211	NA	0.96	NA	0.15	0.00	0.47	0.10	0.14	0.59
KK	4/3/2021	4/25/2021	127	NA	0.22	NA	0.00	NA	0.10	0.06	0.05	0.36
SB	2/16/2020	4/24/2020	310	NA	0.25	NA	0.05	0.00	0.21	0.01	0.02	0.04

SB	4/24/2020	6/20/2020	26	NA	0.05	NA	0.01	NA	0.03	0.01	0.01	0.02
SB	6/20/2020	10/10/2020	66	NA	0.04	NA	0.00	0.00	0.02	0.00	0.00	0.04
SB	10/10/2020	1/11/2021	154	NA	0.11	NA	0.00	0.00	0.04	0.03	0.01	0.07
WAAF	2/16/2020	4/26/2020	366	NA	0.74	NA	0.13	0.00	0.47	0.09	0.06	0.10
WAAF	4/26/2020	6/20/2020	21	NA	0.09	NA	0.00	NA	0.04	0.04	0.01	0.01
WAAF	6/20/2020	10/10/2020	55	NA	0.11	NA	0.00	NA	0.04	0.15	0.01	0.03
WAAF	10/10/2020	1/11/2021	189	NA	0.16	NA	0.01	NA	0.08	0.07	0.03	0.05
WAAF	1/11/2021	4/3/2021	1164	NA	1.42	NA	0.23	0.00	0.74	0.16	0.16	0.32
ER	2/16/2020	3/15/2020	143	NA	1.44	0.01	0.22	0.00	0.82	0.14	0.08	0.07
ER	3/15/2020	4/25/2020	262	NA	0.45	NA	0.11	0.00	0.36	0.03	0.03	0.07
ER	4/25/2020	6/20/2020	79	NA	0.15	NA	0.00	NA	0.08	0.01	0.01	0.09
ER	10/12/2020	1/11/2021	337	NA	0.31	NA	0.03	0.00	0.16	0.01	0.02	0.14
ER	1/11/2021	4/3/2021	894	NA	1.04	NA	0.09	0.00	0.56	0.03	0.07	0.23
D1	10/1/2017	12/31/2017	510	NA	1.01	NA	0.19	NA	0.56	0.04	0.06	0.07
D1	1/1/2018	3/31/2018	778	NA	0.83	NA	0.17	NA	0.44	0.07	0.05	0.08
MT1	4/1/2017	6/30/2017	244	NA	0.30	NA	0.08	NA	0.22	0.00	0.04	0.12
MT1	7/1/2017	9/30/2017	468	NA	0.57	NA	0.15	NA	0.41	0.00	0.07	0.02
MT1	10/1/2017	12/31/2017	595	NA	0.52	NA	0.11	NA	0.26	0.00	0.04	0.48
MT1	1/1/2018	3/31/2018	609	NA	0.69	NA	0.14	NA	0.44	0.04	0.05	0.10
D4	10/1/2017	12/31/2017	89	NA	0.38	NA	0.06	NA	0.24	0.06	0.03	0.02
D4	1/1/2018	3/31/2018	324	NA	0.39	NA	0.04	NA	0.20	0.17	0.05	0.13
D6	4/1/2017	6/30/2017	743	NA	0.91	NA	0.26	NA	0.74	0.00	0.12	0.38
D6	7/1/2017	9/30/2017	531	NA	0.47	NA	0.07	NA	0.29	0.00	0.04	0.34
D6	10/1/2017	12/31/2017	1345	NA	1.40	NA	0.25	NA	0.83	0.06	0.10	0.28
D6	1/1/2018	3/31/2018	1028	NA	1.20	NA	0.20	NA	0.64	0.08	0.12	0.29
D7	4/1/2017	6/30/2017	236	NA	0.55	NA	0.12	NA	0.39	0.00	0.05	0.29
D7	7/1/2017	9/30/2017	96	NA	0.28	NA	0.05	NA	0.18	0.00	0.02	0.22
D7	10/1/2017	12/31/2017	520	NA	0.81	NA	0.17	NA	0.52	0.05	0.07	0.12
D7	1/1/2018	3/31/2018	305	NA	0.39	NA	0.07	NA	0.21	0.01	0.03	0.03
D8	4/1/2017	6/30/2017	360	NA	0.24	NA	0.05	NA	0.20	0.00	0.03	0.14
D9	4/1/2017	6/30/2017	1303	NA	1.01	NA	0.25	NA	0.87	0.00	0.14	0.91
D9	7/1/2017	9/30/2017	568	NA	0.31	NA	0.00	NA	0.19	0.00	0.04	0.37
D9	10/1/2017	12/31/2017	526	NA	0.45	NA	0.11	NA	0.31	0.03	0.04	0.08
D9	1/1/2018	3/31/2018	989	NA	0.92	NA	0.16	NA	0.49	0.06	0.09	0.24
D10	3/1/2017	3/30/2017	299	NA	0.62	NA	0.19	NA	0.41	0.10	0.06	0.29
D10	4/1/2017	6/30/2017	843	NA	1.03	NA	0.12	NA	0.66	0.00	0.07	0.56
D10	7/1/2017	9/30/2017	758	NA	0.42	NA	0.10	NA	0.25	0.00	0.07	0.32
D10	10/1/2017	12/31/2017	1672	NA	1.51	NA	0.33	NA	1.03	0.07	0.20	0.26
D10	1/1/2018	3/31/2018	1200	NA	0.80	NA	0.17	NA	0.43	0.05	0.12	0.22

D11	4/1/2017	6/30/2017	297	NA	0.86	NA	0.24	NA	0.59	0.00	0.07	0.16
D11	7/1/2017	9/30/2017	134	NA	0.63	NA	0.12	NA	0.35	0.00	0.05	0.20
D11	10/1/2017	12/31/2017	240	NA	2.78	NA	0.40	NA	1.58	0.11	0.18	0.24
D11	1/1/2018	3/31/2018	681	NA	1.68	NA	0.29	NA	0.90	0.09	0.15	0.24
D12	10/1/2017	12/31/2017	124	NA	0.19	NA	0.06	NA	0.10	0.10	0.02	0.04
D12	1/1/2018	3/31/2018	178	NA	0.15	NA	0.05	NA	0.08	0.09	0.03	0.10
D13	4/1/2017	6/30/2017	1932	NA	1.93	NA	0.45	NA	1.29	0.00	0.28	1.24
D13	7/1/2017	9/30/2017	919	NA	0.61	NA	0.12	NA	0.30	0.00	0.06	0.30
D13	10/1/2017	12/31/2017	1699	NA	1.77	NA	0.45	NA	1.16	0.07	0.21	0.34
D13	1/1/2018	3/31/2018	1649	NA	2.83	NA	0.46	NA	1.50	0.07	0.28	0.37
D14	4/1/2017	6/30/2017	314	NA	0.21	NA	0.07	NA	0.17	0.00	0.03	0.13
D14	7/1/2017	9/30/2017	220	NA	0.12	NA	0.04	NA	0.10	0.00	0.02	0.09
D14	10/1/2017	12/31/2017	461	NA	0.55	NA	0.09	NA	0.31	0.04	0.06	0.13
D14	1/1/2018	3/31/2018	205	NA	0.18	NA	0.03	NA	0.11	0.07	0.03	0.10
D15	1/1/2018	3/31/2018	342	NA	0.33	NA	0.07	NA	0.18	0.06	0.04	0.10
D16	4/1/2017	6/30/2017	148	NA	0.08	NA	0.14	NA	0.07	0.00	0.02	0.07
D17	4/1/2017	6/30/2017	507	NA	0.73	NA	0.19	NA	0.51	0.00	0.07	0.27
D17	7/1/2017	9/30/2017	352	NA	0.50	NA	0.12	NA	0.31	0.00	0.06	0.33
D17	10/1/2017	12/31/2017	446	NA	0.79	NA	0.03	NA	0.49	0.19	0.10	0.34
D17	1/1/2018	3/31/2018	370	NA	0.34	NA	0.00	NA	0.19	0.06	0.02	0.12
D18	3/1/2017	3/30/2017	263	NA	0.72	NA	0.36	NA	0.54	0.09	0.09	0.40
D18	4/1/2017	6/30/2017	1046	NA	2.09	NA	0.19	NA	1.51	0.00	0.14	0.59
D18	7/1/2017	9/30/2017	1105	NA	0.61	NA	0.12	NA	0.36	0.00	0.07	0.74
D18	10/1/2017	12/31/2017	810	NA	0.93	NA	0.17	NA	0.59	0.06	0.09	0.20
D18	1/1/2018	3/31/2018	1764	NA	1.80	NA	0.32	NA	0.95	0.08	0.20	0.75
D19	4/1/2017	6/30/2017	262	NA	0.32	NA	0.05	NA	0.23	0.00	0.03	0.12
D19	7/1/2017	9/30/2017	421	NA	0.32	NA	0.15	NA	0.18	0.00	0.04	0.35
D19	10/1/2017	12/31/2017	347	NA	0.50	NA	0.08	NA	0.27	0.11	0.04	0.14
D19	1/1/2018	3/31/2018	125	NA	0.16	NA	0.04	NA	0.10	0.06	0.03	0.12
D20	4/1/2017	6/30/2017	1342	NA	1.49	NA	0.22	NA	1.04	0.00	0.16	0.84
D20	7/1/2017	9/30/2017	271	NA	0.30	NA	0.05	NA	0.15	0.00	0.04	0.35
D20	10/1/2017	12/31/2017	351	NA	0.60	NA	0.09	NA	0.37	0.05	0.08	0.44
D20	1/1/2018	3/31/2018	660	NA	0.76	NA	0.10	NA	0.38	0.14	0.09	0.65
A	3/9/2019	5/8/2019	46	0.00	0.09	0.00	0.02	0.00	0.06	0.01	0.00	0.01
A	5/8/2019	6/29/2019	119	0.00	0.09	NA	0.03	NA	0.05	0.00	0.01	0.02
A	6/29/2019	8/5/2019	14	0.00	0.05	0.00	0.01	NA	0.03	0.00	0.00	0.00
A	8/5/2019	10/1/2019	69	0.00	0.06	NA	0.01	0.00	0.04	0.00	0.00	0.01
A	10/1/2019	10/14/2019	49	0.00	0.24	NA	0.05	NA	0.14	0.01	0.02	0.02
A	10/14/2019	11/15/2019	35	0.00	0.06	NA	0.03	0.00	0.04	0.00	0.02	0.02

A	11/15/2019	12/11/2019	50	0.00	0.24	0.00	0.05	0.00	0.15	0.01	0.02	0.02
A	12/11/2019	12/20/2019	50	NA	0.23	NA	0.06	0.00	0.13	0.01	0.01	0.01
A	12/20/2019	1/8/2020	61	0.00	0.74	0.00	0.12	0.00	0.43	0.02	0.03	0.03
A	1/8/2020	1/15/2020	84	NA	1.81	0.00	0.27	0.00	1.06	0.04	0.07	0.07
A	1/15/2020	2/13/2020	22	0.00	0.19	0.00	0.03	0.00	0.11	0.01	0.01	0.01
A	2/13/2020	3/7/2020	72	NA	0.81	0.00	0.12	0.00	0.48	0.02	0.05	0.05
A	3/7/2020	3/20/2020	99	NA	0.30	NA	0.08	NA	0.18	0.01	0.02	0.01
A	3/20/2020	4/17/2020	116	NA	0.27	NA	0.06	NA	0.16	0.01	0.02	0.02
A	11/6/2020	12/11/2020	18	0.00	0.21	NA	0.04	NA	0.11	0.01	0.01	0.01
A	12/11/2020	1/13/2021	47	NA	0.22	NA	0.04	NA	0.12	0.01	0.02	0.02
A	1/13/2021	2/2/2021	145	NA	0.45	NA	0.08	NA	0.24	0.01	0.03	0.03
A	2/2/2021	3/3/2021	55	NA	0.42	NA	0.07	0.00	0.22	0.01	0.03	0.03
A	3/3/2021	3/16/2021	134	NA	0.46	NA	0.10	NA	0.24	0.01	0.03	0.05
A	3/16/2021	3/31/2021	30	NA	0.55	NA	0.09	0.00	0.30	0.01	0.04	0.03
A	3/31/2021	6/11/2021	44	0.00	0.15	0.00	0.03	NA	0.08	0.00	0.01	0.02
A	6/11/2021	8/4/2021	21	0.00	0.13	0.00	0.02	0.00	0.08	0.00	0.01	0.01
DOH	4/9/2018	6/27/2018	286	0.00	0.54	0.00	0.10	NA	0.30	0.01	0.02	0.01
DOH	6/27/2018	8/21/2018	53	0.00	0.24	0.00	0.03	0.00	0.13	0.01	0.01	0.00
DOH	8/21/2018	8/28/2018	214	0.00	4.49	0.02	0.67	0.00	2.38	0.12	0.21	0.06
DOH	11/26/2018	12/13/2018	98	NA	0.81	0.00	0.13	NA	0.45	0.02	0.05	0.02
DOH	12/13/2018	1/24/2019	36	NA	0.19	0.00	0.03	0.00	0.13	0.01	0.01	0.00
DOH	1/24/2019	2/14/2019	104	NA	0.87	0.00	0.14	0.00	0.49	0.03	0.05	0.02
DOH	2/14/2019	3/31/2019	41	NA	0.32	0.00	0.05	0.00	0.18	0.02	0.02	0.01
DOH	3/31/2019	5/8/2019	69	0.00	0.35	0.00	0.07	0.00	0.20	0.03	0.02	0.01
DOH	5/8/2019	6/28/2019	98	0.00	0.17	0.00	0.05	NA	0.10	0.01	0.01	0.01
DOH	6/28/2019	8/5/2019	34	0.00	0.23	0.00	0.04	NA	0.13	0.01	0.02	0.01
DOH	8/5/2019	9/9/2019	36	0.00	0.20	0.00	0.04	0.00	0.11	0.02	0.02	0.01
DOH	9/9/2019	10/1/2019	64	NA	0.25	NA	0.05	0.00	0.15	0.01	0.01	0.01
DOH	10/1/2019	10/14/2019	87	NA	0.40	NA	0.09	NA	0.25	0.01	0.03	0.02
DOH	10/14/2019	11/15/2019	16	0.00	0.10	0.00	0.02	0.00	0.06	0.02	0.01	0.01
DOH	11/15/2019	12/11/2019	69	0.00	0.63	0.00	0.00	0.00	0.37	0.06	0.04	0.02
DOH	12/11/2019	12/20/2019	41	NA	0.54	0.00	0.12	0.00	0.33	0.02	0.02	0.02
DOH	12/20/2019	1/8/2020	144	NA	1.49	0.00	0.24	0.00	0.85	0.07	0.04	0.04
DOH	1/8/2020	1/15/2020	176	NA	3.47	0.01	0.54	0.00	2.01	0.08	0.08	0.08
DOH	1/15/2020	2/13/2020	40	NA	0.30	0.00	0.05	0.00	0.17	0.02	0.02	0.01
DOH	2/13/2020	3/6/2020	61	NA	0.66	0.00	0.09	0.00	0.38	0.02	0.04	0.02
DOH	3/6/2020	3/20/2020	119	NA	0.49	NA	0.13	NA	0.30	0.02	0.03	0.02
DOH	3/20/2020	4/17/2020	121	NA	0.43	NA	0.04	NA	0.25	0.04	0.03	0.01
DOH	4/17/2020	6/10/2020	58	0.00	0.20	NA	NA	0.00	0.12	0.06	0.02	0.01

DOH	7/24/2020	10/2/2020	19	NA	0.06	NA	0.01	0.00	0.03	0.00	0.00	0.00
DOH	10/2/2020	11/6/2020	87	0.00	0.13	NA	0.07	NA	0.08	0.02	0.01	0.01
DOH	11/6/2020	12/11/2020	18	0.00	0.17	NA	0.03	NA	0.09	0.02	0.01	0.01
DOH	12/11/2020	1/13/2021	47	NA	0.19	NA	0.02	NA	0.11	0.01	0.01	0.00
DOH	1/13/2021	2/2/2021	145	NA	0.77	NA	0.11	NA	0.42	0.03	0.05	0.02
DOH	2/2/2021	3/3/2021	55	NA	0.41	NA	0.06	0.00	0.22	0.02	0.03	0.04
DOH	3/3/2021	3/16/2021	134	NA	0.58	NA	0.12	NA	0.34	0.05	0.04	0.06
DOH	3/16/2021	3/31/2021	29	0.00	0.30	NA	0.01	0.00	0.19	0.08	0.02	0.02
DOH	3/31/2021	6/11/2021	44	NA	0.17	0.00	0.11	NA	0.11	0.13	0.02	0.08
DOH	6/11/2021	8/4/2021	21	0.00	0.07	0.00	NA	0.00	0.05	0.02	0.01	0.03
WU	5/1/2019	6/28/2019	154	NA	0.12	NA	0.04	NA	0.07	0.00	0.01	0.01
WU	6/28/2019	8/5/2019	63	0.00	0.20	0.00	0.04	NA	0.12	0.01	0.02	0.01
WU	8/5/2019	9/9/2019	93	NA	0.20	0.00	0.04	0.00	0.12	0.01	0.02	0.01
WU	9/9/2019	10/1/2019	98	NA	0.19	NA	0.04	NA	0.12	0.00	0.01	0.01
WU	10/1/2019	10/14/2019	127	NA	0.38	NA	0.08	NA	0.24	0.01	0.03	0.01
WU	10/14/2019	11/15/2019	37	0.00	0.12	0.00	0.03	0.00	0.07	0.00	0.01	0.01
WU	11/15/2019	12/11/2019	84	0.00	0.54	0.00	0.09	0.00	0.32	0.02	0.04	0.02
WU	12/11/2019	12/20/2019	64	NA	0.62	NA	0.13	0.00	0.36	0.02	0.02	0.02
WU	12/20/2019	1/8/2020	188	NA	1.52	0.00	0.23	0.00	0.87	0.05	0.04	0.04
WU	1/8/2020	1/15/2020	167	NA	4.01	0.01	0.55	0.00	2.27	0.10	0.10	0.10
WU	1/15/2020	2/13/2020	56	0.00	0.27	0.00	0.04	0.00	0.16	0.01	0.02	0.01
WU	2/13/2020	3/6/2020	105	NA	0.72	NA	0.11	0.00	0.42	0.02	0.05	0.02
WU	3/6/2020	3/20/2020	112	NA	0.41	NA	0.08	NA	0.25	0.01	0.03	0.01
WU	3/20/2020	4/17/2020	175	NA	0.41	NA	0.07	NA	0.23	0.01	0.03	0.01
WU	4/17/2020	6/10/2020	107	0.00	0.17	NA	0.03	NA	0.09	0.01	0.01	0.01
WU	7/24/2020	10/2/2020	130	NA	0.17	NA	0.03	0.00	0.09	0.01	0.01	0.01
WU	10/2/2020	11/6/2020	117	NA	0.09	NA	0.04	NA	0.05	0.00	0.01	0.00
WU	11/6/2020	12/11/2020	110	NA	0.38	NA	0.05	0.00	0.20	0.02	0.03	0.01
WU	12/11/2020	1/13/2021	139	NA	0.40	NA	0.06	NA	0.21	0.01	0.03	0.01
WU	1/13/2021	2/3/2021	174	NA	0.90	NA	0.15	NA	0.47	0.02	0.06	0.02
WU	2/3/2021	3/3/2021	135	NA	0.68	NA	0.11	0.00	0.36	0.01	0.05	0.02
WU	3/3/2021	3/16/2021	197	NA	0.57	NA	0.11	NA	0.30	0.02	0.04	0.04
WU	3/16/2021	3/31/2021	90	NA	0.67	NA	0.12	NA	0.35	0.01	0.04	0.02
WU	3/31/2021	6/11/2021	161	0.00	0.23	0.00	0.04	NA	0.13	0.01	0.02	0.01
WU	6/11/2021	8/4/2021	114	0.00	0.20	0.00	0.04	NA	0.12	0.01	0.01	0.01

## APPENDIX A: CHAPTER 2 SUPPLEMENTARY MATERIALS

### TAB A.3. CRUSTAL ENRICHMENT FACTORS

Collector	From Date	To Date	Precipitation (mm)	Crustal Enrichment Factors							
				Cl <sup>-</sup>	δ	K <sup>+</sup>	δ	Na <sup>+</sup>	δ	Mg <sup>2+</sup>	δ
K1	12/19/2018	3/18/2019	461	58.97	2807.40	1.75	0.12	21.57	1085.79	4.07	20.10
K1	3/18/2019	7/12/2019	541	38.84	975.90	2.45	0.19	12.07	272.81	2.33	5.62
K1	7/12/2019	10/12/2019	181	8.66	33.45	3.01	0.18	2.75	9.69	0.87	0.74
K1	10/12/2019	1/5/2020	504	24.97	405.67	1.05	0.03	11.33	240.55	1.86	3.79
K1	1/5/2020	3/28/2020	673	30.06	488.90	0.88	0.02	11.91	221.47	2.33	4.69
K1	3/28/2020	5/2/2020	26	13.87	91.40	1.25	0.03	6.69	60.33	1.33	1.55
K1	5/2/2020	6/20/2020	31	6.04	5.85	0.75	0.00	1.69	1.35	0.64	0.17
K1	6/20/2020	9/19/2020	43	7.91	7.05	0.66	0.00	2.20	1.60	0.68	0.13
K1	9/19/2020	1/4/2021	222	5.80	8.09	1.11	0.01	1.52	1.68	0.56	0.21
K1	1/4/2021	3/13/2021	516	26.10	461.60	1.61	0.08	7.70	116.25	1.89	4.05
K1	3/13/2021	4/21/2021	270	6.76	12.69	0.25	0.00	1.96	3.10	0.64	0.30
K2	7/12/2019	10/12/2019	198	7.03	18.39	2.46	0.10	2.25	5.38	0.60	0.37
K2	10/12/2019	1/5/2020	366	43.94	3121.42	2.63	0.53	25.26	2979.03	2.33	14.08
K2	1/5/2020	3/28/2020	540	20.81	236.05	0.59	0.01	9.04	127.84	1.55	2.32
K2	3/28/2020	5/2/2020	85	6.08	5.10	0.52	0.00	2.65	2.61	0.52	0.11
K2	5/2/2020	6/20/2020	35	2.09	0.36	0.23	0.00	0.59	0.09	0.24	0.02
K2	6/20/2020	9/19/2020	99	2.44	0.62	0.15	0.00	0.68	0.15	0.21	0.02
K2	9/19/2020	1/4/2021	246	2.10	0.72	0.25	0.00	0.54	0.16	0.17	0.02
K2	1/4/2021	3/13/2021	539	6.63	7.71	0.18	0.00	1.93	1.91	0.46	0.13
K2	3/13/2021	4/21/2021	309	1.12	0.20	0.03	0.00	0.32	0.05	0.09	0.01
K3	7/12/2019	10/12/2019	264	10.00	69.75	1.14	0.04	3.59	25.65	0.76	0.99
K3	10/12/2019	1/5/2020	410	34.67	1296.99	2.92	0.44	18.06	1015.40	2.33	9.36
K3	1/5/2020	3/28/2020	619	19.78	142.32	1.36	0.03	7.80	63.67	1.55	1.55
K3	3/28/2020	5/2/2020	90	12.22	71.55	1.25	0.03	6.34	54.22	1.33	1.55
K3	5/2/2020	6/20/2020	94	8.45	19.63	1.42	0.02	2.60	5.36	0.92	0.49
K3	6/20/2020	9/19/2020	153	7.08	8.81	1.56	0.02	2.13	2.32	0.84	0.27
K3	9/19/2020	1/4/2021	390	5.62	8.06	1.05	0.01	1.88	2.54	0.72	0.30
K3	1/4/2021	3/13/2021	759	11.25	47.51	1.32	0.03	3.70	14.73	0.75	0.53
K3	3/13/2021	4/21/2021	261	11.12	60.63	0.99	0.02	3.29	15.33	0.67	0.60
KS	12/19/2018	3/18/2019	750	50.84	2782.36	2.92	0.44	20.94	1363.60	3.88	24.37

KS	3/18/2019	7/12/2019	711	32.95	880.14	1.75	0.12	10.78	272.44	2.33	7.03
KS	7/12/2019	10/12/2019	244	12.61	100.49	0.63	0.01	4.12	30.81	0.79	0.96
KS	10/12/2019	1/5/2020	438	36.98	1474.72	1.17	0.07	18.88	1109.65	2.33	9.36
KS	1/5/2020	3/28/2020	844	22.74	281.13	0.59	0.01	9.65	145.74	1.55	2.32
KS	3/28/2020	5/2/2020	300	11.56	90.00	0.70	0.02	7.39	102.91	0.93	1.28
KS	5/2/2020	6/20/2020	89	9.71	26.48	2.79	0.10	2.60	5.57	0.52	0.25
KS	6/20/2020	9/19/2020	192	11.81	55.85	1.65	0.05	3.02	10.75	1.19	1.09
KS	9/19/2020	1/4/2021	480	7.69	26.21	0.07	0.00	2.06	5.59	0.58	0.43
KS	1/4/2021	3/13/2021	1077	17.40	237.00	0.38	0.01	4.99	56.49	1.22	2.26
KS	3/13/2021	4/21/2021	333	10.19	55.32	0.16	0.00	2.87	12.79	0.76	0.76
MT1	5/10/2019	7/11/2019	255	34.29	92.94	1.28	0.01	10.28	24.16	2.78	0.95
MT1	7/11/2019	9/29/2019	216	4.16	1.88	0.21	0.00	1.37	0.57	0.47	0.07
MT1	9/29/2019	1/9/2020	592	25.90	218.24	1.05	0.02	9.37	82.34	2.09	2.33
MT1	1/9/2020	3/31/2020	1614	25.85	197.66	0.64	0.01	8.85	66.86	1.90	1.79
MT1	6/15/2020	9/17/2020	240	5.14	2.68	0.22	0.00	1.45	0.63	0.42	0.06
MT1	9/17/2020	12/30/2020	753	5.35	4.54	0.22	0.00	1.53	1.09	0.65	0.16
MT1	12/30/2020	3/27/2021	1301	10.52	25.75	0.22	0.00	3.06	6.31	1.16	0.60
MT1	3/27/2021	4/29/2021	97	6.89	2.78	0.35	0.00	2.03	0.70	0.81	0.08
MT2	5/10/2019	7/11/2019	697	33.70	131.44	0.81	0.00	10.39	36.13	2.49	1.14
MT2	7/11/2019	9/25/2019	387	8.22	13.23	0.23	0.00	2.56	3.70	0.79	0.29
MT2	9/25/2019	1/7/2020	1041	35.85	520.21	0.66	0.01	12.79	191.25	2.91	5.31
MT2	1/7/2020	3/31/2020	1263	39.31	833.67	0.88	0.02	14.58	331.45	3.10	7.98
MT2	6/15/2020	9/17/2020	504	12.10	39.31	0.25	0.00	3.51	9.60	0.89	0.48
MT2	9/17/2020	12/22/2020	652	18.19	130.92	0.44	0.00	5.14	30.28	1.26	1.20
MT2	12/22/2020	3/27/2021	1416	33.04	736.97	0.58	0.01	9.62	181.02	2.33	5.86
MT2	3/27/2021	4/29/2021	249	21.11	125.60	0.62	0.01	6.17	31.09	1.67	1.35
MT3	5/10/2019	7/11/2019	597	3.67	2.07	0.12	0.00	1.19	0.61	0.88	0.20
MT3	7/11/2019	9/25/2019	1064	9.57	17.28	0.32	0.00	3.29	5.83	0.79	0.28
MT3	9/25/2019	1/7/2020	1270	23.45	255.98	0.50	0.01	9.33	116.66	1.66	2.23
MT3	1/7/2020	3/31/2020	2032	25.76	308.37	0.50	0.01	10.56	149.29	1.66	2.23
MT3	6/11/2020	9/17/2020	712	3.24	1.33	0.11	0.00	0.92	0.32	0.23	0.03
MT3	9/17/2020	12/22/2020	684	13.78	54.44	0.29	0.00	3.94	12.94	0.92	0.54
MT3	12/22/2020	3/27/2021	1588	24.91	360.65	0.66	0.01	7.17	86.69	1.75	3.03
MT3	3/27/2021	4/26/2021	351	15.76	58.99	0.92	0.01	4.65	14.86	1.09	0.58
MTS	7/11/2019	9/25/2019	323	26.70	275.95	1.34	0.03	8.51	81.00	0.91	0.74
MTS	9/25/2019	1/7/2020	605	52.61	2235.55	2.19	0.19	22.18	1148.65	2.33	7.03
MTS	1/7/2020	3/31/2020	479	22.84	212.62	0.66	0.01	9.40	103.60	1.75	2.12
MTS	6/11/2020	9/17/2020	92	3.85	1.21	0.13	0.00	1.06	0.28	0.26	0.03
MTS	9/17/2020	12/22/2020	376	4.31	2.33	0.39	0.00	1.24	0.57	0.33	0.05

MTS	12/22/2020	4/26/2021	671	11.41	37.51	0.39	0.00	3.33	9.27	0.76	0.41
EB	7/13/2019	9/27/2019	83	3.21	1.95	0.12	0.00	1.31	0.81	0.25	0.05
EB	9/27/2019	1/9/2020	169	2.73	1.19	0.11	0.00	1.31	0.62	0.21	0.03
EB	1/10/2020	3/31/2020	115	3.10	0.88	0.07	0.00	1.28	0.37	0.26	0.03
EB	3/31/2020	6/23/2020	23	1.13	0.14	0.06	0.00	0.30	0.03	0.15	0.01
EB	6/23/2020	10/16/2020	13	0.72	0.02	0.03	0.00	0.18	0.00	0.10	0.00
EB	10/16/2020	1/19/2021	41	1.58	0.15	0.03	0.00	0.43	0.04	0.17	0.01
EB	1/19/2021	4/7/2021	404	3.15	1.17	0.12	0.00	0.94	0.30	0.29	0.04
EB	4/7/2021	5/6/2021	58	2.30	0.53	0.12	0.00	0.67	0.13	0.23	0.02
TR	7/26/2019	10/19/2019	1351	26.15	207.82	0.72	0.01	8.21	59.25	1.39	1.09
TR	10/19/2019	1/9/2020	502	38.93	817.48	1.17	0.04	14.79	340.83	2.72	6.22
TR	1/9/2020	3/15/2020	537	18.09	63.21	0.41	0.00	6.31	22.12	1.23	0.57
TR	3/15/2020	5/4/2020	272	15.41	87.27	0.58	0.01	7.53	59.32	1.03	0.82
TR	5/4/2020	6/20/2020	183	6.15	4.61	0.19	0.00	1.73	1.07	0.44	0.08
TR	6/20/2020	10/12/2020	280	4.05	1.55	0.26	0.00	1.16	0.38	0.29	0.04
TR	1/20/2021	2/1/2021	211	93.49	14838.91	2.22	0.40	28.09	3875.74	5.76	83.05
TR	2/1/2021	2/17/2021	31	40.33	1223.81	2.28	0.19	11.98	312.38	2.81	9.27
TR	2/17/2021	3/2/2021	138	116.30	18961.03	2.59	0.45	34.01	4692.98	7.29	109.04
TR	3/2/2021	3/17/2021	284	66.80	9608.52	1.99	0.41	19.24	2306.04	4.04	52.79
TR	3/17/2021	4/7/2021	105	68.39	3353.63	2.10	0.15	19.79	813.14	4.45	21.18
TR	4/7/2021	4/29/2021	48	34.69	672.35	1.78	0.09	9.90	158.60	2.45	5.32
EB	8/5/2019	8/7/2019	8	9.71	32.35	1.05	0.02	3.94	15.02	0.70	0.43
MHS	10/18/2019	1/9/2020	243	14.90	40.87	0.68	0.00	5.34	15.07	1.03	0.41
M	10/23/2019	1/9/2020	262	10.81	10.71	0.33	0.00	3.53	3.28	0.82	0.14
M	1/9/2020	3/25/2020	731	12.63	41.05	0.54	0.00	5.02	18.50	0.90	0.46
M	3/25/2020	6/23/2020	38	3.83	0.90	0.17	0.00	1.19	0.25	0.25	0.02
M	6/23/2020	10/12/2020	55	1.26	0.12	0.04	0.00	0.33	0.03	0.11	0.00
M	10/12/2020	1/19/2021	140	2.08	0.56	0.03	0.00	0.56	0.13	0.18	0.02
M	1/19/2021	2/8/2021	149	46.50	5833.71	1.17	0.18	14.19	1571.94	2.91	35.49
M	2/8/2021	3/2/2021	20	18.33	45.20	0.37	0.00	5.50	11.78	1.17	0.37
M	3/2/2021	3/17/2021	123	32.52	2018.22	0.72	0.05	9.06	454.04	2.05	13.25
M	3/17/2021	4/7/2021	101	46.56	2500.93	0.94	0.05	13.59	616.95	2.99	15.95
M	4/7/2021	5/3/2021	30	6.96	9.68	0.76	0.00	2.08	2.50	0.62	0.21
PW	10/31/2019	1/29/2020	1086	35.01	567.07	0.75	0.01	13.38	239.08	2.66	5.13
KK	2/16/2020	4/24/2020	244	8.38	15.36	0.66	0.00	3.08	5.85	0.73	0.29
KK	4/24/2020	6/20/2020	27	15.72	38.89	3.49	0.09	2.97	4.16	1.33	0.52
KK	6/20/2020	10/10/2020	142	4.27	1.73	0.88	0.00	0.93	0.28	0.37	0.05
KK	10/10/2020	1/2/2021	148	7.42	7.89	1.94	0.02	1.27	0.79	1.06	0.31
KK	1/2/2021	4/3/2021	1211	3.78	1.43	0.30	0.00	0.99	0.30	0.55	0.07

KK	4/3/2021	4/25/2021	127	1.42	0.28	0.30	0.00	0.34	0.06	0.30	0.03
SB	2/16/2020	4/24/2020	310	15.61	100.66	0.66	0.01	7.24	61.77	1.16	1.10
SB	4/24/2020	6/20/2020	26	7.03	4.93	1.19	0.01	1.93	1.09	0.89	0.17
SB	6/20/2020	10/10/2020	66	2.64	0.58	0.22	0.00	0.73	0.13	0.19	0.02
SB	10/10/2020	1/11/2021	154	3.43	1.20	0.64	0.00	0.69	0.18	0.40	0.05
WAAF	2/16/2020	4/26/2020	366	17.16	50.99	1.66	0.02	5.84	17.00	1.35	0.58
WAAF	4/26/2020	6/20/2020	21	18.69	38.71	6.59	0.23	4.35	6.15	1.05	0.26
WAAF	6/20/2020	10/10/2020	55	9.11	4.96	9.61	0.25	1.86	0.64	0.79	0.09
WAAF	10/10/2020	1/11/2021	189	7.02	6.83	2.40	0.03	1.82	1.38	1.12	0.32
WAAF	1/11/2021	4/3/2021	1164	10.21	15.65	0.90	0.01	2.83	3.51	1.15	0.38
ER	2/16/2020	3/15/2020	143	46.58	501.03	3.51	0.14	14.17	134.18	2.66	2.57
ER	3/15/2020	4/25/2020	262	14.92	67.05	0.64	0.01	6.27	33.83	1.06	0.70
ER	4/25/2020	6/20/2020	79	3.81	0.97	0.11	0.00	1.08	0.23	0.26	0.02
ER	10/12/2020	1/11/2021	337	5.01	2.60	0.13	0.00	1.41	0.61	0.32	0.05
ER	1/11/2021	4/3/2021	894	10.49	17.83	0.23	0.00	3.00	4.25	0.70	0.21
D1	10/1/2017	12/31/2017	510	34.74	326.30	1.17	0.02	10.28	82.75	2.14	2.02
D1	1/1/2018	3/31/2018	778	24.37	214.41	1.56	0.04	6.83	48.87	1.55	1.54
MT1	4/1/2017	6/30/2017	244	5.71	2.78	0.00	NA	2.21	1.14	0.73	0.10
MT1	7/1/2017	9/30/2017	468	57.19	2373.85	0.00	NA	22.16	1030.82	7.32	56.99
MT1	10/1/2017	12/31/2017	595	2.49	0.47	0.00	NA	0.66	0.10	0.19	0.01
MT1	1/1/2018	3/31/2018	609	16.70	65.67	0.75	0.01	5.64	21.58	1.33	0.78
D4	10/1/2017	12/31/2017	89	37.47	189.37	4.24	0.12	12.37	59.67	2.71	1.55
D4	1/1/2018	3/31/2018	324	6.63	4.33	2.18	0.02	1.87	1.01	0.82	0.14
D6	4/1/2017	6/30/2017	743	5.51	2.52	0.00	0.00	2.40	1.28	0.71	0.10
D6	7/1/2017	9/30/2017	531	3.21	0.85	0.00	NA	1.07	0.26	0.28	0.03
D6	10/1/2017	12/31/2017	1345	11.57	23.73	0.37	0.00	3.63	6.75	0.86	0.30
D6	1/1/2018	3/31/2018	1028	9.62	12.70	0.49	0.00	2.71	2.94	0.93	0.25
D7	4/1/2017	6/30/2017	236	4.33	0.70	0.00	0.00	1.65	0.27	0.39	0.02
D7	7/1/2017	9/30/2017	96	2.96	0.21	0.00	0.00	0.99	0.06	0.24	0.01
D7	10/1/2017	12/31/2017	520	15.53	37.94	0.67	0.00	5.34	12.91	1.33	0.52
D7	1/1/2018	3/31/2018	305	33.18	445.19	0.66	0.01	9.53	106.38	2.32	3.50
D8	4/1/2017	6/30/2017	360	4.01	1.99	0.00	NA	1.78	0.99	0.47	0.08
D9	4/1/2017	6/30/2017	1303	2.58	0.58	0.00	NA	1.18	0.28	0.37	0.03
D9	7/1/2017	9/30/2017	568	1.95	0.43	0.00	NA	0.62	0.12	0.24	0.02
D9	10/1/2017	12/31/2017	526	12.90	39.72	0.75	0.01	4.67	14.91	1.16	0.63
D9	1/1/2018	3/31/2018	989	8.72	12.02	0.40	0.00	2.46	2.80	0.85	0.25
D10	3/1/2017	3/30/2017	299	4.95	3.47	0.63	0.00	1.76	1.20	0.50	0.10
D10	4/1/2017	6/30/2017	843	4.29	1.29	0.00	0.00	1.45	0.41	0.31	0.03
D10	7/1/2017	9/30/2017	758	3.05	1.21	0.00	NA	0.98	0.35	0.49	0.07

D10	10/1/2017	12/31/2017	1672	13.56	43.76	0.50	0.00	4.93	16.61	1.83	1.32
D10	1/1/2018	3/31/2018	1200	8.53	15.87	0.44	0.00	2.47	3.86	1.31	0.66
D11	4/1/2017	6/30/2017	297	12.58	11.07	0.00	0.00	4.64	4.31	0.97	0.14
D11	7/1/2017	9/30/2017	134	7.18	1.34	0.00	0.00	2.14	0.34	0.52	0.02
D11	10/1/2017	12/31/2017	240	26.76	25.57	0.83	0.00	8.12	6.82	1.74	0.19
D11	1/1/2018	3/31/2018	681	15.84	25.90	0.66	0.00	4.55	6.19	1.46	0.39
D12	10/1/2017	12/31/2017	124	12.18	19.15	4.72	0.13	3.55	4.73	1.16	0.34
D12	1/1/2018	3/31/2018	178	3.45	1.07	1.51	0.01	1.01	0.27	0.59	0.07
D13	4/1/2017	6/30/2017	1932	3.61	1.02	0.00	NA	1.28	0.34	0.52	0.05
D13	7/1/2017	9/30/2017	919	4.68	2.97	0.00	NA	1.25	0.64	0.47	0.09
D13	10/1/2017	12/31/2017	1699	12.21	27.79	0.39	0.00	4.25	9.63	1.42	0.67
D13	1/1/2018	3/31/2018	1649	17.69	51.45	0.35	0.00	4.99	11.88	1.75	0.85
D14	4/1/2017	6/30/2017	314	3.83	1.77	0.00	NA	1.70	0.88	0.58	0.09
D14	7/1/2017	9/30/2017	220	3.05	1.21	0.00	0.00	1.30	0.54	0.49	0.07
D14	10/1/2017	12/31/2017	461	9.99	13.64	0.56	0.00	3.06	3.69	1.02	0.29
D14	1/1/2018	3/31/2018	205	4.21	1.69	1.20	0.01	1.32	0.47	0.79	0.12
D15	1/1/2018	3/31/2018	342	7.36	7.17	0.97	0.01	2.10	1.71	0.86	0.21
D16	4/1/2017	6/30/2017	148	2.60	0.82	0.00	NA	1.11	0.36	0.52	0.07
D17	4/1/2017	6/30/2017	507	6.29	3.06	0.00	0.00	2.32	1.16	0.63	0.08
D17	7/1/2017	9/30/2017	352	3.51	0.66	0.00	0.00	1.15	0.20	0.43	0.03
D17	10/1/2017	12/31/2017	446	5.32	1.56	0.98	0.00	1.74	0.47	0.70	0.06
D17	1/1/2018	3/31/2018	370	6.85	6.07	0.88	0.00	2.02	1.54	0.50	0.10
D18	3/1/2017	3/30/2017	263	4.21	1.69	0.40	0.00	1.68	0.71	0.53	0.07
D18	4/1/2017	6/30/2017	1046	8.14	4.55	0.00	0.00	3.13	1.89	0.55	0.06
D18	7/1/2017	9/30/2017	1105	1.90	0.40	0.00	NA	0.61	0.11	0.23	0.02
D18	10/1/2017	12/31/2017	810	10.56	16.46	0.53	0.00	3.54	5.29	1.01	0.31
D18	1/1/2018	3/31/2018	1764	5.54	3.09	0.18	0.00	1.56	0.72	0.61	0.10
D19	4/1/2017	6/30/2017	262	5.93	3.08	0.00	0.00	2.30	1.27	0.60	0.08
D19	7/1/2017	9/30/2017	421	2.13	0.37	0.00	NA	0.65	0.10	0.25	0.02
D19	10/1/2017	12/31/2017	347	8.48	6.98	1.46	0.01	2.40	1.63	0.65	0.11
D19	1/1/2018	3/31/2018	125	3.11	0.56	0.94	0.00	1.03	0.17	0.58	0.04
D20	4/1/2017	6/30/2017	1342	4.13	1.29	0.00	0.00	1.54	0.48	0.46	0.05
D20	7/1/2017	9/30/2017	271	1.95	0.21	0.00	0.00	0.52	0.05	0.29	0.01
D20	10/1/2017	12/31/2017	351	3.14	0.42	0.18	0.00	1.03	0.12	0.45	0.02
D20	1/1/2018	3/31/2018	660	2.71	0.45	0.38	0.00	0.72	0.10	0.32	0.02
A	3/9/2019	5/8/2019	46	27.02	234.93	2.50	0.10	9.39	82.03	1.29	1.03
A	5/8/2019	6/29/2019	119	12.88	74.91	0.36	0.00	3.88	19.69	0.91	0.84
A	6/29/2019	8/5/2019	14	47.41	1210.79	1.46	0.06	14.99	350.34	3.88	12.21
A	8/5/2019	10/1/2019	69	12.84	61.26	0.58	0.01	3.97	16.91	0.78	0.55

A	10/1/2019	10/14/2019	49	24.28	320.10	0.59	0.01	7.80	95.57	1.55	2.32
A	10/14/2019	11/15/2019	35	6.85	9.50	0.28	0.00	2.20	2.81	2.33	1.57
A	11/15/2019	12/11/2019	50	36.71	545.55	0.88	0.02	11.71	160.46	2.62	4.36
A	12/11/2019	12/20/2019	50	46.25	3292.35	1.08	0.09	14.08	883.19	2.33	13.40
A	12/20/2019	1/8/2020	61	65.43	1685.01	1.45	0.04	20.14	461.86	2.33	3.43
A	1/8/2020	1/15/2020	84	60.21	2018.40	1.00	0.03	18.70	563.23	2.33	4.85
A	1/15/2020	2/13/2020	22	37.45	300.75	0.84	0.01	11.45	81.36	2.53	2.17
A	2/13/2020	3/7/2020	72	40.07	348.64	0.67	0.00	12.72	101.61	2.64	2.38
A	3/7/2020	3/20/2020	99	48.33	3973.08	1.29	0.14	15.44	1172.84	3.06	24.58
A	3/20/2020	4/17/2020	116	30.03	574.04	0.72	0.02	9.09	152.16	2.15	4.77
A	11/6/2020	12/11/2020	18	32.86	121.57	0.65	0.00	9.30	28.20	2.33	0.98
A	12/11/2020	1/13/2021	47	29.04	224.43	0.72	0.01	8.16	51.35	2.14	1.98
A	1/13/2021	2/2/2021	145	34.19	901.85	0.58	0.01	9.68	209.39	2.44	7.29
A	2/2/2021	3/3/2021	55	29.80	166.61	0.52	0.00	8.33	37.76	2.10	1.35
A	3/3/2021	3/16/2021	134	20.99	293.91	0.43	0.01	5.91	67.49	1.52	2.74
A	3/16/2021	3/31/2021	30	40.49	337.95	0.67	0.00	11.73	82.15	2.79	2.50
A	3/31/2021	6/11/2021	44	19.96	43.90	0.43	0.00	5.74	10.53	1.72	0.56
A	6/11/2021	8/4/2021	21	20.11	35.78	0.50	0.00	6.32	10.21	1.50	0.35
DOH	4/9/2018	6/27/2018	286	173.44	48493.86	3.51	0.95	51.14	12200.34	6.98	115.34
DOH	6/27/2018	8/21/2018	53	192.59	39831.58	5.26	1.42	57.47	10263.59	9.30	135.66
DOH	8/21/2018	8/28/2018	214	169.98	46574.48	3.51	0.95	48.06	10774.93	8.15	156.42
DOH	11/26/2018	12/13/2018	98	116.47	15615.29	2.13	0.25	34.09	3870.71	7.23	88.17
DOH	12/13/2018	1/24/2019	36	123.92	12076.27	3.47	0.45	46.01	4817.84	8.12	75.78
DOH	1/24/2019	2/14/2019	104	103.60	8876.12	2.83	0.32	31.19	2327.93	6.39	49.60
DOH	2/14/2019	3/31/2019	41	84.88	2396.33	3.24	0.17	24.77	590.79	6.02	17.78
DOH	3/31/2019	5/8/2019	69	72.36	2725.00	4.87	0.59	22.06	732.99	3.83	11.52
DOH	5/8/2019	6/28/2019	98	27.29	327.07	1.49	0.05	8.69	96.01	2.14	3.27
DOH	6/28/2019	8/5/2019	34	49.14	650.36	2.34	0.07	14.79	170.42	3.69	5.53
DOH	8/5/2019	9/9/2019	36	37.39	377.13	2.92	0.11	11.19	97.83	4.07	6.70
DOH	9/9/2019	10/1/2019	64	49.72	1997.24	1.75	0.12	15.71	577.00	2.91	10.61
DOH	10/1/2019	10/14/2019	87	46.22	2300.51	1.17	0.07	15.19	718.52	3.10	15.93
DOH	10/14/2019	11/15/2019	16	34.61	283.24	3.88	0.17	10.52	75.80	2.33	2.06
DOH	11/15/2019	12/11/2019	69	78.28	2823.45	6.01	0.80	24.46	797.95	4.99	17.01
DOH	12/11/2019	12/20/2019	41	80.29	6119.35	2.32	0.25	26.11	1871.78	2.33	8.29
DOH	12/20/2019	1/8/2020	144	94.40	5986.33	3.54	0.40	28.74	1606.13	2.33	5.86
DOH	1/8/2020	1/15/2020	176	106.31	12141.39	1.93	0.19	32.84	3352.62	2.33	9.36
DOH	1/15/2020	2/13/2020	40	52.95	943.67	2.74	0.12	15.73	240.86	3.52	6.32
DOH	2/13/2020	3/6/2020	61	83.87	3437.74	1.70	0.07	25.91	949.46	5.47	21.58
DOH	3/6/2020	3/20/2020	119	74.66	9995.41	2.43	0.51	24.51	3117.83	5.30	74.67

DOH	3/20/2020	4/17/2020	121	87.48	9491.06	5.60	1.86	27.95	2803.42	5.55	56.39
DOH	4/17/2020	6/10/2020	58	34.78	321.27	8.65	0.95	11.47	101.09	2.94	3.54
DOH	7/24/2020	10/2/2020	19	54.98	1061.61	2.35	0.09	15.79	253.56	3.62	6.97
DOH	10/2/2020	11/6/2020	87	23.93	359.01	3.14	0.29	7.40	99.16	1.84	3.56
DOH	11/6/2020	12/11/2020	18	41.66	306.83	2.88	0.07	11.32	65.59	2.71	2.03
DOH	12/11/2020	1/13/2021	47	96.67	9424.52	3.34	0.54	28.55	2378.67	6.33	59.47
DOH	1/13/2021	2/2/2021	145	79.20	6531.71	2.32	0.27	23.07	1603.92	5.26	42.64
DOH	2/2/2021	3/3/2021	55	25.79	112.11	1.05	0.01	7.33	26.25	1.76	0.89
DOH	3/3/2021	3/16/2021	134	23.59	329.89	1.44	0.06	7.40	93.72	1.82	3.32
DOH	3/16/2021	3/31/2021	29	28.49	207.63	5.87	0.42	9.49	66.53	2.09	1.83
DOH	3/31/2021	6/11/2021	44	5.01	0.76	2.78	0.01	1.68	0.24	0.64	0.03
DOH	6/11/2021	8/4/2021	21	6.18	2.03	1.14	0.00	2.30	0.78	0.56	0.05
WU	5/1/2019	6/28/2019	154	45.18	2748.59	1.02	0.07	14.32	799.03	3.49	24.92
WU	6/28/2019	8/5/2019	63	47.41	1210.79	1.46	0.06	14.99	350.34	3.88	12.21
WU	8/5/2019	9/9/2019	93	59.32	3784.70	1.17	0.07	19.29	1158.35	4.65	34.65
WU	9/9/2019	10/1/2019	98	48.57	3811.37	0.88	0.06	16.02	1199.49	3.49	29.93
WU	10/1/2019	10/14/2019	127	90.01	26081.25	1.75	0.47	30.75	8804.64	6.97	229.32
WU	10/14/2019	11/15/2019	37	46.27	1357.43	1.14	0.04	14.26	373.12	2.33	5.53
WU	11/15/2019	12/11/2019	84	77.21	3845.63	2.10	0.14	24.14	1088.03	5.58	29.71
WU	12/11/2019	12/20/2019	64	59.20	3329.30	1.19	0.06	18.49	939.95	2.33	8.29
WU	12/20/2019	1/8/2020	188	86.86	5935.83	2.05	0.16	26.45	1592.63	2.33	6.87
WU	1/8/2020	1/15/2020	167	97.13	7607.42	1.89	0.14	29.27	1998.72	2.33	7.03
WU	1/15/2020	2/13/2020	56	67.88	3163.49	1.45	0.07	21.10	884.42	4.85	24.01
WU	2/13/2020	3/6/2020	105	87.36	6154.62	1.71	0.11	27.20	1726.94	6.46	49.46
WU	3/6/2020	3/20/2020	112	66.05	7825.39	1.27	0.14	21.57	2414.63	4.40	51.86
WU	3/20/2020	4/17/2020	175	68.42	6866.65	1.27	0.11	20.22	1734.95	4.87	51.59
WU	4/17/2020	6/10/2020	107	74.48	6626.40	1.69	0.16	21.67	1623.08	5.08	45.78
WU	7/24/2020	10/2/2020	130	73.64	6030.43	1.81	0.18	20.77	1387.98	4.73	37.07
WU	10/2/2020	11/6/2020	117	43.32	4338.26	1.63	0.29	12.77	1091.86	2.83	28.76
WU	11/6/2020	12/11/2020	110	79.91	5887.64	2.91	0.37	22.65	1368.62	5.72	44.54
WU	12/11/2020	1/13/2021	139	91.03	11133.17	1.97	0.25	25.87	2602.44	6.30	78.51
WU	1/13/2021	2/3/2021	174	89.48	9218.81	1.69	0.16	24.72	2036.31	5.73	55.83
WU	2/3/2021	3/3/2021	135	90.92	7408.34	1.51	0.10	25.30	1660.53	6.21	50.84
WU	3/3/2021	3/16/2021	197	32.27	1250.33	0.71	0.03	9.12	289.33	2.33	10.42
WU	3/16/2021	3/31/2021	90	99.57	12294.14	1.62	0.16	28.00	2813.04	6.53	77.76
WU	3/31/2021	6/11/2021	161	41.43	974.17	1.02	0.03	12.11	240.85	2.94	7.60
WU	6/11/2021	8/4/2021	114	42.16	1085.18	0.89	0.02	13.37	315.82	3.03	8.64

## APPENDIX A: CHAPTER 2 SUPPLEMENTARY MATERIALS

### TAB A.4. MARINE ENRICHMENT FACTORS

Collector	From Date	To Date	Precipitation (mm)	Marine Enrichment Factors									
				Ca <sup>2+</sup>	δ	SO <sub>4</sub> <sup>2-</sup>	δ	Na <sup>+</sup>	δ	K <sup>+</sup>	δ	Mg <sup>2+</sup>	δ
K1	12/19/2018	3/18/2019	461	1.84	0.11	1.19	0.08	1.23	0.17	1.80	0.01	1.03	0.05
K1	3/18/2019	7/12/2019	541	2.79	0.19	1.61	0.13	1.05	0.16	3.82	0.04	0.89	0.05
K1	7/12/2019	10/12/2019	181	12.50	2.70	0.15	0.03	1.07	0.47	21.01	3.03	1.49	0.25
K1	10/12/2019	1/5/2020	504	4.33	0.47	0.79	0.10	1.53	0.45	2.54	0.03	1.11	0.10
K1	1/5/2020	3/28/2020	673	3.60	0.27	0.37	0.03	1.33	0.25	1.76	0.01	1.15	0.07
K1	3/28/2020	5/2/2020	26	7.80	1.12	0.34	0.05	1.62	0.64	5.45	0.15	1.43	0.17
K1	5/2/2020	6/20/2020	31	17.90	1.98	0.15	0.02	0.94	0.18	7.44	0.19	1.57	0.13
K1	6/20/2020	9/19/2020	43	13.69	0.82	0.00	NA	0.94	0.10	5.05	0.05	1.27	0.06
K1	9/19/2020	1/4/2021	222	18.65	3.23	0.36	0.06	0.88	0.26	11.51	0.68	1.44	0.18
K1	1/4/2021	3/13/2021	516	4.15	0.45	0.92	0.11	0.99	0.23	3.72	0.06	1.08	0.10
K1	3/13/2021	4/21/2021	270	16.00	2.75	1.12	0.20	0.97	0.31	2.27	0.04	1.41	0.18
K2	7/12/2019	10/12/2019	198	15.39	3.40	1.86	0.43	1.08	0.47	21.11	3.03	1.27	0.21
K2	10/12/2019	1/5/2020	366	2.46	0.38	0.75	0.13	1.94	0.96	3.61	0.08	0.79	0.10
K2	1/5/2020	3/28/2020	540	5.20	0.57	1.06	0.13	1.46	0.42	1.70	0.02	1.11	0.10
K2	3/28/2020	5/2/2020	85	17.80	1.69	0.40	0.04	1.47	0.32	5.16	0.08	1.27	0.09
K2	5/2/2020	6/20/2020	35	51.76	8.60	0.13	0.01	0.95	0.17	6.66	0.14	1.70	0.12
K2	6/20/2020	9/19/2020	99	44.34	7.94	0.42	0.05	0.94	0.20	3.60	0.05	1.26	0.11
K2	9/19/2020	1/4/2021	246	51.48	16.75	0.00	NA	0.87	0.29	7.06	0.30	1.20	0.17
K2	1/4/2021	3/13/2021	539	16.33	1.81	1.20	0.14	0.98	0.20	1.61	0.02	1.03	0.08
K2	3/13/2021	4/21/2021	309	96.85	59.17	0.00	NA	0.97	0.37	1.74	0.03	1.18	0.18
K3	7/12/2019	10/12/2019	264	10.82	3.16	1.79	0.57	1.21	0.78	6.91	0.48	1.13	0.26
K3	10/12/2019	1/5/2020	410	3.12	0.41	0.63	0.09	1.75	0.68	5.09	0.13	1.00	0.11
K3	1/5/2020	3/28/2020	619	5.47	0.42	1.11	0.10	1.33	0.25	4.16	0.05	1.17	0.07
K3	3/28/2020	5/2/2020	90	8.86	1.45	0.19	0.04	1.75	0.82	6.19	0.22	1.62	0.22
K3	5/2/2020	6/20/2020	94	12.81	1.74	0.00	NA	1.04	0.28	10.16	0.46	1.61	0.17
K3	6/20/2020	9/19/2020	153	15.28	1.58	0.00	NA	1.01	0.20	13.27	0.57	1.76	0.14
K3	9/19/2020	1/4/2021	390	19.26	3.66	0.00	NA	1.13	0.41	11.26	0.71	1.90	0.26
K3	1/4/2021	3/13/2021	759	9.62	1.34	0.00	NA	1.11	0.33	7.11	0.24	0.99	0.11
K3	3/13/2021	4/21/2021	261	9.73	1.79	0.00	NA	0.99	0.37	5.38	0.19	0.90	0.13
KS	12/19/2018	3/18/2019	750	2.13	0.19	1.08	0.11	1.39	0.31	3.47	0.04	1.13	0.08

KS	3/18/2019	7/12/2019	711	3.28	0.34	1.63	0.19	1.10	0.25	3.21	0.05	1.05	0.09
KS	7/12/2019	10/12/2019	244	8.58	1.80	0.54	0.13	1.10	0.49	3.01	0.08	0.93	0.15
KS	10/12/2019	1/5/2020	438	2.93	0.36	1.04	0.15	1.72	0.62	1.91	0.02	0.94	0.09
KS	1/5/2020	3/28/2020	844	4.76	0.48	0.73	0.08	1.43	0.37	1.55	0.02	1.01	0.08
KS	3/28/2020	5/2/2020	300	9.36	2.28	0.57	0.15	2.15	1.77	3.67	0.13	1.20	0.23
KS	5/2/2020	6/20/2020	89	11.15	1.35	0.40	0.05	0.90	0.21	17.35	1.18	0.79	0.07
KS	6/20/2020	9/19/2020	192	9.16	1.30	0.00	NA	0.86	0.23	8.43	0.34	1.50	0.17
KS	9/19/2020	1/4/2021	480	14.07	3.39	0.00	NA	0.90	0.40	0.52	0.01	1.13	0.20
KS	1/4/2021	3/13/2021	1077	6.22	1.17	1.13	0.24	0.97	0.37	1.30	0.02	1.04	0.16
KS	3/13/2021	4/21/2021	333	10.62	2.32	0.76	0.18	0.95	0.40	0.97	0.02	1.12	0.19
MT1	5/10/2019	7/11/2019	255	3.16	0.03	1.17	0.01	1.01	0.02	2.26	0.00	1.21	0.01
MT1	7/11/2019	9/29/2019	216	26.00	2.83	0.13	0.01	1.11	0.21	3.00	0.03	1.66	0.12
MT1	9/29/2019	1/9/2020	592	4.18	0.22	0.83	0.05	1.22	0.15	2.45	0.02	1.20	0.05
MT1	1/9/2020	3/31/2020	1614	4.19	0.20	0.93	0.05	1.15	0.12	1.49	0.01	1.10	0.04
MT1	6/15/2020	9/17/2020	240	21.07	1.74	0.00	NA	0.95	0.13	2.57	0.02	1.21	0.07
MT1	9/17/2020	12/30/2020	753	20.21	2.50	1.39	0.17	0.96	0.21	2.51	0.03	1.80	0.16
MT1	12/30/2020	3/27/2021	1301	10.29	0.95	1.07	0.11	0.98	0.18	1.24	0.01	1.65	0.12
MT1	3/27/2021	4/29/2021	97	15.70	0.56	0.85	0.03	0.99	0.07	3.03	0.01	1.74	0.05
MT2	5/10/2019	7/11/2019	697	3.21	0.05	1.19	0.02	1.04	0.03	1.46	0.00	1.10	0.01
MT2	7/11/2019	9/25/2019	387	13.17	1.31	1.16	0.12	1.05	0.21	1.66	0.02	1.44	0.11
MT2	9/25/2019	1/7/2020	1041	3.02	0.14	1.15	0.06	1.20	0.13	1.11	0.00	1.21	0.05
MT2	1/7/2020	3/31/2020	1263	2.75	0.16	1.12	0.07	1.25	0.17	1.35	0.01	1.17	0.06
MT2	6/15/2020	9/17/2020	504	8.95	0.83	0.00	NA	0.98	0.18	1.26	0.01	1.10	0.08
MT2	9/17/2020	12/22/2020	652	5.95	0.54	0.44	0.04	0.95	0.18	1.47	0.01	1.03	0.08
MT2	12/22/2020	3/27/2021	1416	3.28	0.28	0.94	0.09	0.98	0.17	1.07	0.01	1.05	0.07
MT2	3/27/2021	4/29/2021	249	5.13	0.29	1.15	0.07	0.98	0.11	1.77	0.01	1.17	0.05
MT3	5/10/2019	7/11/2019	597	29.51	5.19	1.55	0.23	1.09	0.31	1.99	0.03	3.58	0.46
MT3	7/11/2019	9/25/2019	1064	11.31	0.93	1.08	0.10	1.16	0.20	2.01	0.02	1.23	0.08
MT3	9/25/2019	1/7/2020	1270	4.62	0.38	1.31	0.12	1.34	0.27	1.29	0.01	1.05	0.07
MT3	1/7/2020	3/31/2020	2032	4.20	0.32	0.92	0.08	1.38	0.26	1.18	0.01	0.96	0.06
MT3	6/11/2020	9/17/2020	712	33.35	5.43	0.17	0.02	0.96	0.22	2.08	0.03	1.05	0.09
MT3	9/17/2020	12/22/2020	684	7.86	0.68	0.93	0.09	0.96	0.17	1.26	0.01	1.00	0.07
MT3	12/22/2020	3/27/2021	1588	4.35	0.42	1.07	0.12	0.97	0.20	1.59	0.02	1.04	0.08
MT3	3/27/2021	4/26/2021	351	6.87	0.43	0.75	0.05	0.99	0.13	3.53	0.03	1.03	0.05
MTS	7/11/2019	9/25/2019	323	4.05	0.25	0.71	0.05	1.07	0.14	3.02	0.02	0.51	0.02
MTS	9/25/2019	1/7/2020	605	2.06	0.13	0.71	0.05	1.42	0.24	2.52	0.02	0.66	0.03
MTS	1/7/2020	3/31/2020	479	4.74	0.35	0.99	0.08	1.39	0.26	1.74	0.01	1.14	0.07
MTS	6/11/2020	9/17/2020	92	28.12	2.51	0.08	0.01	0.93	0.12	1.96	0.01	1.01	0.05
MTS	9/17/2020	12/22/2020	376	25.10	3.05	0.81	0.09	0.97	0.19	5.40	0.10	1.14	0.09

MTS	12/22/2020	4/26/2021	671	9.49	1.00	0.99	0.12	0.98	0.21	2.06	0.02	0.99	0.08
EB	7/13/2019	9/27/2019	83	33.73	8.33	2.38	0.46	1.37	0.58	2.22	0.04	1.15	0.16
EB	9/27/2019	1/9/2020	169	39.60	9.67	2.01	0.35	1.61	0.68	2.35	0.04	1.15	0.14
EB	1/10/2020	3/31/2020	115	34.94	4.35	0.80	0.08	1.39	0.29	1.29	0.01	1.27	0.09
EB	3/31/2020	6/23/2020	23	95.65	38.11	0.00	NA	0.88	0.21	3.15	0.05	2.00	0.21
EB	6/23/2020	10/16/2020	13	150.10	35.27	0.23	0.01	0.83	0.08	2.40	0.01	2.07	0.09
EB	10/16/2020	1/19/2021	41	68.58	11.30	1.07	0.08	0.91	0.12	1.06	0.01	1.57	0.09
EB	1/19/2021	4/7/2021	404	34.32	5.37	1.28	0.15	1.00	0.22	2.29	0.03	1.37	0.12
EB	4/7/2021	5/6/2021	58	46.96	8.50	0.00	NA	0.97	0.20	3.03	0.04	1.47	0.12
TR	7/26/2019	10/19/2019	1351	4.14	0.20	1.11	0.06	1.06	0.11	1.66	0.01	0.79	0.03
TR	10/19/2019	1/9/2020	502	2.78	0.16	1.13	0.08	1.28	0.18	1.81	0.01	1.04	0.05
TR	1/9/2020	3/15/2020	537	5.98	0.27	1.13	0.06	1.17	0.12	1.38	0.01	1.01	0.04
TR	3/15/2020	5/4/2020	272	7.02	0.70	1.19	0.13	1.64	0.46	2.29	0.03	1.00	0.08
TR	5/4/2020	6/20/2020	183	17.60	1.46	0.27	0.02	0.95	0.14	1.86	0.01	1.05	0.06
TR	6/20/2020	10/12/2020	280	26.71	2.61	0.00	NA	0.97	0.15	3.82	0.04	1.08	0.07
TR	1/20/2021	2/1/2021	211	1.16	0.09	0.93	0.08	1.01	0.16	1.43	0.01	0.92	0.06
TR	2/1/2021	2/17/2021	31	2.68	0.21	1.05	0.09	1.00	0.16	3.42	0.04	1.04	0.07
TR	2/17/2021	3/2/2021	138	0.93	0.05	0.99	0.06	0.98	0.10	1.35	0.01	0.93	0.04
TR	3/2/2021	3/17/2021	284	1.62	0.22	1.15	0.18	0.97	0.27	1.80	0.03	0.90	0.10
TR	3/17/2021	4/7/2021	105	1.58	0.07	1.13	0.06	0.97	0.09	1.86	0.01	0.97	0.03
TR	4/7/2021	4/29/2021	48	3.12	0.21	1.23	0.10	0.96	0.13	3.11	0.03	1.05	0.06
EB	8/5/2019	8/7/2019	8	11.14	1.65	2.04	0.33	1.37	0.48	6.54	0.22	1.07	0.12
MHS	10/18/2019	1/9/2020	243	7.26	0.38	1.42	0.08	1.21	0.14	2.76	0.02	1.03	0.04
M	10/23/2019	1/9/2020	262	10.01	0.35	1.44	0.06	1.10	0.08	1.85	0.01	1.13	0.03
M	1/9/2020	3/25/2020	731	8.57	0.73	1.61	0.15	1.34	0.27	2.58	0.03	1.05	0.07
M	3/25/2020	6/23/2020	38	28.28	1.90	2.45	0.14	1.05	0.11	2.76	0.02	0.98	0.04
M	6/23/2020	10/12/2020	55	85.90	21.67	2.18	0.22	0.89	0.15	1.87	0.02	1.29	0.09
M	10/12/2020	1/19/2021	140	52.10	13.57	1.78	0.27	0.92	0.25	0.83	0.01	1.26	0.14
M	1/19/2021	2/8/2021	149	2.33	0.56	2.37	0.67	1.03	0.53	1.52	0.04	0.93	0.18
M	2/8/2021	3/2/2021	20	5.90	0.18	1.48	0.05	1.01	0.06	1.21	0.00	0.95	0.02
M	3/2/2021	3/17/2021	123	3.33	0.82	2.69	0.77	0.94	0.47	1.34	0.03	0.94	0.19
M	3/17/2021	4/7/2021	101	2.32	0.24	2.15	0.26	0.98	0.21	1.22	0.01	0.96	0.08
M	4/7/2021	5/3/2021	30	15.54	1.86	2.62	0.33	1.00	0.23	6.55	0.17	1.32	0.12
PW	10/31/2019	1/29/2020	1086	3.09	0.17	1.28	0.08	1.29	0.17	1.30	0.01	1.13	0.05
KK	2/16/2020	4/24/2020	244	12.91	1.41	1.48	0.17	1.24	0.30	4.74	0.09	1.29	0.11
KK	4/24/2020	6/20/2020	27	6.88	0.29	0.29	0.01	0.64	0.05	13.40	0.25	1.26	0.04
KK	6/20/2020	10/10/2020	142	25.32	2.34	0.17	0.01	0.73	0.10	12.50	0.39	1.30	0.08
KK	10/10/2020	1/2/2021	148	14.58	1.18	0.00	NA	0.57	0.07	15.82	0.63	2.12	0.14
KK	1/2/2021	4/3/2021	1211	28.64	3.18	1.09	0.10	0.88	0.14	4.71	0.07	2.17	0.15

KK	4/3/2021	4/25/2021	127	76.00	30.90	0.00	NA	0.82	0.24	12.67	0.85	3.13	0.46
SB	2/16/2020	4/24/2020	310	6.93	0.77	1.59	0.20	1.56	0.47	2.54	0.03	1.11	0.10
SB	4/24/2020	6/20/2020	26	15.39	0.91	1.37	0.08	0.92	0.10	10.23	0.19	1.89	0.09
SB	6/20/2020	10/10/2020	66	40.98	5.39	0.00	NA	0.93	0.15	5.07	0.08	1.09	0.07
SB	10/10/2020	1/11/2021	154	31.57	3.94	0.00	NA	0.67	0.11	11.28	0.39	1.72	0.13
WAAF	2/16/2020	4/26/2020	366	6.31	0.27	1.21	0.06	1.15	0.11	5.85	0.05	1.17	0.04
WAAF	4/26/2020	6/20/2020	21	5.79	0.14	0.00	NA	0.78	0.04	21.31	0.38	0.84	0.02
WAAF	6/20/2020	10/10/2020	55	11.88	0.33	0.00	NA	0.69	0.03	63.70	3.55	1.28	0.03
WAAF	10/10/2020	1/11/2021	189	15.42	1.28	0.54	0.05	0.87	0.13	20.66	1.08	2.37	0.16
WAAF	1/11/2021	4/3/2021	1164	10.60	0.65	1.14	0.08	0.93	0.11	5.30	0.06	1.67	0.08
ER	2/16/2020	3/15/2020	143	2.32	0.05	1.09	0.03	1.02	0.05	4.55	0.02	0.85	0.01
ER	3/15/2020	4/25/2020	262	7.25	0.61	1.71	0.16	1.42	0.30	2.58	0.03	1.05	0.07
ER	4/25/2020	6/20/2020	79	28.39	2.08	0.19	0.01	0.95	0.11	1.73	0.01	1.02	0.05
ER	10/12/2020	1/11/2021	337	21.59	1.86	0.78	0.06	0.95	0.14	1.61	0.01	0.96	0.06
ER	1/11/2021	4/3/2021	894	10.31	0.67	0.60	0.04	0.96	0.12	1.30	0.01	0.99	0.05
D1	10/1/2017	12/31/2017	510	3.12	0.10	1.31	0.05	1.00	0.07	2.04	0.01	0.92	0.02
D1	1/1/2018	3/31/2018	778	4.44	0.28	1.43	0.10	0.94	0.12	3.86	0.04	0.95	0.05
MT1	4/1/2017	6/30/2017	244	18.94	1.18	1.94	0.12	1.31	0.17	0.00	NA	1.91	0.09
MT1	7/1/2017	9/30/2017	468	1.89	0.10	1.94	0.12	1.31	0.17	0.00	NA	1.91	0.09
MT1	10/1/2017	12/31/2017	595	43.41	5.48	1.52	0.13	0.90	0.13	0.00	NA	1.12	0.07
MT1	1/1/2018	3/31/2018	609	6.48	0.38	1.49	0.10	1.14	0.15	2.71	0.02	1.19	0.06
D4	10/1/2017	12/31/2017	89	2.89	0.04	1.06	0.02	1.11	0.04	6.82	0.03	1.08	0.01
D4	1/1/2018	3/31/2018	324	16.33	1.02	0.74	0.05	0.95	0.11	19.88	0.75	1.84	0.09
D6	4/1/2017	6/30/2017	743	19.64	1.24	2.08	0.13	1.47	0.21	0.02	0.00	1.91	0.09
D6	7/1/2017	9/30/2017	531	33.75	3.66	1.07	0.09	1.12	0.18	0.00	NA	1.31	0.08
D6	10/1/2017	12/31/2017	1345	9.36	0.60	1.28	0.09	1.06	0.14	1.92	0.01	1.10	0.06
D6	1/1/2018	3/31/2018	1028	11.25	0.67	1.17	0.08	0.95	0.11	3.08	0.02	1.44	0.07
D7	4/1/2017	6/30/2017	236	24.99	0.89	1.60	0.05	1.28	0.09	0.01	0.00	1.35	0.03
D7	7/1/2017	9/30/2017	96	36.58	1.23	1.32	0.03	1.13	0.05	0.01	0.00	1.22	0.02
D7	10/1/2017	12/31/2017	520	6.97	0.30	1.47	0.07	1.16	0.11	2.60	0.01	1.27	0.04
D7	1/1/2018	3/31/2018	305	3.26	0.17	1.24	0.07	0.97	0.10	1.20	0.01	1.04	0.04
D8	4/1/2017	6/30/2017	360	27.00	3.49	1.54	0.17	1.49	0.39	0.00	NA	1.75	0.15
D9	4/1/2017	6/30/2017	1303	41.89	5.90	1.73	0.17	1.54	0.35	0.00	NA	2.14	0.16
D9	7/1/2017	9/30/2017	568	55.57	13.41	0.00	NA	1.08	0.28	0.00	NA	1.80	0.18
D9	10/1/2017	12/31/2017	526	8.39	0.65	1.74	0.15	1.22	0.21	3.51	0.04	1.34	0.08
D9	1/1/2018	3/31/2018	989	12.41	0.94	1.21	0.10	0.95	0.14	2.76	0.02	1.44	0.09
D10	3/1/2017	3/30/2017	299	21.84	2.61	2.14	0.24	1.20	0.27	7.64	0.20	1.50	0.12
D10	4/1/2017	6/30/2017	843	25.25	1.73	0.84	0.05	1.14	0.14	0.02	0.00	1.09	0.05
D10	7/1/2017	9/30/2017	758	35.50	6.33	1.71	0.23	1.08	0.28	0.00	NA	2.39	0.25

D10	10/1/2017	12/31/2017	1672	7.98	0.59	1.56	0.13	1.23	0.21	2.23	0.02	2.01	0.12
D10	1/1/2018	3/31/2018	1200	12.69	1.36	1.57	0.18	0.97	0.20	3.10	0.04	2.28	0.20
D11	4/1/2017	6/30/2017	297	8.61	0.20	2.00	0.05	1.24	0.07	0.01	0.00	1.15	0.02
D11	7/1/2017	9/30/2017	134	15.07	0.23	1.34	0.02	1.00	0.03	0.00	0.00	1.08	0.01
D11	10/1/2017	12/31/2017	240	4.04	0.02	1.03	0.01	1.02	0.01	1.87	0.00	0.97	0.00
D11	1/1/2018	3/31/2018	681	6.83	0.19	1.24	0.04	0.97	0.05	2.51	0.01	1.37	0.03
D12	10/1/2017	12/31/2017	124	8.88	0.39	2.29	0.11	0.98	0.09	23.39	0.80	1.42	0.05
D12	1/1/2018	3/31/2018	178	31.41	3.45	2.16	0.19	0.99	0.16	26.50	1.85	2.56	0.18
D13	4/1/2017	6/30/2017	1932	30.00	2.72	1.67	0.13	1.20	0.18	0.00	NA	2.16	0.12
D13	7/1/2017	9/30/2017	919	23.14	2.82	1.43	0.16	0.90	0.18	0.00	NA	1.50	0.12
D13	10/1/2017	12/31/2017	1699	8.86	0.57	1.80	0.13	1.17	0.17	1.92	0.01	1.73	0.09
D13	1/1/2018	3/31/2018	1649	6.12	0.24	1.17	0.05	0.95	0.07	1.19	0.00	1.47	0.05
D14	4/1/2017	6/30/2017	314	28.28	3.74	2.26	0.26	1.49	0.39	0.00	NA	2.24	0.19
D14	7/1/2017	9/30/2017	220	35.50	6.33	2.14	0.29	1.44	0.44	0.04	0.00	2.39	0.25
D14	10/1/2017	12/31/2017	461	10.83	0.62	1.19	0.07	1.03	0.12	3.40	0.03	1.53	0.07
D14	1/1/2018	3/31/2018	205	25.74	2.45	1.16	0.10	1.05	0.17	17.16	0.74	2.81	0.19
D15	1/1/2018	3/31/2018	342	14.70	1.10	1.41	0.11	0.96	0.13	7.99	0.15	1.74	0.10
D16	4/1/2017	6/30/2017	148	41.68	8.20	12.00	2.20	1.44	0.44	0.00	NA	2.99	0.33
D17	4/1/2017	6/30/2017	507	17.21	0.89	1.81	0.09	1.24	0.13	0.01	0.00	1.50	0.06
D17	7/1/2017	9/30/2017	352	30.87	1.96	1.70	0.09	1.10	0.11	0.01	0.00	1.84	0.07
D17	10/1/2017	12/31/2017	446	20.35	0.88	0.26	0.01	1.10	0.09	11.09	0.16	1.95	0.06
D17	1/1/2018	3/31/2018	370	15.80	1.25	0.00	NA	0.99	0.15	7.72	0.15	1.08	0.06
D18	3/1/2017	3/30/2017	263	25.74	2.45	3.56	0.31	1.35	0.25	5.73	0.09	1.87	0.12
D18	4/1/2017	6/30/2017	1046	13.29	0.47	0.64	0.02	1.30	0.10	0.01	0.00	1.00	0.03
D18	7/1/2017	9/30/2017	1105	57.11	14.07	1.43	0.19	1.08	0.28	0.00	NA	1.80	0.18
D18	10/1/2017	12/31/2017	810	10.25	0.60	1.29	0.08	1.13	0.14	3.05	0.02	1.42	0.07
D18	1/1/2018	3/31/2018	1764	19.54	1.48	1.26	0.09	0.95	0.12	2.01	0.01	1.64	0.09
D19	4/1/2017	6/30/2017	262	18.24	1.12	1.10	0.07	1.31	0.17	0.02	0.00	1.50	0.07
D19	7/1/2017	9/30/2017	421	50.71	8.16	3.37	0.33	1.03	0.18	0.00	NA	1.71	0.12
D19	10/1/2017	12/31/2017	347	12.76	0.61	1.19	0.06	0.95	0.09	10.40	0.17	1.13	0.04
D19	1/1/2018	3/31/2018	125	34.78	2.71	1.64	0.10	1.11	0.13	18.23	0.59	2.78	0.13
D20	4/1/2017	6/30/2017	1342	26.24	2.01	1.07	0.07	1.26	0.18	0.02	0.00	1.65	0.08
D20	7/1/2017	9/30/2017	271	55.55	6.70	1.21	0.08	0.90	0.11	0.02	0.00	2.25	0.12
D20	10/1/2017	12/31/2017	351	34.49	1.94	1.05	0.05	1.10	0.09	3.52	0.02	2.11	0.07
D20	1/1/2018	3/31/2018	660	39.92	3.74	0.91	0.06	0.90	0.10	8.53	0.15	1.76	0.09
A	3/9/2019	5/8/2019	46	4.01	0.20	1.32	0.08	1.17	0.13	5.59	0.06	0.71	0.03
A	5/8/2019	6/29/2019	119	8.40	1.23	2.25	0.37	1.01	0.31	1.67	0.02	1.05	0.12
A	6/29/2019	8/5/2019	14	2.28	0.11	1.28	0.07	1.06	0.11	1.86	0.01	1.22	0.05
A	8/5/2019	10/1/2019	69	8.43	1.02	1.57	0.21	1.04	0.26	2.75	0.04	0.90	0.09

A	10/1/2019	10/14/2019	49	4.46	0.42	1.36	0.15	1.08	0.22	1.46	0.01	0.95	0.07
A	10/14/2019	11/15/2019	35	15.80	1.96	3.08	0.40	1.08	0.26	2.51	0.03	5.06	0.65
A	11/15/2019	12/11/2019	50	2.95	0.14	1.35	0.07	1.07	0.11	1.44	0.01	1.06	0.04
A	12/11/2019	12/20/2019	50	2.34	0.33	1.89	0.31	1.03	0.30	1.42	0.02	0.75	0.08
A	12/20/2019	1/8/2020	61	1.65	0.04	1.14	0.03	1.04	0.06	1.34	0.00	0.53	0.01
A	1/8/2020	1/15/2020	84	1.80	0.07	1.05	0.05	1.05	0.09	1.00	0.00	0.58	0.02
A	1/15/2020	2/13/2020	22	2.89	0.07	1.22	0.03	1.03	0.05	1.35	0.00	1.00	0.02
A	2/13/2020	3/7/2020	72	2.70	0.06	1.03	0.03	1.07	0.05	1.01	0.00	0.98	0.02
A	3/7/2020	3/20/2020	99	2.24	0.33	1.96	0.34	1.08	0.35	1.61	0.02	0.94	0.11
A	3/20/2020	4/17/2020	116	3.60	0.32	1.58	0.16	1.02	0.19	1.45	0.01	1.06	0.08
A	11/6/2020	12/11/2020	18	3.29	0.05	1.27	0.02	0.95	0.03	1.19	0.00	1.05	0.01
A	12/11/2020	1/13/2021	47	3.73	0.14	1.20	0.05	0.95	0.07	1.49	0.01	1.09	0.03
A	1/13/2021	2/2/2021	145	3.17	0.30	1.32	0.14	0.95	0.18	1.03	0.01	1.06	0.08
A	2/2/2021	3/3/2021	55	3.63	0.10	1.13	0.03	0.94	0.05	1.05	0.00	1.05	0.02
A	3/3/2021	3/16/2021	134	5.15	0.68	1.56	0.24	0.95	0.26	1.24	0.02	1.08	0.12
A	3/16/2021	3/31/2021	30	2.67	0.06	1.19	0.03	0.98	0.04	1.00	0.00	1.02	0.02
A	3/31/2021	6/11/2021	44	5.42	0.13	1.39	0.04	0.97	0.05	1.30	0.00	1.28	0.02
A	6/11/2021	8/4/2021	21	5.38	0.10	1.04	0.02	1.06	0.04	1.51	0.00	1.11	0.02
DOH	4/9/2018	6/27/2018	286	0.62	0.02	1.33	0.06	0.99	0.08	1.22	0.00	0.60	0.02
DOH	6/27/2018	8/21/2018	53	0.56	0.01	1.00	0.03	1.00	0.05	1.65	0.00	0.72	0.01
DOH	8/21/2018	8/28/2018	214	0.64	0.03	1.07	0.05	0.95	0.08	1.25	0.00	0.71	0.02
DOH	11/26/2018	12/13/2018	98	0.93	0.04	1.12	0.05	0.99	0.09	1.10	0.00	0.92	0.03
DOH	12/13/2018	1/24/2019	36	0.87	0.02	1.18	0.04	1.25	0.08	1.69	0.00	0.97	0.02
DOH	1/24/2019	2/14/2019	104	1.04	0.03	1.14	0.04	1.01	0.07	1.65	0.01	0.92	0.03
DOH	2/14/2019	3/31/2019	41	1.28	0.02	1.19	0.02	0.98	0.03	2.30	0.00	1.06	0.01
DOH	3/31/2019	5/8/2019	69	1.50	0.05	1.39	0.05	1.03	0.07	4.06	0.02	0.79	0.02
DOH	5/8/2019	6/28/2019	98	3.97	0.27	2.34	0.18	1.07	0.16	3.30	0.03	1.17	0.06
DOH	6/28/2019	8/5/2019	34	2.20	0.05	1.26	0.03	1.01	0.05	2.87	0.01	1.12	0.02
DOH	8/5/2019	9/9/2019	36	2.89	0.09	1.40	0.05	1.01	0.06	4.72	0.03	1.62	0.04
DOH	9/9/2019	10/1/2019	64	2.18	0.15	1.41	0.11	1.06	0.16	2.13	0.02	0.87	0.05
DOH	10/1/2019	10/14/2019	87	2.34	0.23	1.55	0.17	1.11	0.24	1.53	0.01	1.00	0.08
DOH	10/14/2019	11/15/2019	16	3.13	0.09	1.72	0.06	1.02	0.06	6.77	0.05	1.00	0.02
DOH	11/15/2019	12/11/2019	69	1.38	0.03	0.00	NA	1.05	0.06	4.64	0.02	0.95	0.02
DOH	12/11/2019	12/20/2019	41	1.35	0.07	1.57	0.09	1.09	0.12	1.75	0.01	0.43	0.02
DOH	12/20/2019	1/8/2020	144	1.15	0.03	1.14	0.04	1.03	0.07	2.27	0.01	0.37	0.01
DOH	1/8/2020	1/15/2020	176	1.02	0.04	1.10	0.05	1.04	0.09	1.10	0.00	0.33	0.01
DOH	1/15/2020	2/13/2020	40	2.04	0.05	1.13	0.03	1.00	0.06	3.12	0.01	0.99	0.02
DOH	2/13/2020	3/6/2020	61	1.29	0.03	1.01	0.03	1.04	0.05	1.22	0.00	0.97	0.02
DOH	3/6/2020	3/20/2020	119	1.45	0.15	1.86	0.22	1.11	0.25	1.97	0.02	1.06	0.09

DOH	3/20/2020	4/17/2020	121	1.24	0.07	0.75	0.05	1.08	0.14	3.86	0.04	0.94	0.05
DOH	4/17/2020	6/10/2020	58	3.11	0.10	NA	NA	1.11	0.08	15.02	0.25	1.26	0.03
DOH	7/24/2020	10/2/2020	19	1.97	0.05	1.01	0.03	0.97	0.05	2.58	0.01	0.98	0.02
DOH	10/2/2020	11/6/2020	87	4.52	0.50	3.50	0.45	1.04	0.24	7.92	0.24	1.14	0.10
DOH	11/6/2020	12/11/2020	18	2.60	0.05	1.15	0.02	0.91	0.03	4.17	0.01	0.97	0.01
DOH	12/11/2020	1/13/2021	47	1.12	0.05	0.62	0.03	0.99	0.09	2.09	0.01	0.97	0.03
DOH	1/13/2021	2/2/2021	145	1.37	0.08	0.98	0.06	0.98	0.11	1.77	0.01	0.99	0.04
DOH	2/2/2021	3/3/2021	55	4.20	0.11	1.08	0.03	0.96	0.05	2.47	0.01	1.02	0.02
DOH	3/3/2021	3/16/2021	134	4.59	0.48	1.51	0.18	1.06	0.24	3.67	0.06	1.15	0.10
DOH	3/16/2021	3/31/2021	29	3.80	0.14	0.20	0.01	1.12	0.09	12.44	0.20	1.09	0.03
DOH	3/31/2021	6/11/2021	44	21.62	0.54	4.47	0.11	1.13	0.05	33.53	0.79	1.90	0.03
DOH	6/11/2021	8/4/2021	21	17.52	0.63	NA	NA	1.26	0.09	11.10	0.13	1.36	0.04
WU	5/1/2019	6/28/2019	154	2.40	0.30	2.01	0.29	1.07	0.29	1.37	0.02	1.15	0.12
WU	6/28/2019	8/5/2019	63	2.28	0.11	1.28	0.07	1.06	0.11	1.86	0.01	1.22	0.05
WU	8/5/2019	9/9/2019	93	1.82	0.14	1.39	0.12	1.10	0.18	1.19	0.01	1.17	0.07
WU	9/9/2019	10/1/2019	98	2.23	0.31	1.70	0.27	1.11	0.34	1.09	0.01	1.07	0.12
WU	10/1/2019	10/14/2019	127	1.20	0.18	1.46	0.25	1.15	0.39	1.18	0.02	1.15	0.14
WU	10/14/2019	11/15/2019	37	2.34	0.13	1.68	0.11	1.04	0.13	1.48	0.01	0.75	0.03
WU	11/15/2019	12/11/2019	84	1.40	0.05	1.20	0.05	1.05	0.08	1.65	0.01	1.08	0.03
WU	12/11/2019	12/20/2019	64	1.83	0.12	1.52	0.12	1.05	0.15	1.21	0.01	0.59	0.03
WU	12/20/2019	1/8/2020	188	1.25	0.05	1.09	0.05	1.03	0.08	1.43	0.01	0.40	0.01
WU	1/8/2020	1/15/2020	167	1.11	0.04	0.99	0.04	1.01	0.07	1.17	0.00	0.36	0.01
WU	1/15/2020	2/13/2020	56	1.59	0.07	1.15	0.06	1.05	0.10	1.29	0.01	1.06	0.04
WU	2/13/2020	3/6/2020	105	1.24	0.05	1.11	0.05	1.05	0.09	1.18	0.00	1.10	0.04
WU	3/6/2020	3/20/2020	112	1.64	0.19	1.47	0.19	1.10	0.28	1.16	0.01	0.99	0.09
WU	3/20/2020	4/17/2020	175	1.58	0.14	1.31	0.14	1.00	0.19	1.12	0.01	1.06	0.08
WU	4/17/2020	6/10/2020	107	1.45	0.10	1.40	0.11	0.98	0.14	1.37	0.01	1.02	0.06
WU	7/24/2020	10/2/2020	130	1.47	0.09	1.29	0.09	0.95	0.12	1.49	0.01	0.96	0.05
WU	10/2/2020	11/6/2020	117	2.50	0.56	2.89	0.76	0.99	0.47	2.27	0.06	0.97	0.18
WU	11/6/2020	12/11/2020	110	1.35	0.07	0.93	0.05	0.95	0.10	2.20	0.01	1.07	0.04
WU	12/11/2020	1/13/2021	139	1.19	0.07	1.05	0.07	0.96	0.12	1.31	0.01	1.03	0.05
WU	1/13/2021	2/3/2021	174	1.21	0.07	1.18	0.07	0.93	0.10	1.14	0.01	0.95	0.04
WU	2/3/2021	3/3/2021	135	1.19	0.05	1.12	0.05	0.94	0.08	1.00	0.00	1.02	0.03
WU	3/3/2021	3/16/2021	197	3.35	0.52	1.40	0.25	0.95	0.30	1.33	0.02	1.07	0.14
WU	3/16/2021	3/31/2021	90	1.09	0.06	1.29	0.08	0.95	0.10	0.98	0.00	0.98	0.04
WU	3/31/2021	6/11/2021	161	2.61	0.15	1.34	0.09	0.98	0.12	1.48	0.01	1.06	0.05
WU	6/11/2021	8/4/2021	114	2.57	0.16	1.27	0.09	1.07	0.14	1.28	0.01	1.07	0.05

**APPENDIX A: CHAPTER 2 SUPPLEMENTARY MATERIAL**  
**TAB A.5. NON-SEA SALT MAJOR ION CONCENTRATIONS**

Note: cells highlighted red are those for which the sea-salt aerosol correction calculations produced negative non-sea salt values that fell out of the propagated non-sea salt uncertainty range.

Collector	From Date	To Date	Non-Sea Salt Bulk Concentration ( $\mu\text{M}$ )				
			$\text{SO}_4^{2-}$	$\text{Na}^+$	$\text{K}^+$	$\text{Mg}^{2+}$	$\text{Ca}^{2+}$
K1	12/19/2018	3/18/2019	2.82	57.23	4.53	0.77	4.54
K1	3/18/2019	7/12/2019	7.53	9.53	13.21	-2.51	8.00
K1	7/12/2019	10/12/2019	-3.64	4.91	32.64	3.91	17.90
K1	10/12/2019	1/5/2020	-1.63	69.19	4.65	1.61	9.60
K1	1/5/2020	3/28/2020	-7.22	63.21	3.31	3.25	10.81
K1	3/28/2020	5/2/2020	-4.05	63.48	10.44	4.91	15.23
K1	5/2/2020	6/20/2020	-7.53	-8.86	21.92	9.60	54.88
K1	6/20/2020	9/19/2020	-15.60	-16.21	24.20	8.03	72.39
K1	9/19/2020	1/4/2021	-3.67	-11.12	23.12	4.80	37.07
K1	1/4/2021	3/13/2021	-0.61	-0.89	8.22	1.15	9.09
K1	3/13/2021	4/21/2021	0.66	-2.37	2.72	4.29	30.64
K2	7/12/2019	10/12/2019	3.72	5.48	33.13	2.17	22.63
K2	10/12/2019	1/5/2020	-1.38	86.23	5.55	-2.21	2.96
K2	1/5/2020	3/28/2020	0.45	60.49	2.10	1.61	12.09
K2	3/28/2020	5/2/2020	-6.19	80.18	16.49	5.17	63.58
K2	5/2/2020	6/20/2020	-8.68	-8.88	21.74	13.19	186.20
K2	6/20/2020	9/19/2020	-4.80	-8.16	8.32	4.02	132.18
K2	9/19/2020	1/4/2021	-5.10	-10.89	11.86	1.90	94.19
K2	1/4/2021	3/13/2021	1.72	-2.67	2.04	0.50	48.72
K2	3/13/2021	4/21/2021	-4.61	-2.22	1.31	1.60	161.49
K3	7/12/2019	10/12/2019	2.43	10.81	7.00	0.76	11.10
K3	10/12/2019	1/5/2020	-2.40	82.31	10.28	-0.02	5.09
K3	1/5/2020	3/28/2020	1.26	61.28	13.60	3.52	18.35
K3	3/28/2020	5/2/2020	-4.36	66.90	10.72	6.28	15.50
K3	5/2/2020	6/20/2020	-6.77	4.10	23.75	7.82	29.22
K3	6/20/2020	9/19/2020	-9.16	2.19	43.04	13.19	47.80
K3	9/19/2020	1/4/2021	-5.28	10.99	20.74	8.97	35.25
K3	1/4/2021	3/13/2021	-6.39	11.27	14.94	-0.10	20.12
K3	3/13/2021	4/21/2021	-4.84	-0.44	8.12	-0.89	15.45
KS	12/19/2018	3/18/2019	0.78	61.86	9.10	2.44	3.97
KS	3/18/2019	7/12/2019	5.22	14.07	7.05	0.79	6.94

KS	7/12/2019	10/12/2019	-1.92	6.94	3.25	-0.54	11.68
KS	10/12/2019	1/5/2020	0.29	83.74	2.44	-0.85	4.93
KS	1/5/2020	3/28/2020	-2.35	61.43	1.82	0.24	11.82
KS	3/28/2020	5/2/2020	-1.57	69.89	3.72	1.36	11.15
KS	5/2/2020	6/20/2020	-4.45	-12.32	46.76	-2.96	27.71
KS	6/20/2020	9/19/2020	-6.26	-14.39	17.80	5.90	18.67
KS	9/19/2020	1/4/2021	-3.88	-6.19	-0.72	0.92	18.54
KS	1/4/2021	3/13/2021	0.60	-2.65	0.54	0.37	8.80
KS	3/13/2021	4/21/2021	-0.99	-3.55	-0.05	0.89	14.47
MT1	5/10/2019	7/11/2019	15.43	13.82	42.77	34.51	69.88
MT1	7/11/2019	9/29/2019	-8.89	18.61	7.84	12.80	93.57
MT1	9/29/2019	1/9/2020	-2.80	59.09	9.09	6.25	18.98
MT1	1/9/2020	3/31/2020	-1.28	45.48	3.36	3.23	20.89
MT1	6/15/2020	9/17/2020	-12.47	-9.77	7.50	4.89	91.50
MT1	9/17/2020	12/30/2020	3.21	-5.16	4.77	12.45	57.87
MT1	12/30/2020	3/27/2021	0.73	-3.50	0.89	11.79	32.89
MT1	3/27/2021	4/29/2021	-4.01	-2.68	20.90	37.75	144.60
MT2	5/10/2019	7/11/2019	11.29	37.54	10.46	11.31	48.11
MT2	7/11/2019	9/25/2019	1.44	7.64	2.33	7.62	41.27
MT2	9/25/2019	1/7/2020	2.74	60.46	0.74	7.07	13.35
MT2	1/7/2020	3/31/2020	1.78	61.58	1.97	4.89	9.53
MT2	6/15/2020	9/17/2020	-9.54	-3.68	0.95	1.77	27.70
MT2	9/17/2020	12/22/2020	-5.36	-7.78	1.72	0.57	17.23
MT2	12/22/2020	3/27/2021	-0.63	-3.17	0.26	0.89	8.32
MT2	3/27/2021	4/29/2021	2.26	-3.98	4.58	5.04	23.29
MT3	5/10/2019	7/11/2019	3.70	10.29	2.55	32.61	69.91
MT3	7/11/2019	9/25/2019	0.89	28.88	4.23	4.81	41.40
MT3	9/25/2019	1/7/2020	3.18	58.44	1.15	1.06	13.68
MT3	1/7/2020	3/31/2020	-0.97	71.91	0.76	-0.86	13.31
MT3	6/11/2020	9/17/2020	-6.36	-5.56	3.19	0.69	91.24
MT3	9/17/2020	12/22/2020	-0.71	-6.12	1.00	-0.07	25.26
MT3	12/22/2020	3/27/2021	0.58	-4.37	2.00	0.71	10.76
MT3	3/27/2021	4/26/2021	-3.40	-1.62	13.38	0.72	29.63
MTS	7/11/2019	9/25/2019	-4.05	17.16	10.95	-13.08	15.79
MTS	9/25/2019	1/7/2020	-3.90	92.60	7.71	-8.55	5.13
MTS	1/7/2020	3/31/2020	-0.07	73.83	3.26	2.97	15.75
MTS	6/11/2020	9/17/2020	-11.90	-14.92	4.77	0.31	128.25
MTS	9/17/2020	12/22/2020	-1.74	-5.19	15.21	2.32	79.53
MTS	12/22/2020	4/26/2021	-0.08	-2.41	3.43	-0.22	26.11
EB	7/13/2019	9/27/2019	7.06	31.49	2.39	1.47	61.25
EB	9/27/2019	1/9/2020	5.76	57.71	2.94	1.63	80.26

EB	1/10/2020	3/31/2020	-2.02	67.13	1.15	5.17	128.45
EB	3/31/2020	6/23/2020	-6.99	-13.89	5.76	13.17	241.71
EB	6/23/2020	10/16/2020	-13.91	-51.96	9.70	36.30	984.91
EB	10/16/2020	1/19/2021	0.90	-18.53	0.28	13.64	312.00
EB	1/19/2021	4/7/2021	2.26	0.65	4.04	5.62	99.32
EB	4/7/2021	5/6/2021	-8.59	-3.58	6.68	7.68	144.32
TR	7/26/2019	10/19/2019	1.92	16.83	4.49	-6.92	20.25
TR	10/19/2019	1/9/2020	1.93	68.36	4.59	1.04	9.59
TR	1/9/2020	3/15/2020	2.46	56.04	2.80	0.48	35.33
TR	3/15/2020	5/4/2020	1.66	93.79	4.32	-0.03	19.26
TR	5/4/2020	6/20/2020	-8.60	-10.41	3.91	1.17	71.78
TR	6/20/2020	10/12/2020	-11.55	-6.68	12.46	1.69	108.55
TR	1/20/2021	2/1/2021	-0.79	2.18	1.85	-1.77	0.65
TR	2/1/2021	2/17/2021	0.51	0.02	10.13	0.78	6.73
TR	2/17/2021	3/2/2021	-0.21	-4.25	2.24	-2.17	-0.43
TR	3/2/2021	3/17/2021	0.98	-3.17	1.93	-1.20	1.43
TR	3/17/2021	4/7/2021	2.45	-8.15	6.38	-1.19	4.13
TR	4/7/2021	4/29/2021	2.93	-8.19	10.23	1.19	9.83
EB	8/5/2019	8/7/2019	6.36	37.38	13.00	0.80	22.71
MHS	10/18/2019	1/9/2020	7.02	58.10	11.42	1.04	38.73
M	10/23/2019	1/9/2020	11.21	41.72	8.24	5.95	83.10
M	1/9/2020	3/25/2020	6.31	58.44	6.26	1.06	28.65
M	3/25/2020	6/23/2020	24.95	13.23	11.57	-0.75	171.60
M	6/23/2020	10/12/2020	11.84	-18.63	3.32	5.39	310.96
M	10/12/2020	1/19/2021	5.02	-9.03	-0.41	3.10	120.15
M	1/19/2021	2/8/2021	4.82	1.61	0.70	-0.45	1.71
M	2/8/2021	3/2/2021	13.43	4.88	2.24	-2.54	50.57
M	3/2/2021	3/17/2021	5.88	-3.56	0.46	-0.40	2.97
M	3/17/2021	4/7/2021	9.47	-2.30	0.69	-0.69	3.98
M	4/7/2021	5/3/2021	12.87	0.56	16.91	4.77	42.25
PW	10/31/2019	1/29/2020	4.32	73.64	1.75	3.79	11.82
KK	2/16/2020	4/24/2020	4.03	33.40	12.11	4.63	36.83
KK	4/24/2020	6/20/2020	-14.69	-126.04	98.93	10.13	44.79
KK	6/20/2020	10/10/2020	-9.84	-53.19	52.47	6.76	105.92
KK	10/10/2020	1/2/2021	-11.65	-82.33	66.13	24.53	57.87
KK	1/2/2021	4/3/2021	0.96	-21.17	14.91	23.03	105.95
KK	4/3/2021	4/25/2021	-5.59	-17.15	24.97	22.39	153.15
SB	2/16/2020	4/24/2020	4.61	73.54	4.65	1.61	17.08
SB	4/24/2020	6/20/2020	6.01	-20.69	56.77	26.93	84.45
SB	6/20/2020	10/10/2020	-10.79	-13.21	16.84	1.88	157.73
SB	10/10/2020	1/11/2021	-9.77	-52.80	38.46	13.26	109.20

WAAF	2/16/2020	4/26/2020	4.42	49.69	38.16	6.51	39.89
WAAF	4/26/2020	6/20/2020	-34.88	-124.83	271.29	-10.60	61.10
WAAF	6/20/2020	10/10/2020	-33.19	-172.40	797.01	17.68	132.08
WAAF	10/10/2020	1/11/2021	-5.26	-24.22	86.64	29.74	60.66
WAAF	1/11/2021	4/3/2021	2.05	-16.26	24.07	18.54	51.30
ER	2/16/2020	3/15/2020	3.63	16.74	55.86	-11.66	19.90
ER	3/15/2020	4/25/2020	7.35	71.48	6.26	1.06	23.66
ER	4/25/2020	6/20/2020	-12.77	-12.41	4.44	0.68	158.15
ER	10/12/2020	1/11/2021	-2.68	-11.01	2.81	-0.89	90.66
ER	1/11/2021	4/3/2021	-5.57	-8.30	1.59	-0.26	47.32
D1	10/1/2017	12/31/2017	8.14	-1.39	10.44	-4.17	20.30
D1	1/1/2018	3/31/2018	5.94	-12.81	15.19	-1.42	17.43
MT1	4/1/2017	6/30/2017	15.16	81.33	-6.14	27.36	105.22
MT1	7/1/2017	9/30/2017	15.16	81.33	-6.14	27.36	5.23
MT1	10/1/2017	12/31/2017	6.03	-19.96	-4.47	2.70	180.92
MT1	1/1/2018	3/31/2018	7.17	33.57	9.66	5.14	29.52
D4	10/1/2017	12/31/2017	3.66	105.30	126.56	8.29	39.16
D4	1/1/2018	3/31/2018	-3.96	-13.36	111.77	24.36	86.65
D6	4/1/2017	6/30/2017	17.26	124.83	-6.04	27.36	109.32
D6	7/1/2017	9/30/2017	0.83	23.54	-4.47	6.80	139.72
D6	10/1/2017	12/31/2017	3.84	13.29	4.89	2.68	42.33
D6	1/1/2018	3/31/2018	2.53	-12.94	12.09	12.51	56.85
D7	4/1/2017	6/30/2017	18.27	143.40	-11.63	20.48	268.59
D7	7/1/2017	9/30/2017	12.72	85.00	-14.98	16.29	512.17
D7	10/1/2017	12/31/2017	9.64	54.03	12.62	10.65	44.88
D7	1/1/2018	3/31/2018	4.03	-9.08	1.28	1.29	13.87
D8	4/1/2017	6/30/2017	4.75	72.01	-3.35	12.30	83.20
D9	4/1/2017	6/30/2017	7.49	91.27	-3.91	21.85	152.66
D9	7/1/2017	9/30/2017	-7.29	9.33	-2.79	10.96	145.42
D9	10/1/2017	12/31/2017	8.42	41.44	10.94	7.36	30.74
D9	1/1/2018	3/31/2018	2.50	-9.78	8.16	10.09	50.48
D10	3/1/2017	3/30/2017	9.95	28.51	22.25	8.20	66.70
D10	4/1/2017	6/30/2017	-2.54	37.83	-6.04	2.66	142.22
D10	7/1/2017	9/30/2017	5.21	9.33	-2.79	19.16	91.93
D10	10/1/2017	12/31/2017	6.74	44.83	5.62	22.76	30.53
D10	1/1/2018	3/31/2018	4.90	-3.80	6.91	20.78	36.75
D11	4/1/2017	6/30/2017	38.08	152.73	-14.42	10.84	105.43
D11	7/1/2017	9/30/2017	21.58	1.47	-23.92	9.41	322.65
D11	10/1/2017	12/31/2017	4.62	57.09	51.18	-9.60	170.94
D11	1/1/2018	3/31/2018	7.66	-17.63	18.47	22.10	68.12
D12	10/1/2017	12/31/2017	25.82	-5.95	171.34	15.84	57.59

D12	1/1/2018	3/31/2018	12.81	-1.55	108.25	32.61	123.24
D13	4/1/2017	6/30/2017	8.77	42.81	-5.03	28.76	139.19
D13	7/1/2017	9/30/2017	3.75	-14.99	-3.35	8.20	70.86
D13	10/1/2017	12/31/2017	11.14	39.39	4.89	19.18	39.83
D13	1/1/2018	3/31/2018	3.68	-18.61	1.65	19.65	41.74
D14	4/1/2017	6/30/2017	11.05	72.01	-3.35	20.50	87.30
D14	7/1/2017	9/30/2017	8.31	52.83	-2.69	19.16	91.93
D14	10/1/2017	12/31/2017	2.95	7.85	14.47	15.61	56.64
D14	1/1/2018	3/31/2018	1.83	10.44	72.23	39.70	105.52
D15	1/1/2018	3/31/2018	5.16	-8.38	33.60	17.46	62.81
D16	4/1/2017	6/30/2017	80.21	52.83	-2.79	27.36	108.42
D17	4/1/2017	6/30/2017	15.44	76.37	-7.16	17.77	112.36
D17	7/1/2017	9/30/2017	13.34	32.87	-7.16	30.07	207.06
D17	10/1/2017	12/31/2017	-17.28	40.27	90.71	42.14	166.10
D17	1/1/2018	3/31/2018	-12.10	-1.08	31.16	1.89	65.48
D18	3/1/2017	3/30/2017	29.93	67.04	21.13	19.10	105.52
D18	4/1/2017	6/30/2017	-9.56	129.10	-9.96	-0.07	117.99
D18	7/1/2017	9/30/2017	3.11	9.33	-2.79	10.96	149.52
D18	10/1/2017	12/31/2017	4.48	32.55	12.03	12.24	51.80
D18	1/1/2018	3/31/2018	3.43	-11.80	5.12	16.09	89.95
D19	4/1/2017	6/30/2017	1.66	81.33	-6.04	15.06	101.12
D19	7/1/2017	9/30/2017	24.19	4.27	-3.91	13.65	185.56
D19	10/1/2017	12/31/2017	3.65	-15.53	69.33	4.82	82.76
D19	1/1/2018	3/31/2018	10.62	30.53	108.78	55.33	203.56
D20	4/1/2017	6/30/2017	1.01	62.07	-5.49	17.81	134.56
D20	7/1/2017	9/30/2017	3.11	-24.93	-5.49	34.21	290.86
D20	10/1/2017	12/31/2017	1.14	39.39	21.99	47.61	278.57
D20	1/1/2018	3/31/2018	-1.38	-25.44	42.90	21.37	211.65
A	3/9/2019	5/8/2019	5.59	48.90	30.24	-9.38	18.91
A	5/8/2019	6/29/2019	7.52	1.48	1.54	0.61	16.26
A	6/29/2019	8/5/2019	4.96	19.38	5.92	7.35	8.41
A	8/5/2019	10/1/2019	4.16	4.94	4.88	-1.40	19.79
A	10/1/2019	10/14/2019	3.30	12.58	1.60	-0.86	11.61
A	10/14/2019	11/15/2019	16.11	10.72	4.46	59.07	41.83
A	11/15/2019	12/11/2019	6.46	22.74	3.14	2.13	13.19
A	12/11/2019	12/20/2019	5.43	2.58	0.97	-2.90	3.00
A	12/20/2019	1/8/2020	4.79	20.50	4.43	-30.01	8.09
A	1/8/2020	1/15/2020	1.19	16.76	0.01	-17.63	6.42
A	1/15/2020	2/13/2020	7.75	17.61	4.75	0.28	24.63
A	2/13/2020	3/7/2020	0.96	43.12	0.16	-1.42	23.41
A	3/7/2020	3/20/2020	5.56	7.29	1.36	-0.63	2.62

A	3/20/2020	4/17/2020	5.65	3.08	1.67	1.14	9.19
A	11/6/2020	12/11/2020	16.10	-46.50	4.25	6.01	50.04
A	12/11/2020	1/13/2021	4.41	-19.90	4.23	3.98	22.27
A	1/13/2021	2/2/2021	2.91	-6.99	0.11	1.04	7.17
A	2/2/2021	3/3/2021	4.34	-31.38	0.59	2.93	31.28
A	3/3/2021	3/16/2021	3.61	-5.65	0.58	0.93	9.86
A	3/16/2021	3/31/2021	7.69	-16.07	0.00	1.80	24.51
A	3/31/2021	6/11/2021	14.67	-19.27	4.35	19.67	60.44
A	6/11/2021	8/4/2021	2.10	45.54	9.14	9.48	75.16
DOH	4/9/2018	6/27/2018	7.27	-2.57	1.85	-16.53	-3.01
DOH	6/27/2018	8/21/2018	-0.02	2.96	9.06	-19.33	-5.84
DOH	8/21/2018	8/28/2018	1.46	-17.05	2.02	-11.60	-2.85
DOH	11/26/2018	12/13/2018	2.53	-4.93	0.82	-2.98	-0.53
DOH	12/13/2018	1/24/2019	5.75	133.39	8.45	-1.54	-1.48
DOH	1/24/2019	2/14/2019	3.56	5.85	6.35	-3.99	0.42
DOH	2/14/2019	3/31/2019	10.02	-14.74	25.90	5.44	5.22
DOH	3/31/2019	5/8/2019	10.96	12.57	33.15	-11.34	5.13
DOH	5/8/2019	6/28/2019	17.04	15.45	11.23	3.98	13.81
DOH	6/28/2019	8/5/2019	9.66	8.25	26.68	8.10	16.34
DOH	8/5/2019	9/9/2019	11.27	3.87	40.31	33.08	19.60
DOH	9/9/2019	10/1/2019	5.16	13.37	5.43	-3.06	5.39
DOH	10/1/2019	10/14/2019	4.78	15.50	1.77	-0.03	4.29
DOH	10/14/2019	11/15/2019	21.42	12.00	66.04	0.04	23.25
DOH	11/15/2019	12/11/2019	-34.56	30.12	48.14	-3.42	4.83
DOH	12/11/2019	12/20/2019	9.75	27.15	4.92	-18.43	2.19
DOH	12/20/2019	1/8/2020	3.90	12.07	13.86	-34.11	1.53
DOH	1/8/2020	1/15/2020	2.04	13.47	0.73	-25.58	0.13
DOH	1/15/2020	2/13/2020	4.06	0.05	26.08	-0.74	12.23
DOH	2/13/2020	3/6/2020	0.38	23.44	3.00	-2.02	3.71
DOH	3/6/2020	3/20/2020	7.25	14.89	3.14	0.91	1.39
DOH	3/20/2020	4/17/2020	-3.63	18.11	15.73	-1.54	1.24
DOH	4/17/2020	6/10/2020	NA	49.33	143.71	12.93	20.66
DOH	7/24/2020	10/2/2020	0.16	-17.30	19.24	-1.27	11.29
DOH	10/2/2020	11/6/2020	19.63	5.30	20.79	2.09	10.10
DOH	11/6/2020	12/11/2020	7.30	-67.99	58.32	-2.97	28.08
DOH	12/11/2020	1/13/2021	-7.32	-1.77	8.13	-0.94	0.85
DOH	1/13/2021	2/2/2021	-0.38	-4.90	4.56	-0.36	2.07
DOH	2/2/2021	3/3/2021	2.66	-22.29	17.65	0.93	36.68
DOH	3/3/2021	3/16/2021	4.21	7.56	8.38	2.28	10.73
DOH	3/16/2021	3/31/2021	-18.34	46.04	99.96	3.89	23.35
DOH	3/31/2021	6/11/2021	143.35	87.72	514.86	70.22	311.49

DOH	6/11/2021	8/4/2021	NA	115.81	105.19	18.31	164.21
WU	5/1/2019	6/28/2019	6.90	7.67	0.96	1.92	3.49
WU	6/28/2019	8/5/2019	4.96	19.38	5.92	7.35	8.41
WU	8/5/2019	9/9/2019	4.39	17.79	0.82	3.52	3.38
WU	9/9/2019	10/1/2019	4.28	11.28	0.21	0.80	2.75
WU	10/1/2019	10/14/2019	2.64	14.21	0.38	1.63	0.42
WU	10/14/2019	11/15/2019	10.10	9.38	2.74	-7.04	7.28
WU	11/15/2019	12/11/2019	4.79	21.46	6.02	3.48	3.58
WU	12/11/2019	12/20/2019	6.57	10.95	1.02	-9.91	3.84
WU	12/20/2019	1/8/2020	2.00	9.49	3.68	-25.44	2.02
WU	1/8/2020	1/15/2020	-0.35	5.99	1.62	-29.71	1.02
WU	1/15/2020	2/13/2020	3.08	15.64	2.26	2.39	4.37
WU	2/13/2020	3/6/2020	2.42	17.82	1.53	4.15	1.92
WU	3/6/2020	3/20/2020	3.53	12.43	0.45	-0.13	1.75
WU	3/20/2020	4/17/2020	2.90	-0.78	0.45	1.03	2.02
WU	4/17/2020	6/10/2020	5.11	-4.28	1.79	0.37	2.10
WU	7/24/2020	10/2/2020	3.90	-11.28	2.51	-1.12	2.31
WU	10/2/2020	11/6/2020	7.21	-0.44	1.86	-0.21	2.09
WU	11/6/2020	12/11/2020	-1.29	-13.37	8.08	2.16	2.28
WU	12/11/2020	1/13/2021	0.69	-9.83	1.63	0.78	0.95
WU	1/13/2021	2/3/2021	2.82	-18.31	0.86	-1.40	1.21
WU	2/3/2021	3/3/2021	2.37	-21.55	0.03	0.61	1.44
WU	3/3/2021	3/16/2021	2.20	-4.40	0.70	0.75	4.73
WU	3/16/2021	3/31/2021	4.70	-14.42	-0.12	-0.74	0.52
WU	3/31/2021	6/11/2021	5.10	-3.91	2.74	1.57	8.78
WU	6/11/2021	8/4/2021	3.82	15.95	1.51	1.84	8.07

**APPENDIX A: CHAPTER 2 SUPPLEMENTARY MATERIAL**

**TAB A.6. MAJOR ION RAW DATA**

Collector	From Date	To Date	Precipitation (mm)	Bulk Concentration ( $\mu\text{M}$ )								
				F <sup>-</sup>	Cl <sup>-</sup>	Br <sup>-</sup>	SO <sub>4</sub> <sup>2-</sup>	Li <sup>+</sup>	Na <sup>+</sup>	K <sup>+</sup>	Mg <sup>2+</sup>	Ca <sup>2+</sup>
K1	12/19/2018	3/18/2019	461	NA	287.73	NA	17.70	0.00	304.48	10.23	28.79	9.98
K1	3/18/2019	7/12/2019	541	NA	236.95	0.75	19.78	NA	213.14	17.90	20.57	12.48
K1	7/12/2019	10/12/2019	181	NA	82.37	NA	0.62	0.00	75.69	34.27	11.93	19.46
K1	10/12/2019	1/5/2020	504	NA	152.33	NA	6.25	0.00	200.09	7.67	16.45	12.48
K1	1/5/2020	3/28/2020	673	NA	220.03	NA	4.16	0.00	252.28	7.67	24.68	14.97
K1	3/28/2020	5/2/2020	26	NA	118.48	NA	2.08	0.00	165.29	12.79	16.45	17.47
K1	5/2/2020	6/20/2020	31	NA	171.79	NA	1.35	NA	138.76	25.32	26.33	58.13
K1	6/20/2020	9/19/2020	43	0.53	301.83	NA	0.00	NA	243.15	30.18	37.43	78.09
K1	9/19/2020	1/4/2021	222	NA	111.14	NA	2.08	NA	84.38	25.32	15.63	39.17
K1	1/4/2021	3/13/2021	516	NA	152.89	NA	7.29	NA	130.49	11.25	16.04	11.98
K1	3/13/2021	4/21/2021	270	NA	108.04	NA	6.25	NA	90.47	4.86	14.81	32.68
K2	7/12/2019	10/12/2019	198	NA	83.22	NA	8.02	0.00	76.99	34.78	10.28	24.20
K2	10/12/2019	1/5/2020	366	NA	107.19	NA	4.16	0.00	178.34	7.67	8.23	4.99
K2	1/5/2020	3/28/2020	540	NA	152.33	NA	8.33	0.00	191.39	5.12	16.45	14.97
K2	3/28/2020	5/2/2020	85	NA	200.28	NA	4.16	0.00	252.28	20.46	24.68	67.37
K2	5/2/2020	6/20/2020	35	NA	194.08	NA	1.35	NA	157.89	25.58	32.09	189.87
K2	6/20/2020	9/19/2020	99	NA	161.35	NA	3.54	0.00	130.49	11.51	19.74	135.23
K2	9/19/2020	1/4/2021	246	NA	98.73	NA	0.00	0.00	73.95	13.81	11.52	96.06
K2	1/4/2021	3/13/2021	539	NA	168.12	NA	10.41	0.00	141.80	5.37	16.87	51.90
K2	3/13/2021	4/21/2021	309	NA	89.14	NA	0.00	0.00	74.38	3.07	10.28	163.17
K3	7/12/2019	10/12/2019	264	NA	59.80	NA	5.52	0.00	62.20	8.18	6.58	12.23
K3	10/12/2019	1/5/2020	410	NA	126.94	NA	4.16	0.00	191.39	12.79	12.34	7.49
K3	1/5/2020	3/28/2020	619	NA	217.21	NA	12.49	0.00	247.93	17.90	24.68	22.46
K3	3/28/2020	5/2/2020	90	NA	104.37	NA	1.04	0.00	156.59	12.79	16.45	17.47
K3	5/2/2020	6/20/2020	94	NA	130.89	NA	0.00	NA	116.57	26.34	20.57	31.69
K3	6/20/2020	9/19/2020	153	NA	177.15	NA	0.00	NA	154.41	46.55	30.44	51.15
K3	9/19/2020	1/4/2021	390	NA	102.12	NA	0.00	NA	98.74	22.76	18.92	37.18
K3	1/4/2021	3/13/2021	759	NA	123.55	NA	0.00	0.00	117.44	17.39	11.93	22.46
K3	3/13/2021	4/21/2021	261	NA	93.65	NA	0.00	0.00	80.03	9.97	8.23	17.22
KS	12/19/2018	3/18/2019	750	NA	186.18	NA	10.41	0.00	221.84	12.79	20.57	7.49

KS	3/18/2019	7/12/2019	711	NA	160.79	0.63	13.53	NA	152.24	10.23	16.45	9.98
KS	7/12/2019	10/12/2019	244	NA	81.52	NA	2.29	0.00	76.99	4.86	7.40	13.22
KS	10/12/2019	1/5/2020	438	NA	135.40	NA	7.29	0.00	200.09	5.12	12.34	7.49
KS	1/5/2020	3/28/2020	844	NA	166.43	NA	6.25	0.00	204.44	5.12	16.45	14.97
KS	3/28/2020	5/2/2020	300	NA	70.52	NA	2.08	0.00	130.49	5.12	8.23	12.48
KS	5/2/2020	6/20/2020	89	NA	144.43	NA	3.02	NA	111.79	49.62	11.11	30.44
KS	6/20/2020	9/19/2020	192	NA	121.02	NA	0.00	NA	89.60	20.20	17.69	20.96
KS	9/19/2020	1/4/2021	480	NA	75.04	NA	0.00	NA	58.29	0.77	8.23	19.96
KS	1/4/2021	3/13/2021	1077	NA	89.14	NA	5.21	0.00	73.95	2.30	9.05	10.48
KS	3/13/2021	4/21/2021	333	NA	79.55	NA	3.12	0.00	64.81	1.53	8.64	15.97
MT1	5/10/2019	7/11/2019	255	0.53	1715.09	2.25	104.10	0.00	1487.60	76.73	201.56	102.30
MT1	7/11/2019	9/29/2019	216	NA	198.03	NA	1.35	0.00	188.78	11.76	32.09	97.31
MT1	9/29/2019	1/9/2020	592	NA	315.94	NA	13.53	0.00	330.58	15.35	37.02	24.95
MT1	1/9/2020	3/31/2020	1614	NA	346.97	NA	16.66	0.00	343.63	10.23	37.02	27.45
MT1	6/15/2020	9/17/2020	240	NA	241.18	NA	0.00	NA	197.48	12.28	28.38	96.06
MT1	9/17/2020	12/30/2020	753	NA	159.38	NA	11.45	0.00	131.80	7.93	27.97	60.88
MT1	12/30/2020	3/27/2021	1301	NA	187.31	NA	10.41	0.00	157.46	4.60	30.03	36.43
MT1	3/27/2021	4/29/2021	97	NA	520.45	NA	22.90	0.00	444.54	31.20	88.44	154.44
MT2	5/10/2019	7/11/2019	697	0.53	1150.92	1.38	70.79	0.00	1026.53	33.25	123.41	69.86
MT2	7/11/2019	9/25/2019	387	NA	179.41	NA	10.72	0.00	161.81	5.88	25.09	44.66
MT2	9/25/2019	1/7/2020	1041	NA	349.79	NA	20.82	0.00	361.03	7.67	41.14	19.96
MT2	1/7/2020	3/31/2020	1263	NA	287.73	NA	16.66	0.00	308.83	7.67	32.91	14.97
MT2	6/15/2020	9/17/2020	504	NA	184.49	NA	0.00	1.44	154.85	4.60	19.74	31.19
MT2	9/17/2020	12/22/2020	652	NA	184.20	NA	4.16	0.00	150.50	5.37	18.51	20.71
MT2	12/22/2020	3/27/2021	1416	NA	193.51	NA	9.37	0.00	163.11	4.09	19.74	11.98
MT2	3/27/2021	4/29/2021	249	NA	298.73	NA	17.70	0.00	252.72	10.49	34.14	28.94
MT3	5/10/2019	7/11/2019	597	NA	129.76	0.50	10.41	0.00	121.79	5.12	45.25	72.36
MT3	7/11/2019	9/25/2019	1064	NA	212.41	NA	11.87	0.00	211.40	8.44	25.50	45.41
MT3	9/25/2019	1/7/2020	1270	NA	200.28	NA	13.53	0.00	230.54	5.12	20.57	17.47
MT3	1/7/2020	3/31/2020	2032	NA	220.03	NA	10.41	0.00	260.98	5.12	20.57	17.47
MT3	6/11/2020	9/17/2020	712	NA	149.22	NA	1.35	0.00	122.66	6.14	15.22	94.06
MT3	9/17/2020	12/22/2020	684	NA	194.92	NA	9.37	0.00	161.37	4.86	18.92	28.94
MT3	12/22/2020	3/27/2021	1588	NA	170.10	NA	9.37	0.00	141.80	5.37	17.28	13.97
MT3	3/27/2021	4/26/2021	351	NA	267.14	NA	10.41	0.00	227.93	18.67	26.74	34.68
MTS	7/11/2019	9/25/2019	323	NA	273.62	0.75	10.10	0.00	252.28	16.37	13.57	20.96
MTS	9/25/2019	1/7/2020	605	NA	256.70	NA	9.37	0.00	313.18	12.79	16.45	9.98
MTS	1/7/2020	3/31/2020	479	NA	222.85	NA	11.45	0.00	265.33	7.67	24.68	19.96
MTS	6/11/2020	9/17/2020	92	NA	250.21	NA	1.04	NA	200.09	9.72	24.68	132.98
MTS	9/17/2020	12/22/2020	376	NA	174.61	NA	7.29	0.00	144.85	18.67	19.33	82.83

MTS	12/22/2020	4/26/2021	671	NA	162.76	NA	8.33	0.00	137.45	6.65	15.63	29.19
EB	7/13/2019	9/27/2019	83	0.53	99.01	NA	12.18	0.00	116.57	4.35	11.11	63.12
EB	9/27/2019	1/9/2020	169	NA	110.01	NA	11.45	0.00	152.24	5.12	12.34	82.34
EB	1/10/2020	3/31/2020	115	NA	200.28	NA	8.33	0.00	239.23	5.12	24.68	132.24
EB	3/31/2020	6/23/2020	23	NA	135.12	NA	0.00	NA	102.22	8.44	26.33	244.26
EB	6/23/2020	10/16/2020	13	NA	349.51	NA	4.16	0.00	248.37	16.62	70.34	991.52
EB	10/16/2020	1/19/2021	41	NA	244.29	NA	13.53	0.00	191.39	5.12	37.43	316.62
EB	1/19/2021	4/7/2021	404	NA	157.69	NA	10.41	0.00	136.15	7.16	20.98	102.30
EB	4/7/2021	5/6/2021	58	NA	166.15	NA	0.00	0.00	139.19	9.97	23.86	147.46
TR	7/26/2019	10/19/2019	1351	NA	341.33	0.50	19.57	0.00	310.13	11.25	26.33	26.70
TR	10/19/2019	1/9/2020	502	NA	284.91	NA	16.66	0.00	313.18	10.23	28.79	14.97
TR	1/9/2020	3/15/2020	537	NA	375.18	NA	21.86	0.00	378.43	10.23	37.02	42.42
TR	3/15/2020	5/4/2020	272	NA	169.25	NA	10.41	0.00	239.23	7.67	16.45	22.46
TR	5/4/2020	6/20/2020	183	NA	228.77	NA	3.23	NA	186.17	8.44	23.45	76.10
TR	6/20/2020	10/12/2020	280	NA	223.41	NA	0.00	NA	185.30	16.88	23.45	112.77
TR	1/20/2021	2/1/2021	211	NA	216.64	NA	10.41	NA	188.34	6.14	19.33	4.74
TR	2/1/2021	2/17/2021	31	NA	211.57	NA	11.45	NA	181.82	14.32	21.39	10.73
TR	2/17/2021	3/2/2021	138	NA	326.38	NA	16.66	0.00	276.21	8.70	29.62	5.74
TR	3/2/2021	3/17/2021	284	NA	122.14	NA	7.29	NA	101.78	4.35	10.70	3.74
TR	3/17/2021	4/7/2021	105	NA	375.46	NA	21.86	0.00	314.48	13.81	35.38	11.23
TR	4/7/2021	4/29/2021	48	NA	245.42	NA	15.62	NA	202.70	15.09	25.09	14.47
EB	8/5/2019	8/7/2019	8	0.00	118.48	NA	12.49	NA	139.19	15.35	12.34	24.95
MHS	10/18/2019	1/9/2020	243	NA	327.22	NA	23.94	0.00	339.28	17.90	32.91	44.91
M	10/23/2019	1/9/2020	262	NA	488.01	NA	36.44	0.00	461.07	17.90	53.48	92.32
M	1/9/2020	3/25/2020	731	NA	200.28	NA	16.66	0.00	230.54	10.23	20.57	32.44
M	3/25/2020	6/23/2020	38	NA	332.86	NA	42.16	NA	299.26	18.16	31.67	177.89
M	6/23/2020	10/12/2020	55	NA	193.79	NA	21.86	NA	147.89	7.16	24.27	314.62
M	10/12/2020	1/19/2021	140	NA	124.40	NA	11.45	NA	97.87	2.05	15.22	122.50
M	1/19/2021	2/8/2021	149	NA	67.98	NA	8.33	NA	60.03	2.05	6.17	2.99
M	2/8/2021	3/2/2021	20	1.05	545.56	NA	41.64	0.00	473.68	13.04	50.60	60.88
M	3/2/2021	3/17/2021	123	NA	67.42	NA	9.37	NA	54.37	1.79	6.17	4.24
M	3/17/2021	4/7/2021	101	NA	159.10	NA	17.70	NA	134.41	3.84	14.81	6.99
M	4/7/2021	5/3/2021	30	NA	153.74	NA	20.82	NA	132.67	19.95	19.74	45.16
PW	10/31/2019	1/29/2020	1086	NA	299.01	NA	19.78	0.00	330.58	7.67	32.91	17.47
KK	2/16/2020	4/24/2020	244	NA	163.61	NA	12.49	0.00	173.99	15.35	20.57	39.92
KK	4/24/2020	6/20/2020	27	NA	402.82	NA	6.14	NA	220.10	106.91	49.36	52.40
KK	6/20/2020	10/10/2020	142	NA	230.47	NA	2.08	NA	144.85	57.03	29.21	110.28
KK	10/10/2020	1/2/2021	148	NA	225.39	NA	0.00	0.00	111.35	70.59	46.48	62.13
KK	1/2/2021	4/3/2021	1211	NA	202.82	NA	11.45	0.00	153.11	18.93	42.78	109.78

KK	4/3/2021	4/25/2021	127	NA	108.04	NA	0.00	NA	75.69	27.11	32.91	155.19
SB	2/16/2020	4/24/2020	310	NA	152.33	NA	12.49	0.00	204.44	7.67	16.45	19.96
SB	4/24/2020	6/20/2020	26	NA	310.58	NA	22.07	NA	246.19	62.92	57.18	90.32
SB	6/20/2020	10/10/2020	66	NA	208.74	NA	0.00	0.00	166.16	20.97	22.21	161.68
SB	10/10/2020	1/11/2021	154	NA	189.00	NA	0.00	0.00	109.61	42.20	31.67	112.77
WAAF	2/16/2020	4/26/2020	366	NA	397.74	NA	24.98	0.00	391.47	46.04	45.25	47.41
WAAF	4/26/2020	6/20/2020	21	NA	674.75	NA	0.00	NA	454.98	284.65	55.12	73.85
WAAF	6/20/2020	10/10/2020	55	NA	642.03	NA	0.00	NA	379.30	809.72	80.21	144.21
WAAF	10/10/2020	1/11/2021	189	NA	222.57	NA	6.25	NA	167.03	91.05	51.42	64.87
WAAF	1/11/2021	4/3/2021	1164	NA	282.65	NA	16.66	0.00	226.62	29.67	46.07	56.64
ER	2/16/2020	3/15/2020	143	NA	795.49	1.25	44.76	0.00	700.30	71.61	65.82	34.93
ER	3/15/2020	4/25/2020	262	NA	200.28	NA	17.70	0.00	243.58	10.23	20.57	27.45
ER	4/25/2020	6/20/2020	79	NA	305.50	NA	3.02	NA	250.11	10.49	30.44	163.92
ER	10/12/2020	1/11/2021	337	NA	233.00	NA	9.37	0.00	189.21	7.42	21.80	95.06
ER	1/11/2021	4/3/2021	894	NA	268.83	NA	8.33	0.00	222.71	6.91	25.92	52.40
D1	10/1/2017	12/31/2017	510	NA	507.84	NA	34.40	NA	435.00	20.50	45.29	29.90
D1	1/1/2018	3/31/2018	778	NA	268.02	NA	19.80	NA	217.50	20.50	24.69	22.50
MT1	4/1/2017	6/30/2017	244	NA	310.33	NA	31.20	NA	348.00	0.00	57.59	111.09
MT1	7/1/2017	9/30/2017	468	NA	310.33	NA	31.20	NA	348.00	0.00	57.59	11.10
MT1	10/1/2017	12/31/2017	595	NA	225.72	NA	17.70	NA	174.00	0.00	24.69	185.19
MT1	1/1/2018	3/31/2018	609	NA	284.92	NA	21.90	NA	278.40	15.30	32.89	34.90
D4	10/1/2017	12/31/2017	89	NA	1097.39	NA	60.40	NA	1048.29	148.29	115.18	59.90
D4	1/1/2018	3/31/2018	324	NA	299.03	NA	11.50	NA	243.60	117.69	53.49	92.30
D6	4/1/2017	6/30/2017	743	NA	310.33	NA	33.30	NA	391.50	0.10	57.59	115.19
D6	7/1/2017	9/30/2017	531	NA	225.72	NA	12.50	NA	217.50	0.00	28.79	143.99
D6	10/1/2017	12/31/2017	1345	NA	268.02	NA	17.70	NA	243.60	10.20	28.79	47.40
D6	1/1/2018	3/31/2018	1028	NA	293.42	NA	17.70	NA	239.20	17.90	41.09	62.40
D7	4/1/2017	6/30/2017	236	NA	592.45	NA	48.90	NA	652.49	0.10	78.18	279.79
D7	7/1/2017	9/30/2017	96	NA	761.66	NA	52.10	NA	739.49	0.10	90.48	526.57
D7	10/1/2017	12/31/2017	520	NA	397.73	NA	30.20	NA	395.80	20.50	49.39	52.40
D7	1/1/2018	3/31/2018	305	NA	324.43	NA	20.80	NA	269.70	7.70	32.89	20.00
D8	4/1/2017	6/30/2017	360	NA	169.31	NA	13.50	NA	217.50	0.00	28.79	86.40
D9	4/1/2017	6/30/2017	1303	NA	197.52	NA	17.70	NA	261.00	0.00	41.09	156.39
D9	7/1/2017	9/30/2017	568	NA	141.01	NA	0.00	NA	130.50	0.00	24.69	148.09
D9	10/1/2017	12/31/2017	526	NA	220.02	NA	19.80	NA	230.50	15.30	28.79	34.90
D9	1/1/2018	3/31/2018	989	NA	234.12	NA	14.60	NA	191.40	12.80	32.89	54.90
D10	3/1/2017	3/30/2017	299	NA	169.31	NA	18.70	NA	174.00	25.60	24.69	69.90
D10	4/1/2017	6/30/2017	843	NA	310.33	NA	13.50	NA	304.50	0.10	32.89	148.09
D10	7/1/2017	9/30/2017	758	NA	141.01	NA	12.50	NA	130.50	0.00	32.89	94.60

D10	10/1/2017	12/31/2017	1672	NA	231.32	NA	18.70	NA	243.60	10.20	45.29	34.90
D10	1/1/2018	3/31/2018	1200	NA	166.41	NA	13.50	NA	139.20	10.20	36.99	39.90
D11	4/1/2017	6/30/2017	297	NA	733.46	NA	76.00	NA	782.99	0.10	82.28	119.29
D11	7/1/2017	9/30/2017	134	NA	1213.10	NA	84.30	NA	1043.89	0.10	127.57	345.58
D11	10/1/2017	12/31/2017	240	NA	2970.65	NA	158.20	NA	2609.77	110.00	279.74	227.09
D11	1/1/2018	3/31/2018	681	NA	617.85	NA	39.60	NA	513.29	30.70	82.28	79.80
D12	10/1/2017	12/31/2017	124	NA	386.53	NA	45.80	NA	326.20	178.99	53.49	64.90
D12	1/1/2018	3/31/2018	178	NA	214.42	NA	23.90	NA	182.70	112.50	53.49	127.29
D13	4/1/2017	6/30/2017	1932	NA	253.92	NA	21.90	NA	261.00	0.00	53.49	143.99
D13	7/1/2017	9/30/2017	919	NA	169.31	NA	12.50	NA	130.50	0.00	24.69	74.06
D13	10/1/2017	12/31/2017	1699	NA	268.02	NA	25.00	NA	269.70	10.20	45.29	44.90
D13	1/1/2018	3/31/2018	1649	NA	431.64	NA	26.00	NA	352.30	10.20	61.69	49.90
D14	4/1/2017	6/30/2017	314	NA	169.31	NA	19.80	NA	217.50	0.00	36.99	90.50
D14	7/1/2017	9/30/2017	220	NA	141.01	NA	15.60	NA	174.00	0.10	32.89	94.60
D14	10/1/2017	12/31/2017	461	NA	304.73	NA	18.70	NA	269.70	20.50	45.29	62.40
D14	1/1/2018	3/31/2018	205	NA	225.72	NA	13.50	NA	204.40	76.70	61.69	109.79
D15	1/1/2018	3/31/2018	342	NA	242.62	NA	17.70	NA	200.10	38.40	41.09	67.40
D16	4/1/2017	6/30/2017	148	NA	141.01	NA	87.50	NA	174.00	0.00	41.09	111.09
D17	4/1/2017	6/30/2017	507	NA	366.73	NA	34.40	NA	391.50	0.10	53.49	119.29
D17	7/1/2017	9/30/2017	352	NA	366.73	NA	32.30	NA	348.00	0.10	65.79	213.99
D17	10/1/2017	12/31/2017	446	NA	454.24	NA	6.20	NA	430.60	99.70	86.38	174.69
D17	1/1/2018	3/31/2018	370	NA	234.12	NA	0.00	NA	200.10	35.80	24.69	69.90
D18	3/1/2017	3/30/2017	263	NA	225.72	NA	41.60	NA	261.00	25.60	41.09	109.79
D18	4/1/2017	6/30/2017	1046	NA	507.84	NA	16.70	NA	565.49	0.10	49.39	127.59
D18	7/1/2017	9/30/2017	1105	NA	141.01	NA	10.40	NA	130.50	0.00	24.69	152.19
D18	10/1/2017	12/31/2017	810	NA	296.23	NA	19.80	NA	287.10	17.90	41.09	57.40
D18	1/1/2018	3/31/2018	1764	NA	256.72	NA	16.70	NA	208.80	10.20	41.09	94.80
D19	4/1/2017	6/30/2017	262	NA	310.33	NA	17.70	NA	348.00	0.10	45.29	106.99
D19	7/1/2017	9/30/2017	421	NA	197.52	NA	34.40	NA	174.00	0.00	32.89	189.29
D19	10/1/2017	12/31/2017	347	NA	372.43	NA	22.90	NA	304.50	76.70	41.09	89.80
D19	1/1/2018	3/31/2018	125	NA	318.83	NA	27.10	NA	304.50	115.09	86.38	209.59
D20	4/1/2017	6/30/2017	1342	NA	282.12	NA	15.60	NA	304.50	0.10	45.29	139.89
D20	7/1/2017	9/30/2017	271	NA	282.12	NA	17.70	NA	217.50	0.10	61.69	296.19
D20	10/1/2017	12/31/2017	351	NA	440.14	NA	23.90	NA	417.60	30.70	90.48	286.89
D20	1/1/2018	3/31/2018	660	NA	287.72	NA	13.50	NA	221.80	48.60	49.39	217.09
A	3/9/2019	5/8/2019	46	1.05	332.86	0.63	22.80	0.00	334.93	36.83	23.04	25.20
A	5/8/2019	6/29/2019	119	0.53	116.22	NA	13.53	NA	101.35	3.84	11.93	18.46
A	6/29/2019	8/5/2019	14	0.00	346.97	0.63	22.90	NA	317.53	12.79	41.14	14.97
A	8/5/2019	10/1/2019	69	0.53	141.04	NA	11.45	0.00	126.14	7.67	12.34	22.46

A	10/1/2019	10/14/2019	49	0.53	177.72	NA	12.49	NA	165.29	5.12	16.45	14.97
A	10/14/2019	11/15/2019	35	0.53	149.51	NA	23.84	0.00	139.19	7.42	73.63	44.66
A	11/15/2019	12/11/2019	50	0.53	358.25	0.63	24.98	0.00	330.58	10.23	37.02	19.96
A	12/11/2019	12/20/2019	50	NA	118.48	NA	11.56	0.00	104.39	3.32	8.64	5.24
A	12/20/2019	1/8/2020	61	0.53	654.44	0.88	38.62	0.00	582.86	17.39	33.73	20.46
A	1/8/2020	1/15/2020	84	NA	425.95	0.50	23.21	0.00	382.78	8.44	23.86	14.47
A	1/15/2020	2/13/2020	22	0.53	689.70	0.75	43.41	0.00	610.27	18.41	67.46	37.67
A	2/13/2020	3/7/2020	72	NA	728.35	0.88	38.62	0.00	668.99	14.58	69.52	37.18
A	3/7/2020	3/20/2020	99	NA	111.99	NA	11.35	NA	103.52	3.58	10.28	4.74
A	3/20/2020	4/17/2020	116	NA	186.74	NA	15.30	NA	163.55	5.37	19.33	12.72
A	11/6/2020	12/11/2020	18	1.05	1154.58	NA	75.79	NA	945.63	27.11	118.47	71.86
A	12/11/2020	1/13/2021	47	NA	432.16	NA	26.75	NA	351.46	12.79	46.07	30.44
A	1/13/2021	2/2/2021	145	NA	175.18	NA	11.97	NA	143.54	3.58	18.10	10.48
A	2/2/2021	3/3/2021	55	NA	628.77	NA	36.85	0.00	508.92	13.04	64.17	43.16
A	3/3/2021	3/16/2021	134	NA	125.53	NA	10.10	NA	102.22	3.07	13.16	12.23
A	3/16/2021	3/31/2021	30	NA	775.46	NA	47.78	0.00	650.28	15.35	77.33	39.17
A	3/31/2021	6/11/2021	44	1.05	722.99	1.00	52.05	NA	602.00	18.67	90.09	74.10
A	6/11/2021	8/4/2021	21	1.58	907.76	1.13	49.03	0.00	825.58	27.11	97.90	92.32
DOH	4/9/2018	6/27/2018	286	0.53	423.13	0.88	29.15	NA	361.03	10.23	24.68	4.99
DOH	6/27/2018	8/21/2018	53	0.53	705.22	1.13	36.44	0.00	608.96	23.02	49.36	7.49
DOH	8/21/2018	8/28/2018	214	0.53	414.67	1.00	22.90	0.00	339.28	10.23	28.79	4.99
DOH	11/26/2018	12/13/2018	98	NA	398.03	0.63	23.11	NA	337.10	8.70	35.79	6.99
DOH	12/13/2018	1/24/2019	36	NA	619.75	1.13	37.79	0.00	665.94	20.72	58.82	10.23
DOH	1/24/2019	2/14/2019	104	NA	492.81	0.88	29.04	0.00	429.32	16.11	44.01	9.73
DOH	2/14/2019	3/31/2019	41	NA	1004.23	1.25	61.94	0.00	848.19	45.78	103.25	24.20
DOH	3/31/2019	5/8/2019	69	0.53	547.25	0.88	39.25	0.00	482.82	43.99	41.96	15.47
DOH	5/8/2019	6/28/2019	98	0.53	246.26	0.63	29.77	NA	227.06	16.11	27.97	18.46
DOH	6/28/2019	8/5/2019	34	0.53	719.32	1.13	46.85	NA	626.36	40.92	78.16	29.94
DOH	8/5/2019	9/9/2019	36	0.53	547.25	0.75	39.56	0.00	474.12	51.15	86.38	29.94
DOH	9/9/2019	10/1/2019	64	NA	242.60	NA	17.70	0.00	221.84	10.23	20.57	9.98
DOH	10/1/2019	10/14/2019	87	NA	169.25	NA	13.53	NA	160.94	5.12	16.45	7.49
DOH	10/14/2019	11/15/2019	16	0.53	578.28	0.63	51.32	0.00	508.92	77.49	56.36	34.18
DOH	11/15/2019	12/11/2019	69	0.00	668.55	1.00	0.00	0.00	604.61	61.38	61.70	17.47
DOH	12/11/2019	12/20/2019	41	NA	332.86	0.63	26.96	0.00	313.18	11.51	13.99	8.48
DOH	12/20/2019	1/8/2020	144	NA	552.89	0.75	32.48	0.00	487.17	24.81	19.74	11.98
DOH	1/8/2020	1/15/2020	176	NA	389.28	0.63	22.17	0.00	347.98	8.44	12.34	7.49
DOH	1/15/2020	2/13/2020	40	NA	620.03	0.50	36.12	0.00	532.84	38.36	59.65	23.95
DOH	2/13/2020	3/6/2020	61	NA	675.32	1.25	35.29	0.00	603.74	16.37	63.76	16.47
DOH	3/6/2020	3/20/2020	119	NA	163.89	NA	15.72	NA	155.72	6.39	16.87	4.49

DOH	3/20/2020	4/17/2020	121	NA	277.57	NA	10.72	NA	256.63	21.23	25.50	6.49
DOH	4/17/2020	6/10/2020	58	2.63	517.63	NA	NA	0.00	494.13	153.96	63.35	30.44
DOH	7/24/2020	10/2/2020	19	NA	616.93	NA	32.06	0.00	512.83	31.46	58.82	22.95
DOH	10/2/2020	11/6/2020	87	0.53	151.76	NA	27.48	NA	135.71	23.79	16.87	12.97
DOH	11/6/2020	12/11/2020	18	0.53	930.04	NA	55.38	NA	731.19	76.73	87.62	45.66
DOH	12/11/2020	1/13/2021	47	NA	377.15	NA	12.18	NA	322.31	15.60	35.79	7.98
DOH	1/13/2021	2/2/2021	145	NA	299.29	NA	15.09	NA	252.28	10.49	28.79	7.73
DOH	2/2/2021	3/3/2021	55	NA	607.05	NA	34.04	0.00	499.35	29.67	60.06	48.15
DOH	3/3/2021	3/16/2021	134	NA	158.25	NA	12.39	NA	143.54	11.51	17.69	13.72
DOH	3/16/2021	3/31/2021	29	1.58	441.47	NA	4.48	0.00	425.40	108.70	46.89	31.69
DOH	3/31/2021	6/11/2021	44	NA	799.44	1.38	184.68	NA	774.68	530.69	148.09	326.60
DOH	6/11/2021	8/4/2021	21	0.53	525.81	0.75	NA	0.00	567.64	115.60	69.52	174.15
WU	5/1/2019	6/28/2019	154	NA	132.30	NA	13.74	NA	121.36	3.58	14.81	5.99
WU	6/28/2019	8/5/2019	63	0.00	346.97	0.63	22.90	NA	317.53	12.79	41.14	14.97
WU	8/5/2019	9/9/2019	93	NA	217.21	0.50	15.62	0.00	204.44	5.12	24.68	7.49
WU	9/9/2019	10/1/2019	98	NA	118.48	NA	10.41	NA	113.09	2.56	12.34	4.99
WU	10/1/2019	10/14/2019	127	NA	110.01	NA	8.33	NA	108.74	2.56	12.34	2.50
WU	10/14/2019	11/15/2019	37	0.53	287.73	0.50	24.98	0.00	256.63	8.44	20.98	12.72
WU	11/15/2019	12/11/2019	84	0.53	471.09	1.00	29.15	0.00	426.27	15.35	49.36	12.48
WU	12/11/2019	12/20/2019	64	NA	245.42	NA	19.26	0.00	221.84	5.88	13.99	8.48
WU	12/20/2019	1/8/2020	188	NA	434.41	0.50	24.46	0.00	382.78	12.28	16.87	10.23
WU	1/8/2020	1/15/2020	167	NA	473.91	0.50	24.15	0.00	413.22	11.00	16.45	9.98
WU	1/15/2020	2/13/2020	56	0.00	389.28	0.75	23.21	0.00	350.15	9.97	40.31	11.73
WU	2/13/2020	3/6/2020	105	NA	426.23	NA	24.46	0.00	384.08	9.97	45.66	9.98
WU	3/6/2020	3/20/2020	112	NA	144.99	NA	11.03	NA	137.02	3.32	13.99	4.49
WU	3/20/2020	4/17/2020	175	NA	183.64	NA	12.39	NA	157.02	4.09	18.92	5.49
WU	4/17/2020	6/10/2020	107	0.53	245.42	NA	17.80	NA	206.61	6.65	24.27	6.74
WU	7/24/2020	10/2/2020	130	NA	260.65	NA	17.38	0.00	212.70	7.67	24.27	7.24
WU	10/2/2020	11/6/2020	117	NA	73.91	NA	11.03	NA	63.07	3.32	6.99	3.49
WU	11/6/2020	12/11/2020	110	NA	341.04	NA	16.34	0.00	279.69	14.83	35.38	8.73
WU	12/11/2020	1/13/2021	139	NA	266.57	NA	14.47	NA	219.23	6.91	26.74	5.99
WU	1/13/2021	2/3/2021	174	NA	305.78	NA	18.63	NA	244.45	6.91	28.38	6.99
WU	2/3/2021	3/3/2021	135	NA	399.15	NA	23.01	0.00	321.44	7.93	39.49	8.98
WU	3/3/2021	3/16/2021	197	NA	106.35	NA	7.70	NA	86.99	2.81	11.11	6.74
WU	3/16/2021	3/31/2021	90	NA	315.94	NA	21.03	NA	257.07	6.14	30.03	6.49
WU	3/31/2021	6/11/2021	161	0.53	288.01	0.38	19.99	NA	243.58	8.44	29.62	14.22
WU	6/11/2021	8/4/2021	114	0.00	272.50	0.50	17.91	NA	250.11	6.91	28.38	13.22

**APPENDIX B: CHAPTER 3 SUPPLEMENTARY MATERIAL**  
**WATER STABLE ISOTOPE RAW DATA**

Collector Abbreviation	Latitude	Longitude	Elevation (m)	From Date	To Date	Period	Point Precipitation (mm)	$\delta^{18}\text{O}$ (‰)	$\delta^2\text{H}$ (‰)
K1	21.54118	-158.16010	290	12/19/2018	3/18/2019	89	461	-3.4	-12.2
K1	21.54118	-158.16010	290	3/18/2019	7/12/2019	116	541	-2.5	-7.7
K1	21.54118	-158.16010	290	7/12/2019	10/12/2019	92	181	-3.8	-20.1
K1	21.54118	-158.16010	290	10/12/2019	1/5/2020	85	504	-2.8	-9.4
K1	21.54118	-158.16010	290	1/5/2020	3/28/2020	83	673	-4.2	-19.2
K1	21.54118	-158.16010	290	3/28/2020	5/2/2020	35	26	-3.6	-16.9
K1	21.54118	-158.16010	290	5/2/2020	6/20/2020	49	31	-1.5	0.6
K1	21.54118	-158.16010	290	6/20/2020	9/19/2020	91	43	-3.5	-17.9
K1	21.54118	-158.16010	290	9/19/2020	1/4/2021	107	222	-2.2	-5.0
K1	21.54118	-158.16010	290	1/4/2021	3/13/2021	68	516	-4.7	-26.9
K1	21.54118	-158.16010	290	3/13/2021	4/21/2021	39	270	-2.9	-12.0
K2	21.52963	-158.16487	553	7/12/2019	10/12/2019	92	198	-4.2	-21.6
K2	21.52963	-158.16487	553	10/12/2019	1/5/2020	85	366	-3.2	-10.7
K2	21.52963	-158.16487	553	1/5/2020	3/28/2020	83	540	-5.3	-27.3
K2	21.52963	-158.16487	553	3/28/2020	5/2/2020	35	85	-4.5	-23.3
K2	21.52963	-158.16487	553	5/2/2020	6/20/2020	49	35	-2.0	-2.6
K2	21.52963	-158.16487	553	6/20/2020	9/19/2020	91	99	-4.4	-23.7
K2	21.52963	-158.16487	553	9/19/2020	1/4/2021	107	246	-2.9	-7.8
K2	21.52963	-158.16487	553	1/4/2021	3/13/2021	68	539	-4.1	-14.3
K2	21.52963	-158.16487	553	3/13/2021	4/21/2021	39	309	-3.6	-14.9
K3	21.51185	-158.15778	930	7/12/2019	10/12/2019	92	264	-4.4	-20.9
K3	21.51185	-158.15778	930	10/12/2019	1/5/2020	85	410	-3.6	-12.6
K3	21.51185	-158.15778	930	1/5/2020	3/28/2020	83	619	-4.4	-18.1
K3	21.51185	-158.15778	930	3/28/2020	5/2/2020	35	90	-4.8	-23.9

K3	21.51185	-158.15778	930	5/2/2020	6/20/2020	49	94	-2.4	-3.8
K3	21.51185	-158.15778	930	6/20/2020	9/19/2020	91	153	-3.7	-15.6
K3	21.51185	-158.15778	930	9/19/2020	1/4/2021	107	390	-3.2	-8.8
K3	21.51185	-158.15778	930	1/4/2021	3/13/2021	68	759	-4.8	-20.3
K3	21.51185	-158.15778	930	3/13/2021	4/21/2021	39	261	-4.2	-18.4
KS	21.50827	-158.14395	1212	12/19/2018	3/18/2019	89	750	-5.1	-23.5
KS	21.50827	-158.14395	1212	3/18/2019	7/12/2019	116	711	-3.2	-9.9
KS	21.50827	-158.14395	1212	7/12/2019	10/12/2019	92	244	-4.0	-18.5
KS	21.50827	-158.14395	1212	10/12/2019	1/5/2020	85	438	-3.7	-12.7
KS	21.50827	-158.14395	1212	1/5/2020	3/28/2020	83	844	-5.1	-23.5
KS	21.50827	-158.14395	1212	3/28/2020	5/2/2020	35	300	-4.2	-20.8
KS	21.50827	-158.14395	1212	5/2/2020	6/20/2020	49	89	-2.4	-4.7
KS	21.50827	-158.14395	1212	6/20/2020	9/19/2020	91	192	-3.8	-16.9
KS	21.50827	-158.14395	1212	9/19/2020	1/4/2021	107	480	-3.5	-10.6
KS	21.50827	-158.14395	1212	1/4/2021	3/13/2021	68	1077	-5.8	-28.4
KS	21.50827	-158.14395	1212	3/13/2021	4/21/2021	39	333	-4.6	-21.7
MT1	21.43008	-157.93803	291	3/10/2019	5/10/2019	61	190		
MT1	21.43008	-157.93803	291	5/10/2019	7/11/2019	62	255	-2.8	-11.4
MT1	21.43008	-157.93803	291	7/11/2019	9/29/2019	80	216	-2.9	-12.8
MT1	21.43008	-157.93803	291	9/29/2019	1/9/2020	102	592	-2.4	-6.8
MT1	21.43008	-157.93803	291	1/9/2020	3/31/2020	82	1614	-2.5	-8.4
MT1	21.43008	-157.93803	291	3/31/2020	6/15/2020	76	109	-2.0	-8.3
MT1	21.43008	-157.93803	291	6/15/2020	9/17/2020	94	240	-1.4	-0.6
MT1	21.43008	-157.93803	291	9/17/2020	12/30/2020	104	753	-1.8	-1.7
MT1	21.43008	-157.93803	291	12/30/2020	3/27/2021	87	1301	-3.1	-11.4
MT1	21.43008	-157.93803	291	3/27/2021	4/29/2021	33	97	-1.1	1.3
MT2	21.44235	-157.91015	452	5/10/2019	7/11/2019	62	697	-2.2	-7.1
MT2	21.44235	-157.91015	452	7/11/2019	9/25/2019	76	387	-2.6	-9.6
MT2	21.44235	-157.91015	452	9/25/2019	1/7/2020	104	1041	-2.5	-3.8
MT2	21.44235	-157.91015	452	1/7/2020	3/31/2020	84	1263	-3.2	-10.4
MT2	21.44235	-157.91015	452	3/31/2020	6/15/2020	76	114	-2.9	-11.1

MT2	21.44235	-157.91015	452	6/15/2020	9/17/2020	94	504	-2.0	-3.3
MT2	21.44235	-157.91015	452	9/17/2020	12/22/2020	96	652	-2.0	-2.2
MT2	21.44235	-157.91015	452	12/22/2020	3/27/2021	95	1416	-3.3	-11.4
MT2	21.44235	-157.91015	452	3/27/2021	4/29/2021	33	249	-2.2	-1.7
MT3	21.44780	-157.89497	549	5/10/2019	7/11/2019	62	597	-2.9	-11.5
MT3	21.44780	-157.89497	549	7/11/2019	9/25/2019	76	1064	-3.5	-16.0
MT3	21.44780	-157.89497	549	9/25/2019	1/7/2020	104	1270	-2.9	-7.3
MT3	21.44780	-157.89497	549	1/7/2020	3/31/2020	84	2032	-2.9	-8.2
MT3	21.44780	-157.89497	549	3/31/2020	6/11/2020	72	552	-2.5	-4.6
MT3	21.44780	-157.89497	549	6/11/2020	9/17/2020	98	712	-2.4	-4.7
MT3	21.44780	-157.89497	549	9/17/2020	12/22/2020	96	684	-2.0	-2.0
MT3	21.44780	-157.89497	549	12/22/2020	3/27/2021	95	1588	-3.4	-11.4
MT3	21.44780	-157.89497	549	3/27/2021	4/26/2021	30	351	-2.6	-2.1
MTS	21.45677	-157.87535	806	7/11/2019	9/25/2019	76	323	-3.1	-11.5
MTS	21.45677	-157.87535	806	9/25/2019	1/7/2020	104	605	-3.2	-9.3
MTS	21.45677	-157.87535	806	1/7/2020	3/31/2020	84	479	-3.8	-14.8
MTS	21.45677	-157.87535	806	3/31/2020	6/11/2020	72	135	-3.2	-10.1
MTS	21.45677	-157.87535	806	6/11/2020	9/17/2020	98	92	-2.8	-8.2
MTS	21.45677	-157.87535	806	9/17/2020	12/22/2020	96	376	-2.9	-6.8
MTS	21.45677	-157.87535	806	12/22/2020	4/26/2021	125	671	-4.5	-21.5
EB	21.31592	-158.03555	7	6/16/2020	6/16/2020	1	1	-1.1	3.4
EB	21.31592	-158.03555	7	7/13/2019	9/27/2019	76	83	-2.9	-10.6
EB	21.31592	-158.03555	7	9/27/2019	1/9/2020	104	169	-5.9	-35.7
EB	21.31592	-158.03555	7	1/10/2020	3/31/2020	81	115	-5.5	-33.8
EB	21.31592	-158.03555	7	3/31/2020	6/23/2020	84	23	-5.1	-29.0
EB	21.31592	-158.03555	7	6/23/2020	10/16/2020	115	13	-1.3	-2.1
EB	21.31592	-158.03555	7	10/16/2020	1/19/2021	95	41	-1.8	-0.7
EB	21.31592	-158.03555	7	1/19/2021	4/7/2021	78	404	-4.0	-21.8
EB	21.31592	-158.03555	7	4/7/2021	5/6/2021	29	58	-2.2	-5.2
TR	21.37067	-157.87018	380	7/26/2019	10/19/2019	85	1351	-2.1	-7.6
TR	21.37067	-157.87018	380	10/19/2019	1/9/2020	82	502	-2.0	-3.0

TR	21.37067	-157.87018	380	1/9/2020	3/15/2020	66	537	-2.3	-6.4
TR	21.37067	-157.87018	380	3/15/2020	5/4/2020	50	272	-4.8	-25.7
TR	21.37067	-157.87018	380	5/4/2020	6/20/2020	47	183	-1.8	-1.9
TR	21.37067	-157.87018	380	6/20/2020	10/12/2020	114	280	-1.9	-3.3
TR	21.37067	-157.87018	380	1/20/2021	2/1/2021	12	211	-3.1	-9.4
TR	21.37067	-157.87018	380	2/1/2021	2/17/2021	16	31	-3.1	-9.4
TR	21.37067	-157.87018	380	2/17/2021	3/2/2021	13	138	-1.8	-2.6
TR	21.37067	-157.87018	380	3/2/2021	3/17/2021	15	284	-4.0	-18.8
TR	21.37067	-157.87018	380	3/17/2021	4/7/2021	21	105	-1.7	3.7
TR	21.37067	-157.87018	380	4/7/2021	4/29/2021	22	48	-1.8	-0.4
EB	21.31592	-158.03555	7	8/5/2019	8/7/2019	2	8	-5.7	-38.5
MHS	21.45508	-158.00838	222	10/18/2019	1/9/2020	83	243	-2.2	-4.1
M	21.37140	-158.08641	335	10/23/2019	1/9/2020	78	262	-2.5	-9.0
M	21.37140	-158.08641	335	1/9/2020	3/25/2020	76	731	-5.3	-30.4
M	21.37140	-158.08641	335	3/25/2020	6/23/2020	90	38	-3.7	-16.7
M	21.37140	-158.08641	335	6/23/2020	10/12/2020	111	55	-3.2	-12.5
M	21.37140	-158.08641	335	10/12/2020	1/19/2021	99	140	-2.8	-6.0
M	21.37140	-158.08641	335	1/19/2021	2/8/2021	20	149	-4.8	-22.5
M	21.37140	-158.08641	335	2/8/2021	3/2/2021	22	20	-1.7	-0.4
M	21.37140	-158.08641	335	3/2/2021	3/17/2021	15	123	-5.0	-28.0
M	21.37140	-158.08641	335	3/17/2021	4/7/2021	21	101	-1.9	-4.2
M	21.37140	-158.08641	335	4/7/2021	5/3/2021	26	30	-1.8	-0.3
PW	21.46866	-157.89450	677	10/31/2019	1/29/2020	90	1086	-2.8	-5.8
KK	21.47352	-158.11030	557	2/16/2020	4/24/2020	68	244	-4.7	-24.4
KK	21.47352	-158.11030	557	4/24/2020	6/20/2020	57	27	-1.9	-2.8
KK	21.47352	-158.11030	557	6/20/2020	10/10/2020	112	142	-3.4	-16.2
KK	21.47352	-158.11030	557	10/10/2020	1/2/2021	84	148	-2.8	-6.6
KK	21.47352	-158.11030	557	1/2/2021	4/3/2021	91	1211	-2.8	-8.4
KK	21.47352	-158.11030	557	4/3/2021	4/25/2021	22	127	-3.4	-12.6
SB	21.48850	-158.09840	371	2/16/2020	4/24/2020	68	310	-4.7	-26.0
SB	21.48850	-158.09840	371	4/24/2020	6/20/2020	57	26	-1.7	-1.1

SB	21.48850	-158.09840	371	6/20/2020	10/10/2020	112	66	-3.0	-14.2
SB	21.48850	-158.09840	371	10/10/2020	1/11/2021	93	154	-2.3	-4.1
WAAF	21.48269	-158.04210	270	2/16/2020	4/26/2020	70	366	-2.9	-12.6
WAAF	21.48269	-158.04210	270	4/26/2020	6/20/2020	55	21	-1.4	1.6
WAAF	21.48269	-158.04210	270	6/20/2020	10/10/2020	112	55	-1.8	-3.4
WAAF	21.48269	-158.04210	270	10/10/2020	1/11/2021	93	189	-1.8	-2.0
WAAF	21.48269	-158.04210	270	1/11/2021	4/3/2021	82	1164	-3.3	-14.1
ER	21.48753	-158.00480	306	2/16/2020	3/15/2020	28	143	-1.8	-1.3
ER	21.48753	-158.00480	306	3/15/2020	4/25/2020	41	262	-3.4	-15.9
ER	21.48753	-158.00480	306	4/25/2020	6/20/2020	56	79	-1.2	1.3
ER	21.48753	-158.00480	306	10/12/2020	1/11/2021	91	337	-2.2	-3.5
ER	21.48753	-158.00480	306	1/11/2021	4/3/2021	82	894	-2.9	-10.5
A	21.37949	-157.93322	13	3/31/2019	5/8/2019	38	46	-1.1	1.2
A	21.37949	-157.93322	13	5/8/2019	6/29/2019	52	119	-6.3	-41.7
A	21.37949	-157.93322	13	6/29/2019	8/5/2019	37	14	-0.5	0.2
A	21.37949	-157.93322	13	8/5/2019	9/9/2019	35	16	-1.4	-8.7
A	21.37949	-157.93322	13	9/9/2019	10/1/2019	22	89	-2.0	-6.7
A	21.37949	-157.93322	13	10/1/2019	10/14/2019	13	49	-3.4	-26.3
A	21.37949	-157.93322	13	10/14/2019	11/15/2019	32	35	-1.9	-1.7
A	21.37949	-157.93322	13	11/15/2019	12/11/2019	26	50	-2.8	-12.5
A	21.37949	-157.93322	13	12/11/2019	12/20/2019	9	50	-2.5	-11.2
A	21.37949	-157.93322	13	12/20/2019	1/8/2020	19	61	-1.1	-0.2
A	21.37949	-157.93322	13	1/8/2020	1/15/2020	7	84	-1.7	-0.6
A	21.37949	-157.93322	13	1/15/2020	2/13/2020	29	22	-2.1	-7.3
A	21.37949	-157.93322	13	2/13/2020	3/7/2020	23	72	-1.4	-2.5
A	21.37949	-157.93322	13	3/7/2020	3/20/2020	13	99	-7.5	-48.4
A	21.37949	-157.93322	13	3/20/2020	4/17/2020	28	116	-4.3	-23.8
A	21.37949	-157.93322	13	4/17/2020	6/10/2020	54	14	0.3	5.8
A	21.37949	-157.93322	13	6/10/2020	10/2/2020	114	37	0.4	3.4
A	21.37949	-157.93322	13	10/2/2020	11/6/2020	35	87	-2.3	-6.6
A	21.37949	-157.93322	13	11/6/2020	12/11/2020	35	18	-0.5	4.5

A	21.37949	-157.93322	13	12/11/2020	1/13/2021	33	47	-2.0	-5.1
A	21.37949	-157.93322	13	1/13/2021	2/2/2021	20	145	-4.4	-22.1
A	21.37949	-157.93322	13	2/2/2021	3/3/2021	29	55	-1.6	-3.3
A	21.37949	-157.93322	13	3/3/2021	3/16/2021	13	134	-4.1	-23.4
A	21.37949	-157.93322	13	3/16/2021	3/31/2021	15	30	-0.9	2.5
A	21.37949	-157.93322	13	3/31/2021	6/11/2021	73	44	-1.1	0.6
A	21.37949	-157.93322	13	6/11/2021	8/4/2021	53	21	-0.1	2.4
DOH	21.41723	-157.94814	154	3/1/2018	4/9/2018	39	121	-1.4	0.3
DOH	21.41723	-157.94814	154	4/9/2018	6/27/2018	79	286	-2.1	-7.6
DOH	21.41723	-157.94814	154	6/27/2018	8/21/2018	55	53	-1.1	-3.4
DOH	21.41723	-157.94814	154	8/21/2018	8/28/2018	7	214	-2.8	-14.4
DOH	21.41723	-157.94814	154	8/28/2018	8/29/2018	1	0	-2.7	-13.3
DOH	21.41723	-157.94814	154	8/29/2018	9/21/2018	23	173	-3.8	-22.7
DOH	21.41723	-157.94814	154	9/21/2018	10/8/2018	17	72	-3.6	-19.7
DOH	21.41723	-157.94814	154	10/8/2018	11/26/2018	49	194	-2.4	-7.1
DOH	21.41723	-157.94814	154	11/26/2018	11/26/2018	1	0	-2.4	-7.0
DOH	21.41723	-157.94814	154	11/26/2018	12/13/2018	17	98	-1.6	2.1
DOH	21.41723	-157.94814	154	12/13/2018	1/24/2019	42	36	-1.4	-0.3
DOH	21.41723	-157.94814	154	1/24/2019	2/14/2019	21	104	-3.3	-13.7
DOH	21.41723	-157.94814	154	2/14/2019	3/31/2019	45	41	-2.1	-5.6
DOH	21.41723	-157.94814	154	3/31/2019	5/8/2019	38	69	-1.3	-0.5
DOH	21.41723	-157.94814	154	5/8/2019	6/28/2019	51	98	-5.3	-32.8
DOH	21.41723	-157.94814	154	6/28/2019	8/5/2019	38	34	-1.3	-3.3
DOH	21.41723	-157.94814	154	8/5/2019	9/9/2019	35	36	-2.1	-10.5
DOH	21.41723	-157.94814	154	9/9/2019	10/1/2019	22	64	-2.0	-6.9
DOH	21.41723	-157.94814	154	10/1/2019	10/14/2019	13	87	-4.8	-26.9
DOH	21.41723	-157.94814	154	10/14/2019	11/15/2019	32	16	-0.6	4.3
DOH	21.41723	-157.94814	154	11/15/2019	12/11/2019	26	69	-1.6	-0.9
DOH	21.41723	-157.94814	154	12/11/2019	12/20/2019	9	41	-1.6	-3.2
DOH	21.41723	-157.94814	154	12/20/2019	1/8/2020	19	144	-1.6	-1.4
DOH	21.41723	-157.94814	154	1/8/2020	1/15/2020	7	176	-2.5	-8.9

DOH	21.41723	-157.94814	154	1/15/2020	2/13/2020	29	40	-1.9	-6.1
DOH	21.41723	-157.94814	154	2/13/2020	3/6/2020	22	61	-1.9	-3.2
DOH	21.41723	-157.94814	154	3/6/2020	3/20/2020	14	119	-6.8	-41.9
DOH	21.41723	-157.94814	154	3/20/2020	4/17/2020	28	121	-3.3	-13.4
DOH	21.41723	-157.94814	154	4/17/2020	6/10/2020	54	58	-0.6	4.1
DOH	21.41723	-157.94814	154	6/10/2020	10/2/2020	114	19	-0.8	-0.2
DOH	21.41723	-157.94814	154	10/2/2020	11/6/2020	35	87	-2.4	-6.0
DOH	21.41723	-157.94814	154	11/6/2020	12/11/2020	35	18	-1.0	3.4
DOH	21.41723	-157.94814	154	12/11/2020	1/13/2021	33	47	-2.7	-9.3
DOH	21.41723	-157.94814	154	1/13/2021	2/2/2021	20	145	-3.2	-11.0
DOH	21.41723	-157.94814	154	2/2/2021	3/3/2021	29	55	-1.7	-2.1
DOH	21.41723	-157.94814	154	3/3/2021	3/16/2021	13	134	-4.2	-21.5
DOH	21.41723	-157.94814	154	3/16/2021	3/31/2021	15	29	-1.3	1.6
DOH	21.41723	-157.94814	154	3/31/2021	6/11/2021	72	44	-0.8	2.5
DOH	21.41723	-157.94814	154	6/11/2021	8/4/2021	54	21	-1.0	-0.5
WU	21.42663	-157.92957	330	5/8/2019	6/28/2019	51	154	-4.5	-25.1
WU	21.42663	-157.92957	330	6/28/2019	8/5/2019	38	63	-2.0	-5.8
WU	21.42663	-157.92957	330	8/5/2019	9/9/2019	35	93	-2.7	-13.3
WU	21.42663	-157.92957	330	9/9/2019	10/1/2019	22	98	-2.3	-8.4
WU	21.42663	-157.92957	330	10/1/2019	10/14/2019	13	127	-5.1	-29.1
WU	21.42663	-157.92957	330	10/14/2019	11/15/2019	32	37	-1.3	2.0
WU	21.42663	-157.92957	330	11/15/2019	12/11/2019	26	84	-2.0	-3.4
WU	21.42663	-157.92957	330	12/11/2019	12/11/2019	1	107	-2.3	-5.3
WU	21.42663	-157.92957	330	12/11/2019	12/20/2019	9	64	-1.9	-4.3
WU	21.42663	-157.92957	330	12/20/2019	1/8/2020	19	188	-1.9	-2.9
WU	21.42663	-157.92957	330	1/8/2020	1/15/2020	7	167	-2.8	-10.7
WU	21.42663	-157.92957	330	1/15/2020	2/13/2020	29	56	-2.7	-7.6
WU	21.42663	-157.92957	330	2/13/2020	3/6/2020	22	105	-3.3	-14.3
WU	21.42663	-157.92957	330	3/6/2020	3/20/2020	14	112	-7.0	-43.2
WU	21.42663	-157.92957	330	3/20/2020	4/17/2020	28	175	-3.1	-10.6
WU	21.42663	-157.92957	330	4/17/2020	6/10/2020	54	107	-1.4	-0.1

WU	21.42663	-157.92957	330	6/10/2020	10/2/2020	114	130	-1.4	-2.1
WU	21.42663	-157.92957	330	10/2/2020	11/6/2020	35	117	-2.4	-6.1
WU	21.42663	-157.92957	330	11/6/2020	12/11/2020	35	110	-1.5	1.0
WU	21.42663	-157.92957	330	12/11/2020	1/13/2021	33	139	-2.5	-6.8
WU	21.42663	-157.92957	330	1/13/2021	2/3/2021	21	174	-2.9	-7.7
WU	21.42663	-157.92957	330	2/3/2021	3/3/2021	28	135	-2.1	-4.1
WU	21.42663	-157.92957	330	3/3/2021	3/16/2021	13	197	-4.4	-24.0
WU	21.42663	-157.92957	330	3/16/2021	3/31/2021	15	90	-1.9	-0.5
WU	21.42663	-157.92957	330	3/31/2021	6/11/2021	72	161	-1.4	0.5
WU	21.42663	-157.92957	330	6/11/2021	8/4/2021	54	114	-1.5	-1.7
SK1	21.51187	-158.15775	945	10/12/2019	10/12/2019	1	NA	-3.5	-10.8
SK1	21.51187	-158.15775	945	1/5/2020	1/5/2020	1	NA	-3.5	-10.8
SK1	21.51187	-158.15775	945	3/28/2020	3/28/2020	1	NA	-3.5	-10.4
SK1	21.51187	-158.15775	945	5/2/2020	5/2/2020	1	NA	-3.5	-10.4
SK1	21.51187	-158.15775	945	6/20/2020	6/20/2020	1	NA	-3.2	-8.5
SK1	21.51187	-158.15775	945	9/19/2020	9/19/2020	1	NA	-3.2	-8.7
SK1	21.51187	-158.15775	945	1/4/2021	1/4/2021	1	NA	-3.4	-9.7
SK1	21.51187	-158.15775	945	3/13/2021	3/13/2021	1	NA	-4.0	-14.0
SK1	21.51187	-158.15775	945	4/21/2021	4/21/2021	1	NA	-3.5	-10.3

## APPENDIX C: CHAPTER 4 SUPPLEMENTARY MATERIAL

**TAB C.1. LOWER MANANA SOIL AND WATER BUDGET DATA**

Date	Temperature (°C)	RH	Precipitation (mm)	Tension (kPa)	Soil Water Potential (cm)		Soil Water Content	Tension (kPa)	Soil Water Potential (cm)		Soil Water Content	Tension (kPa)	Soil Water Potential (cm)		Soil Water Content	Tension (kPa)	Soil Water Potential (cm)		Soil Water Content	Soil Water Column Height (mm)	Soil Water Change (mm)	Soil Water Potential Gradient	PET (mm)	AET (mm)	Infiltration (mm)
					100 cm Depth				91 cm Depth				72 cm Depth				52 cm Depth								
12/30/2020	22.11	85.80	3.81	10.11	-103.13	0.44	15.40	-148.08	0.42	28.93	-267.12	0.40	17.27	-128.12	0.42	186.97	-0.89	0.90	7.01	4.70	0.00				
12/31/2020	21.30	87.17	1.02	11.54	-117.73	0.43	16.46	-158.88	0.42	29.46	-272.48	0.40	18.46	-140.28	0.41	186.02	-0.82	0.84	8.72	1.84	0.00				
1/1/2021	20.61	91.80	3.30	12.79	-130.48	0.43	17.33	-167.80	0.42	29.96	-277.58	0.40	19.58	-151.75	0.41	185.22	-0.78	0.81	4.84	4.08	0.00				
1/2/2021	20.93	90.45	3.56	13.50	-137.70	0.43	18.00	-174.60	0.42	31.46	-292.88	0.40	20.42	-160.25	0.41	184.56	-0.48	0.88	6.64	4.03	0.00				
1/3/2021	21.00	91.30	2.29	14.00	-142.80	0.42	18.96	-184.38	0.41	31.50	-293.30	0.40	21.00	-166.20	0.41	184.12	-0.26	0.83	3.95	2.55	0.00				
1/4/2021	22.06	87.33	8.13	14.00	-142.80	0.42	19.17	-186.50	0.41	31.83	-296.70	0.40	21.00	-166.20	0.41	184.06	0.14	0.83	7.79	7.79	0.00				
1/5/2021	21.37	91.13	4.57	14.00	-142.80	0.42	19.42	-189.05	0.41	27.96	-257.18	0.40	18.67	-142.40	0.41	185.39	1.85	0.14	6.16	2.72	0.00				
1/6/2021	21.78	87.64	0.51	14.00	-142.80	0.42	18.75	-182.25	0.41	29.46	-272.48	0.40	17.54	-130.93	0.42	185.81	-0.46	0.05	6.41	0.97	0.00				
1/7/2021	21.86	83.41	0.25	14.00	-142.80	0.42	19.00	-184.80	0.41	30.46	-282.68	0.40	19.13	-147.08	0.41	184.97	-1.05	0.40	11.24	1.30	0.00				
1/8/2021	19.73	89.76	0.00	14.00	-142.80	0.42	19.00	-184.80	0.41	31.63	-294.58	0.40	20.21	-158.13	0.41	184.41	-0.49	0.68	2.85	0.49	0.00				
1/9/2021	20.84	87.81	0.00	14.17	-144.50	0.42	19.38	-188.63	0.41	31.75	-295.85	0.40	21.25	-168.75	0.41	183.93	-0.61	0.83	3.57	0.61	0.00				
1/10/2021	20.82	90.40	2.29	15.00	-153.00	0.42	20.00	-195.00	0.41	31.96	-297.98	0.40	22.00	-176.40	0.41	183.46	0.00	0.80	7.26	2.29	0.00				
1/11/2021	21.50	89.78	1.78	15.00	-153.00	0.42	20.25	-197.55	0.41	32.50	-303.50	0.40	23.00	-186.60	0.41	183.02	-0.60	1.00	7.76	2.38	0.00				
1/12/2021	22.24	85.61	0.00	15.13	-154.28	0.42	21.00	-205.20	0.41	32.46	-303.08	0.40	23.58	-192.55	0.41	182.70	-0.42	1.03	7.53	0.42	0.00				
1/13/2021	21.74	86.19	0.25	16.00	-163.20	0.42	21.29	-208.18	0.41	32.54	-303.93	0.40	24.25	-199.35	0.41	182.36	-0.47	1.00	6.92	0.72	0.00				
1/14/2021	22.34	85.47	0.25	16.00	-163.20	0.42	22.00	-215.40	0.41	33.21	-310.73	0.39	25.00	-207.00	0.40	181.95	-0.09	1.12	11.13	0.35	0.00				
1/15/2021	21.84	85.27	0.00	16.00	-163.20	0.42	22.29	-218.38	0.41	33.42	-312.85	0.39	25.71	-214.23	0.40	181.67	-0.36	1.25	6.83	0.36	0.00				
1/16/2021	21.73	88.39	0.51	16.33	-166.60	0.42	23.00	-225.60	0.41	34.21	-320.93	0.39	26.54	-222.73	0.40	181.22	-0.55	1.34	8.21	1.06	0.00				
1/17/2021	20.61	93.89	5.33	16.92	-172.55	0.42	23.00	-225.60	0.41	33.33	-312.00	0.39	27.00	-227.40	0.40	181.12	0.27	1.29	3.74	3.74	0.00				
1/18/2021	18.51	97.75	12.19	17.00	-173.40	0.42	23.00	-225.60	0.41	30.00	-278.00	0.40	27.75	-235.05	0.40	181.23	0.64	1.26	1.95	1.95	0.00				
1/19/2021	20.89	92.48	12.19	6.00	-61.20	0.46	20.83	-203.50	0.41	12.42	-98.65	0.43	14.46	-99.48	0.42	191.39	9.09	-0.34	5.27	3.10	0.00				
1/20/2021	20.76	92.74	6.86	10.71	-109.23	0.43	18.50	-179.70	0.41	14.33	-118.20	0.42	15.58	-110.95	0.42	189.35	-3.09	-0.56	3.84	3.84	6.11				
1/21/2021	20.62	92.33	10.92	4.96	-50.58	0.46	17.29	-167.38	0.42	14.63	-121.18	0.42	12.79	-82.48	0.43	192.20	5.41	-0.07	7.25	5.51	0.00				
1/22/2021	21.47	83.38	1.02	7.92	-80.75	0.44	16.00	-154.20	0.42	14.29	-117.78	0.42	12.63	-80.78	0.43	191.84	-2.61	-0.48	13.94	3.63	0.00				
1/23/2021	20.52	96.12	20.07	4.42	-45.05	0.47	14.08	-134.65	0.42	13.50	-109.70	0.43	6.42	-17.45	0.46	201.06	15.20	-1.03	5.55	4.87	0.00				
1/24/2021	21.66	92.20	5.84	3.13	-31.88	0.48	12.00	-113.40	0.43	12.67	-101.20	0.43	4.79	-0.87	0.46	201.98	-5.81	-1.00	8.22	8.22	3.43				
1/25/2021	19.97	99.70	65.53	3.04	-31.03	0.48	7.92	-71.75	0.45	9.17	-65.50	0.44	5.00	-3.00	0.46	205.80	12.18	-0.75	0.97	0.97	52.39				

1/26/2021	20.96	94.44	3.30	3.00	-30.60	0.48	3.21	-23.73	0.47	5.17	-24.70	0.46	4.17	5.50	0.47	209.93	-5.67	-0.68	3.73	3.73	5.23		
1/27/2021	21.15	88.08	2.03	3.75	-38.25	0.47	9.42	-87.05	0.44	9.79	-71.88	0.44	8.79	-41.68	0.44	198.77	-	12.42	-0.20	10.59	10.59	3.87	
1/28/2021	20.12	86.68	1.02	6.50	-66.30	0.45	13.21	-125.73	0.43	15.25	-127.55	0.42	13.79	-92.68	0.42	191.77	-4.18	0.29	8.89	5.20	0.00		
1/29/2021	19.88	92.89	9.40	9.71	-99.03	0.44	14.96	-143.58	0.42	17.92	-154.75	0.42	15.50	-110.10	0.42	189.44	-0.16	0.09	4.34	4.34	0.00		
1/30/2021	20.84	91.16	9.14	10.50	-107.10	0.43	15.00	-144.00	0.42	17.17	-147.10	0.42	14.58	-100.75	0.42	189.96	0.27	-0.26	6.82	6.82	2.05		
1/31/2021	20.25	90.76	10.67	10.29	-104.98	0.43	11.42	-107.45	0.43	15.04	-125.43	0.42	5.08	-3.85	0.46	200.83	10.10	-1.91	6.55	0.57	0.00		
2/1/2021	19.55	97.33	17.78	9.50	-96.90	0.44	7.46	-67.08	0.45	9.58	-69.75	0.44	5.75	-10.65	0.46	202.85	8.62	-1.56	2.62	2.62	6.54		
2/2/2021	21.14	92.19	3.30	7.25	-73.95	0.45	3.79	-29.68	0.47	6.71	-40.43	0.45	4.58	1.25	0.46	207.05	-7.97	-1.24	6.66	6.66	4.61		
2/3/2021	18.13	98.88	15.49	6.79	-69.28	0.45	4.29	-34.78	0.47	6.54	-38.73	0.45	4.79	-0.87	0.46	206.91	8.51	-1.18	1.26	1.26	5.73		
2/4/2021	17.15	86.53	0.00	5.96	-60.78	0.45	6.17	-53.90	0.46	7.71	-50.63	0.44	6.88	-22.13	0.45	202.66	-	12.99	-0.75	7.46	7.46	5.54	
2/5/2021	17.55	83.37	0.00	8.67	-88.40	0.44	11.71	-110.43	0.43	11.50	-89.30	0.43	13.33	-88.00	0.43	192.95	-5.27	-0.20	8.07	5.27	0.00		
2/6/2021	18.64	79.71	0.00	10.21	-104.13	0.43	14.58	-139.75	0.42	14.83	-123.30	0.42	16.38	-119.03	0.42	189.61	-2.19	0.07	6.53	2.19	0.00		
2/7/2021	19.37	75.31	0.00	11.58	-118.15	0.43	16.25	-156.75	0.42	16.67	-142.00	0.42	18.17	-137.30	0.42	187.93	-1.74	0.15	8.31	1.74	0.00		
2/8/2021	19.80	83.92	1.27	12.71	-129.63	0.43	17.33	-167.80	0.42	17.83	-153.90	0.42	19.54	-151.33	0.41	186.83	-0.68	0.20	10.31	1.95	0.00		
2/9/2021	17.90	77.15	0.00	13.71	-139.83	0.42	18.00	-174.60	0.42	18.00	-155.60	0.42	20.58	-161.95	0.41	186.18	-0.48	0.20	7.79	0.48	0.00		
2/10/2021	19.04	76.08	0.00	14.00	-142.80	0.42	19.00	-184.80	0.41	18.58	-161.55	0.41	21.58	-172.15	0.41	185.51	-0.70	0.29	12.44	0.70	0.00		
2/11/2021	20.52	78.95	0.00	14.75	-150.45	0.42	19.50	-189.90	0.41	19.00	-165.80	0.41	22.58	-182.35	0.41	184.94	-0.59	0.35	10.01	0.59	0.00		
2/12/2021	22.00	78.31	1.78	15.00	-153.00	0.42	20.25	-197.55	0.41	19.25	-168.35	0.41	23.67	-193.40	0.41	184.39	-0.65	0.47	11.00	2.43	0.00		
2/13/2021	21.66	89.26	1.52	15.96	-162.78	0.42	21.00	-205.20	0.41	20.00	-176.00	0.41	24.54	-202.33	0.40	183.80	-0.40	0.46	7.44	1.93	0.00		
2/14/2021	21.43	92.25	1.52	16.00	-163.20	0.42	21.79	-213.28	0.41	20.25	-178.55	0.41	25.00	-207.00	0.40	183.49	-0.29	0.49	3.40	1.82	0.00		
2/15/2021	22.07	88.87	0.00	16.25	-165.75	0.42	22.13	-216.68	0.41	21.00	-186.20	0.41	25.75	-214.65	0.40	183.08	-0.38	0.60	7.32	0.38	0.00		
2/16/2021	22.69	84.29	0.00	17.00	-173.40	0.42	22.92	-224.75	0.41	21.04	-186.63	0.41	27.00	-227.40	0.40	182.54	-0.58	0.66	5.56	0.58	0.00		
2/17/2021	21.91	82.36	0.00	17.00	-173.40	0.42	22.96	-225.18	0.41	21.96	-195.98	0.41	28.29	-240.58	0.40	182.03	-0.29	0.97	5.34	0.29	0.00		
2/18/2021	22.36	86.53	14.22	13.33	-136.00	0.43	23.63	-231.98	0.41	18.08	-156.45	0.42	29.38	-251.63	0.40	183.16	5.68	1.51	7.03	7.03	0.00		
2/19/2021	20.93	97.08	18.03	9.96	-101.58	0.44	22.08	-216.25	0.41	7.63	-49.78	0.45	12.96	-84.18	0.44	196.32	14.11	-1.63	2.46	2.46	1.46		
2/20/2021	21.73	92.10	3.56	14.00	-142.80	0.42	18.88	-183.53	0.41	8.67	-60.40	0.44	7.63	-29.78	0.45	196.64	-8.89	-2.99	3.20	3.20	9.25		
2/21/2021	21.81	88.99	6.86	13.96	-142.38	0.42	18.00	-174.60	0.42	10.88	-82.93	0.43	12.46	-79.08	0.43	191.75	-1.81	-1.83	6.26	6.26	2.42		
2/22/2021	21.06	89.24	4.57	13.00	-132.60	0.43	17.58	-170.35	0.42	12.00	-94.40	0.43	13.00	-84.60	0.43	191.24	0.17	-1.47	8.65	4.40	0.00		
2/23/2021	21.72	83.08	4.57	13.00	-132.60	0.43	17.04	-164.83	0.42	12.29	-97.38	0.43	13.71	-91.83	0.42	190.85	-1.57	-1.26	12.26	6.14	0.00		
2/24/2021	21.44	84.21	1.52	13.00	-132.60	0.43	17.63	-170.78	0.42	13.17	-106.30	0.43	15.58	-110.95	0.42	189.50	-1.23	-0.90	13.46	2.76	0.00		
2/25/2021	21.72	86.60	10.92	13.00	-132.60	0.43	18.00	-174.60	0.42	14.25	-117.35	0.42	17.54	-130.93	0.42	188.24	-0.67	-0.49	13.18	11.59	0.00		
2/26/2021	19.47	47.84	5.59	13.08	-133.45	0.43	18.21	-176.73	0.42	14.50	-119.90	0.42	17.21	-127.53	0.42	188.31	1.16	-0.57	43.28	4.43	0.00		
2/27/2021	19.78	97.83	28.96	5.96	-60.78	0.47	9.13	-84.08	0.45	8.83	-62.10	0.44	7.92	-32.75	0.45	202.90	20.89	-0.75	2.88	2.88	5.18		
2/28/2021	19.59	87.83	15.49	3.00	-30.60	0.48	3.00	-21.60	0.48	6.00	-33.20	0.45	3.67	10.60	0.47	210.69	0.00	-0.71	10.61	10.61	4.88		
3/1/2021	19.93	85.09	2.54	3.13	-31.88	0.48	3.58	-27.55	0.47	6.33	-36.60	0.45	4.38	3.38	0.46	208.80	-7.09	-0.63	11.72	9.63	0.00		
3/2/2021	19.45	85.89	8.89	4.67	-47.60	0.46	9.54	-88.33	0.44	9.42	-68.05	0.44	11.04	-64.63	0.43	196.54	-9.60	0.07	9.94	9.94	0.00		
3/3/2021	20.14	88.10	4.06	7.71	-78.63	0.44	12.29	-116.38	0.43	11.08	-85.05	0.43	13.25	-87.15	0.43	193.04	-0.65	-0.14	6.01	4.71	0.00		
3/4/2021	18.25	98.30	6.10	9.83	-100.30	0.44	14.00	-133.80	0.42	12.46	-99.08	0.43	14.63	-101.18	0.42	191.21	-2.47	-0.29	2.87	2.87	5.70		

3/5/2021	19.85	92.12	39.12	6.00	-61.20	0.46	6.04	-52.63	0.46	6.88	-42.13	0.45	3.79	9.33	0.47	208.61	22.12	-1.40	2.19	2.19	14.81		
3/6/2021	19.92	94.25	15.49	3.00	-30.60	0.48	3.08	-22.45	0.48	5.96	-32.78	0.45	4.00	7.20	0.47	210.04	-2.31	-0.66	2.12	2.12	15.68		
3/7/2021	20.07	97.72	1.27	3.88	-39.53	0.47	5.58	-47.95	0.46	7.21	-45.53	0.45	4.83	-1.30	0.46	206.32	-	11.08	-0.80	5.71	5.71	6.63	
3/8/2021	22.46	87.98	59.69	3.63	-36.98	0.47	4.67	-38.60	0.47	6.92	-42.55	0.45	3.83	8.90	0.47	209.17	13.85	-0.89	10.38	10.38	35.46		
3/9/2021	22.91	89.02	14.99	2.04	-20.83	0.49	3.17	-23.30	0.47	6.04	-33.63	0.45	3.50	12.30	0.47	211.48	-2.78	-0.61	2.90	2.90	14.86		
3/10/2021	21.45	96.57	13.46	3.54	-36.13	0.47	7.96	-72.18	0.45	8.04	-54.03	0.44	5.33	-6.40	0.46	204.09	-5.80	-0.82	6.12	6.12	13.14		
3/11/2021	20.32	94.71	9.91	5.21	-53.13	0.46	9.96	-92.58	0.44	7.96	-53.18	0.44	3.96	7.63	0.47	205.03	-0.21	-1.55	6.53	6.53	3.59		
3/12/2021	20.35	92.39	16.51	6.71	-68.43	0.45	11.46	-107.88	0.43	8.88	-62.53	0.44	5.63	-9.38	0.46	201.70	2.79	-1.54	9.05	9.05	4.67		
3/13/2021	19.96	95.91	3.05	7.08	-72.25	0.45	10.25	-95.55	0.43	7.00	-43.40	0.45	4.04	6.78	0.47	204.78	-2.35	-1.90	5.09	5.09	0.31		
3/14/2021	20.11	98.05	12.45	8.75	-89.25	0.44	11.08	-104.05	0.43	7.75	-51.05	0.44	5.79	-11.08	0.46	201.37	0.16	-1.86	3.37	3.37	8.92		
3/15/2021	20.45	84.20	46.48	5.88	-59.93	0.46	7.21	-64.53	0.45	6.67	-40.00	0.45	3.83	8.90	0.47	207.59	6.85	-1.49	4.40	4.40	35.23		
3/16/2021	17.89	98.67	23.62	3.00	-30.60	0.48	3.50	-26.70	0.47	6.00	-33.20	0.45	3.00	17.40	0.48	211.82	0.88	-0.89	2.58	2.58	20.16		
3/17/2021	20.47	84.72	1.52	3.04	-31.03	0.48	3.46	-26.28	0.47	6.17	-34.90	0.45	3.38	13.58	0.47	210.91	-4.68	-0.81	15.78	6.20	0.00		
3/18/2021	19.52	93.21	30.48	4.00	-40.80	0.47	6.79	-60.28	0.45	6.71	-40.43	0.45	3.46	12.73	0.47	208.49	4.68	-1.23	4.09	4.09	21.71		
3/19/2021	19.35	88.80	3.30	3.29	-33.58	0.47	5.17	-43.70	0.46	6.46	-37.88	0.45	3.17	15.70	0.47	210.05	-6.88	-1.04	12.65	10.18	0.00		
3/20/2021	21.60	78.21	2.03	5.00	-51.00	0.46	10.54	-98.49	0.43	8.92	-63.02	0.44	6.92	-22.62	0.45	200.08	-8.28	-0.92	8.50	8.50	1.81		
3/21/2021	NA	NA	NA	NA	NA	NA	NA	NA	NA	NA	NA	NA	NA	NA	NA	NA	NA	NA	NA	NA	NA		
3/22/2021	21.89	82.52	0.00	10.00	-102.00	0.44	13.93	-133.07	0.42	11.57	-90.03	0.43	11.50	-69.30	0.43	193.38	-4.84	-0.98	10.82	4.84	0.00		
3/23/2021	22.68	88.19	6.86	11.00	-112.20	0.43	15.13	-145.28	0.42	13.08	-105.45	0.43	14.54	-100.33	0.42	190.76	-2.76	-0.56	8.73	8.73	0.88		
3/24/2021	21.72	97.71	10.92	12.25	-124.95	0.43	16.00	-154.20	0.42	14.25	-117.35	0.42	16.13	-116.48	0.42	189.35	0.43	-0.47	3.73	3.73	6.76		
3/25/2021	22.65	92.55	16.26	5.13	-52.28	0.46	6.58	-58.15	0.46	8.13	-54.88	0.44	5.75	-10.65	0.46	205.46	18.33	-0.86	6.79	0.00	0.00		
3/26/2021	23.98	81.25	0.00	6.17	-62.90	0.45	9.13	-84.08	0.44	8.46	-58.28	0.44	6.63	-19.58	0.45	201.26	-	12.34	-1.06	12.98	12.34	0.00	
3/27/2021	21.86	84.60	4.83	9.63	-98.18	0.44	13.71	-130.83	0.42	10.83	-82.50	0.43	12.29	-77.38	0.43	193.19	-4.47	-0.78	11.72	9.29	0.00		
3/28/2021	20.82	84.02	0.25	11.50	-117.30	0.43	16.04	-154.63	0.42	13.38	-108.43	0.43	15.54	-110.53	0.42	189.91	-2.35	-0.51	10.32	2.60	0.00		
3/29/2021	23.07	82.03	0.00	12.83	-130.90	0.43	17.25	-166.95	0.42	15.33	-128.40	0.42	17.54	-130.93	0.42	188.17	-1.41	-0.34	16.60	1.41	0.00		
3/30/2021	23.41	80.86	0.51	14.00	-142.80	0.42	18.33	-178.00	0.41	16.79	-143.28	0.42	19.04	-146.23	0.41	186.95	-1.28	-0.25	14.20	1.79	0.00		
3/31/2021	23.38	82.72	2.03	14.83	-151.30	0.42	19.29	-187.78	0.41	17.71	-152.63	0.42	20.50	-161.10	0.41	185.96	-0.80	-0.13	12.10	2.83	0.00		
4/1/2021	22.15	84.32	6.60	15.29	-155.98	0.42	20.04	-195.43	0.41	18.00	-155.60	0.42	21.17	-167.90	0.41	185.50	-0.22	-0.12	10.97	6.83	0.00		
4/2/2021	21.83	82.50	1.02	16.00	-163.20	0.42	21.00	-205.20	0.41	18.88	-164.53	0.41	21.67	-173.00	0.41	184.97	-0.54	-0.18	8.42	1.56	0.00		
4/3/2021	21.86	79.66	0.25	16.00	-163.20	0.42	21.04	-205.63	0.41	19.00	-165.80	0.41	22.58	-182.35	0.41	184.61	-0.36	0.01	14.81	0.61	0.00		
4/4/2021	21.07	86.68	4.32	16.21	-165.33	0.42	22.00	-215.40	0.41	19.71	-173.03	0.41	23.50	-191.70	0.41	184.03	-0.37	0.11	10.72	4.69	0.00		
4/5/2021	21.69	79.07	0.51	17.00	-173.40	0.42	22.13	-216.68	0.41	20.00	-176.00	0.41	24.50	-201.90	0.40	183.58	-0.81	0.18	22.14	1.31	0.00		
4/6/2021	21.07	72.27	0.25	17.00	-173.40	0.42	23.00	-225.60	0.41	20.29	-178.98	0.41	25.38	-210.83	0.40	183.14	-0.46	0.29	19.35	0.72	0.00		
4/7/2021	20.31	80.74	5.59	17.08	-174.25	0.42	23.17	-227.30	0.41	21.00	-186.20	0.41	26.71	-224.43	0.40	182.59	-0.43	0.57	11.77	6.02	0.00		
4/8/2021	20.95	76.39	0.25	17.88	-182.33	0.42	23.83	-234.10	0.41	21.00	-186.20	0.41	27.63	-233.78	0.40	182.18	-0.36	0.56	15.76	0.61	0.00		
4/9/2021	21.46	75.93	0.25	18.00	-183.60	0.42	24.25	-238.35	0.41	21.50	-191.30	0.41	29.38	-251.63	0.40	181.56	-0.82	0.88	15.00	1.08	0.00		
4/10/2021	20.44	76.36	0.25	18.00	-183.60	0.42	25.00	-246.00	0.40	22.00	-196.40	0.41	30.67	-264.80	0.40	181.05	-0.26	1.10	7.76	0.52	0.00		
4/11/2021	20.11	83.31	1.02	18.29	-186.58	0.41	25.04	-246.43	0.40	22.17	-198.10	0.41	31.79	-276.28	0.40	180.71	-0.57	1.28	4.97	1.59	0.00		

4/12/2021	21.93	78.65	2.29	18.96	-193.38	0.41	25.96	-255.78	0.40	22.96	-206.18	0.41	34.83	-307.30	0.39	179.74	-0.72	1.74	13.68	3.01	0.00
4/13/2021	21.94	76.38	0.76	19.21	-195.93	0.41	26.83	-264.70	0.40	23.42	-210.85	0.41	38.96	-349.38	0.39	178.67	-1.38	2.47	15.88	2.14	0.00
4/14/2021	22.69	74.93	1.52	19.88	-202.73	0.41	27.29	-269.38	0.40	24.08	-217.65	0.41	44.25	-403.35	0.39	177.49	-1.36	3.41	15.76	2.88	0.00
4/15/2021	22.06	76.22	0.00	20.00	-204.00	0.41	28.08	-277.45	0.40	24.96	-226.58	0.40	51.21	-474.33	0.38	176.11	-1.40	4.76	13.28	1.40	0.00
4/16/2021	20.76	80.46	0.00	20.21	-206.13	0.41	28.79	-284.68	0.40	25.00	-227.00	0.40	58.29	-546.58	0.38	174.97	-0.85	6.08	8.51	0.85	0.00
4/17/2021	22.37	76.94	0.00	20.71	-211.23	0.41	29.17	-288.50	0.40	25.46	-231.68	0.40	67.71	-642.63	0.37	173.66	-1.96	7.87	15.21	1.96	0.00
4/18/2021	23.49	73.65	0.00	21.04	-214.63	0.41	30.17	-298.70	0.40	26.33	-240.60	0.40	79.21	-759.93	0.37	172.15	-1.23	10.08	17.03	1.23	0.00
4/19/2021	25.47	70.46	0.00	21.83	-222.70	0.41	31.25	-309.75	0.40	27.25	-249.95	0.40	90.58	-875.95	0.36	170.82	-1.58	12.18	14.65	1.58	0.00
4/20/2021	21.92	87.14	9.91	14.50	-147.90	0.43	31.50	-312.30	0.40	17.50	-150.50	0.42	55.75	-520.65	0.39	179.48	13.53	5.85	3.10	0.00	0.00
4/21/2021	24.31	77.31	0.00	19.71	-201.03	0.41	31.13	-308.48	0.40	15.92	-134.35	0.42	46.79	-429.28	0.38	178.12	-8.45	3.18	12.80	8.45	0.00
4/22/2021	24.84	70.70	0.00	23.00	-234.60	0.41	31.96	-316.98	0.40	26.13	-238.48	0.40	60.08	-564.85	0.37	174.10	-1.50	5.76	17.25	1.50	0.00
4/23/2021	21.24	86.14	5.59	23.00	-234.60	0.41	32.29	-320.38	0.40	28.33	-261.00	0.40	61.50	-579.30	0.37	173.62	0.19	6.13	5.94	5.40	0.00
4/24/2021	22.62	80.73	3.81	23.25	-237.15	0.41	32.75	-325.05	0.40	29.00	-267.80	0.40	59.50	-558.90	0.37	173.76	-0.05	5.68	11.40	3.86	0.00
4/25/2021	22.92	81.74	1.78	23.75	-242.25	0.41	33.13	-328.88	0.39	29.00	-267.80	0.40	58.75	-551.25	0.38	173.80	0.04	5.41	12.76	1.73	0.00
4/26/2021	23.30	79.80	0.51	24.00	-244.80	0.41	33.71	-334.83	0.39	29.29	-270.78	0.40	58.42	-547.85	0.38	173.75	0.03	5.27	5.77	0.47	0.00
4/27/2021	23.74	80.32	1.02	24.00	-244.80	0.41	34.21	-339.93	0.39	29.63	-274.18	0.40	59.50	-558.90	0.37	173.53	-0.27	5.46	9.40	1.29	0.00
4/28/2021	22.12	87.50	12.19	24.00	-244.80	0.41	33.96	-337.38	0.39	19.08	-166.65	0.42	60.17	-565.70	0.37	175.42	3.59	5.08	3.52	3.52	0.00
4/29/2021	26.76	70.45	0.25	24.00	-244.80	0.41	33.00	-327.60	0.39	12.29	-97.31	0.43	56.86	-531.94	0.38	176.71	-1.10	4.16	11.36	1.36	0.00

**APPENDIX C: CHAPTER 4 SUPPLEMENTARY MATERIAL**  
**TAB C.2. UPPER MANANA SOIL AND WATER BUDGET DATA**

Date	Temperature (°C)	RH	Precipitation (mm)	Tension (kPa)	Soil Water Potential (cm)		Soil Water Content		Tension (kPa)	Soil Water Potential (cm)		Soil Water Content		Tension (kPa)	Soil Water Potential (cm)		Soil Water Content		Soil Water Column Height (mm)	Soil Water Change (mm)	Soil Water Potential Gradient	PET (mm)	AET (mm)	Infiltration (mm)
				122 cm Depth			57 cm Depth			37 cm Depth														
10/2/2020	23.29	93.08	NA	NA	NA	NA	NA	NA	NA	NA	NA	NA	NA	NA	NA	NA	NA	NA	NA	NA	NA	NA	NA	NA
10/3/2020	25.62	79.01	NA	NA	NA	NA	NA	NA	NA	NA	NA	NA	NA	NA	NA	NA	NA	NA	NA	NA	NA	NA	NA	NA
10/4/2020	24.81	76.23	NA	NA	NA	NA	NA	NA	NA	NA	NA	NA	NA	NA	NA	NA	NA	NA	NA	NA	NA	NA	NA	NA
10/5/2020	23.86	85.56	NA	NA	NA	NA	NA	NA	NA	NA	NA	NA	NA	NA	NA	NA	NA	NA	NA	NA	NA	NA	NA	NA
10/6/2020	25.91	76.39	0.00	19.00	-193.80	0.41	16.00	-98.20	0.42	16.76	-85.97	0.42	228.46	-0.37	-1.32	0.37	11.04	0.00						
10/7/2020	25.44	78.19	1.52	19.00	-193.80	0.41	16.73	-105.64	0.42	18.42	-102.85	0.41	227.73	-0.90	-1.14	2.43	13.72	0.00						
10/8/2020	25.17	76.27	0.00	19.00	-193.80	0.41	17.00	-108.40	0.42	19.67	-115.60	0.41	227.27	-0.61	-1.02	0.61	14.46	0.00						
10/9/2020	25.28	74.23	0.00	19.58	-199.75	0.41	17.02	-108.61	0.42	21.67	-136.00	0.41	226.41	-1.11	-0.91	1.11	10.64	0.00						
10/10/2020	25.35	75.19	4.06	20.00	-204.00	0.41	17.96	-118.18	0.42	24.10	-160.86	0.41	225.38	-0.61	-0.71	4.68	19.90	0.00						
10/11/2020	24.21	84.85	3.30	20.00	-204.00	0.41	18.00	-118.60	0.42	26.40	-184.24	0.40	224.82	-0.47	-0.50	3.77	8.45	0.00						
10/12/2020	24.85	83.63	12.19	20.17	-205.70	0.41	18.00	-118.60	0.42	24.96	-169.58	0.40	225.09	0.54	-0.65	9.77	9.77	1.88						
10/13/2020	24.69	78.12	0.76	21.00	-214.20	0.41	18.00	-118.60	0.42	22.83	-147.90	0.41	225.26	0.85	-0.95	0.00	16.64	0.00						
10/14/2020	25.19	79.63	2.54	21.00	-214.20	0.41	18.00	-118.60	0.42	21.00	-129.20	0.41	225.77	-0.30	-1.12	2.84	10.62	0.00						
10/15/2020	24.32	86.46	0.00	21.00	-214.20	0.41	18.00	-118.60	0.42	21.77	-137.06	0.41	225.55	-0.28	-1.05	0.28	10.70	0.00						
10/16/2020	25.50	84.06	0.00	21.00	-214.20	0.41	18.00	-118.60	0.42	22.98	-149.39	0.41	225.22	-0.53	-0.94	0.53	9.83	0.00						
10/17/2020	24.10	87.34	0.00	21.00	-214.20	0.41	18.54	-124.13	0.41	21.71	-136.43	0.41	225.51	1.22	-1.03	0.00	3.37	0.00						
10/18/2020	22.98	96.37	19.05	21.13	-215.48	0.41	18.15	-120.09	0.42	13.98	-57.59	0.43	228.39	4.74	-1.76	3.54	3.54	10.77						
10/19/2020	24.70	88.26	8.64	21.21	-216.33	0.41	16.31	-101.39	0.42	9.02	-7.01	0.44	231.19	1.55	-2.29	7.08	7.73	0.00						
10/20/2020	23.96	92.23	6.10	21.00	-214.20	0.41	13.38	-71.43	0.43	0.92	75.65	0.59	259.83	41.38	-3.11	0.00	4.22	0.00						
10/21/2020	23.72	91.71	3.05	20.31	-207.19	0.41	11.02	-47.41	0.43	0.30	82.03	0.62	266.16	0.89	-3.17	2.16	3.28	0.00						
10/22/2020	24.21	88.20	8.89	18.42	-187.85	0.41	11.81	-55.49	0.43	1.09	73.95	0.54	252.07	-31.57	-2.82	6.20	6.20	34.26						

10/23/2020	22.30	99.07	39.62	9.19	-93.71	0.44	7.17	-8.10	0.45	0.09	84.15	0.66	282.35	48.49	-1.90	0.00	1.87	0.00
10/24/2020	25.96	83.45	1.52	3.69	-37.61	0.47	6.46	-0.87	0.45	0.20	83.09	0.64	286.30	-1.75	-1.21	3.28	10.36	0.00
10/25/2020	25.25	81.31	3.30	3.94	-40.16	0.47	9.67	-33.60	0.44	1.75	67.15	0.52	262.74	-35.79	-0.98	4.10	4.10	34.99
10/26/2020	23.87	88.15	4.06	4.75	-48.45	0.46	11.33	-50.60	0.43	5.44	29.54	0.46	249.13	-7.44	-0.68	2.59	2.59	8.91
10/27/2020	22.02	93.43	0.00	6.77	-69.06	0.45	12.00	-57.40	0.43	7.73	6.16	0.44	243.47	-5.69	-0.71	0.81	0.81	4.88
10/28/2020	23.72	86.48	6.86	9.00	-91.80	0.44	12.27	-60.16	0.43	9.40	-10.84	0.44	239.61	-2.28	-0.84	7.29	7.29	1.84
10/29/2020	23.36	78.32	0.00	10.00	-102.00	0.44	12.40	-61.44	0.43	7.69	6.59	0.44	239.87	1.82	-1.12	0.00	11.07	0.00
10/30/2020	23.44	79.69	0.00	10.00	-102.00	0.44	12.67	-64.20	0.43	8.54	-2.13	0.44	239.14	-1.82	-1.03	1.82	9.90	0.00
10/31/2020	23.13	79.17	0.25	10.00	-102.00	0.44	13.00	-67.60	0.43	9.98	-16.79	0.44	238.08	-0.64	-0.89	0.89	6.58	0.00
11/1/2020	22.30	80.38	0.00	10.00	-102.00	0.44	13.10	-68.66	0.43	10.94	-26.56	0.43	237.50	-1.38	-0.80	1.38	2.70	0.00
11/2/2020	24.87	77.60	0.00	10.88	-110.93	0.43	14.00	-77.80	0.42	12.21	-39.53	0.43	235.84	-0.85	-0.76	0.85	11.19	0.00
11/3/2020	23.60	91.77	2.79	11.13	-113.48	0.43	14.19	-79.71	0.42	12.60	-43.56	0.43	235.40	-1.51	-0.75	4.31	6.12	0.00
11/4/2020	24.36	87.95	1.52	12.00	-122.40	0.43	15.00	-88.00	0.42	13.52	-52.91	0.43	234.09	-0.45	-0.75	1.97	5.80	0.00
11/5/2020	25.34	80.97	0.25	12.08	-123.25	0.43	15.00	-88.00	0.42	13.94	-57.16	0.42	233.84	-0.35	-0.72	0.61	6.53	0.00
11/6/2020	23.34	86.69	3.05	13.00	-132.60	0.43	15.35	-91.61	0.42	14.29	-60.78	0.42	232.95	-0.60	-0.79	3.64	5.94	0.00
11/7/2020	23.22	89.74	14.48	13.00	-132.60	0.43	15.67	-94.80	0.42	12.44	-41.86	0.43	233.80	2.28	-0.95	7.58	7.58	4.62
11/8/2020	23.54	82.36	13.72	13.27	-135.36	0.43	14.21	-79.93	0.42	9.58	-12.75	0.44	235.50	1.25	-1.30	10.68	10.68	1.78
11/9/2020	21.47	95.24	17.53	12.25	-124.95	0.43	9.31	-29.99	0.44	2.42	60.35	0.49	247.29	20.08	-2.00	0.00	2.94	0.00
11/10/2020	22.90	85.56	2.29	3.35	-34.21	0.47	7.00	-6.40	0.45	1.88	65.88	0.49	260.68	3.34	-0.99	0.00	10.07	0.00
11/11/2020	21.44	91.13	15.75	3.29	-33.58	0.47	8.44	-21.06	0.44	2.31	61.41	0.49	258.64	0.94	-0.89	7.38	7.38	7.43
11/12/2020	22.51	84.01	19.81	3.04	-31.03	0.48	8.48	-21.49	0.44	2.31	61.41	0.49	259.27	2.66	-0.86	13.04	13.04	4.11
11/13/2020	22.52	87.48	6.86	4.38	-44.63	0.47	6.17	2.10	0.45	2.21	62.48	0.49	258.04	-3.89	-1.13	5.46	5.46	5.28
11/14/2020	22.98	81.90	3.81	3.15	-32.09	0.47	8.92	-25.95	0.44	2.81	56.31	0.48	257.60	-4.31	-0.81	8.12	9.33	0.00
11/15/2020	23.49	82.70	3.56	3.92	-39.95	0.47	10.50	-42.10	0.43	4.00	44.20	0.47	252.76	-2.91	-0.74	6.46	9.57	0.00
11/16/2020	23.08	86.03	1.52	4.69	-47.81	0.46	11.00	-47.20	0.43	4.85	35.49	0.46	249.92	-5.25	-0.74	5.69	5.69	1.08
11/17/2020	23.62	84.59	0.51	6.56	-66.94	0.45	11.56	-52.94	0.43	7.81	5.31	0.44	243.83	-5.28	-0.69	5.79	6.74	0.00
11/18/2020	21.65	97.98	39.62	6.23	-63.54	0.45	8.79	-24.68	0.44	5.75	26.35	0.46	248.20	10.23	-0.94	1.92	1.92	27.47
11/19/2020	21.88	87.42	1.78	4.00	-40.80	0.47	8.75	-24.25	0.44	4.60	38.04	0.46	252.42	-0.71	-0.76	2.48	4.82	0.00
11/20/2020	20.99	96.88	21.08	4.17	-42.50	0.47	8.50	-21.70	0.44	4.35	40.59	0.46	252.57	2.69	-0.82	2.60	2.60	15.80
11/21/2020	22.05	83.14	40.39	5.50	-56.10	0.46	5.48	9.11	0.46	4.00	44.20	0.47	252.62	0.58	-1.14	6.54	6.54	33.27
11/22/2020	22.23	84.85	28.96	3.56	-36.34	0.47	5.50	8.90	0.46	4.00	44.20	0.47	256.09	3.23	-0.89	9.41	9.41	16.32

11/23/2020	22.49	83.52	51.82	4.54	-46.33	0.46	4.69	17.19	0.46	4.00	44.20	0.47	254.96	0.83	-1.04	8.14	8.14	42.84
11/24/2020	21.76	88.39	61.21	6.77	-69.06	0.45	4.31	21.01	0.46	3.31	51.21	0.47	252.64	-2.63	-1.41	4.52	4.52	59.32
11/25/2020	21.00	85.34	3.30	3.38	-34.43	0.47	4.94	14.64	0.46	3.56	48.66	0.47	257.75	2.86	-0.92	0.44	3.33	0.00
11/26/2020	22.04	76.38	1.52	3.04	-31.03	0.48	8.19	-18.51	0.44	3.88	45.48	0.47	256.19	-6.88	-0.73	6.05	6.05	2.35
11/27/2020	20.41	89.60	1.52	4.02	-41.01	0.47	10.50	-42.10	0.43	5.83	25.50	0.45	250.28	-4.06	-0.59	2.17	2.17	3.42
11/28/2020	21.18	74.51	4.06	5.90	-60.14	0.45	11.42	-51.45	0.43	8.58	-2.55	0.44	244.26	-6.46	-0.54	3.97	3.97	6.56
11/29/2020	21.86	42.68	19.56	7.85	-80.11	0.44	11.21	-49.33	0.43	7.31	10.41	0.45	243.05	5.06	-0.92	8.70	8.70	5.80
11/30/2020	22.29	72.16	8.64	4.63	-47.18	0.46	7.19	-8.31	0.45	4.29	41.23	0.46	252.94	10.03	-0.93	0.00	4.57	0.00
12/1/2020	23.39	72.73	0.00	3.00	-30.60	0.48	8.44	-21.06	0.44	4.75	36.55	0.46	254.92	-2.69	-0.63	2.69	6.74	0.00
12/2/2020	22.08	78.47	0.00	3.75	-38.25	0.47	10.17	-38.70	0.43	6.94	14.24	0.45	250.00	-5.76	-0.46	5.54	5.54	0.22
12/3/2020	23.53	74.42	0.00	5.15	-52.49	0.46	11.25	-49.75	0.43	9.46	-11.48	0.44	244.94	-5.27	-0.37	4.88	4.88	0.40
12/4/2020	23.49	74.07	1.27	7.65	-77.99	0.44	12.08	-58.25	0.43	10.73	-24.44	0.43	240.35	-4.47	-0.55	5.69	5.69	0.05
12/5/2020	22.21	77.23	0.00	9.48	-96.69	0.44	13.00	-67.60	0.43	12.21	-39.53	0.43	237.34	-1.95	-0.62	1.95	6.26	0.00
12/6/2020	21.91	79.89	0.00	10.00	-102.00	0.44	13.25	-70.15	0.43	13.31	-50.79	0.43	236.26	-0.73	-0.57	0.73	2.23	0.00
12/7/2020	22.39	77.71	2.03	10.60	-108.16	0.43	14.00	-77.80	0.42	14.21	-59.93	0.42	235.15	-1.26	-0.54	3.30	3.86	0.00
12/8/2020	22.75	75.59	1.52	11.00	-112.20	0.43	14.00	-77.80	0.42	15.00	-68.00	0.42	234.48	0.00	-0.52	1.52	3.57	0.00
12/9/2020	22.73	74.47	0.25	11.88	-121.13	0.43	14.96	-87.58	0.42	15.83	-76.50	0.42	233.23	-1.42	-0.52	1.67	1.88	0.00
12/10/2020	23.06	74.08	0.76	12.10	-123.46	0.43	15.00	-88.00	0.42	16.00	-78.20	0.42	232.99	-0.71	-0.54	1.47	3.51	0.00
12/11/2020	22.14	77.60	1.27	13.00	-132.60	0.43	15.06	-88.64	0.42	16.58	-84.15	0.42	232.12	-0.61	-0.60	1.88	4.51	0.00
12/12/2020	22.22	77.99	6.35	13.10	-133.66	0.43	16.00	-98.20	0.42	16.81	-86.49	0.42	231.74	-0.66	-0.55	5.73	5.73	1.28
12/13/2020	21.50	84.00	0.00	14.00	-142.80	0.42	16.00	-98.20	0.42	17.00	-88.40	0.42	231.08	0.00	-0.65	0.00	2.46	0.00
12/14/2020	20.92	82.38	1.52	14.00	-142.80	0.42	16.00	-98.20	0.42	17.17	-90.10	0.42	231.03	-0.35	-0.64	1.87	3.92	0.00
12/15/2020	20.94	80.19	14.22	14.90	-151.94	0.42	16.00	-98.20	0.42	17.48	-93.29	0.42	230.37	0.10	-0.72	4.71	4.71	9.41
12/16/2020	20.87	81.03	30.73	8.75	-89.25	0.45	11.13	-48.48	0.43	6.88	14.88	0.45	245.77	25.77	-1.08	4.30	4.30	0.67
12/17/2020	22.18	81.07	12.45	3.00	-30.60	0.48	7.48	-11.29	0.45	4.00	44.20	0.47	256.37	0.00	-0.74	4.15	4.15	8.30
12/18/2020	22.80	72.76	11.43	2.88	-29.33	0.48	6.23	1.46	0.45	3.67	47.60	0.47	258.10	1.75	-0.80	9.68	14.28	0.00
12/19/2020	22.94	71.51	17.78	2.56	-26.14	0.48	5.96	4.23	0.45	2.94	55.04	0.48	260.72	6.63	-0.83	10.27	10.27	0.88
12/20/2020	21.52	77.16	8.64	2.25	-22.95	0.49	5.92	4.65	0.45	2.00	64.60	0.49	264.14	-3.59	-0.88	4.27	4.27	7.96
12/21/2020	20.07	82.24	5.59	3.00	-30.60	0.48	6.77	-4.06	0.45	2.00	64.60	0.49	260.94	-0.58	-0.94	4.84	4.84	1.32
12/22/2020	20.45	85.96	0.00	3.00	-30.60	0.48	8.31	-19.79	0.44	2.33	61.20	0.49	259.37	-3.79	-0.85	3.61	3.61	0.19
12/23/2020	23.81	78.52	0.00	3.65	-37.19	0.47	10.25	-39.55	0.43	4.46	39.53	0.46	253.03	-7.11	-0.67	7.11	8.81	0.00

12/24/2020	21.75	86.81	2.03	5.08	-51.85	0.46	11.33	-50.60	0.43	8.10	2.34	0.44	246.01	-7.02	-0.48	2.69	2.69	6.36
12/25/2020	22.24	76.87	12.45	7.00	-71.40	0.45	12.00	-57.40	0.43	9.81	-15.09	0.44	241.64	-0.73	-0.55	0.01	0.01	13.16
12/26/2020	NA	NA	NA	NA	NA	NA	NA	NA	NA	NA	NA	NA	NA	NA	NA	NA	NA	
12/27/2020	NA	NA	NA	NA	NA	NA	NA	NA	NA	NA	NA	NA	NA	NA	NA	NA	NA	
12/28/2020	NA	NA	NA	NA	NA	NA	NA	NA	NA	NA	NA	NA	NA	NA	NA	NA	NA	
12/29/2020	NA	NA	NA	NA	NA	NA	NA	NA	NA	NA	NA	NA	NA	NA	NA	NA	NA	
12/30/2020	20.84	88.21	2.54	5.62	-57.28	0.46	11.38	-51.12	0.43	6.77	15.95	0.45	246.10	2.08	-0.67	0.46	4.57	0.00
12/31/2020	20.49	87.10	1.02	7.75	-79.05	0.44	12.00	-57.40	0.43	9.17	-8.50	0.44	241.20	-4.95	-0.71	5.96	6.80	0.00
1/1/2021	20.53	89.31	6.10	9.29	-94.78	0.44	12.29	-60.38	0.43	10.00	-17.00	0.44	238.94	-1.23	-0.82	5.00	5.00	2.33
1/2/2021	20.88	89.27	6.86	10.00	-102.00	0.44	12.50	-62.50	0.43	9.83	-15.30	0.44	238.32	0.94	-0.92	4.57	4.57	1.35
1/3/2021	21.71	82.24	3.05	10.00	-102.00	0.44	11.33	-50.60	0.43	7.04	13.18	0.45	240.76	2.78	-1.22	0.26	4.42	0.00
1/4/2021	20.86	83.68	7.11	8.67	-88.40	0.44	10.38	-40.83	0.43	6.00	23.80	0.45	243.29	1.98	-1.17	5.13	5.46	0.00
1/5/2021	20.87	84.08	16.26	4.29	-43.78	0.47	7.79	-14.48	0.45	3.38	50.58	0.47	255.39	17.05	-0.95	0.00	4.38	0.00
1/6/2021	21.56	78.78	1.52	3.00	-30.60	0.48	8.38	-20.43	0.44	2.79	56.53	0.48	258.22	-3.79	-0.81	5.32	5.45	0.00
1/7/2021	21.26	77.29	0.76	3.79	-38.68	0.47	10.17	-38.70	0.43	4.25	41.65	0.47	252.94	-6.01	-0.71	6.77	7.87	0.00
1/8/2021	21.74	78.79	0.00	5.38	-54.83	0.46	11.13	-48.48	0.43	7.21	11.48	0.45	246.34	-8.85	-0.61	2.36	2.36	6.49
1/9/2021	20.71	84.18	0.76	8.00	-81.60	0.44	12.00	-57.40	0.43	9.67	-13.60	0.44	240.59	-2.87	-0.69	2.61	2.61	1.02
1/10/2021	21.31	84.45	2.03	9.63	-98.18	0.44	12.67	-64.20	0.43	10.63	-23.38	0.43	238.15	-1.81	-0.79	3.84	5.03	0.00
1/11/2021	22.94	77.83	7.62	10.00	-102.00	0.44	13.00	-67.60	0.43	11.54	-32.73	0.43	237.20	-0.53	-0.74	6.14	6.14	2.01
1/12/2021	22.77	77.89	0.00	10.29	-104.98	0.43	13.00	-67.60	0.43	10.75	-24.65	0.43	237.38	0.26	-0.85	0.00	4.06	0.00
1/13/2021	25.15	69.31	0.76	11.00	-112.20	0.43	13.00	-67.60	0.43	10.67	-23.80	0.43	236.83	-0.58	-0.95	1.34	4.25	0.00
1/14/2021	22.74	78.03	0.76	11.00	-112.20	0.43	13.00	-67.60	0.43	11.00	-27.20	0.43	236.64	0.00	-0.92	0.76	8.55	0.00
1/15/2021	19.95	85.83	0.00	11.00	-112.20	0.43	13.29	-70.58	0.43	11.75	-34.85	0.43	236.16	-0.80	-0.84	0.80	3.00	0.00
1/16/2021	19.34	91.65	1.27	11.67	-119.00	0.43	14.00	-77.80	0.42	12.50	-42.50	0.43	235.08	-1.26	-0.83	2.53	3.51	0.00
1/17/2021	19.80	85.45	7.11	12.00	-122.40	0.43	14.00	-77.80	0.42	13.00	-47.60	0.43	234.58	0.00	-0.83	2.75	2.75	4.36
1/18/2021	18.59	73.37	51.05	10.08	-102.85	0.44	12.58	-63.35	0.43	9.25	-9.35	0.45	241.17	24.26	-0.98	9.01	9.01	17.78
1/19/2021	19.17	68.08	34.54	7.54	-76.93	0.45	4.63	17.83	0.46	1.54	69.28	0.50	257.22	1.29	-1.66	8.37	8.37	24.88
1/20/2021	20.30	67.66	9.91	3.83	-39.10	0.47	5.92	4.65	0.45	1.00	74.80	0.51	263.59	5.47	-1.18	4.44	8.60	0.00
1/21/2021	20.54	62.30	8.64	3.00	-30.60	0.48	5.58	8.05	0.46	1.00	74.80	0.51	265.88	0.00	-1.08	8.64	19.33	0.00
1/22/2021	20.43	72.38	2.03	3.00	-30.60	0.48	7.08	-7.25	0.45	1.33	71.40	0.51	263.61	-5.72	-0.99	7.75	20.50	0.00
1/23/2021	19.10	64.74	40.13	6.58	-67.15	0.45	6.33	0.40	0.45	1.67	68.00	0.50	256.69	0.25	-1.45	19.34	19.34	20.54

1/24/2021	20.09	61.72	10.67	3.71	-37.83	0.47	5.00	14.00	0.46	1.38	70.98	0.50	262.96	6.15	-1.16	4.52	17.73	0.00
1/25/2021	21.31	65.82	54.10	5.25	-53.55	0.46	4.92	14.85	0.46	1.75	67.15	0.50	260.53	-14.88	-1.33	7.90	7.90	61.08
1/26/2021	22.13	67.66	9.91	5.58	-56.95	0.46	4.79	16.13	0.46	1.83	66.30	0.49	257.90	14.88	-1.37	0.00	11.57	0.00
1/27/2021	20.67	81.41	4.57	3.17	-32.30	0.47	6.83	-4.70	0.45	1.38	70.98	0.50	263.12	-1.75	-1.02	6.33	10.98	0.00
1/28/2021	22.51	80.11	3.30	3.17	-32.30	0.47	9.04	-27.23	0.44	1.67	68.00	0.50	260.84	-7.59	-0.91	10.89	12.19	0.00
1/29/2021	21.90	81.20	8.38	3.96	-40.38	0.47	9.67	-33.60	0.44	1.38	70.98	0.50	259.79	4.60	-1.01	3.78	7.34	0.00
1/30/2021	22.19	76.17	7.62	3.46	-35.28	0.47	8.38	-20.43	0.44	1.00	74.80	0.51	263.19	2.99	-1.03	4.63	9.17	0.00
1/31/2021	21.03	76.96	13.97	4.00	-40.80	0.47	5.75	6.35	0.45	1.00	74.80	0.51	263.57	1.07	-1.20	8.55	8.55	4.35
2/1/2021	20.15	83.14	52.58	5.92	-60.35	0.46	5.50	8.90	0.46	1.00	74.80	0.51	260.62	-8.02	-1.46	3.12	3.12	57.47
2/2/2021	19.72	89.37	4.06	5.33	-54.40	0.46	5.08	13.15	0.46	0.96	75.23	0.52	262.58	5.47	-1.41	0.00	4.25	0.00
2/3/2021	20.45	83.77	19.05	5.38	-54.83	0.46	5.33	10.60	0.46	0.75	77.35	0.55	268.11	28.62	-1.42	0.00	7.73	0.00
2/4/2021	20.94	77.74	0.00	3.58	-36.55	0.47	6.38	-0.02	0.45	0.63	78.63	0.57	274.40	0.80	-1.16	0.00	7.03	0.00
2/5/2021	20.52	73.88	0.00	3.46	-35.28	0.47	9.71	-34.03	0.44	1.54	69.28	0.52	263.46	-37.99	-0.93	6.61	6.61	31.38
2/6/2021	20.24	77.16	0.00	4.88	-49.73	0.46	10.92	-46.35	0.43	4.54	38.68	0.46	250.13	-9.09	-0.80	4.46	4.46	4.63
2/7/2021	21.34	70.44	0.00	7.33	-74.80	0.45	11.92	-56.55	0.43	8.88	-5.53	0.44	241.96	-6.08	-0.68	5.72	5.72	0.36
2/8/2021	20.28	75.07	1.78	9.33	-95.20	0.44	12.58	-63.35	0.43	11.63	-33.58	0.43	237.90	-2.34	-0.67	4.12	7.10	0.00
2/9/2021	20.32	73.98	0.00	10.00	-102.00	0.44	13.00	-67.60	0.43	12.92	-46.75	0.43	236.51	-0.94	-0.62	0.94	5.93	0.00
2/10/2021	19.06	82.69	0.00	10.63	-108.38	0.43	13.67	-74.40	0.42	14.25	-60.35	0.42	235.20	-1.54	-0.55	1.54	6.91	0.00
2/11/2021	19.14	79.66	0.00	11.00	-112.20	0.43	14.00	-77.80	0.42	15.21	-70.13	0.42	234.40	-0.39	-0.50	0.39	5.74	0.00
2/12/2021	19.39	80.23	1.02	11.88	-121.13	0.43	14.50	-82.90	0.42	16.08	-79.05	0.42	233.25	-1.40	-0.52	2.41	7.83	0.00
2/13/2021	18.91	78.27	2.79	12.54	-127.93	0.43	15.00	-88.00	0.42	17.00	-88.40	0.42	232.31	-0.71	-0.50	3.50	7.82	0.00
2/14/2021	19.35	82.76	5.59	13.00	-132.60	0.43	15.00	-88.00	0.42	17.25	-90.95	0.42	231.90	-0.35	-0.54	2.97	2.97	2.97
2/15/2021	19.45	83.58	0.00	13.83	-141.10	0.42	15.58	-93.95	0.42	17.54	-93.93	0.42	231.11	-0.90	-0.60	0.90	4.56	0.00
2/16/2021	20.40	83.55	0.76	14.00	-142.80	0.42	16.00	-98.20	0.42	18.00	-98.60	0.42	230.74	0.00	-0.56	0.76	3.35	0.00
2/17/2021	20.76	81.96	0.00	14.92	-152.15	0.42	16.00	-98.20	0.42	18.00	-98.60	0.42	230.18	-0.61	-0.68	0.61	4.13	0.00
2/18/2021	22.80	78.94	9.14	15.00	-153.00	0.42	16.00	-98.20	0.42	18.00	-98.60	0.42	230.13	0.00	-0.69	4.72	4.72	4.42
2/19/2021	NA	NA	NA	NA	NA	NA	NA	NA	NA	NA	NA	NA	NA	NA	NA	NA	NA	
2/20/2021	NA	NA	NA	NA	NA	NA	NA	NA	NA	NA	NA	NA	NA	NA	NA	NA	NA	
2/21/2021	NA	NA	NA	NA	NA	NA	NA	NA	NA	NA	NA	NA	NA	NA	NA	NA	NA	
2/22/2021	NA	NA	NA	NA	NA	NA	NA	NA	NA	NA	NA	NA	NA	NA	NA	NA	NA	
2/23/2021	NA	NA	NA	NA	NA	NA	NA	NA	NA	NA	NA	NA	NA	NA	NA	NA	NA	

2/24/2021	NA	NA	NA	NA	NA	NA	NA	NA	NA	NA	NA	NA	NA	NA	NA	NA	NA	NA
2/25/2021	NA	NA	NA	NA	NA	NA	NA	NA	NA	NA	NA	NA	NA	NA	NA	NA	NA	NA
2/26/2021	NA	NA	NA	NA	NA	NA	NA	NA	NA	NA	NA	NA	NA	NA	NA	NA	NA	NA
2/27/2021	NA	NA	NA	NA	NA	NA	NA	NA	NA	NA	NA	NA	NA	NA	NA	NA	NA	NA
2/28/2021	NA	NA	NA	NA	NA	NA	NA	NA	NA	NA	NA	NA	NA	NA	NA	NA	NA	NA
3/1/2021	NA	NA	NA	NA	NA	NA	NA	NA	NA	NA	NA	NA	NA	NA	NA	NA	NA	NA
3/2/2021	NA	NA	NA	NA	NA	NA	NA	NA	NA	NA	NA	NA	NA	NA	NA	NA	NA	NA
3/3/2021	NA	NA	NA	NA	NA	NA	NA	NA	NA	NA	NA	NA	NA	NA	NA	NA	NA	NA
3/4/2021	NA	NA	NA	NA	NA	NA	NA	NA	NA	NA	NA	NA	NA	NA	NA	NA	NA	NA
3/5/2021	NA	NA	NA	NA	NA	NA	NA	NA	NA	NA	NA	NA	NA	NA	NA	NA	NA	NA
3/6/2021	NA	NA	NA	NA	NA	NA	NA	NA	NA	NA	NA	NA	NA	NA	NA	NA	NA	NA
3/7/2021	NA	NA	NA	NA	NA	NA	NA	NA	NA	NA	NA	NA	NA	NA	NA	NA	NA	NA
3/8/2021	NA	NA	NA	NA	NA	NA	NA	NA	NA	NA	NA	NA	NA	NA	NA	NA	NA	NA
3/9/2021	NA	NA	NA	NA	NA	NA	NA	NA	NA	NA	NA	NA	NA	NA	NA	NA	NA	NA
3/10/2021	NA	NA	NA	NA	NA	NA	NA	NA	NA	NA	NA	NA	NA	NA	NA	NA	NA	NA
3/11/2021	NA	NA	NA	NA	NA	NA	NA	NA	NA	NA	NA	NA	NA	NA	NA	NA	NA	NA
3/12/2021	NA	NA	NA	NA	NA	NA	NA	NA	NA	NA	NA	NA	NA	NA	NA	NA	NA	NA
3/13/2021	NA	NA	NA	NA	NA	NA	NA	NA	NA	NA	NA	NA	NA	NA	NA	NA	NA	NA
3/14/2021	NA	NA	NA	NA	NA	NA	NA	NA	NA	NA	NA	NA	NA	NA	NA	NA	NA	NA
3/15/2021	NA	NA	NA	NA	NA	NA	NA	NA	NA	NA	NA	NA	NA	NA	NA	NA	NA	NA
3/16/2021	NA	NA	NA	NA	NA	NA	NA	NA	NA	NA	NA	NA	NA	NA	NA	NA	NA	NA
3/17/2021	NA	NA	NA	NA	NA	NA	NA	NA	NA	NA	NA	NA	NA	NA	NA	NA	NA	NA
3/18/2021	NA	NA	NA	NA	NA	NA	NA	NA	NA	NA	NA	NA	NA	NA	NA	NA	NA	NA
3/19/2021	NA	NA	NA	NA	NA	NA	NA	NA	NA	NA	NA	NA	NA	NA	NA	NA	NA	NA
3/20/2021	NA	NA	NA	NA	NA	NA	NA	NA	NA	NA	NA	NA	NA	NA	NA	NA	NA	NA
3/21/2021	NA	NA	NA	NA	NA	NA	NA	NA	NA	NA	NA	NA	NA	NA	NA	NA	NA	NA
3/22/2021	22.32	70.22	0.00	3.00	-30.60	0.48	8.00	-16.60	0.44	2.27	61.88	0.49	259.68	27.29	-0.87	0.00	9.75	0.00
3/23/2021	22.10	70.96	3.05	3.54	-36.13	0.47	10.08	-37.85	0.44	3.33	51.00	0.47	255.06	-6.40	-0.77	6.89	6.89	2.55
3/24/2021	22.25	75.28	0.00	4.63	-47.18	0.46	11.00	-47.20	0.43	5.38	30.18	0.46	249.36	-3.08	-0.69	3.08	3.27	0.00

**APPENDIX C: CHAPTER 4 SUPPLEMENTARY MATERIAL**

**TAB C.3. ULUAKUPU SOIL CHEMISTRY DATA**

Sample Date	Sample Time	Depth (cm)	$\delta^2\text{H}$ (‰)	$\delta^{18}\text{O}$ (‰)	$\delta^2\text{H}$ Excess (‰)
10/1/2019	15:40	30	-10.3	-1.9	4.9
10/9/2019	7:15	30	-5.1	-1	2.8
12/7/2019	13:20	30	-13.2	-2.4	6.3
12/14/2019	10:30	30	-11.5	-2	4.9
12/16/2019	15:15	30	-8.8	-1.9	6.4
12/18/2019	16:40	30	-5.5	-1.5	6.6
12/26/2019	16:30	30	-0.7	-0.9	6.5
1/6/2020	16:30	30	1.7	-0.7	7.4
1/13/2020	14:20	30	-6.9	-2.2	10.9
2/12/2020	7:00	30	-7	-2.1	10.1
3/3/2020	7:20	30	-6.9	-2	8.7
3/7/2020	16:20	30	-5.2	-1.7	8.3
3/19/2020	16:25	30	-13.7	-2.9	9.7
4/16/2020	17:30	30	-14.2	-3.1	10.4
1/8/2021	7:00	30	1.2	-0.6	6
1/27/2021	7:20	30	-3.5	-1.7	10.3
3/5/2021	14:20	30	-3.2	-1.5	9.2
3/12/2021	16:10	30	-11.7	-2.8	10.9
3/18/2021	11:55	30	-21	-3.8	9.8
10/11/2019	16:55	90	-11.9	-2.6	9
10/16/2019	15:30	90	-14.8	-2.9	8.7
12/18/2019	16:30	90	-12.9	-2.7	8.6
12/26/2019	16:30	90	-13.4	-2.7	8.5
1/7/2020	16:00	90	-10.4	-2.3	7.9
1/13/2020	14:30	90	-7.3	-2.1	9.4
2/15/2020	13:45	90	-6.6	-1.9	8.6
3/3/2020	7:25	90	-7.9	-2	7.7
3/7/2020	10:50	90	-6.8	-2	9.2
3/19/2020	16:30	90	-10.3	-2.6	10.2
4/16/2020	17:15	90	-11.4	-2.8	11.2
12/30/2020	7:55	90	-8.4	-2.3	9.9
1/26/2021	11:40	90	-7.7	-2.2	9.7
3/4/2021	8:30	90	-6.2	-2	9.6
3/11/2021	14:45	90	-7.2	-2.2	10
3/17/2021	16:20	90	-9.5	-2.4	9.9
3/25/2021	16:30	90	-9.6	-2.5	10.6

**APPENDIX C: CHAPTER 4 SUPPLEMENTARY MATERIAL**

**TAB C.4. ULUAKUPU SOIL TENSION AND MOISTURE DATA**

Date	Time	Soil Tension 30 cm Depth (kPa)	Soil Tension 60 cm Depth (kPa)	Soil Tension 90 cm Depth (kPa)	Soil Tension 120 cm Depth (kPa)	Soil Moisture Content 0-15 cm Depth	Soil Moisture Content 0-30 cm Depth	Soil Moisture Content 0-68 cm Depth	Soil Moisture Content 90-105 cm Depth
1/24/2022	6:15			29	40	0.27	0.43	0.38	0.53
1/28/2022	7:40		37	32	44	0.26	0.4	0.38	0.5
1/31/2022	7:50		42	34	47	0.25	0.38	0.37	0.46
2/2/2022	6:00		46	36	49	0.25	0.36	0.37	0.49
2/3/2022	16:00		50	47	52	0.25	0.35	0.37	
2/7/2022	6:20		66	41	54	0.25	0.35	0.36	0.43
2/9/2022	9:45		77	43	56	0.24	0.32	0.36	0.48
2/14/2022	7:00		110	50	60	0.24	0.32	0.35	0.47
2/16/2022	6:30		119	53	62	0.24	0.32	0.35	0.48
2/18/2022	6:00		127	56	64	0.24	0.3	0.35	0.49
2/23/2022	6:15		154	66	68	0.24	0.29	0.35	0.43
2/25/2022	6:00		176	71	71	0.23	0.28	0.35	0.47
2/28/2022	6:00		221	80	73	0.24	0.29	0.35	0.45
3/2/2022	6:00			85	73	0.24	0.28	0.35	0.45
3/4/2022	13:50			93	77	0.23	0.29	0.34	0.45
3/7/2022	6:30			104	80	0.23	0.27	0.34	0.45
3/9/2022	6:15			112	84	0.23	0.26	0.35	0.46
3/11/2022	6:15			123	84	0.24	0.31	0.35	0.45
3/14/2022	6:15			133	91	0.23	0.27	0.34	0.42
3/16/2022	6:00			141	96	0.23	0.25	0.34	0.46
3/18/2022	6:15			147	100	0.23	0.25	0.34	0.42
3/21/2022	6:45			159	107	0.23	0.27	0.34	0.44
3/23/2022	10:25			168	106	0.25	0.27	0.35	0.45
3/25/2022	15:30			176	106				
3/28/2022	6:15			182	104	0.25	0.36	0.36	0.43
3/30/2022	6:20			185	105	0.25	0.35	0.36	0.43
4/1/2022	6:10			187	107	0.24	0.34	0.35	0.43
4/4/2022	6:00			189	109	0.24	0.32	0.35	0.41
4/6/2022	6:10			193	114	0.24	0.3	0.35	0.43
4/8/2022	6:15			194	119	0.24		0.34	0.42
4/11/2022	6:10			200	130	0.23	0.26	0.34	0.43
4/13/2022	6:00			205	135	0.23	0.25	0.34	0.45
4/18/2022	6:10			231	154	0.23	0.26	0.34	0.43
4/20/2022	6:00			239	159	0.23	0.27	0.34	0.46
4/22/2022	6:10			239	161	0.24	0.32	0.35	0.45
4/25/2022	6:30			239	161	0.26	0.34	0.36	0.43
4/27/2022	6:00			239	161	0.27	0.37	0.38	0.44
4/29/2022	6:15			239	161	0.25	0.34	0.36	0.41
5/2/2022	6:30			239	161	0.27	0.4	0.37	0.42
5/4/2022	6:00			239	158	0.29	0.48	0.38	0.43
5/6/2022	6:00			239	154	0.29	0.45	0.38	0.42
5/11/2022	9:30			239	146	0.28	0.43	0.39	0.44
5/16/2022	6:00			238	143	0.25	0.38	0.36	0.42
5/18/2022	6:00		230	233	140	0.26	0.36	0.37	0.45
5/20/2022	6:00		230	230	137	0.28	0.42	0.38	0.43

5/23/2022	6:15			121	133	0.29	0.45	0.4	0.44
5/25/2022	6:00		179	213	131	0.27	0.42	0.38	0.44
5/27/2022	6:30		180	215	131	0.25	0.36	0.36	0.45
6/1/2022	6:00		212	203	142	0.24	0.28	0.35	0.45
6/3/2022	8:20			220	151	0.23	0.29	0.35	0.43
6/6/2022	6:15			233	169	0.23	0.26	0.34	0.43
6/8/2022	6:10			226	176	0.22	0.25	0.34	0.43
6/13/2022	6:15			197	204	0.23	0.26	0.34	0.45
7/5/2022	7:40			172		0.24	0.36	0.35	0.4
7/7/2022	7:30			166		0.26	0.39	0.38	0.42
7/11/2022	6:15	31	115			0.27	0.4	0.38	0.45
7/13/2022	7:15			87		0.29	0.44	0.39	0.43
7/15/2022	6:30	21	23	73		0.3	0.46	0.39	0.41
7/18/2022	6:15	51	27	81		0.29	0.44	0.38	0.4
7/20/2022	6:15	68	23	20		0.28	0.44	0.38	0.4
7/22/2022	6:15	98	19	22		0.29	0.44	0.39	0.4
7/25/2022	6:30	140	35	29		0.25	0.4	0.36	0.41
7/27/2022	6:00	163	42	42		0.24	0.34	0.35	0.43
7/29/2022	7:50	197	57	42		0.23	0.29	0.35	0.45
8/1/2022	6:15		62	64		0.23	0.3	0.34	0.41
8/3/2022	6:00		67	77		0.23	0.32	0.35	0.4
8/5/2022	7:35		71	97		0.23	0.27	0.35	0.38
8/8/2022	6:30		85	117		0.23	0.22	0.34	
8/10/2022	6:00		116	130		0.22	0.21	0.34	
8/15/2022	6:30		211	152		0.23	0.2	0.33	
8/17/2022	6:00		228	134		0.23	0.18	0.33	
8/22/2022	6:15			140		0.22	0.17	0.33	
8/24/2022	6:00			164		0.22	0.17	0.33	
8/26/2022	6:05			194		0.22		0.35	0.39
8/29/2022	6:10			203		0.23		0.34	0.42
8/31/2022	6:15			209		0.23		0.34	0.4
9/2/2022	6:15			204		0.26		0.35	0.4
9/6/2022	8:50	143	21	218		0.29	0.39	0.37	0.42
9/8/2022	9:20	182	42	212		0.26	0.27	0.36	0.41
9/12/2022	6:10		82	195		0.36	0.43	0.37	0.4
9/14/2022	6:00		92	24		0.28	0.4	0.36	0.42
9/16/2022	6:10		99	210		0.26	0.38	0.35	0.43
9/19/2022	6:40		110	199		0.36	0.42	0.35	0.39
9/23/2022	6:00		115	169		0.24	0.37	0.35	0.42
9/26/2022	6:00		93	133		0.23	0.31	0.35	0.41
9/28/2022	6:15		125	109		0.23	0.3	0.34	0.42
9/30/2022	13:30		160	112		0.27	0.36	0.35	0.41
10/3/2022	6:15			123		0.23	0.33	0.34	0.4
10/5/2022	6:00		81	129		0.23	0.31	0.33	0.4
10/7/2022	6:15		106	138		0.22	0.28	0.34	0.41
10/12/2022	6:15		199	172		0.26	0.43	0.37	0.43
10/20/2022	7:00	39	18	47		0.31	0.45	0.41	0.49
10/24/2022	6:30	33	34	52		0.3	0.45	0.4	0.5
10/26/2022	6:30	36	33	60		0.34	0.48	0.43	0.47
10/31/2022	9:10	17	25	65		0.31	0.47	0.41	0.51
11/2/2022	6:15	25	28	65		0.3	0.45	0.41	0.5
11/4/2022	11:30	32	31	65		0.31	0.45	0.4	0.52
11/7/2022	7:50	44	35	61		0.29	0.44	0.4	0.5
11/9/2022	6:15	53	37	60		0.3	0.43	0.4	0.51
11/14/2022	6:35		18	65	18	0.32	0.49	0.42	0.5
11/16/2022	6:30	25	39	64		0.33	0.46	0.4	0.47
11/21/2022	11:20	16	35	66		0.33	0.47	0.41	0.45
11/23/2022	6:00	21	32	58		0.33	0.46	0.42	0.52
11/25/2022	8:10	21	32	65		0.33	0.47	0.42	0.53
11/28/2022	6:15	29	33	63		0.32	0.46	0.41	0.49

11/30/2022	10:10	32	34	62		0.31	0.45	0.41	0.48
12/2/2022	6:00	30	35	62		0.31	0.44	0.41	0.49
12/5/2022	6:30	38	34	61		0.33	0.45	0.41	0.49
12/23/2022	6:50	21	19	16		0.33	0.48	0.42	0.56
12/27/2022	6:15	27	23	22		0.32	0.46	0.42	0.56
12/29/2022	7:45	31	25	24		0.3	0.42	0.41	0.52
1/3/2023	7:50	44	29	29		0.28	0.41	0.39	0.52
1/6/2023	6:00	50	30	31		0.3	0.44	0.4	0.49
1/9/2023	6:20	62	35	33		0.27	0.4	0.39	0.49
1/11/2023	6:15	80	34	35		0.26	0.39	0.38	0.52
1/13/2023	6:15	109	35	36		0.25	0.37	0.38	0.52
1/17/2023	8:00	152	39	40		0.24	0.35	0.37	0.5
1/20/2023	6:40	176	42	41		0.23	0.32	0.37	0.51
1/23/2023	6:40	228	47	43		0.23	0.32	0.36	0.51
1/25/2023	6:45		52	44		0.23	0.32	0.36	0.48
1/27/2023	6:00		58	45		0.23	0.3	0.36	0.51
1/30/2023	9:45			49		0.36	0.48	0.41	0.5
2/1/2023	10:40	14		48		0.33	0.48	0.42	
2/3/2023	7:40	22	37	43		0.32		0.41	
2/6/2023	6:30	11	15	8		0.34	0.5	0.43	
2/10/2023	6:40	17	20	18		0.34		0.42	0.51
2/13/2023	6:40	1	14	19		0.35	0.48	0.44	
2/15/2023	7:30	12	17	18		0.34	0.5	0.43	
2/17/2023	9:00	0.1	15	20		0.37	0.53	0.44	
2/21/2023	9:20	4	12	8		0.36	0.51	0.44	
2/24/2023	8:20	0.1	12	13		0.45	0.51	0.44	
2/27/2023	8:30	13	17	16		0.36	0.5	0.44	0.54
3/1/2023	10:00	10	12	5		0.37	0.52	0.44	
3/3/2023	14:15	0.1	11	13		0.37	0.52	0.44	
3/6/2023	6:20	13	16	16		0.36	0.52	0.44	
3/8/2023	9:30	12	18	19		0.36	0.51	0.44	
3/10/2023	7:45	18	20	22		0.34	0.5	0.42	
3/13/2023	8:15	23	23	25		0.32	0.47	0.41	0.51
3/15/2023	9:30	26	29	27		0.33	0.47	0.41	0.5
3/17/2023	8:00	29	25	28		0.3	0.46	0.4	0.51
3/20/2023	8:00	34	28	31					
3/22/2023	8:10	39	29	32		0.32	0.46	0.4	0.52
3/24/2023	6:10	44	30	33		0.29	0.44	0.4	0.49
3/27/2023	8:15	53	34	35		0.25	0.43	0.38	0.48
3/29/2023	7:30	65	34	37		0.34	0.47	0.4	
3/31/2023	12:10	70	36	38		0.31	0.46	0.4	
4/3/2023	6:15	78	37	39		0.35	0.5	0.42	0.5
4/4/2023	11:55	8	16	2					
4/5/2023	11:10	12	17	10					
4/6/2023	9:30	17	17	13		0.35	0.5	0.43	0.55
4/10/2023	6:10	19	22	22		0.36	0.51	0.43	
4/12/2023	9:40	9	20	24		0.36	0.54	0.43	
4/14/2023	9:00	17	20	23		0.34	0.52	0.42	
4/17/2023	6:10	24	23	26		0.31	0.47	0.41	0.5
4/19/2023	6:00	7	12	3		0.38	0.55	0.44	
4/21/2023	15:35	20	17	16		0.34	0.51	0.43	0.52
4/24/2023	8:30	23	20	22		0.32	0.49	0.43	0.55
4/26/2023	11:25	27	22	24		0.31	0.49	0.41	0.51